HUGO GALARNEAU

# INFLUENCE DE LA RÉPONSE INFLAMMATOIRE ET D'UN TRAITEMENT ANTI-INFLAMMATOIRE SUR LE DÉVELOPPEMENT DES GLIOMES

Mémoire présenté
à la Faculté des études supérieures de l'Université Laval
dans le cadre du programme de Maîtrise en physiologie-endocrinologie
pour l'obtention du grade de Maître ès sciences (M. Sc.)

FACULTÉ DE MÉDECINE
UNIVERSITÉ LAVAL
QUÉBEC

2007

# Résumé

Le rôle des macrophages dans le développement des gliomes, des tumeurs attaquant le système nerveux central, est controversé. Nous avons étudié le développement des gliomes chez des souris transgéniques permettant la déplétion spécifique des macrophages par l'administration d'un pro-médicament. Nos résultats indiquent qu'une réduction de la densité de macrophages augmente la croissance tumorale. Selon le modèle, leur activité est apparue dépendante ou non du recrutement des lymphocytes T. Nous avons ensuite émis l'hypothèse que les anti-inflammatoires pourraient favoriser le développement des gliomes. Au contraire, nous avons observé que l'administration de dexaméthasone à des souris implantées avec des cellules gliomales diminuait la progression des tumeurs. Nous avons établi que cet agent affectait le profil d'expression génique des cellules endothéliales en diminuant notamment l'expression de l'angiopoiétine-2, un facteur pro-angiogénique. L'utilisation d'un anticorps synthétique inhibant l'Angpt2 est apparue plus efficace que la dexaméthasone pour réduire la croissance des gliomes. Les inhibiteurs de l'Angpt-2 pourraient donc représenter des outils intéressants pour le traitement des gliomes.

# Avant-Propos

Je tiens tout d'abord à remercier mon directeur, le Dr. Luc Vallières, sans qui, rien de ceci n'aurait été possible. Il est sans contredit un modèle de détermination et de motivation. J'ai pu bénéficier de beaucoup de rigueur dans mon encadremment, une qualité primordiale en recherche.

Sans nommer de noms, pour éviter les oublis, je voudrais mentionner tous ceux et celles qui m'ont apporté leur support durant ces années d'études. Qu'ils soient collègues de travail, parents ou amis, j'ai pu compter sur plusieurs personnes pour m'encourager dans les moments plus difficiles. Et non, la recherche ce n'est pas toujours facile. On cherche beaucoup et on trouve…un peu, la satisfaction est grande par contre! J'ai eu la chance d'évoluer dans un milieu agréable et stimulant, où la bonne humeur qui régnait a permi de rendre chaque journée plus agréable…

# Contribution aux articles

**Chapitre 2 :**

Augmentation de la croissance des gliomes chez des souris déplétées en macrophages, *«Increased glioma growth in mice depleted in macrophages»,* Hugo Galarneau, Jérôme Villeneuve, Geneviève Gowing, Jean-Pierre Julien et Luc Vallières.

Cet article sera soumis prochainement pour publication dans le périodique *Cancer research*.

Les résultats présentés dans cet article sont attribuables à moi-même et Jérôme Villeneuve à parts égales. Geneviève Gowing est l'étudiante ayant réalisé le modèle de souris utilisé (souris CD11b-TK), travail ayant été réalisé dans le laboratoire du Dr. Jean-Pierre Julien.

**Chapitre 3 :**

L'inhibition de l'angiopoiétine 2 par la dexamethasone ou une protéine de fusion peptide-Fc réduit la croissance des gliomes, *«Blockade of angiopoietin 2 with dexamethasone or a peptide-Fc fusion protein reduces glioma growth»,* Jérôme Villeneuve, Hugo Galarneau, Marie-Josée Beaudet, Pierrot Tremblay, Ariel Chernomoretz[1] et Luc Vallières.

Article soumis pour publication dans le périodique *Journal of Neuroscience.*

Ma contribution à cet article est principalement reliée aux expériences de génomiques (Microarray), ainsi qu'à certaines analyses microscopiques. Jérôme Villeneuve, avec l'aide de Pierrot Tremblay, a réalisé la plupart des expériences *in vivo*, ainsi que celles relatives aux lymphocytes. Marie-Josée Beaudet a réalisée les travaux relatifs à l'expression de la MMP-2. Ariel Chernomoretz est le bioinformaticien s'étant chargé de l'analyse des résultats bruts obtenus en génomiques.

# Table des matières

# Liste des abréviations

| | |
|---|---|
| **ACTH** | Hormone adrénocorticotropique |
| **ADN** | Acide désoxyribonucléique |
| **Angpt** | Angiopoiétine |
| **CPA** | Cellule présentatrice d'antigène |
| **BHE** | Barrière hémato-encéphalique |
| **Casp** | Caspase |
| **CCR** | Récepteur de chimiokines C-C |
| **CD** | Cluster of differentiation |
| **CMH** | Complexe majeur d'histocompatibilité |
| **COX2** | Cyclooxygénase 2 |
| **CRF** | Corticolibérine |
| **CVO** | Organe circumventriculaire |
| **CSF-1** | Colony-stimulating factor 1 |
| **DC** | Cellule dendritique |
| **DD** | Death domain |
| **DISC** | Death inducing signaling complex |
| **dNTP** | Désoxyribonucléotide triphosphate |
| **EGF** | Epidermal growth factor |
| **FADD** | Fas-associated death domain |
| **FasL** | Fas ligand |
| **FGF** | Fibroblast growth factor |
| **α-GalCer** | α-galactosylceramide |
| **GCV** | Gancyclovir |
| **GFAP** | Glial fibrillary acidic protein |
| **$H_2O_2$** | Peroxyde d'hydrogène |
| **HGF** | Hepatocyte growth factor |
| **HIF-1** | Hypoxia inducible factor 1 |
| **HPA** | Axe hypothalamo-hypophysaire |
| **HSP** | Protéine de choc thermique |
| **HSV-1** | Virus de l'Herpes simplex type 1 |
| **ICAM** | Intercellular adhesion molecule |

| | |
|---|---|
| **IFN** | Interféron |
| **IL** | Interleukine |
| **IL-1R** | Récepteur de l'interleukine-1 |
| **IRAK** | Interleukin-1 receptor-associated kinase |
| **KO** | Knock out |
| **LCR** | Liquide céphalo-rachidien |
| **LFA-1** | Lymphocyte-function associated antigen |
| **MCP-1** | Monocyte chimioattractant protein 1 |
| **mdr** | Multidrug resistance |
| **MEC** | Matrice extra-cellulaire |
| **MMP** | Matrix metalloproteinase |
| **Myd88** | Myeloid differentiation primary response gene 88 |
| **NF-κB** | Nuclear factor κB |
| **NK** | Natural killer cell |
| **NKT** | Natural killer T cell |
| **NO** | Oxyde nitrique |
| **OMS** | Organisation mondiale de la santé |
| **$PGE_2$** | Prostaglandine $E_2$ |
| **PRR** | Pattern recognition receptor |
| **RANTES** | Regulation on activation normal T-cell expressed and secreted |
| **ROI** | Espèces réactives de l'oxygène |
| **SNC** | Système nerveux central |
| **SODD** | Silencer of death domain |
| **TIL** | Tumor infiltrating lymphocytes |
| **TGF** | Transforming growth factor |
| **TK** | Thymidine kinase |
| **TLR** | Toll-like receptor |
| **TNF** | Tumor necrosis factor |
| **TRADD** | Tumor necrosis factor receptor associated death domain |
| **TRAF** | Tumor necrosis factor receptor factor |
| **Treg** | cellule T régulatrice |
| **VCAM** | Vascular cell adhesion molecule |
| **VEGF** | Vascular endothelial growth factor |

# Liste des figures

# Liste des tableaux

# Introduction

## 1.1 Problématique

Les tumeurs attaquant le système nerveux central (SNC) constituent un problème de santé important. Jusqu'à l'âge de 40 ans, ce type de tumeur représente une des principales causes de décès reliés au cancer [1]. Les glioblastomes, la forme la plus sévère, sont incurables malgré des traitements agressifs tels que la chirurgie, la radiothérapie et la chimiothérapie. Une des alternatives envisageables pour palier à cet échec est l'immunothérapie. Cette approche consiste à utiliser les mécanismes de défenses spécifiques de l'hôte pour combattre la tumeur. Pour parvenir à utiliser efficacement ce principe, il est nécessaire de mieux comprendre les mécanismes fondamentaux de la réponse immunitaire anti-tumorale. Les macrophages jouent un rôle controversé dans ce processus. Comme nous le verrons plus loin, ces cellules peuvent détruire les cellules tumorales en produisant, entre autre, des intermédiaires réactifs de l'oxygène (ROIs). Toutefois, les macrophages peuvent aussi favoriser le développement des cellules tumorales en sécrétant des facteurs pro-angiogéniques et des métalloprotéinases. Par ailleurs, tous les patients atteints d'un gliome sont traités avec de la dexamethasone, un puissant anti-inflammatoire réduisant l'oedéme cérébral. Le mécanisme conduisant à cet effet est méconnu et la dexamethasone engendre de nombreux effets secondaires. En outre, elle pourrait inhiber les mécanismes anti-tumoraux endogènes (entre autre ceux des macrophages) et contrer l'efficacité de l'immunothérapie. Il serait donc avantageux d'éclaircir son mécanisme d'action afin d'identifier des cibles thérapeutiques plus spécifiques épargnant la réponse immunitaire.

# 1.2 Les tumeurs du SNC

## 1.2.1 Origine, classification et incidence

L'origine cellulaire des tumeurs cérébrales ne peut être établie précisément et leur classification est donc complexe. Les cellules tumorales retrouvées dans le système nerveux central (SNC) se caractérisent, entre autre, par l'expression de marqueurs spécifiques aux cellules matures normales en conjonction avec des molécules normalement retrouvées uniquement sur des cellules immatures. Aussi, elles présentent généralement une morphologie spécifique. À titre d'exemple, les cellules d'astrocytomes, des tumeurs dérivées des astrocytes, expriment parfois le *glial fibrillary acidic protein* (GFAP), une protéine retrouvée dans le cytosquelette des astrocytes matures. Toutefois, les cellules d'astrocytomes ne présentent pas des ramifications aussi élaborées que les astrocytes matures [2, 3]. Il existe deux principales hypothèses pour expliquer l'origine des cellules néoplasiques. D'une part, elles pourraient être le résultat de la prolifération incontrôlée de cellules matures qui se sont dé-différenciées [3]. Alternativement, un nombre croissant d'études tend à démontrer qu'elles pourraient dériver directement de cellules progénitrices ayant perdu la capacité de répondre normalement aux signaux de différenciation [4-7]. La classification la plus courante des tumeurs du SNC est celle proposée par l'organisation mondiale de la santé (OMS) [8]. Elles sont nommées en fonction du type cellulaire démontrant le plus de similitudes. Cette nomenclature est jumelée à une valeur de I à IV définissant l'agressivité de la tumeur; les tumeurs bénignes sont associées au niveau I et les plus malignes au niveau IV. Plus de 120 tumeurs cérébrales sont ainsi répertoriées selon qu'elles soient associées principalement aux lignées astrogliales, oligodendrogliales, épendymales ou neuronales [3]. Elles peuvent de plus constituer des métastases de tumeurs situées en périphérie du SNC. Le tableau 1 présente une version abrégée de la liste élaborée par l'OMS.

**Tableau 1**. Classification des tumeurs cérébrales.
***A,*** Version abrégée de la liste de l'OMS [8, 9]. ***B,*** Classification détaillée des astrocytomes avec leur niveau de malignité [10].

**A**

| **Tumors of neuroepithelial tissue** |
|---|
| Astrocytic tumors |
| Astrocytoma |
| Anaplastic astrocytoma |
| Glioblastoma multiforme |
| Pilocytic astrocytoma |
| Pleomorphic xanthoastrocytoma |
| Subependymal giant-cell astrocytoma |
| Oligodendroglial tumors |
| Oligodendroglioma |
| Anaplastic oligodendroglioma |
| Mixed gliomas |
| Oligoastrocytoma |
| Anaplastic oligoastrocytoma |
| Ependymal tumors |
| Ependymoma |
| Anaplastic ependymoma |
| Myxopapillary ependymoma |
| Subependymoma |
| Choroid plexus tumors |
| Choroid-plexus papilloma |
| Choroid-plexus carcinoma |
| Neuronal and mixed neuronal-glial tumors |
| Gangliocytoma |
| Dysembryoplastic neuroepithelial tumor |
| Ganglioglioma |
| Anaplastic ganglioglioma |
| Central neurocytoma |
| Pineal parenchymal tumors |
| Pineocytoma |
| Pineoblastoma |
| Embryonal tumors |
| Medulloblastoma |
| Primitive neuroectodermal tumor |
| **Meningeal tumors** |
| Meningioma |
| Hemangiopericytoma |
| Melanocytic tumor |
| Hemangioblastoma |
| **Primary central nervous system lymphomas** |
| **Germ-cell tumors** |
| Germinoma |
| Embryonal carcinoma |
| Yolk-sac tumor (endodermal-sinus tumor) |
| Choriocarcinoma |
| Teratoma |
| Mixed-germ-cell tumors |
| **Tumors of the sellar region** |
| Pituitary adenoma |
| Pituitary carcinoma |
| Craniopharyngioma |
| **Metastatic tumors** |

**B**

| **Astrocytic tumors** | **WHO Grade** |
|---|---|
| Diffuse astrocytomas | II |
| Fibrillary | |
| Protoplasmic | |
| Gemistocytic | |
| Anaplastic astrocytomas | III |
| Glioblastoma | IV |
| Giant cell glioblastoma | |
| Gliosarcoma | |
| Pilocytic astrocytoma | I |
| Pleomorphic xanthoastrocytoma | I-III |
| Subependymal giant cell astrocytoma | I |

Les tumeurs du SNC ne sont pas particulièrement fréquentes représentant 1.4 % de tous les cancers. Néanmoins, lorsque l'on considère leur contribution au taux de décès associé à cette maladie, le pourcentage double [11]. Les tumeurs dérivées des cellules gliales, ou gliomes, sont les plus courantes et comptent pour 40% de toutes les tumeurs diagnostiquées dans le cerveau. Ce pourcentage augmente à 60% si l'on considère seulement les tumeurs primaires [11]. Il existe plusieurs types de gliomes de niveaux d'agressivités variables, cependant plus de 80% d'entre eux s'avèrent malins et sont associés au niveau IV de l'échelle de l'OMS [9]. Ces derniers, nommés glioblastomes, constituent probablement les tumeurs pour lesquelles le pronostic est le plus pessimiste [12]. La survie des individus atteints dépasse rarement un an malgré les thérapies existantes [13]. Leur incidence est maximale chez les individus âgés de 65 à 74 ans [11]. Toutefois, ce sont les enfants qui sont le plus touchés. Jusqu'à l'âge de 20 ans, les tumeurs du SNC sont la forme de cancer la plus fréquente [11] représentant aussi la principale cause de décès reliée au cancer après la leucemie. Chez les individus âgés de 20 à 39 ans elles occupent la troisième place [1]. Les études démontrent également que les hommes sont plus susceptibles que les femmes de développer ce genre de tumeur. Une étude réalisée dans l'état de New-York a établi que l'écart entre les sexes apparaît vers l'âge de la puberté pour s'amenuiser à la ménopause, ce qui suggère un rôle protecteur des hormones féminines [14].

### 1.2.2 Caractéristiques des glioblastomes

Les glioblastomes se distinguent des tumeurs bénignes d'origine gliale par la présence de zones de nécroses, leur grande capacité d'invasion résultant de la production d'enzymes dégradant la matrice extracellulaire (MEC) et finalement, la formation de nouveaux vaisseaux sanguins (ou la prolifération vasculaire), phénomène nommé angiogénèse. Toutes ces caractéristiques sont intimement reliées du point de vue moléculaire. Le modèle le plus accepté pour expliquer le développement de ces tumeurs comporte 5 phases : l'apparition des premières cellules tumorales, leur organisation en périphérie des vaisseaux sanguins, leur prolifération, la dégénérescence des vaisseaux sanguins, et finalement, la création de zones nécrotiques et hypoxiques favorisant l'angiogénèse (Figure 1) [15]. Tout au long de ce processus les cellules tumorales

envahissent le tissu normal en migrant le long des vaisseaux sanguins. Ainsi, le développement tumoral est non seulement le résultat de la prolifération des cellules, mais aussi celui de l'évasion des cellules qui s'éloignent du foyer initial.

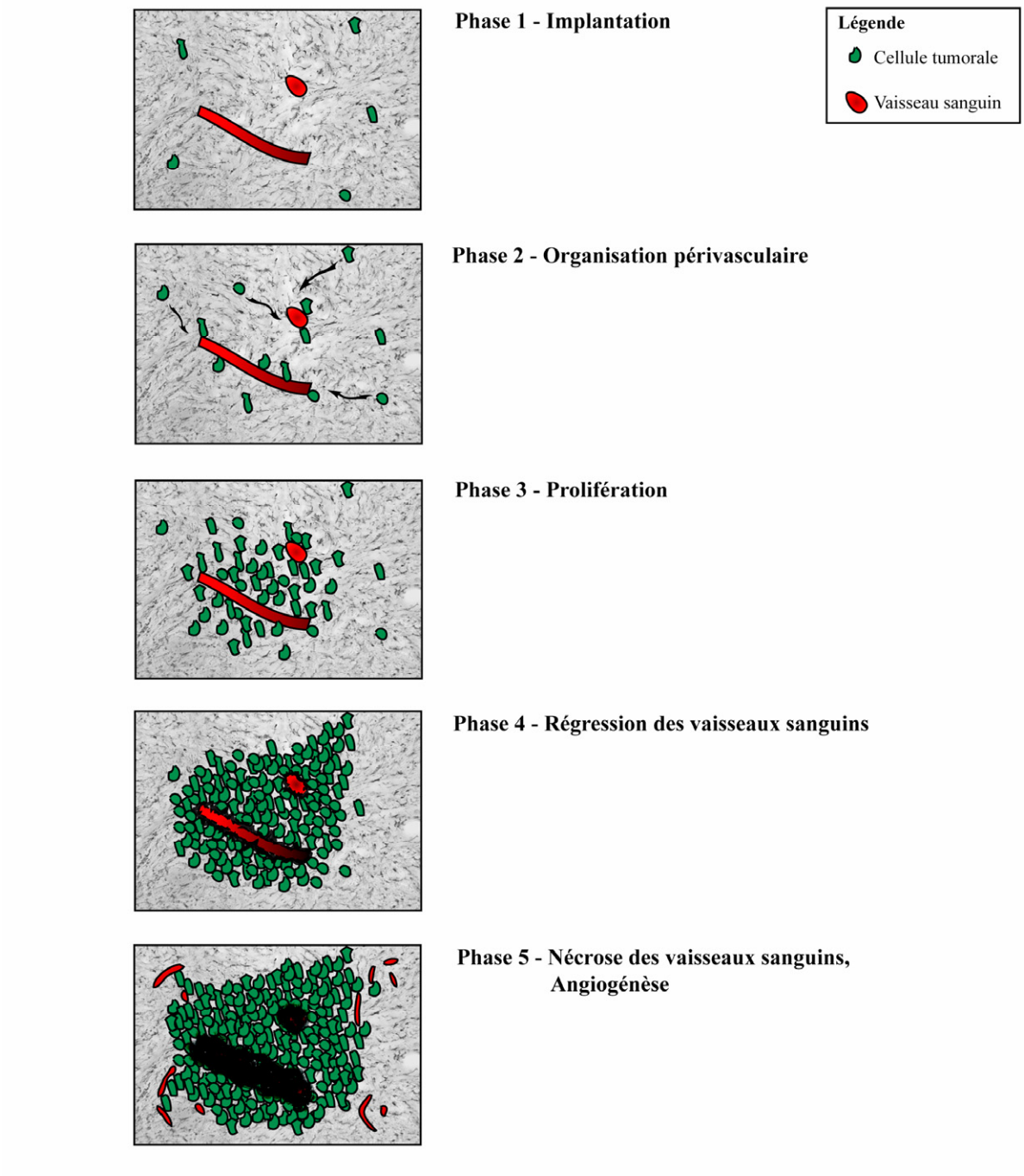


**Figure 1.** Les cinq phases du développement des glioblastomes.

Contrairement à d'autres types de tumeurs, la croissance des glioblastomes ne débute pas par une phase avasculaire [16, 17]. Dès le commencement du processus, les cellules tumorales tendent à s'établir en périphérie des vaisseaux sanguins existants. L'augmentation du nombre de cellules tumorales laisse apparaître une région présentant des vaisseaux hyperplasiques dont la densité semble diminuée comparativement au tissu sain [17]. Éventuellement, les cellules forment une véritable palissade entourant les vaisseaux. Cette forme de «parasitisme» entraîne une déstabilisation de la paroi des vaisseaux sanguins en association avec l'apoptose des cellules endothéliales. Les angiopoiétines, une famille de protéines connue pour jouer un rôle clé dans l'angiogénèse, seraient impliquées dans cet effet. L'augmentation de l'expression de l'*angiopoiétine-2* (Angpt2) favorise la déstabilisation des vaisseaux sanguins en inhibant l'activité consolidatrice de l'*angiopoiétine-1* (Angpt1) [18, 19]. La circulation sanguine ainsi compromise affecte l'acheminement de l'oxygène et entraîne la formation de foyers nécrotiques. Ces zones hypoxiques contribuent à l'induction de facteurs de transcriptions spécifiques à cette condition comme le *hypoxia inducible factor-1* (HIF-1) [20-22]. Celui-ci contribue à l'augmentation de l'expression de plusieurs gènes dont celui du *vascular endothelial growth factor* (VEGF), un facteur pro-angiogénique ayant un effet mitotique sur les cellules endothéliales et favorisant la perméabilité des vaisseaux sanguins [23, 24]. L'action du VEGF, jumelée au pouvoir déstabilisateur de l'Angpt2, permet donc le développement de nouveaux vaisseaux sanguins. La grande capacité invasive des glioblastomes n'est pas étrangère à ces phénomènes. Il a été démontré que l'Angpt2 joue un rôle dans l'activation de l'expression de la *matrix-metalloproteinase-2* (MMP-2) [25]. Cette protéine, surexprimée dans les gliomes, contribue à l'invasion des cellules tumorales en dégradant la matrice extracellulaire [26, 27]. L'analyse de l'expression de l'Angpt2 dans des gliomes humains a révélé que son expression était localisée exclusivement dans les régions invasives et absentes des zones centrales. De même, l'expression de la MMP-2 était plus importante dans ces régions invasives [28]. Toutefois, nous verrons que dans notre modèle murin l'expression de l'Angpt2 était observable de façon uniforme dans toute la tumeur et nous n'avons pu démontrer de relation avec l'expression de la MMP-2 *in vivo*.

### 1.2.3 Traitements

Malgré les efforts investis en recherche et le développement de nouvelles thérapies expérimentales, les glioblastomes demeurent pour l'instant incurables. Les patients reçoivent des traitements courants comprenant la chirurgie, la radiothérapie et la chimiothérapie. Cependant, ces traitements sont administrés à titre palliatif seulement afin de prolonger la survie des individus atteints avec la meilleure qualité de vie possible [13, 29].

La première intervention envisageable est la chirurgie. Une résection du maximum de la masse tumorale est pratiquée en évitant toutefois d'affecter le tissu sain adjacent. De cette façon une amélioration notable et rapide des fonctions neurologiques du patient peut être obtenue [30]. L'effet sur le prolongement de la survie n'a toutefois pas encore été formellement établi [31]. Malheureusement, les propriétés invasives de la tumeur rendent son ablation entière impossible; ainsi de nouveaux foyers de prolifération de cellules tumorales peuvent donc ressurgir. La présence d'œdème dans le cerveau des patients rend également l'opération particulièrement risquée. L'œdème cérébral est une complication résultant de l'accumulation de fluides dans le cerveau à cause de l'affaiblissement de la barrière hémato-encéphalique (BHE), ce qui engendre une augmentation de la pression intra-crânienne. Pour contrer ce phénomène, de la dexaméthasone est souvent administrée aux patients [32, 33]. Il s'agit d'un glucocorticoïde synthétique ayant des effets anti-inflammatoires. Le mécanisme permettant de réduire l'œdème est méconnu, mais conduirait à la diminution de la perméabilité vasculaire ou à l'augmentation de l'évacuation des fluides. Il a été rapporté que la dexamethasone pouvait contribuer à réduire l'expression du *vascular endothelial growth factor a* (VEGF-a), une molécule initialement identifiée comme le *vascular permeability factor* (VPF) [34, 35]. Cependant, les résultats de nos études *in vivo* ne supportent pas cette hypothèse. L'utilisation de cet agent ne doit pas être prolongée puisque de nombreux effets secondaires lui sont associés, notamment la perte de poids et le développement d'infections opportunistes [36].

Le plus souvent, une radiothérapie est prescrite en phase post-opératoire. Ce traitement est, d'après les études, celui permettant d'obtenir l'augmentation la plus significative de la survie des patients [37]. Ce type de rayonnement s'attaque uniquement aux cellules en division et est d'autant plus spécifique que la majorité des cellules du SNC ne prolifèrent peu ou pas. Par contre, l'hypoxie, une caractéristique des glioblastomes, affecte l'efficacité de cette thérapie. En effet, l'oxygène contribue normalement à médier les effets de ces rayons [38]. La surexpression de protéines anti-apoptotiques et la préservation de mécanismes efficace de réparation de l'ADN sont d'autres facteurs pouvant affaiblir les bénéfices reliés à ce traitement.

L'administration d'une chimiothérapie parallèlement à la radiothérapie permettrait d'augmenter les bienfaits de ce traitement [39]. Cependant, les bénéfices de la chimiothérapie, à elle seule, sont controversés [40, 41]. En effet, la localisation et la nature des gliomes les rendent aptes à résister à ces traitements. La BHE constitue un premier obstacle pour la plupart des molécules utilisées en chimiothérapie [42]. De plus, bien que la tumeur soit drainée par un riche réseau de vaisseaux sanguins, ceux-ci présentent une morphologie altérée et ne peuvent ainsi assurer une perfusion adéquate de la tumeur [43]. L'administration efficace de médicaments est donc compromise puisqu'il est difficile d'obtenir des concentrations optimales au site d'action. L'implantation de polymères imprégnés d'agents antinéoplasiques directement dans le lit de la tumeur lors de l'ablation permet une administration plus efficace et ciblée des traitements [44-46]. Par ailleurs, l'évolution rapide des glioblastomes favorise le développement d'une grande diversité cellulaire, résultant de l'accumulation de nombreuses mutations génétiques. L'administration d'une chimiothérapie peut donc engendrer une pression permettant la sélection de clones de cellules tumorales résistants aux traitements. Les mécanismes impliqués sont similaires à ceux associés à la radiothérapie. Les cellules présentent souvent une augmentation de l'expression de gènes encodant des facteurs anti-apoptotiques jumelée à une diminution des facteurs pro-apoptotiques. Certaines cellules sont aussi connues pour exprimer des protéines de transport membranaire, telle que la P-glycoprotéine encodée par le gène *multidrug resistance gene* (mdr), qui permettent l'élimination de drogues [47].

De toute évidence, le traitement des glioblastomes représente un défi considérable. Plusieurs thérapies innovatrices, telles que la thérapie génique, sont présentement en phase d'essais cliniques, mais pour l'instant peu d'entre elles semblent réellement prometteuses [48, 49]. Une alternative imaginée il y a de nombreuses années propose d'utiliser le système immunitaire pour combattre le développement des tumeurs. Après être tombée dans l'oubli, cette avenue est aujourd'hui plus que jamais explorée. Les glioblastomes pourraient constituer une cible spécialement attrayante pour ce type de traitements puisqu'ils sont abondamment infiltrés par des macrophages et des lymphocytes T.

## 1.3 Immunologie tumorale

### 1.3.1 Historique

La découverte de l'immunologie tumorale est généralement attribuée à William Coley, un chirurgien américain de la fin du 19$^{e}$ siècle. Ce dernier avait constaté que des patients atteints d'une tumeur se voyaient presque miraculeusement rétablis lorsqu'ils étaient victime d'une infection nosocomiale [50]. Par la suite, Paul Ehrlich postula au début des années 1900 que les cellules tumorales devaient exprimer des structures antigéniques pouvant être reconnues par le système immunitaire par l'intermédiaire du « magic bullet », identifié plus tard comme les anticorps [51]. Ce système de défense permettait, selon lui, d'expliquer la faible émergence de cellules tumorales. Dans les années 70, Sir MacFarlane Burnet et Lewis Thomas ont officiellement formulé la théorie d'immunosurveillance [52]. Dans les années qui ont suivi, l'engouement pour l'immunologie tumorale s'est dissipé, en partie parce que des expériences menées sur des souris athymiques démontraient qu'elles ne présentaient pas une plus forte propension à développer des tumeurs [53]. Toutefois, ces souris n'étaient pas complètement dépourvues de réponse immunitaire. Thierry Boon, en 1980, apporta un support considérable à la théorie de l'immunologie tumorale. Il établit que l'inoculation à des souris de cellules tumorales manipulées pour ne plus être tumorigènes empêchait le développement d'une tumeur lorsque ces mêmes souris étaient subséquemment inoculées avec des cellules tumorales sauvages [54].

Le système immunitaire agit donc comme un formidable système de défense non seulement contre les agressions extérieures, mais aussi contre des cellules endogènes qui se sont transformées, telles que les cellules tumorales. Lorsque des événements comme ceux-ci surviennent, une réponse complexe finement régulée s'organise. Cette réponse comprend deux phases successives et complémentaires: l'immunité innée et l'immunité acquise [55, 56]. Les macrophages constituent un médiateur important de l'immunité innée. Ils reconnaissent les cellules étrangères de façon non spécifique pour les détruire [57]. À plus long terme, la présentation d'antigènes par des cellules spécialisées, notamment les cellules dendritiques, permet l'activation des lymphocytes T, principaux effecteurs de la réponse acquise, qui reconnaîtront spécifiquement les pathogènes ou les cellules tumorales.

## 1.3.2 Mécanismes anti-tumoraux

### 1.3.2.1 L'immunité innée

Il est bien connu que les macrophages expriment des récepteurs permettant la reconnaissance de structures conservées chez les microbes et absentes de l'hôte. Ces récepteurs se regroupent sous une grande famille nommée *pattern recognition receptor* (PRR)[58-60]. L'expression de molécules dont la structure est altérée ou dont la localisation est modifiée permet la reconnaissance des cellules tumorales par ces mêmes récepteurs. Les *Toll like receptors* (TLR) représentent une importante catégorie de PRRs regroupant plus de 11 membres [61, 62]. La découverte de ligands endogènes pour ces récepteurs est relativement récente et ils ne sont donc pas encore exhaustivement définis. Les protéines de choc thermique (HSP) en constituent un bon exemple. Ces protéines sont présentes de façon ubiquitaire dans le cytoplasme des cellules. Par contre, une variété de stimuli, dont la transformation maligne de cellules, peut provoquer une augmentation de leur expression et même causer leur translocation à la surface de la membrane cytoplasmique [63-65]. Elles sont alors identifiables par les TLRs. D'autres couples de récepteurs/ligands sont connus pour pouvoir jouer un rôle dans cette reconnaissance et sont présentés dans le tableau 2 [66-69].

**Tableau 2.** Quelques exemples de couples récepteurs/ligands impliqués dans la reconnaissance des cellules tumorales par les macrophages.

| Ligands | Récepteurs |
|---|---|
| HSP-60 | TLR-2/4 |
| HSP-70 | TLR-2/4 |
| Fragments d'acide hyaluronique (HA) | TLR-4 |
| Fragments d'heparan sulfate | TLR-4 |
| Phosphatidylsérine (PS) externalisée | PS-specific receptor |
| Molécules anormalement glycosylées | Lectines |

La liaison des TLRs à leurs ligands engendre une signalisation semblable à celle du récepteur de l'*interleukine-1* (IL-1R) puisqu'ils appartiennent à la même famille. La protéine adaptatrice Myd88 se lie au domaine IL-1R du TLR et recrute ainsi IRAK et TRAF6 qui peut mener à l'activation de différents facteurs de transcription tel que NF-κB [70, 71]. Cette signalisation permet d'augmenter l'expression de cytokines pro-inflammatoires (TNF-α, IL-1β, IL-6, IL-12), de chimiokines (MCP-1, RANTES) et de molécules d'adhésion (ICAM, VCAM) [56, 72]. La production de ces molécules permet le recrutement d'autres médiateurs de l'immunité innée au site de la tumeur. Par exemple, la liaison de l'IL-1β à son récepteur IL1-R1 sur les cellules endothéliales engendre l'expression de MCP-1 via NF-κB. À son tour MCP-1 se lie à son récepteur CCR-2 à la surface des monocytes ce qui stimule la synthèse d'intégrines et augmente leur état d'activation. Ces molécules interagissent alors avec les molécules d'adhésion des cellules endothéliales et permettent le passage des monocytes au site de la tumeur ou d'un autre dommage. Ce phénomène est nommé extravasation. Les cellules tumorales elles-mêmes peuvent participer au recrutement des cellules inflammatoires en produisant des chimiokines comme MCP-1 et CSF-1[73-77].

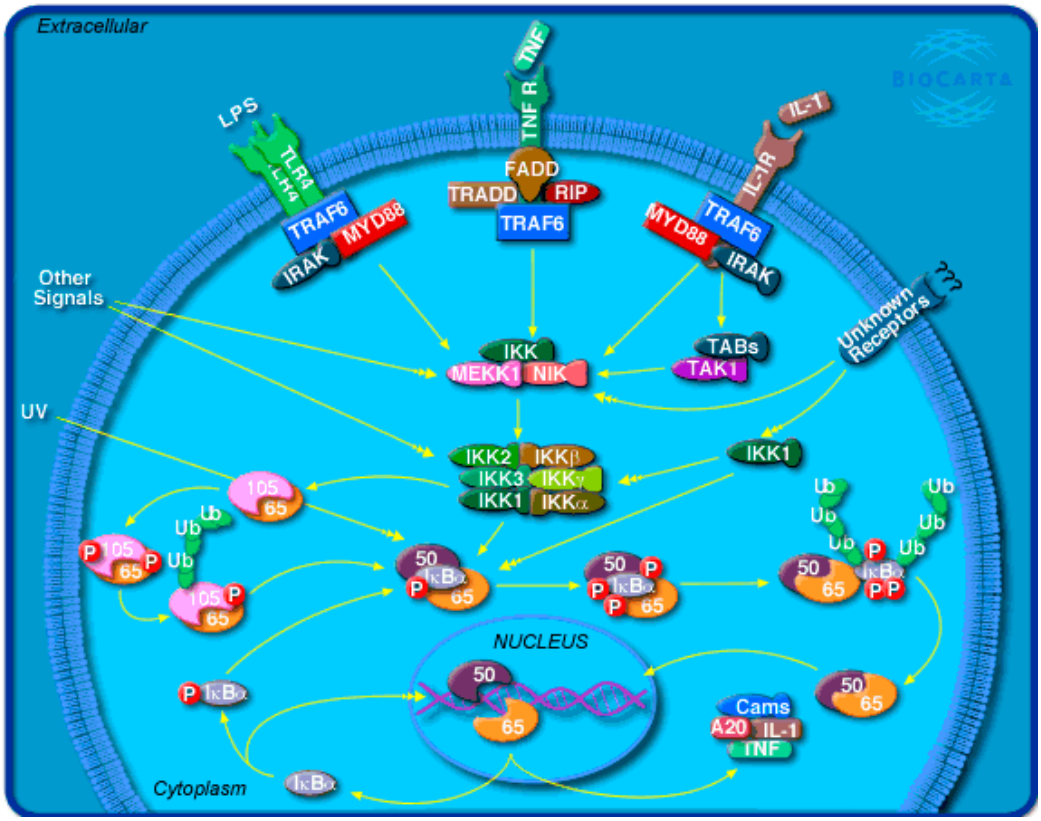


**Figure 2.** Activation de NF-κB par les TLR, le TNF-R1 et l'IL-1R (www.biocarta.com).

Cette réponse est normalement étroitement régulée pour éviter qu'elle ne persiste et puisse ainsi avoir des effets adverses sur l'organisme. Ainsi, l'IL-1β agit aussi comme stimulateur de l'axe hypothalamo-hypophysaire (HPA) en favorisant la production de la corticolibérine (CRF) par des neurones spécialisés. Cette libération est suivie par la sécrétion de l'hormone adrénocorticotropique (ACTH) qui permet la production de glucocorticoïdes par les glandes surrénales [78, 79]. Les glucocorticoïdes sont reconnus pour leurs puissants effets anti-inflammatoires résultant de l'inhibition de NF-κB [80-83]. Le processus de tumorogénèse est plutôt associé à une réponse inflammatoire persistante indiquant que ce mécanisme d'inhibition est probablement insuffisant. Par contre, l'administration de dexamethasone permet de recréer ces effets puisqu'il s'agit d'un glucocorticoïde synthétique.

L'infiltrat leucocytaire des tumeurs peut se composer de la plupart des types cellulaires normalement retrouvés lors d'une infection (neutrophiles, cellules dendritiques, macrophages, éosinophiles, mastocytes et lymphocytes). Généralement, une majorité de ces cellules sont des macrophages. Ceux-ci représentent d'ailleurs la principale source de cytokines et sont responsables d'effets très variés (figure 5). Ils peuvent participer directement à la destruction des cellules tumorales par des mécanismes dépendants ou indépendants d'un contact intercellulaire [57, 84]. Les mécanismes de cytotoxicité dépendant d'un contact permettent la lyse des cellules étrangères principalement par la production de peroxyde d'hydrogène ($H_2O_2$) [57, 85]. Les mécanismes indépendants d'un contact impliquent la production de facteurs variés tels que des cytokines, l'oxyde nitrique (NO) et les espèces réactives de l'oxygène (ROIs) [57, 84]. Parmi les cytokines produites, le TNF joue un rôle majeur dans la réponse immunitaire. Cette molécule présente une signalisation complexe qui peut mener à des résultats opposés. Le récepteur du TNF possède un domaine cytoplasmique nommé *death domain* (DD). Sous sa forme inactive, il se retrouve en association avec une protéine appelée *silencer of death domain* (SODD). Lors de la liaison du TNF, cette molécule est libérée pour permettre au DD d'interagir avec une protéine adaptatrice, *Fas-associated death domain* (FADD) qui permet le recrutement de *TNF-R associated death domain* (TRADD). Cette protéine participe à la formation du *death inducing signaling complex* (DISC) qui nécessite le recrutement de la *caspase-8* (casp-8) pour activer la cascade des caspases menant à l'apoptose. L'utilisation de doses supra-physiologiques de TNF a permis de démontrer son efficacité à tuer les cellules tumorales *in vitro* [86], incluant des cellules gliomales [87]. L'importance de ce mécanisme reste toutefois à être démontré *in vivo*. D'autre part TRADD peut, dans certaines circonstances, recruter *TNF-R associated factor* (TRAF) qui permet plutôt d'activer divers facteurs de transcriptions tel que NF-κB. Les cellules tumorales, exprimant des protéines anti-apoptotiques régulées par NF-κB, peuvent donc tirer profit de cette voie leur permettant d'améliorer leur survie.

Le TNF permet aussi l'activation de NF-κB dans d'autres types cellulaires. Ainsi, il représente un important facteur pro-inflammatoire. Il permet l'activation des cellules endothéliales au même titre que l'IL-1β en plus de contribuer à la production d'une multitude d'autres cytokines, notamment l'interferon-γ (IFN-γ). Cette dernière joue un rôle primordial dans l'immunité anti-tumorale. Elle possède un pouvoir anti-prolifératif sur les cellules tumorales en plus de pouvoir stimuler l'activité des macrophages et des cellules *natural killer* (NK) et NKT. Ces deux derniers types cellulaires représentent des sous-populations de lymphocytes ciblant les cellules tumorales de façon non spécifique pour les éliminer [88-90].

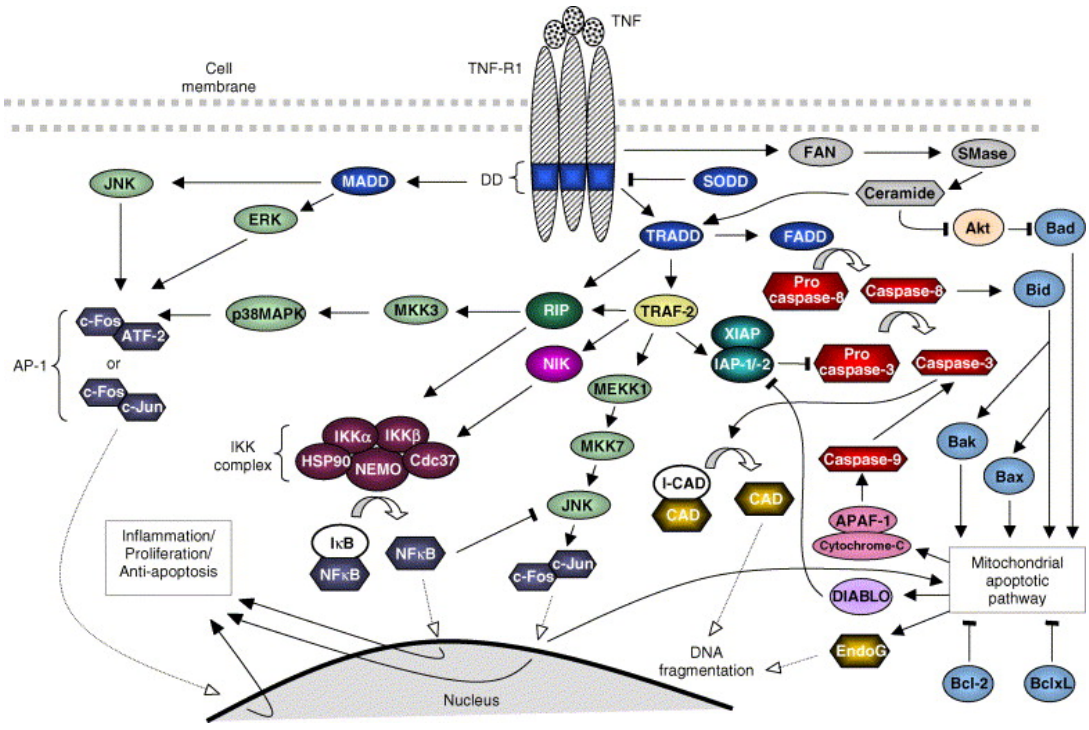


**Figure 3.** La signalisation par le TNF-R1 [86].

### 1.3.2.2 L'immunité acquise

Les lymphocytes T constituent une population de cellules qui se sont spécifiquement développées pour reconnaître des antigènes étrangers au corps humain et attaquer les cellules qui les présentent. Les cellules tumorales, bien qu'elles constituent à l'origine des cellules du soi, produisent des molécules qui peuvent être perçues comme des molécules du soi altéré et ainsi reconnues par les lymphocytes T. Ces antigènes tumoraux sont répertoriés en quatre catégories. On retrouve les antigènes uniques spécifiques de la tumeur; il s'agit de produits de la mutation de protéines endogènes. Elles représentent un avantage en immunothérapie étant donné leur grande spécificité. En deuxième lieu, on retrouve les antigènes viraux qui se retrouvent dans les tumeurs d'origine virale. Il y a les antigènes de différentiation spécifiques de tissus, qui correspondent à des molécules retrouvées normalement dans l'organisme mais dont l'expression est ectopique au site de la tumeur. La dernière catégorie regroupe les antigènes dont l'expression est augmentée dans la tumeur comparativement au tissu sain [91-95]. Au cours des dernières années, une véritable chasse à leur identification s'est amorcée en vue de pouvoir créer un « immunome » complet des tumeurs de l'être humain. Quelques milliers de candidats sont maintenant répertoriés et disponibles dans une base de données sur Internet (http://www2.licr.org/CancerImmunomeDB). Quelques candidats ont été découverts pour les gliomes, mais ils demeurent peu nombreux.

Pour être reconnus par les lymphocytes T, ces antigènes doivent être présentés à la surface de la cellule par l'entremise d'une molécule nommée complexe majeur d'histocompatibilité (CMH) [56, 96]. Il en existe deux classes (CMH I et II). Les molécules de CMH I sont reconnues spécifiquement par les lymphocytes T CD8+, alors que celles du CMH II le sont par les lymphocytes T CD4+ helper. La présentation des antigènes survient dans des organes spécialisés, les ganglions lymphatiques. Pour ce faire, les antigènes doivent pouvoir migrer dans ces structures. Il est possible que les cellules tumorales puissent y migrer directement ou encore que les antigènes y parviennent sous forme libre. Par contre, il est plus probable que les antigènes soient capturés par les cellules présentatrices d'antigènes (CPA) avant d'être acheminés aux ganglions.

Les CPA, particulièrement les cellules dendritiques (DC), patrouillent l'ensemble des tissus de l'organisme et échantillonnent constamment l'environnement par macropinocytose pour détecter la présence d'antigènes. La destruction de cellules tumorales par l'immunité innée constitue un pré-requis à cette étape en permettant aux antigènes tumoraux d'être libérés dans le milieu extra-cellulaire. Ceux-ci, une fois ingérés par les DC, sont apprêtés pour être présentés à la surface cellulaire sous forme d'un complexe avec le CMH I ou II. Lors d'un dommage, les DC reçoivent un signal provoquant leur maturation et leur migration dans les ganglions lymphatiques. Les lymphocytes T circulent constamment dans ces organes pour sonder les antigènes qui y sont présentés. La reconnaissance d'un antigène à la surface des CPAs par l'intermédiaire du récepteur des cellules T (TCR) provoque l'interaction de ces deux types cellulaires. Cette interaction est par la suite stabilisée par des molécules d'adhésion comme le couple LFA-1/ICAM-1 [56]. Les lymphocytes T peuvent ainsi être activés, ce qui provoque leur différentiation et une phase de division rapide, nommée expansion clonale. La reconnaissance du complexe peptide-CMH n'est toutefois pas suffisante pour enclencher ce processus. Des signaux de costimulations sont aussi nécessaires et permettent une régulation plus fine de cette étape critique. L'une des principales molécules impliquée est le CD28, exprimé sur les lymphocytes, qui interagit avec les membres de la famille B7 (exemple : CD80 et CD86) exprimés sur les DC. Ce signal permet l'augmentation de l'expression de l'IL-2, une cytokine qui active la prolifération des lymphocytes T, et l'expression de son récepteur sur ces mêmes cellules (figure 4).

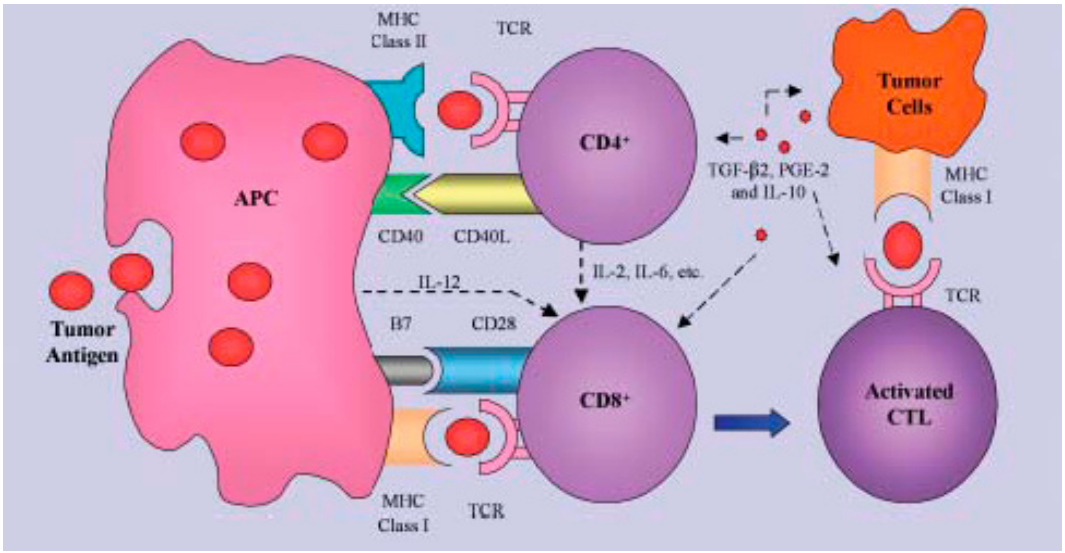


**Figure 4.** La présentation des antigènes tumoraux par les APCs [97].

L'activation des cellules CD4+ engendre la production d'IL-2, d'IFN-γ et de TNF nécessaire à l'activation des lymphocytes T CD8+; c'est pourquoi les cellules CD4+ sont nommées « helper ». Tous ces clones, spécifiques de l'antigène, retournent en circulation afin de gagner le lit de la tumeur où ils pourront exercer leur activité cytotoxique spécifiquement sur les cellules tumorales qui expriment parfois le CMH I. Le mécanisme implique la participation de molécules nommées perforines et granzymes produites par les lymphocytes T CD8+. La perforine forme des pores dans la membrane des cellules tumorales, ce qui permet l'entrée des granzymes qui activent l'apoptose par l'intermédiaire de la cascade des caspases. Alternativement, l'induction de l'apoptose peut dépendre de molécules appelées récepteurs de mort comme Fas. Le liaison du ligand Fas (FasL), exprimé à la surface des lymphocytes, à son récepteur Fas, exprimé sur les cellules tumorales, engendre le recrutement d'un DD qui active la caspase 8.

### 1.3.3 Les effets pro-tumoraux

À première vue, le système immunitaire constitue une arme redoutable contre le développement des tumeurs. En fait, les cellules tumorales semblent capables de contourner et même d'exploiter la réponse immune à leur avantage. La théorie de l'immunosurveillance originalement proposée ne serait donc pas tout à fait véridique. Plus récemment, des chercheurs ont proposé de la modifier pour créer la théorie « d'immunoediting ». Cette dernière propose que, lorsque les mécanismes de défenses sont inefficaces pour contrer le développement de la tumeur, une pression de sélection s'exerce sur les cellules tumorales et donne un avantage aux clones résistants aux mécanismes immunitaires [98, 99]. L'instabilité génétique des cellules tumorales favorise l'apparition de tels clones. Des études de transplantation supportent cette hypothèse en démontrant que des cellules d'une tumeur qui se sont développées dans un organisme dépourvu de réponse immune sont beaucoup plus immunogéniques lorsque transplantées dans un organisme normal [98, 100, 101]. L'hypothèse que l'évasion des défenses de l'organisme soit simplement le résultat de mécanismes inhérents au développement de la tumeur, et donc indépendant d'une pression externe, n'est toutefois pas à écarter.

Les mécanismes d'évasions sont nombreux et peuvent être directs, impliquant la modification des cellules tumorales elles-mêmes, ou encore indirects, résultant de l'altération du comportement d'autres cellules par l'environnement tumoral [98]. Les cellules tumorales peuvent notamment modifier l'expression de plusieurs molécules nécessaires à leur reconnaissance par les cellules du système immunitaire ainsi qu'à la signalisation qui leur est associée. La perte de l'expression de certaines composantes du CMH I est une de ces caractéristiques qui a été observée, empêchant la reconnaissance par les lymphocytes T [102]. De même, la production d'une forme soluble du ligand des cellules NK permet de limiter l'efficacité de ce mécanisme d'attaque [103]. Les cellules néoplasiques peuvent aussi surexprimer plusieurs facteurs anti-apoptotiques [104]. Finalement, de nombreux défauts peuvent être observés dans les voies de signalisations couplées aux récepteurs de mort comme Fas. L'activité apoptotique de FasL peut être véhiculée en sens inverse (des cellules tumorales aux cellules immunitaires) puisque dans

certains cas les cellules immunitaires et les cellules tumorales peuvent exprimer autant le récepteur que le ligand Fas [105-107].

Indirectement, les cellules tumorales peuvent exercer une influence sur les macrophages et les lymphocytes T via la production d'une panoplie de cytokines anti-inflammatoires. C'est le cas particulièrement du TGF-β2 qui a un pouvoir inhibiteur sur les lymphocytes T et les macrophages. Cette cytokine avait d'ailleurs été identifiée à l'origine comme le « glioblastoma cell-derived T-cell suppressor factor »[108, 109]. Elle agit notamment en diminuant la production d'IL-2 et de perforine et l'expression du CMH II [110-113]. En plus, le facteur pro-inflammatoire prostaglandine $E_2$ ($PGE_2$), dont l'expression est augmentée dans les cellules tumorales, agit sur les lymphocytes et les macrophages pour favoriser l'expression de l'IL-10 [114]. Cette molécule inhibe la différentiation des DC, la présentation antigénique et la production d'IL-12 et d'ICAM-1 [115-117]. Il se crée donc un environnement d'immunosuppression dans la tumeur.

Les macrophages sont connus pour produire une quantité exceptionnelle de molécules aux fonctions très diverses (Fig. 5). L'environnement tumoral influence de façon importante le comportement des macrophages et peut favoriser leur participation à la croissance tumorale de plusieurs façons [76, 118, 119]. Parmi les cytokines produites, on retrouve, entre autres, plusieurs facteurs pro-angiogéniques tels que le VEGF [120, 121]. Son expression peut même être augmentée par un mécanisme dépendant de l'IL-1. Celle-ci augmente l'activité de l'enzyme cyclooxygénase 2 (COX2) qui produit du HIF-1 qui, comme nous l'avons vu, favorise la transcription du VEGF [23, 122]. Également, de nombreuses enzymes de dégradation de la matrice extracellulaire contribuant à la migration des cellules tumorales peuvent être produites, comme la MMP-2 et 9 [118]. Les macrophages peuvent aussi contribuer à la prolifération des cellules tumorales en produisant de grandes quantités de facteurs de croissance comme l'epidermal growth factor (EGF), son récepteur l'EGFR se retrouve exprimé autant sur les cellules gliomales que les macrophages eux-mêmes [121, 123, 124]. De surcroît, les macrophages sécrètent d'importantes quantités de TNF, lequel a des effets ambigus sur les tumeurs. D'un point de vue pro-tumoral, il a été démontré que cette cytokine pouvait influencer les principales conditions nécessaires à la croissance tumorale : la prolifération, la migration et

l'angiogénèse. Elle permet donc, notamment, d'augmenter la production du VEGF, de l'EGFR et de la MMP-9 [125-127]. D'autre part, même les mécanismes cytotoxiques des macrophages peuvent s'avérer utiles au développement tumoral. En effet, bien que le NO et les ROIs puissent tuer des cellules, leur action sur l'ADN peut provoquer l'apparition de nouvelles mutations pouvant mener à la transformation cellulaire. Les macrophages auraient donc le potentiel de constituer un facteur initiateur de tumeurs lors d'une réponse inflammatoire persistante [76, 128]. Finalement, ces cellules ne sont pas les seules à pouvoir exercer une action bénéfique au développement tumoral. Une sous-population particulière de lymphocytes T, les cellules T régulatrices (Treg), principalement connues pour jouer un rôle protecteur en matière d'autoimmunité, pourraient aussi agir en supprimant l'action des lymphocytes T anti-tumoraux [129, 130].

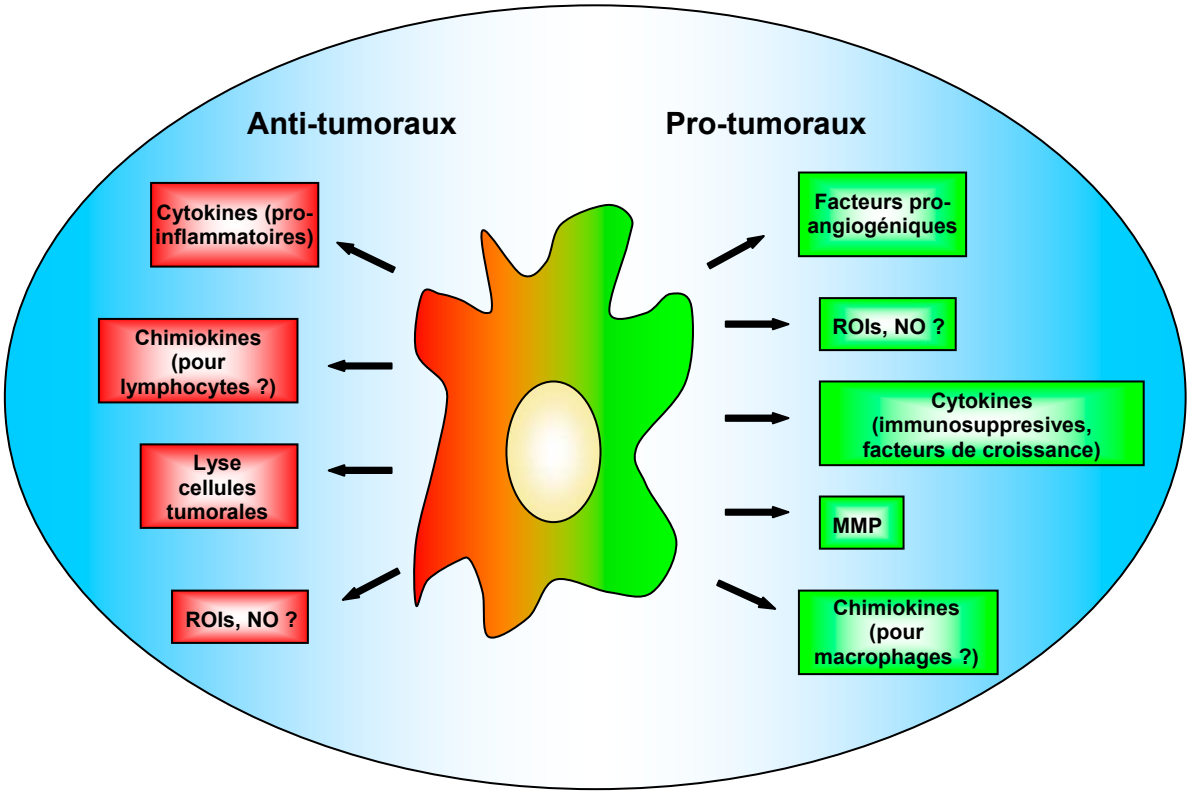


**Figure 5.** Effets possibles anti- et pro-tumoraux des macrophages.

### 1.3.4 Réponse immunitaire dans le SNC et particularités des glioblastomes

À l'origine, des expériences de greffes tissulaires dans le SNC avaient révélé que l'hôte ne rejetait le tissu étranger qu'à très long terme. Cette constatation a mené au développement de la notion de privilège immunitaire, qui voulait que le SNC soit isolé du système immunitaire périphérique. La présence de la barrière hématoencéphalique, l'expression faible des molécules de CMH, l'absence de drainage lymphatique et de DC dans le SNC contribuaient à soutenir cette hypothèse [131]. Aujourd'hui, on sait par contre que ce concept est plus relatif qu'absolu. Lors de différents dommages, une réponse immunitaire s'organise tout de même. Elle débute par les organes circumventriculaires (CVO), le plexus choroïdien et les leptomeninges puisque que ces régions sont dépourvues de BHE [132-134]. Par la suite, le processus peut s'étendre à l'ensemble du SNC. Bien que des jonctions serrées unissent fermement les cellules endothéliales du SNC et forment une barrière imperméable à plusieurs molécules plasmatiques ainsi qu'à plusieurs cellules; les leucocytes peuvent tout de même accéder au cerveau lors d'une réponse immunitaire qui permet l'activation des cellules endothéliales pour produire des molécules d'adhésion [134].

Les acteurs principaux de l'immunité dans le SNC sont les cellules microgliales. Ces dernières représentent les macrophages résidents de ce tissu dont elles constituent environ 8 % de toutes les cellules [135]. Elles sont généralement dans un état de repos et ont alors une morphologie très ramifiée. Elles surveillent ainsi l'environnement et s'activent rapidement lorsqu'elles détectent une altération du tissu. Elles gagnent alors l'apparence de macrophages conventionnels. Les microglies produisent alors une panoplie de molécules tout comme les macrophages [136]. Il est probable que ces cellules jouent le rôle de CPA puisque le SNC est dépourvu de cellules dendritiques, bien qu'elles soient moins efficaces que ces dernières [137]. L'expression des molécules du CMH dans le cerveau, contrairement à la périphérie, n'est pas constitutive. Leur expression peut toutefois être induite à la surface des microglies tout comme celle des molécules de costimulations de la famille B7 [138]. L'absence de drainage lymphatique apparaît toutefois encore comme un obstacle au développement d'une réponse immune complète. Certaines

expériences ont par contre pu démontrer que des antigènes du SNC pouvaient atteindre les ganglions cervicaux probablement par l'intermédiaire d'un système de transport alternatif faisant intervenir le liquide céphalo-rachidien (LCR) [139, 140].

La réponse immunitaire s'établissant dans le SNC est donc distincte de celle en périphérie. En plus, les glioblastomes présentent des caractéristiques particulières comparativement au SNC en général. La BHE y est altérée par la production importante de TNF et les vaisseaux sanguins, modifiés par le processus angiogénique, n'incorporent pas ces caractéristiques. Les cellules microgliales ne représentent probablement qu'une faible proportion des leucocytes dans la tumeur, la majorité étant des macrophages provenant de la périphérie [87]. Ces derniers semblent peu efficaces à présenter les antigènes dans les conditions immunosuppressives des glioblastomes et personne n'a encore réussi à démontrer que ces cellules parvenaient réellement à migrer dans les ganglions lymphatiques. Les glioblastomes constituent donc un environnement tumoral unique encore mal compris. Malgré qu'il soit de plus en plus évident que les macrophages contribuent au développement tumoral dans certains cancers périphériques comme le cancer du sein [141, 142], les résultats des études dans les gliomes demeurent controversés. Certaines rapportent que les densités les plus importantes de macrophages se retrouvent dans les tumeurs les plus malignes, indiquant une corrélation avec un pronostic pessimiste [143]. À l'inverse, une autre étude suggère qu'aucune corrélation n'existe [144]. Le rôle bénéfique des lymphocytes T CD8+ pour freiner le développement tumoral semble quant-à-lui bien établi. Une équipe a démontré que l'infiltration de la tumeur par ces cellules engendrait une plus longue survie des patients [145]. De même, des travaux plus récents proposent que la production plus importante de cellules T dans le thymus chez les individus plus jeunes atteints d'un gliome constitue un facteur positif pour le pronostic de ce cancer [146].

## 1.4 Résultats préalables

Dans le but d'établir plus précisément si la réponse inflammatoire contribue ou non au développement des glioblastomes, notre laboratoire a étudié leur développement chez des souris déficientes en TNF (TNF k.o.). Les résultats ont démontré que les tumeurs de ces souris présentent une diminution de la densité de macrophages intra-tumoraux qui corrèle inversement avec le volume de la tumeur [87]. Il apparaît donc que les macrophages peuvent contribuer à leur propre recrutement par la production de TNF et qu'ils permettent d'entraver le développement de la tumeur. Ce mécanisme de défense n'est toutefois pas entièrement efficace puisque la masse tumorale continue à se développer.

## 1.5 L'ablation sélective de cellules par la HSV-1 TK

L'ablation sélective d'une population cellulaire constitue une méthode efficace et directe pour étudier sa fonction dans un organisme. L'expression d'un gène capable de convertir un pro-médicament en un agent cytotoxique spécifiquement dans les cellules cibles est une façon élégante d'y parvenir. Un modèle pour l'ablation sélective des cellules de la lignée myéloïde a ainsi été élaboré [147]. Le gène utilisé, la thymidine kinase du virus de l'Herpes simplex type 1 (HSV-1 TK), peut phosphoryler une grande variété d'analogues de nucléotides. Son équivalent humain n'est par contre spécifique que de la thymidine. Le Gancyclovir est un de ces analogues couramment utilisé. Après avoir été phosphorylé par la HSV-1 TK le GCV-monophosphate est phosphorylé à nouveau par d'autres enzymes cellulaires pour devenir du GCV-triphosphate, lequel est un analogue toxique de la thymidine. Cette molécule est donc intégrée dans l'ADN nouvellement synthétisée et bloque sa réplication conduisant à la mort de la cellule [148, 149]. Dans le présent modèle le mutant-30 a été utilisé. Il a été démontré que cette forme de l'enzyme lie plus efficacement le GCV que la thymidine comparativement à la forme sauvage [150]. Les doses de GCV utilisées peuvent donc être réduites, ce qui permet de limiter ses effets toxiques.

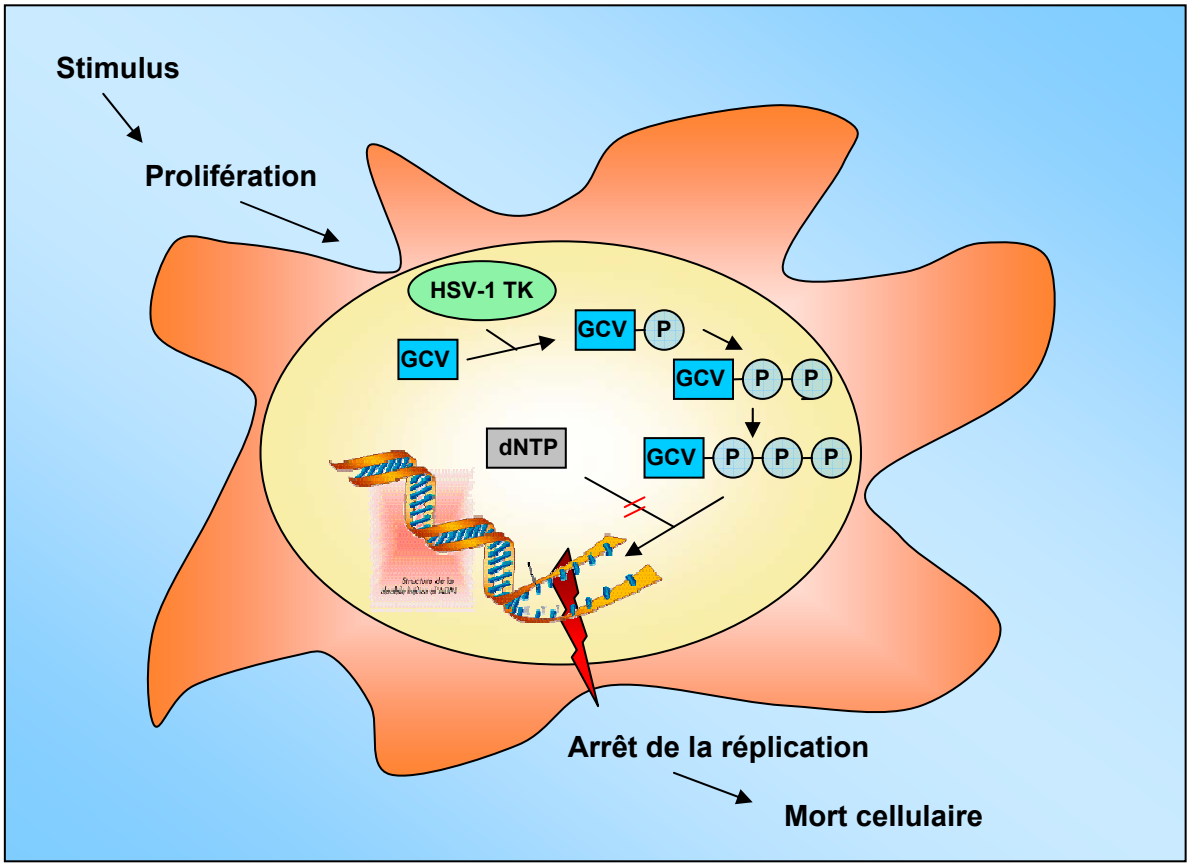


**Figure 6.** Mécanisme d'action du Gancyclovir.

La spécificité de l'expression du gène est obtenue en le couplant au promoteur CD11b. La molécule CD11b constitue une sous-unité du récepteur d'intégrine CD11/CD18. Son expression est principalement spécifique à la lignée myéloïde. Elle est faiblement détectable chez les précurseurs mais elle augmente suivant leur différenciation pour atteindre un niveau maximal chez les cellules matures (neutrophiles, monocytes, macrophages et microglies). Son expression est aussi détectable sur les cellules NK [151]. Il a déjà été démontré que la séquence promotrice de ce gène permettait l'expression de transgènes dans les cellules myéloïdes matures de souris de façon stable [152]. L'efficacité du modèle CD11b-TK a été établie dans diverses conditions [147].

## 1.6 Objectifs du projet

Afin d'élucider avec plus de précision le rôle des macrophages dans la croissance tumorale et tâcher de comprendre leur mécanisme d'action, nous avons étudié le développement des gliomes dans le modèle de souris exprimant la HSV-1 TK sous le contrôle du promoteur CD11b (souris TK). Plus spécifiquement, l'efficacité du modèle à tuer les macrophages tumoraux a été vérifiée par le compte des cellules marquées par immunohistochimie. Par la suite, le volume des tumeurs a été mesuré pour vérifier si l'ablation des macrophages avait bel et bien influencée la croissance des gliomes. Finalement, nous avons examiné l'hypothèse que l'effet des macrophages puisse être médié indirectement via le recrutement des lymphocytes T.

Dans un deuxième volet de l'étude, nous nous sommes questionnés sur l'impact de l'utilisation de la dexamethasone dans la thérapie des glioblastomes. En effet, puisque nos résultats démontrent l'utilité de la réponse immune pour combattre le développement des glioblastomes, nous avons émis l'hypothèse que l'action anti-inflammatoire de ce glucocorticoïde pourrait se révéler nuisible au traitement de ces tumeurs. Les résultats, au contraire, ont démontré que l'administration de cet agent permettait de réduire la croissance tumorale malgré une diminution de la population de lymphocytes T intra-tumorale. Différentes approches *in vitro* et *in vivo* ont été utilisées dans le but d'identifier les mécanismes d'action de la dexamethasone susceptibles d'influencer spécifiquement le développement tumoral.

# Chapitre 2 : Augmentation de la croissance des gliomes chez des souris déplétées en macrophages

# “Increased glioma growth in mice depleted in macrophages”

**Hugo Galarneau*, Jérôme Villeneuve*, Geneviève Gowing, Jean-Pierre Julien et Luc Vallières**

** Ces deux auteurs ont contribués également au travail.*

Département d’Endocrinologie moléculaire et oncologie, Centre de Recherche du Centre Hospitalier de l’Université Laval, Québec, Québec, Canada

## 2.1 Résumé

Les macrophages peuvent promouvoir la croissance de certaines tumeurs, notamment au sein et au foie. Toutefois, cet effet n'a pas été prouvé pour l'ensemble des tumeurs, incluant celles du système nerveux central. Au contraire, nous avons démontré que les macrophages peuvent ralentir la progression des gliomes malins par un processus dépendant du TNF. La présente étude apporte des évidences suggérant que cet effet anti-tumoral soit médié par les lymphocytes T. En effet, leur nombre est réduit de façon importante chez les souris déficientes en TNF et corrèle inversement avec le volume des gliomes. Cependant, cette corrélation a seulement été observée chez des receveurs allogéniques, remettant en question le rôle des macrophages dans un contexte non-immunogénique. En utilisant des souris syngéniques, exprimant la thymidine kinase du virus de l'Herpes simplex sous le contrôle du promoteur CD11b, nous avons démontré que les macrophages peuvent exercer un effet anti-tumoral indépendamment de l'aide des lymphocytes T. La déplétion des macrophages, obtenue par l'administration de ganciclovir, a résulté en une augmentation de 33% du volume de la tumeur. L'effet anti-tumoral des macrophages n'était probablement pas relié à une activité tumoricide. En effet, des cellules gliomales transduitent ex vivo, avant transplantation, avec un vecteur lentiviral exprimant la GFP, ont rarement été observées dans un état apoptotique ou phagocyté. En somme, ces résultats suggèrent que les macrophages peuvent atténuer la croissance des gliomes par eux-mêmes (e.g. en protégeant le tissu adjacent) et indirectement, quand la tumeur est immunogénique, en contribuant à la mise en place de l'immunité antitumorale adaptative. Cette étude pave la voie au développement de protocoles d'immunothérapie du cancer par l'emploi des macrophages et soulève un questionnement quant à l'utilisation d'agents anti-inflammatoires chez les patients atteints de tumeurs cérébrales.

## 2.2 Abstract

Macrophages can promote the growth of some tumors, such as those of the breast and lung, but it is unknown whether this is true for all tumors, including those of the central nervous system. On the contrary, we have shown that macrophages can slow the progression of malignant gliomas through a TNF-dependent mechanism. Here we provide evidence that this antitumor effect was mediated by T lymphocytes, as their number was drastically reduced in TNF-deficient mice and inversely correlated with glioma volume. However, this correlation was only observed in allogeneic recipients, questioning the role of macrophages in a non-immunogenic context. Using syngeneic mice expressing the herpes simplex virus thymidine kinase under the control of the CD11b promoter, we show that macrophages can exert an antitumor effect without the help of T lymphocytes. Macrophage depletion achieved by ganciclovir treatment resulted in a 33% increase in glioma volume. The antitumor effect of macrophages was not likely due to a tumoricidal activity, because phagocytosis or apoptosis of glioma cells, transduced *ex vivo* prior to transplantation with a lentiviral vector expressing GFP, was rarely observed. Altogether, these results suggest that macrophages can attenuate glioma growth by themselves (e.g., by protecting the surrounding tissue) and indirectly, when the tumor is immunogenic, by contributing to the development of adaptive antitumor immunity. This study provides a rationale for the design of macrophage-based cancer immunotherapy protocols, and raises concerns regarding the use of anti-inflammatory drugs in patients with brain tumors.

## 2.3 Introduction

Tumors affecting the central nervous system are a leading cause of cancer-related death in children and young adults[1]. The most frequent types are gliomas, wich derive from glial cells that have acquired the ability to continuously proliferate and diffusely invade the parenchyma. In response to this aggression, immune cells, mainly macrophages, infiltrate the neoplastic tissue [121, 153]. In the mouse glioma model used in the present study, for example, we have shown that macrophages account for ~8% of the cells of the tumor mass [87], which is comparable to the proportion of microglia in the normal brain. In contrast to microglia, glioma-associated macrophages originate from newly recruited monocytes, and exhibit a round, amoeboid or elongated shape with relatively short cytoplasmic processes, rather than a highly ramified morphology [87].

The role of macrophages in glioma biology is unclear, as it has not been directly tested, but rather inferred from observations made *in vitro* or in other tumor types [121]. The traditional belief is that macrophages can potentially detect glioma cells expressing abnormal surface antigens (e.g., via the NKG2D receptor) and kill them by releasing lysosomal enzymes and reactive oxygen intermediates [154]. Macrophages also have the potential to degrade such antigens into peptides that bind to major histocompatibility complex class I (MHC-I) molecules for cross-presentation to cytotoxic T lymphocytes [155]. When activated, the latter can theoretically recognize and kill cells that display the same peptides by releasing the content of their cytotoxic granules. However, the reality is that most glioma cells escape these defense mechanisms, probably due to the lack of abnormal immunogenic antigen, down-regulation of MHC-I, induction of immunologic tolerance and/or secretion of immunosuppressive molecules [156]. In recent years, an alternative hypothesis has been proposed in which macrophages contribute to glioma progression by secreting growth factors, angiogenic molecules, extracellular matrix-degrading enzymes and immunosuppressors [121, 153]. Although this possibility is supported by several observations in the case of some cancers, such as those of the breast and lung [72, 76, 118, 119, 157], it has not been directly tested in gliomas. Therefore, the

question of whether macrophages promote or counteract glioma progression remains unanswered and needs to be addressed in orthotopic models.

In support of a beneficial role for glioma-associated macrophages, we have recently shown that these cells stimulate their own recruitment and reduce glioma growth by expressing TNF [87], but the mechanism responsible for this effect is unknown. In the initial part of the present study, we found evidence that the antitumor effect of TNF can be mediated by T lymphocytes, as their number was drastically reduced in TNF-deficient mice and inversely correlated with glioma volume. However, this correlation was only seen when glioma cells originating from a B6 mouse were transplanted in recipients with a mixed genetic background (B6 × 129S), questioning the role of macrophages in a context where the tumor is weakly or not immunogenic. In the following parts, we confirm that glioma-associated macrophages, in a syngeneic context, exert a beneficial effect without the help of T lymphocytes, as determined using a new model of transgenic mice allowing for temporal depletion of macrophages.

## 2.4 Methods

### 2.4.1 Animals

TNF-deficient and wild-type mice on a B6 × 129S background were generated from breeders originally obtained from the Jackson Laboratory (Bar Harbor, Maine). Their genotypes were confirmed by PCR using DNA extracted from tail biopsies following the protocol provided by the supplier. Heterozygous CD11b-TK$^{mt-30}$ mice and wild-type littermates (B6 background) were generated as previously described [147]. B6 mice were purchased from Charles River (Montréal, QC, Canada) and adapted to standard laboratory conditions for 1 week before any manipulation. All experiments were performed on males aged 2-3 months according to procedures approved by our institution's Animal Welfare Committee.

### 2.4.2 Culture of glioma cells

The glioma cell line GL261, originally derived from a B6 mouse implanted intracerebrally with methylcholanthrene [158], was provided by Dr. Protul Shrikant (Roswell Park Cancer Institute, Buffalo, New York). Cells were cultured in Dulbecco's modified Eagle's medium (Wisent, Saint-Bruno, QC, Canada) supplemented with 10% heat-inactivated fetal bovine serum, 2 mM L-glutamine, 110 mg/L sodium pyruvate, 100 U/ml penicillin and 100 µg/ml streptomycin. Prior to implantation, cells were harvested by brief incubation at room temperature in 0.25% trypsin (Invitrogen, Carlsbad, CA), then washed and resuspended in Dulbecco's phosphate-buffered saline (DPBS, Invitrogen) containing 1 g/L D-glucose.

### 2.4.3 Viral transduction of glioma cells

GL261 cells were incubated for 24 h with vesicular stomatitis virus glycoprotein-pseudotyped lentivirus carrying the green fluorescent protein (GFP) gene at a multiplicity of infection of 10. The viral suspension was provided by Dr. Gary Kobinger (National Microbiology Laboratory, Winnipeg, Manitoba, Canada) and produced as previously described [159]. Four days later, GFP$^+$ cells were sorted using an Epic Elite ESP flow

cytometer (Beckman Coulter, Fullerton, CA), and then expanded *in vitro* before implantation.

### 2.4.4 Intracerebral implantation of glioma cells

Mice were anesthetized, shaved and immobilized in a stereotaxic frame. A midline incision was made on the scalp, followed by a circular craniotomy over the right hemisphere, 1.7 mm lateral and 1 mm rostral from bregma. After removal of the dura mater, a 5-µl Hamilton syringe fitted with a 27-gauge beveled needle was advanced into the caudoputamen at a depth of 3.5 mm from the skull surface. Using a UMPII micropump (World Precision Instruments, Saratoga, Florida), 2 µl of Dulbecco's phosphate-buffered saline (DPBS; Invitrogen, Carlsbad, California) containing $5 \times 10^4$ viable GL261 cells were injected over 2 min. After injection, the syringe was left in place for 2 min before being withdrawn very slowly.

### 2.4.5 Ganciclovir treatment

Starting 7 days after tumor implantation, mice were injected intraperitoneally twice daily for 6 days with 50 mg/kg ganciclovir (GCV; Hoffmann-La Roche, Mississauga, Ontario, Canada) diluted in saline. Control mice were treated identically, except that GCV was substituted by saline.

### 2.4.6 Bromodeoxyuridine labeling

Bromodeoxyuridine (BrdU, Sigma) was dissolved in saline at a concentration of 10 µg/µl. Mice were injected four times with BrdU (100 µg/g) at 3 h intervals, and perfused 2 h after the final injection.

### 2.4.7 Histological preparation

For all histological analyses except *in situ* hybridization, mice were transcardially perfused with 10 ml of saline, followed by ice-cold 4% paraformaldehyde in phosphate buffer, pH 7.4, over 10 min. The brains were removed, postfixed for 4 h at 4 °C, then cryoprotected overnight in 50 mM potassium phosphate-buffered saline (KPBS) supplemented with 20% sucrose. Series of sections through the tumors were cut at 40 µm

using a freezing microtome, collected in cryoprotectant (30% ethylene glycol, 20% glycerol, 50 mM sodium phosphate buffer, pH 7.4) and stored at –20 °C until analysis. For *in situ* hybridization, the following modifications were applied: 1) the fixative was dissolved in borate buffer, pH 9.5, instead of phosphate buffer; 2) the brains were postfixed for 48 h before being cryoprotected overnight in the same fixative supplemented with 20% sucrose; and 3) the tumors were cut at 30 μm.

### 2.4.8 Immunostaining

Immunohistochemistry and immunofluorescence were performed as previously described [160] using the following primary antibodies: rat anti-BrdU (1:1000; Accurate Chemicals, Westbury, New York), rat anti-CD11b (1:1000; BD Biosciences, San Diego, California), rat anti-CD3ε (1:500; Serotec, Raleigh, North Carolina), rat anti-CD45 (1:1000; BD Biosciences), rat anti-F4/80 (1:500; Serotec) and rabbit anti-Iba1 (1:2000; Wako Chemicals, Richmond, Virginia). Fluorescent sections were counterstained for 1 min with 2 μg/ml diamidinophenylindole (DAPI, Invitrogen). Before CD3e immunostaining, sections fixed with paraformaldehyde at pH 9.5 were subjected to an antigen retrieval procedure that consisted of heating the sections in 10 mM sodium citrate buffer, pH 6.0, for 25 min using a microwave oven at 40% power.

### 2.4.9 In situ hybridization

TNF mRNA was detected by radioisotopic *in situ* hybridization according to a previously described protocol [161]. Briefly, sections were mounted onto Superfrost slides (Fisher Scientific, Pittsburgh, PA), postfixed with 4% paraformaldehyde in borate buffer, pH 9.5, for 20 min, digested with 10 μg/ml proteinase K at 37°C for 25 min, acetylated with 0.25% acetic anhydride for 10 min and dehydrated. Antisense and sense cRNA probes were transcribed from a linearized 1.3 kb mouse cDNA in the presence of [$^{35}$S]-UTP and [$^{35}$S]-CTP (Perkin-Elmer, Foster City, CA), purified by phenol-chloroform extraction and ammonium acetate-ethanol precipitation, then applied to the slides at a concentration of $2 \times 10^7$ cpm/ml in hybridization buffer (50% formamide, 0.3 M NaCl, 10 mM Tris, pH 8.0, 1 mM EDTA, 1× Denhardt's solution, 10% dextran sulfate, 2 μg/ml tRNA and 10 mM

dithiothreitol). After incubation at 60 °C for 14 h, the slides were treated with 20 µg/ml ribonuclease A for 30 min at 37 °C, washed in a solution containing 15 mM NaCl and 1.5 mM sodium citrate for 30 min at 65 °C, dehydrated and exposed to Biomax film (Kodak, Rochester, NY) for 22 h. After film autoradiography, slides were defatted in xylene, dipped into Kodak NTB2 emulsion, exposed at 4 °C for 21 days, developed in Kodak D19 developer for 3.5 min at 14-16 °C, fixed in Kodak rapid fixer for 5 min, counterstained with 0.25% thionin, dehydrated and coverslipped with a mixture of distyrene, tricresyl phosphate and xylene (DPX; Electron Microscopy Sciences, Fort Washington, Pennsylvania).

### 2.4.10 Stereological analyses

Systematically sampled sections (every $10^{th}$ section through the tumors) were analyzed in a blind fashion using a Stereo Investigator system (Microbrightfield, Colchester, Vermont) combined with a Nikon E800 microscope.

Tumor volume was estimated from thionin-stained sections by the Cavalieri method. Using a 2× Plan Apochromat objective (numerical aperture 0.1), a point grid of 200 × 200 µm was overlaid on each section and the points that fell within the tumor were counted. Point counts were converted to volume estimates taking into account sampling frequency, magnification, grid size and section thickness.

Immunostained cells were counted by the optical fractionator method. Tumor tissue was traced using a 2× objective and sampled using a 60× Plan Apochromat oil objective (numerical aperture 1.4). The counting parameters were as follows: distance between counting frames, 400 × 400 µm ($Iba1^+$ cells) or 450 × 450 µm ($CD3\varepsilon^+$ cells); counting frame size, 50 × 50 µm ($Iba1^+$ cells) or 100 × 100 µm ($CD3\varepsilon^+$ cells); disector height, 10 µm; guard zone thickness, ≥2 µm. Cells were counted only if their nuclei laid within the disector area, did not intersect forbidden lines and came into the focus as the optical plane moved through the height of the disector.

*In situ* hybridization signals were counted by the fractionator method. Tumor tissue was traced using a 2× objective and sampled using a 40× Plan Apochromat objective (numerical aperture 0.95). The counting parameters were as follows: distance between

counting frames, 450 × 450 µm; counting frame size, 100 × 100 µm. Clusters of emulsion grains were counted only if they laid within the disector area and did not intersect forbidden lines.

The relative area occupied by microcysts was measured by photographing thionin-stained sections using a 2× Plan Apochromat objective and a Retiga EX monochrome camera (QImaging, Burnaby, British Columbia, Canada). The photographs (8-bit, grayscale) were converted to Bitmap images with Photoshop 7 (Adobe Systems, San Jose, California) using a threshold level of 160. The contour of each tumor profile was traced with the freehand selection tool of ImageJ software (National Institutes of Health, Bethesda, Maryland), and the mean gray value of that area was recorded (black = 0, white = 255). The data were averaged and converted to percentages.

### 2.4.11 Confocal microscopy

Confocal images were acquired with a Fluoview confocal microscope (BX-61; Olympus Optical, Tokyo, Japan) and a 60× Uplan Apo oil objective (numerical aperture 1.35) by sequential scanning using a z-separation of 0.25 µm. For each fluorochrome, the upper and lower thresholds were set using the range indicator to minimize data loss. The proportions of cells displaying a given phenotype were evaluated by scoring the colocalization of cell markers using confocal images (5 per mouse) randomly sampled through the neoplastic tissue. A minimum of 110 cells was examined per staining and animal.

### 2.4.12 Bright-field imaging

Photomicrographs were taken using a Retiga EX monochrome camera mounted on a Nikon E800 microscope. The images were adjusted for contrast, brightness and sharpness using Photoshop 7.

### 2.4.13 Splenocyte culture

Spleens harvested from four CD11b-TK$^{mt\text{-}30}$ mice were minced with razor blades in DPBS, passed four times through a 20-G needle, and filtered through 40-µm nylon mesh.

Cells were separated by centrifugation on a cushion of lymphocyte separation medium (Wisent, St-Bruno, Québec, Canada) at 2500 rpm for 20 min. Immediately after isolation, cells were activated for 24 h in RPMI 1640 medium supplemented with 10% fetal bovine serum and 1 µg/ml phytohemagglutinin A (Sigma), and then cultured for 48 h in the presence of 50 U/ml interleukin-2 (Sigma). Activated cells were incubated for 4 days in a 96-well plate (200 000 cells/well) in the same medium containing 10 µM GCV or vehicle. Interleukin-2 (25 U/ml) was added to the cultures after 48 h. Cells were collected by centrifugation, blocked for 5 min with 5 µg/ml anti-CD16/CD32 antibody (BD Biosciences), stained for 30 min on ice with Alexa 488-conjugated anti-CD3ε antibody (BD Biosciences), and counted with an Epic XL flow cytometer (Coulter, Miami, Florida) by excluding dead cells by propidium iodide staining.

### 2.4.14 Primary culture of microglia

Microglia were isolated from brains of 2 or 3-day old CD11b-TK$^{mt-30}$ or wild-type mice. The brains were minced with razor blades in DPBS and passed four times through a 20-G needle. After centrifugation (1,500 rpm), the pellets were resuspended and incubated at 37 °C for 15 min in DPBS containing 0.25% trypsine and 0.05% DNase I. Cells were plated in T-75 flasks (3 brains/flask) and grown in Dulbecco's modified Eagle's medium (Wisent) supplemented with 10% heat-inactivated fetal bovine serum, with medium changed every 2 days. After 1 week, microglia growing on the top of the confluent cell monolayer were separated by shaking the flasks on a rotary shaker (200 rpm) at 37 °C for 4 h. Floating cells were collected and plated in T-25 flasks. After 10 min, the flasks were gently hand-shaken for 30 sec, and the medium was changed to remove contaminating non-adherent cells. Microglia were grown for 2 days and transferred onto four-chamber polystyrene vessel tissue culture-treated glass slides (BD Pharmingen) at a density of 100,000 cells/chamber in medium containing 10 µM GCV or vehicle. After 4 days, the cells were fixed in phosphate buffered-paraformaldehyde (pH 7.4) for 30 min, immunostained for CD11b and counterstained with DAPI as described above. The cultures used were > 99% pure. Microglia were counted at a magnification of 40× using the fractionator method with Stereo Investigator. The counting parameters were as follows: distance between counting frames, 1500 × 1500 µm; counting frame size, 150 × 150 µm.

### 2.4.15 Statistical analysis

Unless otherwise stated, data are expressed as mean ± SE. Means were compared using the unpaired Student's *t* test when the data met the assumptions of homogeneity of variance (Levene's test). As an alternative, the Welch's *t* test was used when the variances were unequal. Relationships between variables were assessed by Pearson correlation. All these tests used an alpha of 0.05 and were done with JMP software (SAS Institute, Cary, North Carolina).

## 2.5 Results

### 2.5.1 Decrease in glioma-infiltrating T cells in TNF-deficient mice

We have shown that macrophage-derived TNF can slow glioma growth through a process leading to the formation of small cavities called microcysts [87]. To examine whether T cells play a role in this process, we implanted GL261 glioma cells into the brains of TNF-knockout and wild-type mice sharing the same genetic background (B6 × 129S). The animals were killed 21 days later and brain sections were immunostained for the T cell marker CD3ε. Labeled cells were found in all compartments of the tumors (Fig. 7a, b), but not in the surrounding non-neoplastic tissue. Stereological analysis revealed that T cell density was 4.4-fold lower in TNF-deficient mice compared to wild-type controls (Fig. 7c). Interestingly, T cell density was directly proportional to the numbers of macrophages and microcysts (Fig. 7d, e), but inversely to glioma volume (Fig. 7f). These results, together with our previous findings [87], support the concept that macrophages can reduce glioma growth, at least in part, by promoting the recruitment of T cells with antitumor activity via the secretion of TNF.

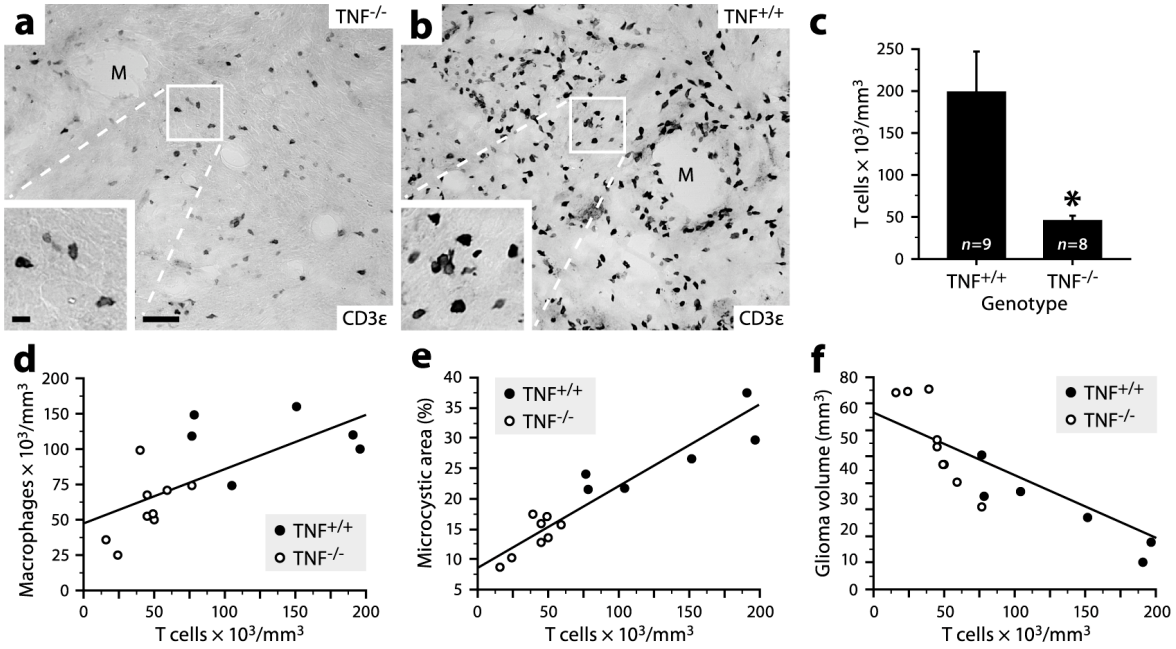


**Figure 7.** Decrease in glioma-infiltrating T lymphocytes in absence of TNF.

**a, b,** T cells immunostained for CD3ε in glioma sections from TNF-knockout and wild-type mice, respectively. Scale bars: 50 μm (main image), 10 μm (insert).

**c,** Stereological analysis revealed a 4.4-fold reduction in the number of glioma-infiltrating T cells in TNF-knockout mice. *Welch *t* test, $P = 0.014$.

**d-f,** Pearson correlation analyses showed that the number of T cells correlated positively with the number of macrophages ($P = 0.0057$, $R = 0.68$) and the percentage of tumor area occupied by microcysts ($P < 0.0001$, $R = 0.94$), but negatively with glioma volume ($P < 0.0001$, $R = -0.88$). Each data point represents a TNF-deficient (white circle) or wild-type mouse (black circle).

### 2.5.3 Proliferation of glioma-associated macrophages

Theoretically, glioma-associated macrophages can arise from three different sources: peritumoral microglia, circulating monocytes and pre-existing macrophages undergoing division. Using lethally irradiated mice reconstituted with bone marrow cells expressing GFP, we have shown that glioma-associated macrophages mainly derive from newly recruited monocytes and not from microglia [87]. To determine whether these cells manifest the ability to proliferate after infiltration, we injected glioma-bearing mice (B6 background) with BrdU prior to sacrifice to label cells in the S phase of the cell cycle. As shown in Figure 8a, $BrdU^+$ cells were found in very large numbers in the tumors and, in lower abundance, the immediate adjacent areas. Confocal microscopic analysis showed that some $BrdU^+$ cells expressed the macrophage marker Iba1 (Fig. 8b-g), which represented 1.4% (SD ± 0.3, $n$ = 3) of the dividing cells in the tumors, but 49.9% (SD ± 10.3) of those in the adjacent normal tissue. These results indicate that macrophages and microglia located within or near gliomas have the potential to proliferate.

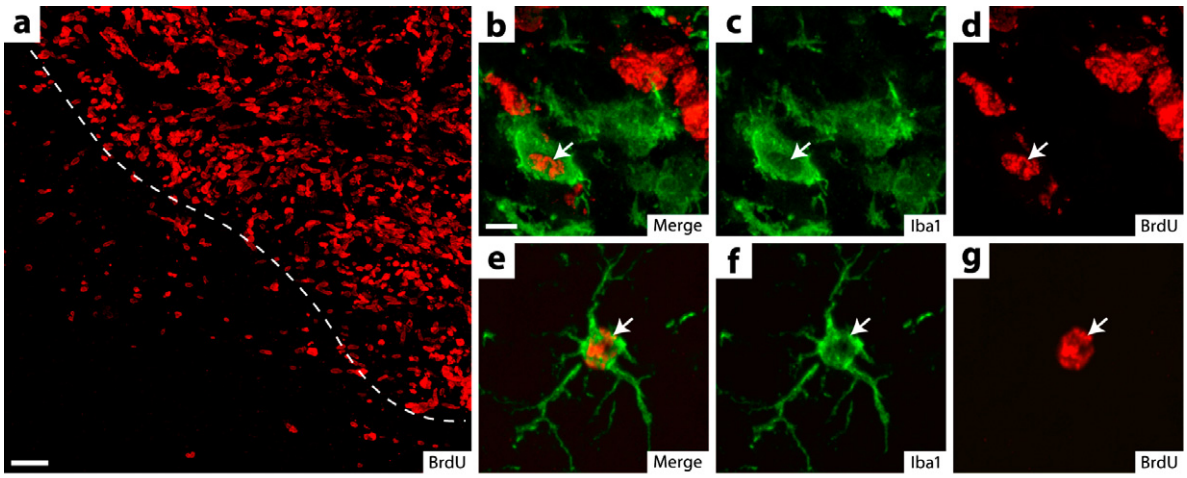


**Figure 8.** Proliferation of monocytic cells within and around gliomas.

**a,** Confocal image showing proliferating cells immunostained for BrdU in a glioma section from a mouse killed 2 weeks after tumor implantation. The dashed line delimits the tumor area (right side). Note the presence of $BrdU^{+}$ cells not only in the tumor, but also in the surrounding area. Scale bar: 50 µm.

**b-d,** A glioma associated-macrophage (arrow) double labeled for Iba1 (green) and BrdU (red). Scale bar: 5 µm (b-g).

**e-g,** A ramified microglia (arrow) double labeled for Iba1 (green) and BrdU (red). This cell was located in the area surrounding the tumor.

### 2.5.6 Macrophage depletion increases glioma growth

To confirm the role of glioma-associated macrophages, we attempted to deplete them by exploiting the proliferative ability of these cells and their precursors. More precisely, we used transgenic mice expressing a mutated form of the herpes simplex virus 1 thymidine kinase ($TK^{mt-30}$) gene under the control of the myeloid-specific CD11b promoter [147]. In these mice, it is possible to deplete macrophages by the administration of GCV, a prodrug that is converted by the viral TK to nucleotide analogues, which kill proliferating cells by inhibiting DNA synthesis. CD11b-$TK^{mt-30}$ mice on a B6 background were implanted with GL261 cells, and the tumors were allowed to grow for 7 days (Fig. 9a). Thereafter, mice were injected twice daily for 6 days with GCV or vehicle before being sacrificed. This treatment resulted in a 45% depletion of glioma-associated macrophages, as determined by stereological analysis (Fig. 9b-d). In agreement with our previous observations suggesting a beneficial role for macrophages in glioma development [87], we found that the tumors were 33% larger in GCV-treated mice (Fig. 9e), and negatively correlated with macrophage density (Fig. 9f). As expected, no difference in macrophage density (33,710 ± 3,704 cells/$mm^3$ versus 30,238 ± 4,141; Student's *t* test, $P = 0.55$; $n = 5$ per group) and glioma volume (5.1 ± 0.7 $mm^3$ versus 4.9 ± 0.8; Student's *t* test, $P = 0.85$; $n = 5$ per group) was detected in non-transgenic mice treated with GCV compared to vehicle-treated controls.

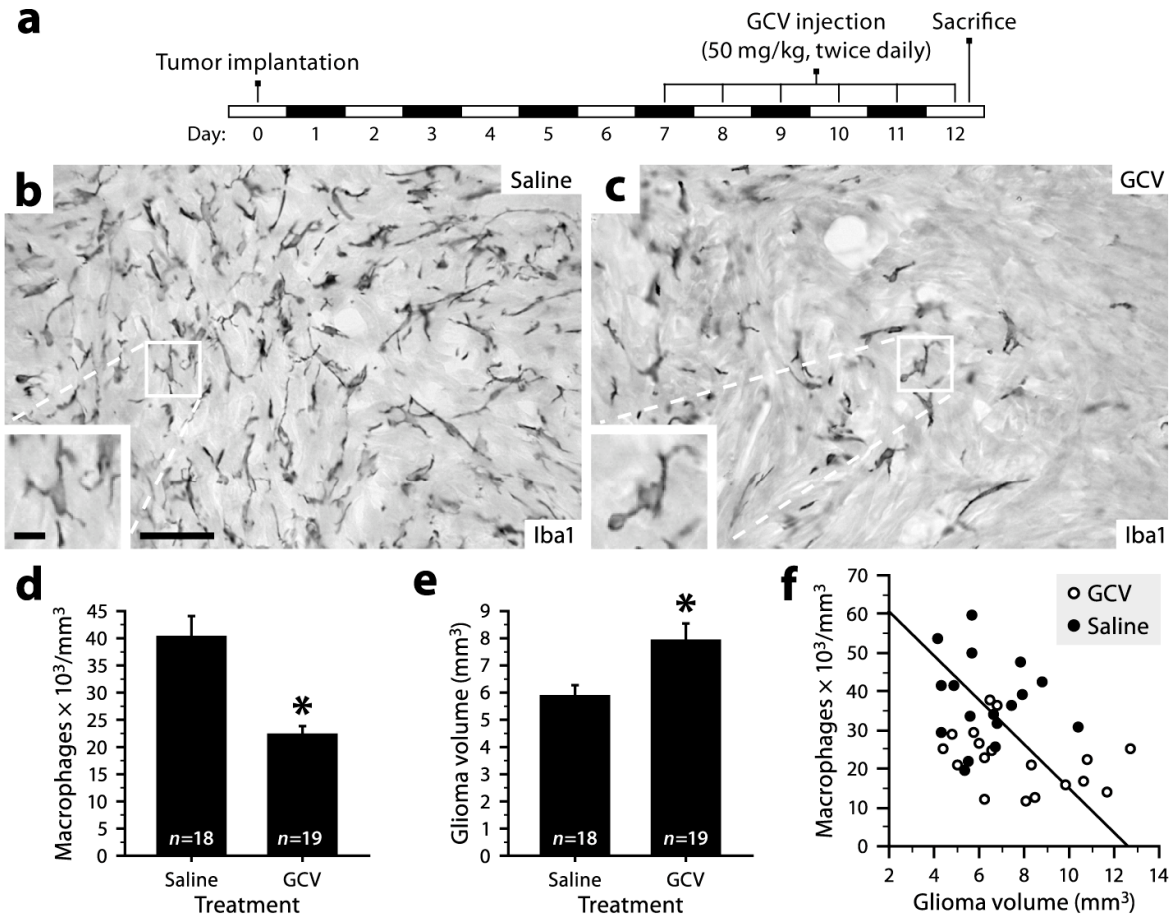


**Figure 9.** Macrophage depletion increases glioma growth.

**a,** Schematic representation of the experiment.
**b, c,** Immunoperoxidase staining for Iba1 showing glioma-associated macrophages in CD11b-TK$^{mt\text{-}30}$ mice treated with saline or GCV, respectively. Scale bars: 50 µm (main image), 10 µm (insert).
**d,** Stereological analysis revealed a 45% reduction in the number of glioma-associated macrophages in GCV-treated CD11b-TK$^{mt\text{-}30}$ mice. *Student's *t* test, $P < 0.0001$.
**e,** A 33% increase in glioma volume was found in GCV-treated CD11b-TK$^{mt\text{-}30}$ mice, as determined by the Cavalieri method. *Student's *t* test, $P = 0.016$.
**f,** The number of macrophages was inversely proportional to glioma volume (Pearson correlation, $P = 0.0054$, $R = -0.45$). Each data point represents a mouse treated with GCV (white circle) or saline (black circle).

To examine whether the increase in glioma growth observed after macrophage depletion was due to a reduction in the recruitment of antitumor T cells, brain sections from GCV-treated mice and their controls were hybridized for TNF mRNA or immunostained for CD3ε. We found that the numbers of TNF-expressing macrophages and T cells were decreased in GCV-treated mice (Fig. 10a-c), and positively correlated to each other (Fig. 10d). Consistently, there was also a direct relationship between the total numbers of macrophages and T cells (Fig. 10e). This effect on T cells was unlikely to be direct, because T cells collected from the spleens of CD11b-TK$^{mt-30}$ mice and cultured in the presence of interleukin-2 did not differ in number after a 4-day exposure to GCV at a concentration as high as 10 μM, as compared with untreated cells (11,444 ± 1,656 versus 10,336 ± 1,656; Student's *t* test, $P = 0.65$; $n = 5$ per group). Surprisingly, we observed no correlation between T cell density and glioma volume (Fig. 10f), contrary to what we found in TNF-knockout mice and their wild-type controls (Fig. 7f). The most likely explanation for this discrepancy is that GL261 cells, which originate from a B6 mouse, are more immunogenic and trigger a more robust adaptive immune response when implanted in a mixed genetic background compared to a pure B6 background. In support of this possibility, we found that glioma-infiltrating T cell were 8.3-fold more numerous in B6 × 129S mice compared to B6 mice (199,038 ± 4,7441 T cells/mm$^3$ versus 24,059 ± 4,063). Altogether, these results suggest that T cells did not mediate the antitumor effect of macrophages observed in CD11b-TK$^{mt-30}$ mice.

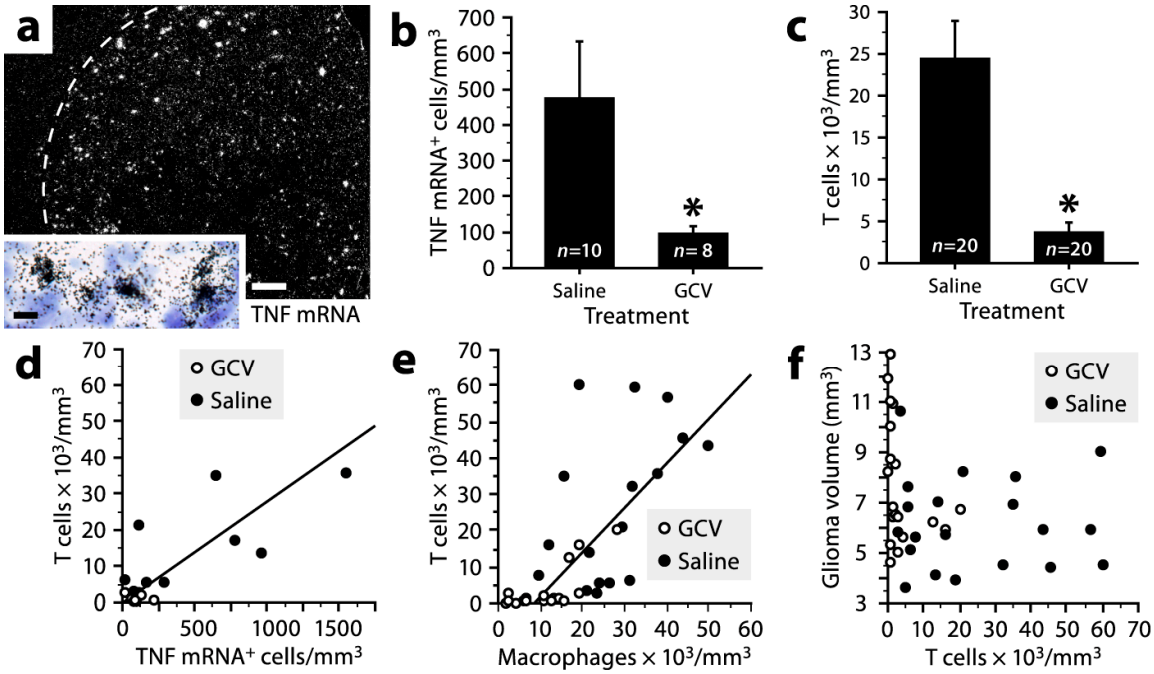


**Figure 10.** Reduction in TNF-expressing cells and T lymphocytes in macrophage-depleted gliomas.

**a,** Dark-field (main image) and bright-field (insert) photomicrographs of *in situ* hybridization signals for TNF mRNA in a 2-week glioma. The dashed line delimits the tumor area (right side). Blue, thionin counterstaining. Scale bars: 200 µm (main image), 10 µm (insert).

**b,** Stereological analysis showed a 5-fold reduction in the number of TNF mRNA$^{+}$ cells in gliomas from CD11b-TK$^{mt\text{-}30}$ mice treated with GCV. Welch *t* test, $P = 0.042$.

**c,** A 6.7-fold reduction in the number of glioma-infiltrating T cells was detected in CD11b-TKmt-30 mice treated with GCV. *Welch *t* test, $P = 0.0002$.

**d-f,** Pearson correlation analyses showed that the number of glioma-infiltrating T cells correlated positively with that of TNF mRNA$^{+}$ cells ($P < 0.0001$, $R = 0.79$) and macrophages ($P = 0.0002$, $R = 0.58$), but not with glioma volume ($P = 0.066$).

### 2.5.7 Phenotypic characterization of glioma-infiltrating leukocytes

We sought to exclude the possibility that our results were due to a depletion of immune cells other than macrophages and T cells, especially granulocytes and natural killer cells, which are known to express CD11b [162]. As we failed to detect unequivocally these cells by immunohistochemistry, we reasoned that, if they were actually absent from our specimen, the proportion of macrophages among the total leukocyte population should be equal the proportion of $Iba1^+$ cells over the sum of $Iba1^+$ (40,219 /$mm^3$) and $CD3^+$ cells (24,423/$mm^3$) found in vehicle-treated CD11b-$TK^{mt\text{-}30}$ mice (Fig. 9d and 10c), i.e., 62%. In addition, almost all $CD11b^+$ cells should express antigens that are highly specific for macrophages, including Iba1 and F4/80. To test these expectations, we immunostained glioma sections with antibodies directed against these markers or the leukocyte common antigen CD45 (Fig. 11). Confocal microscopic analysis revealed that 64% of the $CD45^+$ cells within the tumors expressed Iba1, which is similar to the expected 62%. Furthermore, the vast majority of the $CD11b^+$ cells (> 99%) expressed Iba1 and F4/80 (and vice versa), and none of the leucocytes examined, except one (Fig. 11u-x), had a multilobed nucleus typical of granulocytes. Together, these results indicate that macrophages and T cells are virtually the only immune cells that infiltrate GL261 gliomas, excluding a significant influence of other immune cells on our results.

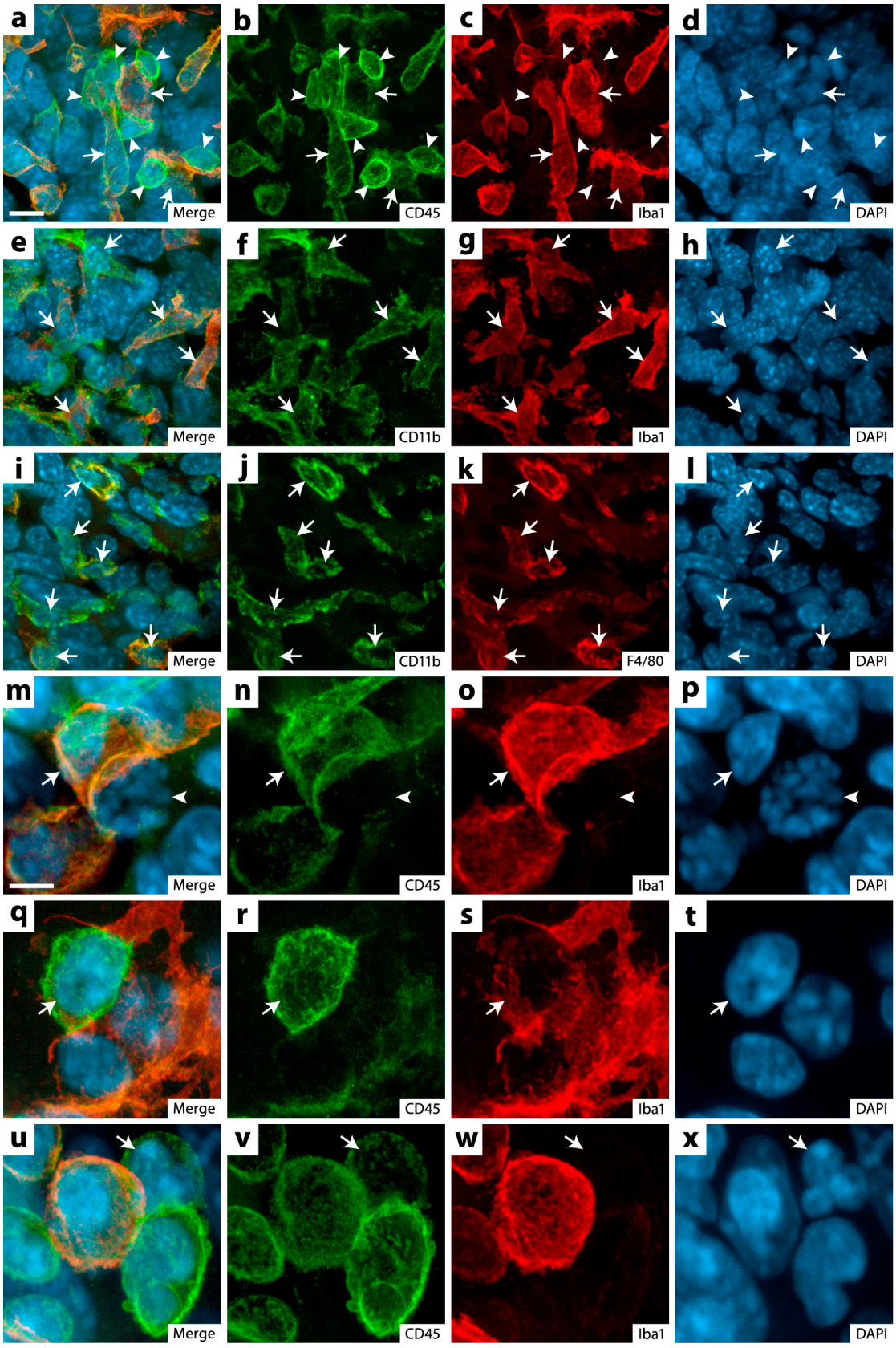
a
Merge
b
CD45
c
Iba1
d
DAPI
e
Merge
f
CD11b
g
Iba1
h
DAPI
i
Merge
j
CD11b
k
F4/80
l
DAPI
m
Merge
n
CD45
o
Iba1
p
DAPI
q
Merge
r
CD45
s
Iba1
t
DAPI
u
Merge
v
CD45
w
Iba1
x
DAPI

**Figure 11.** Phenotypic characterization of glioma-infiltrating leukocytes.

**a-d,** Confocal images showing glioma-infiltrating leukocytes expressing the panhematopoietic marker CD45 (green). Note the associations between $Iba1^{+}$ macrophages (arrows, red) and $Iba1^{-}$ cells (arrowheads), which are most likely T lymphocytes. Blue, DAPI-stained nuclei. Scale bar: 10 μm (a-l).
**e-h,** Macrophages (arrows) coexpressing CD11b (green) and Iba1 (red).
**i-l,** Macrophages (arrows) coexpressing CD11b (green) and F4/80 (red).
**m-p,** Higher magnification of a macrophage (arrow) that seems to interact with a cell showing a pyknotic nucleus (arrowhead). Scale bar: 5 μm (m-x).
**q-t,** An $Iba1^{-}$ leukocyte (arrow) with a typical round nucleus surrounded by cytoplasmic processes of macrophages.
**u-x,** An $Iba1^{-}$ leukocyte (arrow) showing a multilobed nucleus that resembles that of a granulocyte.

### 2.5.8 Physical interaction between macrophages and glioma cells

To provide evidence of the ability of macrophages to kill glioma cells, we implanted B6 mice with GL261 cells transduced with a lentiviral vector expressing GFP. Confocal imaging of brain sections immunostained for Iba1 revealed that most glioma cells were surrounded by macrophages with which many of them established physical contacts (Fig. 12 a-f). However, we found only one clear example of macrophages that was phagocytosing glioma cell fragments (Fig. 12 g-j), and very few glioma cells (~7 per section) completely wrapped by macrophage processes (Fig. 12 k-r). Glioma cells showing signs of apoptosis (e.g., pyknotic nucleus) were rarely observed (< 1 per section; Fig. 12 o-r). These observations suggest that macrophages can physically interact with glioma cells, but that their antitumor activity is unlikely to be due to tumor cell killing.

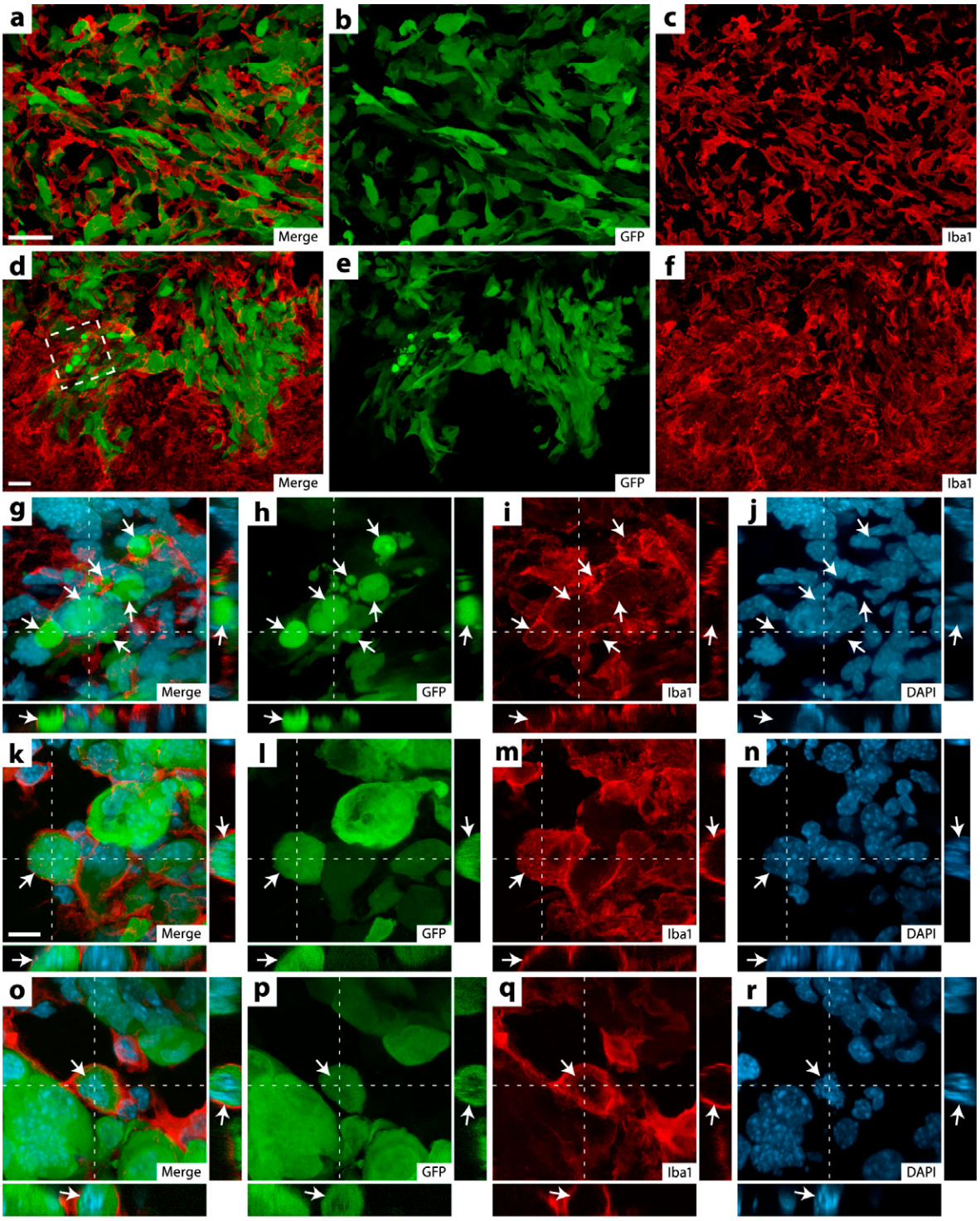
a
Merge
b
GFP
c
Iba1
d
Merge
e
GFP
f
Iba1
g
Merge
h
GFP
i
Iba1
j
DAPI
k
Merge
l
GFP
m
Iba1
n
DAPI
o
Merge
p
GFP
q
Iba1
r
DAPI

**Figure 12.** Physical interaction between macrophages and glioma cells.

**a-c,** Confocal images taken near the center of a tumor showing glioma cells (green), transduced *ex vivo* with a GFP-expressing lentiviral vector, surrounded by $Iba1^{+}$ macrophages (red). Scale bar: 50 μm (a-c).
**d-f,** Glioma cells (green) associated with macrophages (red) at the invasive border of a tumor. Scale bar: 25 μm (d-f).
**g-r,** Higher magnification of the area within the dashed box in d showing macrophages engulfing glioma cell fragments (arrows). Blue, DAPI-stained nuclei. The rectangle images at the right and bottom of the main images are optical z-sections taken at the level of the dashed lines. Scale bar: 10 μm (g-r).
**k-n** and **o-r**, Two examples of glioma cells (arrows) completely wrapped by macrophage processes, one with an apparently normal nucleus (n) and the other with a pyknotic nucleus (r).

## 2.6 Discussion

Accumulating evidence suggests that cancer cells that have escaped immune surveillance can exploit macrophages for their own benefit [72, 76, 118, 119, 157]. For example, it has been proposed that tumor-associated macrophages promote angiogenesis by secreting VEGF or other cytokines with direct or indirect proangiogenic activity. These cells could also facilitate tumor cell invasion and metastasis by releasing matrix-degrading enzymes such as the gelatinase MMP-9. Although this concept seems to be true for different cancers, including those of the breast and lung [72, 76, 118, 119, 157], the present study suggests that it does not apply to all tumors, especially gliomas. On the contrary, we found that gliomas develop faster when macrophages are compromised, suggesting that the sum of their antitumor effects are greater than that of their protumor effects, if any. This functional difference between glioma-associated macrophages and those that populate peripheral tumors may lie, at least in part, in the fact that gliomas do not metastasize outside the nervous system and do not depend on angiogenesis to grow, but rather on an alternative process called vessel co-option [15, 17, 163], in which macrophages are probably not essential.

Our results are in apparent contradiction with clinical studies indicating that a high macrophage content correlates with poor prognosis [143]. However, considering the variable nature of human brain tumors, these studies do not necessarily mean that macrophages promote glioma growth, and may instead suggest that aggressive gliomas are somewhat more immunogenic than low-grade gliomas. Alternatively, it may be that aggressive gliomas cause more severe cellular and physiological disturbances (e.g., neuronal degeneration, edema formation, extracellular matrix remodeling), which would induce the recruitment of a higher number of macrophages to clean up the cellular debris and protect the adjacent normal tissue. Another possibility is that the density of macrophages is determined in part by that of the tumor cells, as it is suggested by the observation that the proportion of macrophages in GL261 gliomas (~8%) is similar to that of microglia in the normal nervous system [87]. This theory would explain why

macrophages were found in larger numbers in high-grade gliomas, which tend to be more homogeneous and densely packed than lower grade tumors [8, 164].

The present study leads us to conclude that macrophages use different mechanisms to slow glioma growth depending on the immunogenicity of the tumor. When it is weakly or not immunogenic, they act without the aid of lymphocytes, suggesting that they could be equipped to directly recognize and kill glioma cells. However, this idea is not supported by the fact that we observed only rare glioma cells being phagocytosed by macrophages or showing apoptotic features. Alternatively, we propose that the antitumor effect of macrophages results from a neuroprotective activity. This hypothesis derives from the property of malignant gliomas to infiltrate the surrounding tissue by causing its destruction. Indeed, it has been reported that glioma cells produce toxic levels of glutamate that facilitate their progression, an effect that can be blocked by the administration of the glutamate receptor antagonist MK801 [165]. Similarly, other potentially toxic molecules secreted by tumor cells or derived from plasma that penetrates the parenchyma through a damaged blood-brain barrier could promote glioma cell invasion. It is possible that macrophages reduce the invasive potential of glioma cells by protecting the surrounding tissue from the accumulation of toxic substances, and by attempting to maintain its structural integrity. Further investigation will be required to validate and characterize this mechanism.

In the case of immunogenic gliomas, our previous [87] and present findings indicate that macrophages contribute to the development of the adaptive antitumor immune response, at least in part, by producing TNF. This cytokine seems to act mainly by increasing the number of infiltrating T cells with potential antitumor activity, but whether this effect is due to an increase in their recruitment, proliferation and/or survival is a question that remains to be addressed. As observed in this study, it has been reported that tumor-infiltrating lymphocytes can physically interact with macrophages, suggesting tumor antigen cross-presentation [166]. Although the magnitude of adaptive immunity may greatly vary depending on the nature of the tumor, its importance is underscored by an early clinical study that found an association between the presence of infiltrating lymphocytes and longer survival [145]. More recently, it has been reported that the production levels of

cytotoxic T cells by the thymus inversely correlates with tumor recurrence and mortality in glioblastoma patients and accounts for the effect of age on their prognosis, suggesting that T cells exert one of the strongest known influences on glioblastoma progression [146]. These observations should be taken into account when considering the administration of certain anti-inflammatory drugs to patients with brain tumors, especially anti-TNF agents, which have recently been associated with an increased risk of malignancies [167]. More importantly, they call for a reevaluation of the routine use of dexamethasone in the management of brain tumor-associated edema. Because this synthetic glucocorticoid can suppress cytokine signaling and induce T cell apoptosis [168, 169], it may be useful to develop a more specific drug able to mimic dexamethasone's beneficial properties without affecting the antitumor immune mechanisms. Such a drug would have the added advantage of being compatible with future immunotherapy.

In conclusion, this study demonstrates that macrophages play beneficial roles against gliomas, either directly or indirectly by recruiting T cells with potential antitumor activity. It raises hope that one day macrophage activity could be therapeutically augmented to control or eradicate malignant brain tumors. This possibility will require a better understanding of the mechanisms underlying the antitumor effects of macrophages, and the strategies used by glioma cells to counter them. This study also validates CD11b-$TK^{mt\text{-}30}$ mice as a tool to investigate the role of macrophages in cancer development.

# Chapitre 3: L'inhibition de l'angiopoiétine 2 par la dexamethasone ou une protéine de fusion peptide-Fc réduit la croissance des gliomes

## "Blockade of angiopoietin 2 with dexamethasone or a peptide-Fc fusion protein reduces glioma growth"

Jérôme Villeneuve, Hugo Galarneau, Marie-Josée Beaudet, Pierrot Tremblay, Ariel Chernomoretz[1] et Luc Vallières

Département d'oncologie et endocrinologie moléculaire, Centre de recherche du centre hospitalier de l'université Laval, Québec, Québec, Canada

[1]Adresse présente : Departemento de Fisica, Facultad de Ciencias Exactas y Naturales, Universidad de Buenos Aires, Pabellon 1 Ciudad Universitaria, 1428, Buenos Aires, Argentina.

## 3.1 Résumé

Tous les patients atteints de glioblastomes, la forme la plus agressive et la plus commune de tumeurs cérébrales, développent de l'œdème. Cette complication est couramment traitée avec de la dexamethasone, un agent anti-inflammatoire stéroïdien dont les effets sur le cerveau son encore mal compris. Nous avons démontré que la dexamethasone peut réduire la croissance de gliomes implantés chez la souris même si cet agent engendre une diminution du nombre de lymphocytes T infiltrant la tumeur. Plus précisément, les cellules T auxiliaires ($T_H$) ou cytotoxiques étaient sensibles à la dexamethasone à l'inverse des populations de cellules CD4 et CD8 négatives, incluant les cellules T γδ et les NKT. L'effet antinéoplasique de la dexamethasone était indirect puisqu'il n'affectait pas la croissance et le profil d'expression génique des cellules de gliomes *in vitro*. Au contraire, plusieurs centaines de gènes sensibles à la dexamethasone, notamment l'angiopoiétine 2 (Angpt2), jouant un rôle dans le remodelage vasculaire, ont été identifiés dans des cellules endothéliales du cerveau par microarray. L'habilité de la dexamethasone à inhiber l'expression de l'Angpt-2 a été confirmé *in vitro* et *in vivo*. L'inhibition de l'Angpt-2 par un anticorps synthétique a permis de réduire la croissance des gliomes et l'élargissement vasculaire de façon plus significative que la dexamethasone sans affecter l'infiltration de lymphocytes T. En somme, cette étude a permis d'identifier un mécanisme par lequel la dexamethasone peut atténuer la croissance des gliomes, fournissant une nouvelle cible thérapeutique pour les tumeurs cérébrales malignes. Ces résultats suggèrent aussi que l'élaboration d'immunothérapies basées sur l'utilisation de cellules T γδ ou NKT pourraient être bénéfique pour les patients traités avec des glucocorticoïdes.

## 3.2 Abstract

All patients with glioblastoma, the most aggressive and common form of brain cancer, develop cerebral edema. This complication is routinely treated with dexamethasone, a steroidal anti- inflammatory drug whose effects on brain tumors are not fully understood. Here we show that dexamethasone can reduce the growth of an experimental glioma in mice, even though it depletes infiltrating T cells with potential antitumor activity. More precisely, T cells with helper or cytotoxic function were sensitive to dexamethasone, but not those that were negative for the CD4 and CD8 molecules, including gammadelta and natural killer (NK) T cells. The antineoplastic effect of dexamethasone was indirect, as it did not meaningfully affect the growth and gene expression profile of glioma cells in vitro. In contrast, hundreds of dexamethasone-sensitive genes, notably angiopoietin 2 (Angpt2), which is involved in vascular remodeling, were identified in cultured cerebral endothelial cells by microarray analysis. The ability of dexamethasone to inhibit Angpt2 expression in glioma endothelium was confirmed in vitro and in vivo. Selective neutralization of Angpt2 using a synthetic antibody reduced glioma growth and vascular enlargement to a greater extent than dexamethasone, without affecting T cell infiltration. In summary, this study identifies a mechanism by which dexamethasone can attenuate glioma growth, providing a new therapeutic target for malignant brain tumors. It also suggests that cancer immunotherapy based on gammadelta or NK T cells might be beneficial in patients treated with glucocorticoids.

## 3.3 Introduction

Brain tumors are a leading cause of cancer-related death in children and young adults [1]. The most frequent and aggressive brain tumor, glioblastoma, carries a very poor prognosis, with a median survival of about a year, despite radical treatments, including surgical resection, irradiation and chemotherapy [170, 171]. New, more targeted approaches, such as immunotherapy, antiangiogenic therapy and gene therapy, have shown promise in experimental models, but their effectiveness in clinical settings remains to be proven [170, 172-174].

Vascular edema is a serious complication of brain tumors [175]. It results from the disruption of the blood-brain barrier, allowing plasma to enter the interstitial space [176]. Because this condition can cause neurological deficits and death, patients with brain tumors are treated with dexamethasone [32], a synthetic glucocorticoid with broad anti-inflammatory actions. Although this drug is routinely used since decades in the management of cerebral edema, its precise mechanism of action is still poorly understood, but is thought to result in a reduction in the permeability of tumor capillaries and/or an increase in the clearance of extracellular fluid. Despite its usefulness, dexamethasone can produce many side effects, including Cushing's syndrome, myopathy (muscle weakness, wasting) and opportunistic infections (e.g., Pneumocystis carinii pneumonitis) [36]. Furthermore, recent studies suggest that dexamethasone can potentially interfere with current and prospective anticancer treatments. For example, it has been shown that dexamethasone protects glioma cells from the chemotherapeutic agent temozolomide [177, 178] reduces the bystander effect of the thymidine kinase/ganciclovir system in suicide-gene therapy [179], and inhibits the antitumor effect of interleukin-4 when delivered using retroviruses [180].

An interesting feature of brain tumors is that they are infiltrated by immune cells with potential antitumor activity, particularly macrophages and T lymphocytes. Despite their presence in large numbers, these cells are normally unable to eradicate malignant tumors, but some evidence suggests that they can slow their progression to some extent. For example, we have shown in mice that glioma-associated macrophages, by expressing the

cytokine tumor necrosis factor, promote their own recruitment and reduce glioma growth through a process that culminates in the formation of microcysts [87]. The exact mechanism by which macrophages can mount an attack against glioma cells is unclear, but possibly involves contact-dependent interactions, the secretion of cytotoxic and cytostatic humoral factors, and/or the recruitment of effector T cells. The ability of the latter to reduce glioma growth is suggested by an early clinical study that found an association between the presence of tumor-infiltrating lymphocytes and longer survival [145]. More recently, it has been reported that the production levels of cytotoxic T cells by the thymus inversely correlates with tumor recurrence and mortality in glioblastoma patients and accounts for the effect of age on their prognosis, suggesting that T cells exert one of the strongest known influences on glioblastoma progression [146].

Considering that glucocorticoids can suppress cytokine signaling and induce T cell apoptosis [168, 169], the question arises as to whether dexamethasone may facilitate the growth of brain tumors by interfering with antitumor immune responses. In the present study, we have tested this hypothesis and report that dexamethasone can, on the contrary, slow glioma growth, even though it depletes infiltrating T cells. Through the combined use of in vitro and in vivo techniques, we provide evidence that dexamethasone exerts this antitumor effect by acting on the tumor endothelium through a mechanism involving down-regulation of the angiogenic factor Angpt2.

## 3.4 Methods

### 3.4.1 Intracerebral implantation of glioma cells

Eight week-old male C57BL/6 mice (Charles River Laboratories, Montréal, Québec, Canada) were anesthetized, shaved and immobilized in a stereotaxic frame. A midline incision was made on the scalp, followed by a circular craniotomy over the right hemisphere, 1.7 mm lateral and 1 mm rostral from bregma. After removal of the dura mater, a 5-µl Hamilton syringe fitted with a 27-gauge beveled needle was advanced into the caudoputamen at a depth of 3.5 mm from the skull surface. Using a UMPII micropump (World Precision Instruments, Saratoga, Florida), 2 µl of Dulbecco's phosphate-buffered saline (DPBS; Invitrogen, Carlsbad, California) containing 5 × 104 viable GL261 cells were injected over 2 min. After the injection, the syringe was left in place for 2 min before being withdrawn very slowly.

### 3.4.2 Dexamethasone treatment

From the day of tumor implantation to the day of death, mice were injected intraperitoneally twice daily with 0.1 or 1.0 mg/kg dexamethasone phosphate (Sabex, Boucherville, Québec, Canada) diluted in saline. Control mice were treated identically, except that dexamethasone was substituted by saline.

### 3.4.3 L1-10 treatment

From the day of tumor implantation to the day of death, mice were injected subcutaneously every other day with 4 mg/kg L1-10 (kindly provided by Amgen, Thousand Oaks, California) diluted in PBS. Control mice were treated identically, except that dexamethasone was substituted by PBS.

### 3.4.4Survival analysis

After tumor implantation, mice were monitored daily and killed when any of the following criteria were observed: >20% weight loss, paralysis or lethargy. The survival time was calculated from the day of tumor implantation to the day of euthanasia or death. The Kaplan-Meier method was used to create survival curves, which were compared using the log-rank test.

### 3.4.5 Flow cytometry

Twenty days after tumor implantation, mice were anesthetized and transcardially perfused with DPBS for 5 min. The tumors were dissected out, minced with rasor blades in DPBS containing 2% goat serum, processed with the Medimachine (Dako, Carpinteria, California) and filtered through 40-μm nylon mesh. Myelin debris were removed by centrifugation through 35% Percoll. The cells were rinced, blocked for 5 min with 5 μg/ml anti-CD16/CD32 antibody (BD Biosciences, San Diego, California) and stained for 30 min on ice with combinations of the following rat antibodies (2 μg/ml each; all from BD Biosciences): CD11b-Alexa 488 (clone M1/70), CD3ε-Alexa 488 (clone 145-2C11), CD4-APC (clone RM4-5), CD4-PE (clone H129.19), CD8a-APC (clone 53-6.7), NK-1.1-PE (clone PK136), TCRβ-PE (clone H57-597) and TCRγδ-PE (clone GL3). Apoptotic cells (annexin V+, propidium iodide-) were labeled using the Vybrant Apoptosis Assay Kit #2 (Molecular Probes, Eugene, Oregon). Cells were analyzed using a two-laser, four-color FACSCalibur flow cytometer and CellQuest Pro software (BD Biosciences).

### 3.4.6 Histological preparation

For all histological analyses except in situ hybridization, mice were transcardially perfused with 10 ml of saline, followed by ice-cold 4% paraformaldehyde in phosphate buffer, pH 7.4, over 10 min. The brains were removed, postfixed for 4 h at 4 °C, then cryoprotected overnight in 50 mM potassium phosphate-buffered saline (KPBS) supplemented with 20% sucrose. Series of sections through the tumors were cut at 40 μm using a freezing microtome, collected in cryoprotectant (30% ethylene glycol, 20% glycerol, 50 mM sodium phosphate buffer, pH 7.4) and stored at –20°C until analysis. For in situ hybridization, the following modifications were applied: 1) the fixative was

dissolved in borate buffer, pH 9.5, instead of phosphate buffer; 2) the brains were postfixed for 48 h before being cryoprotected overnight in the same fixative supplemented with 20% sucrose; and 3) the tumors were cut at 30 μm.

### 3.4.7 Immunostaining

Immunohistochemistry was performed as described previously [87] using the following primary antibodies: rabbit anti-Iba1 (1:2000; Wako Chemicals, Richmond, Virginia), rat anti-CD3ε (1:500; Serotec, Raleigh, North Carolina) and rat anti-CD31 (1:1000; BD Biosciences).

### 3.4.8 In situ hybridization

Transcripts were detected by radioisotopic in situ hybridization according to a previously described protocol [161]. Briefly, sections were mounted onto Superfrost slides (Fisher Scientific, Pittsburgh, Pennsylvania), postfixed with 4% paraformaldehyde in borate buffer, pH 9.5, for 20 min, digested with 10 μg/ml proteinase K at 37 °C for 25 min, acetylated with 0.25% acetic anhydride for 10 min and dehydrated. Antisense and sense cRNA probes were transcribed from linearized cDNAs (Supplementary Table 3) in the presence of [35S]-UTP and [35S]-CTP (Perkin- Elmer, Foster City, California), purified by phenol-chloroform extraction and ammonium acetate- ethanol precipitation, then applied to the slides at a concentration of 2 × 107 cpm/ml in hybridization buffer (50% formamide, 0.3 M NaCl, 10 mM Tris, pH 8.0, 1 mM EDTA, 1× Denhardt's solution, 10% dextran sulfate, 2 μg/ml tRNA and 10 mM dithiothreitol). After overnight incubation at 60 °C, the slides were treated with 20 μg/ml ribonuclease A for 30 min at 37 °C, washed in a solution containing 15 mM NaCl and 1.5 mM sodium citrate for 30 min at 65°C and dehydrated. After film autoradiography, slides were defatted in xylene, dipped into Kodak NTB2 emulsion, exposed at 4 °C for 7 (Tnc, MMP2) or 14 (Angpt2, ESM1, TGFß2, VEGFa) days, developed in Kodak D19 developer for 3.5 min at 14-16 °C, fixed in Kodak rapid fixer for 5 min, counterstained with 0.25% thionin, dehydrated and coverslipped.

### 3.4.9 Quantitative histological analyses

For all the analyses, systematically sampled sections (every 10th section through the tumors) were examined in a blinded manner using a Stereo Investigator system (Microbrightfield, Colchester, Vermont) with a Nikon E800 microscope.

Tumor volume was estimated from thionin-stained sections by the Cavalieri method. Using a 2× Plan Apochromat objective (numerical aperture 0.1), a point grid of 200 × 200 μm was overlaid on each section and the points that fell within the tumor were counted. Point counts were converted to volume estimates taking into account sampling frequency, magnification, grid size and section thickness.

Labeled cells were counted by the optical fractionator method. Tumor tissue was traced using a 2× objective and sampled using a 60× Plan Apochromat oil objective (numerical aperture 1.4). The counting parameters were as follow: distance between counting frames, 400 × 400 μm (Iba1+ cells) or 450 × 450 μm (CD3ε+ cells); counting frame size, 50 × 50 μm (Iba1+ cells) or 100 × 100 μm (CD3ε+ cells); disector height, 10 μm; guard zone thickness, ≥2 μm. Cells were counted only if their nuclei laid within the disector area, did not intersect forbidden lines and came into the focus as the optical plane moved through the height of the disector.

Tumor vessel density was evaluated from CD31-immunostained section by the area fraction fractionator method. Tumor tissue was traced using a 2× objective and sampled using a 40× Plan Apochromat oil objective (numerical aperture 0.95). The analysis parameters were as follows: counting frame size, 400 × 400 μm; distance between counting frame, 1000 × 1000 μm; grid size within counting frame, 35 × 35 μm. The number of points that fell on the vasculature in each counting frames were converted to area estimates taking into account sampling frequency, magnification and grid size.

Tumor vessel caliber was measured using the Quick Measure Line tool of Stereo Investigator. For unbiased sampling, a point grid of 325 × 325 μm was overlaid on each section and the vessel diameter was recorded systematically where points fell on the vasculature.

In situ hybridization signals for Angpt2 were quantified at the single-cell level by optical densitometry. For unbiased sampling, all the tumor area was photographed (12-bit, grayscale) in dark-field microscopy using a 20× Plan objective and a Retiga EX monochrome camera (QImaging, Burnaby, British Columbia, Canada), and then one image out of three was used for quantification. The intensity of each hybridization signal on each image (100-150 per mouse) was analyzed with ImageJ software 1.36. To this end, the signal was circled using the round selection tool of a fixed dimension (50 × 50 pixels) and the mean optical intensity of that area was recorded. The value was subtracted from an average of 6 background measurements.

In situ hybridization signals for MMP2 were quantified by exposing the slides to PhosphorImager screens (Molecular Dynamics, Sunnyvale, California) for 3 h, after which the screens were scanned using a Storm 860 PhosphorImager. The tumor area on each section was traced with the freehand selection tool of ImageJ and the mean optical intensity of that area was recorded.

### 3.4.10 Cell culture and RNA preparation

The glioma cell line GL261, originally derived from a B6 mice implanted intracerebrally with methylcholanthrene [158], was provided by Dr. Protul Shrikant (Roswell Park Cancer Institute, Buffalo, New York). The murine brain endothelial cell line bEnd.3 was obtained from American Type Culture Collection (Manassas, Virginia). Cells were cultured in 6-well plates for 24 h with Dulbecco's modified Eagle's medium (Wisent, Saint-Bruno, Québec, Canada) supplemented with 10% heat-inactivated fetal bovine serum, 2 mM L-glutamine, 110 mg/L sodium pyruvate, 100 U/ml penicillin and 100 µg/ml streptomycin. Thereafter, the medium was replaced with fresh medium supplemented or not with different concentrations of dexamethasone or L1-10. For cell growth assay, GL261 cells were seeded at 10,000 cells/well, collected by trypsinization 3 or 5 days after drug addition and counted with an Epic XL flow cytometer (Coulter, Miami, Florida) by excluding dead cells by propidium iodide staining. For microarray and qRT-PCR analyses, cells were seeded at 50,000 (GL261) or 20,000 (dEnd.3) cells/well and total RNA was extracted, 24 h after stimulation, using the GenElute Mammalian Total RNA Miniprep Kit

(Sigma-Aldrich, St. Louis, Missouri). RNA integrity and yield were assessed by microcapillary electrophoresis (Bioanalyzer 2100, Agilent Technologies, Palo Alto, California).

### 3.4.11 Microarray analysis

RNA (12 ng) was converted to cDNA, which was amplified and transcribed to produce biotinylated cRNA using the Small Sample Labeling Protocol Version 2 (Affymetrix, Santa Clara, California). cRNA (15 µg) was fragmented and hybridized to Affymetrix Mouse Genome 430 2.0 arrays for 16 h at 45 °C with constant rotation at 60 rpm. The arrays were washed and stained with streptavidin-phycoerythrin (10 µg/ml; Molecular Probes) and biotinylated goat anti- streptavidin (3 mg/ml; Vector Laboratories, Burlingame, California) using the Affymetrix Fluidics Station 400 (protocol EukGE-WS2Av5), then read using the Affymetrix GeneChip Scanner 3000.

Microarray data were analyzed with the statistical software R (version 2.3.1; http://www.r-project.org) and add-on packages from the Bioconductor project (version 1.8; http://www.bioconductor.org). Briefly, after assessing array quality using the AffyPLM and AffyQCReport packages, the hybridization signals were background-corrected, normalized and summarized with the GCRMA package. To identify differentially expressed genes, empirical Bayes moderated t-statistics were computed with the LIMMA package, adjusting the corresponding P-values to control the false discovery rate at 5%. Annotations were obtained from the Affymetrix web site (www.affymetrix.com).

### 3.4.12 Real-time qRT-PCR

RNA (1.25 µg) was reverse transcribed for 10 min at 25 °C and 120 min at 42 °C using a random primer hexamer and Superscript II reverse transcriptase (Invitrogen). Quantitative PCR was conducted in duplicate in a final volume of 15 µl containing 1× Universal PCR Master Mix (Applied Biosystems, Foster City, California), 10 nM Z-tailed forward primer (Annexe I), 100 nM untailed reverse primer (Annexe I), 100 nM Amplifluor Uniprimer (Chemicon, Temecula, California) and 2 µl cDNA (40-50 ng/µl). Amplification was performed using the ABI PRISM 7900 sequence detector (Applied

Biosystems) under the following conditions: 2 min at 50 °C, 4 min at 95 °C, followed by 55 cycles of 15 sec at 95°C and 40 sec at 55 °C. Ribosomal 18S RNA or GAPDH mRNA was used as an internal control to normalize the expression levels of each transcript.

### 3.4.13 cDNA cloning

RNA (5 μg) from bEnd.3 cells was reverse transcribed for 50 min at 42 °C with Superscript II reverse transcriptase (Invitrogen). Partial cDNAs were PCR amplified with Platinum Pfx DNA polymerase (Invitrogen) and the primers listed in Supplementary Table 3. The PCR conditions consisted of an initial denaturation step (94 °C, 2 min), followed by 30 cycles of PCR reaction (94 °C for 15 sec, 63 °C for 30 sec, 68 °C for 100 sec), and then by a final extension step (68 °C, 2 min). Amplicons were cloned into the PCR-Blunt II-TOPO vector (Invitrogen) and automatically sequenced from both ends to confirm identity. Before riboprobe synthesis for in situ hybridization, the plasmids were linearized with restriction enzymes (Annexe II) and purified with the QIAquick PCR purification kit (Qiagen).

### 3.4.14 Statistical analysis

Unless otherwise stated, means were compared using the unpaired Student's t test or one-way ANOVA when the data met the assumptions of normality (Shapiro-Wilk W test) and homogeneity of variance (Levene's test). As an alternative, the Wilcoxon rank-sum or Kruskal-Wallis test was used when the distribution was abnormal or the Welch's t test or Welch's ANOVA when the variances were unequal. The Tukey-Kramer HSD or Dunn's test was used for parametric or nonparametric post hoc multiple comparisons, respectively. A two-way ANOVA, followed by the Tukey test, was used when more than one independent variable was being evaluated. Relationships between variables were assessed by Pearson correlation. All these tests used an alpha of 0.05 and were done with JMP software (SAS Institute, Cary, North Carolina) or Prism 4 (GraphPad Software, San Diego, California).

## 3.5 Results

### 3.5.1 Dexamethasone reduces glioma growth

To assess the effect of dexamethasone on glioma growth, we implanted GL261 glioma cells into the brains of syngeneic immunocompetent mice, and then treated the animals with either dexamethasone or vehicle. Some mice were killed after 20 days for histological analysis and the remaining mice were monitored for survival. We found that dexamethasone reduced glioma volume by 33% when given twice daily at 1 mg/kg (Fig. 13b), but not at a lower dose of 0.1 mg/kg (Student's t test, $P = 0.9$; data not shown). However, glioma-bearing mice treated with the highest dose of dexamethasone did not survive longer than control mice (Fig. 13c) and suffered from chronic weight loss (Fig. 13d). Therefore, these results indicate that dexamethasone can slow the growth of malignant gliomas, contrary to our expectation, but only at a relatively high concentration and without improving survival, perhaps due to a toxic side effect, such as muscle wasting or cachexia [181].

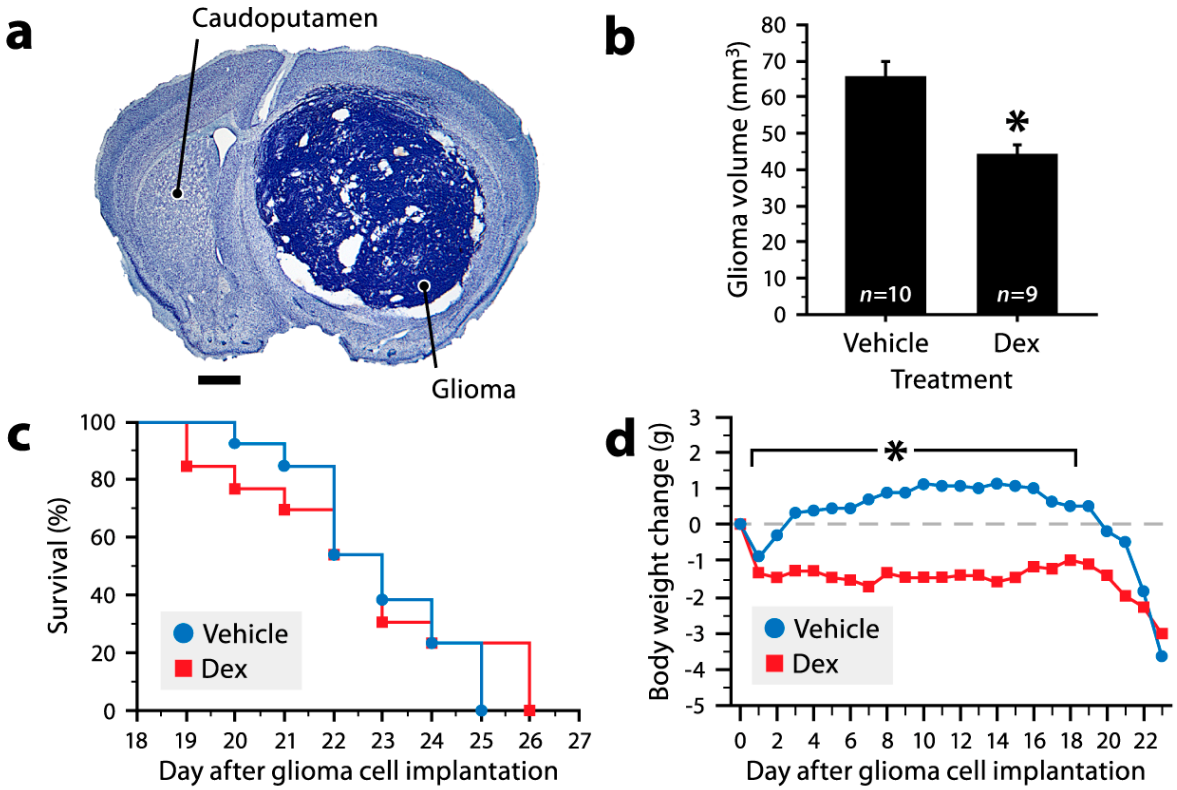


**Figure 13.** Dexamethasone reduces the growth of malignant gliomas in mice without increasing survival.

***a***, Representative section of a glioma stained with thionin from a mouse killed 20 days after implantation of GL261 cells into the right caudoputamen. Scale bar, 1mm.

***b***, Stereological analysis revealed a 33% decrease in glioma volume in mice injected twice daily with 1 mg/kg dexamethasone (Dex) compared to sham-treated mice. *Student's *t* test, $P$=0.0008. Data are mean ± SE.

***c***, Kaplan-Meier curves showing no difference in the probability of survival between glioma-bearing mice treated or not with dexamethasone ($n$ = 13 per group). Log-rank test, $P$ = 0.68.

***d***, A chronic reduction in body weight was recorded in glioma-bearing mice treated with dexamethasone ($n$ = 13 per group). *MANOVA with repeated measures ($P$ < 0.0001) followed by Student's *t* tests ($P$ < 0.02). Data are mean change in body weight from the day of tumor implantation.

### 3.5.2 Dexamethasone depletes tumor-infiltrating T lymphocytes

To determine whether dexamethasone had affected, as anticipated, the recruitment of immune cells into the tumors, we immunostained glioma sections for the T-cell marker CD3ε (Fig. 14a,b) or the macrophage marker Iba1 (Fig. 14d,e). Stereological analysis revealed that dexamethasone (1 mg/kg, twice daily) reduced the density of T cells in the tumors by 51% (Fig. 14c), but not that of macrophages (Fig. 14f). To confirm this decrease and characterize the phenotype of infiltrating T cells, we repeated the experiment, except that tumors were exsanguinated and dissociated into single-cell suspensions for flow cytometric analysis. Multiple labeling with CD3ε, CD4 and CD8 antibodies showed 3 predominant populations of T cells: CD4+ helper T cells, CD8+ cytotoxic T cells and double negative (CD4–CD8–) T cells (Fig. 15a-c). In gliomas not exposed to dexamethasone, these populations accounted for 45, 39 and 15% of the infiltrating T cells, respectively. In agreement with our histological observation, the overall number of infiltrating T cells was 43% lower in dexamethasone-treated mice (Fig. 15d). Interestingly, all populations of T cells were equally sensitive to dexamethasone, except double negative T cells, which were not affected at all (Fig. 15e). Further characterization showed that 42% of double negative T cells expressed the T cell receptor (TCR) ß chain (Fig. 15f,i), while another 24% expressed the alternative TCR γδ (Fig. 15g,i). Furthermore, 36% of double negative T cells were positive for the NK cell marker NK-1.1 (Fig. 15h,i), which correlated positively with TCR ß (Fig. 15j), but negatively with TCR γδ (Fig. 15k). Most double negative T cells were viable, as only 11% of them on average labeled positively for the apoptotic marker annexin V (data not shown). In summary, our results indicate that dexamethasone can reduce glioma growth, while depleting most infiltrating T cells with potential antitumor activity, except a subpopulation including gammadelta and NK T cells.

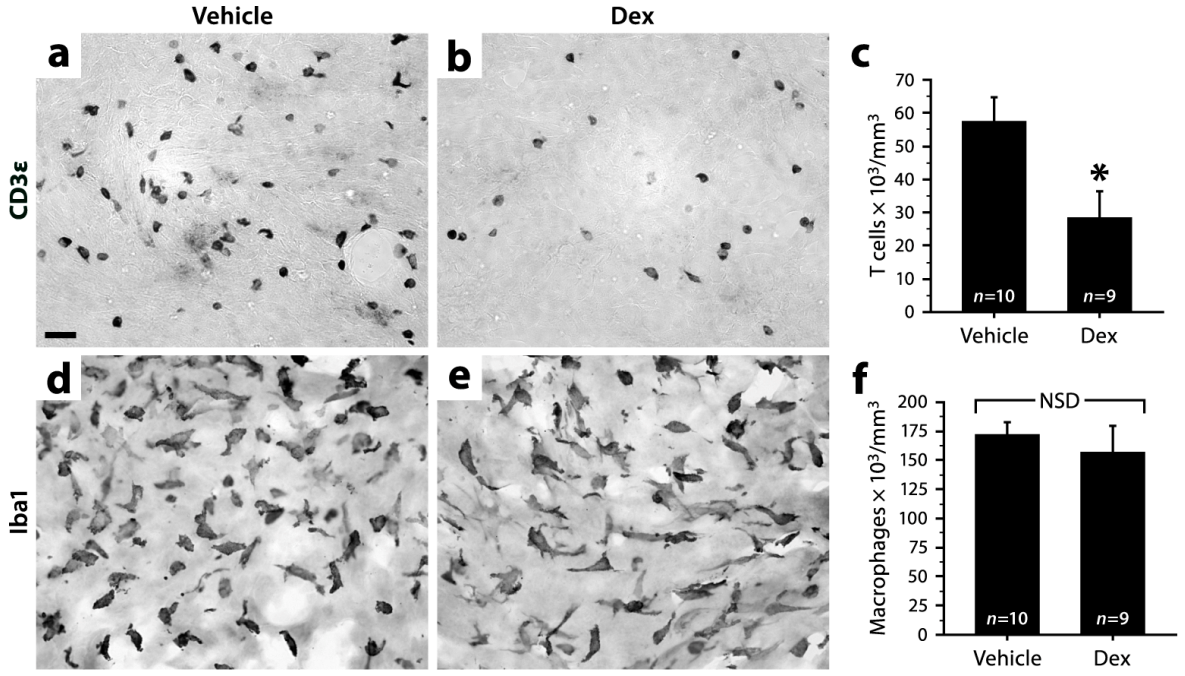


**Figure 14.** Dexamethasone depletes tumor-infiltrating T cells, but not macrophages.

***a,b,*** T cells immunostained for CD3ε in glioma sections from mice injected twice daily for 20 days with vehicle or 1 mg/kg dexamethasone (Dex), respectively. Scale bar: 20 μm (*a,b,d,e*).

***c,*** Stereological analysis revealeed a 51% decrease in the number of tumor-infiltrating T cells in mice treated with dexamethasone. *Student's *t* test, $P < 0.017$. Data are mean ± SE.

***d,e,*** Macrophages immunostained for Iba1 in glioma sections from mice treated with vehicle or dexamethasone, respectively.

***f,*** Stereological analysis showed no intergroup difference in the number of tumor-associated macrophages. Student's *t* test, $P = 0.5$. Data are mean ± SE. NSD, not statistically different.

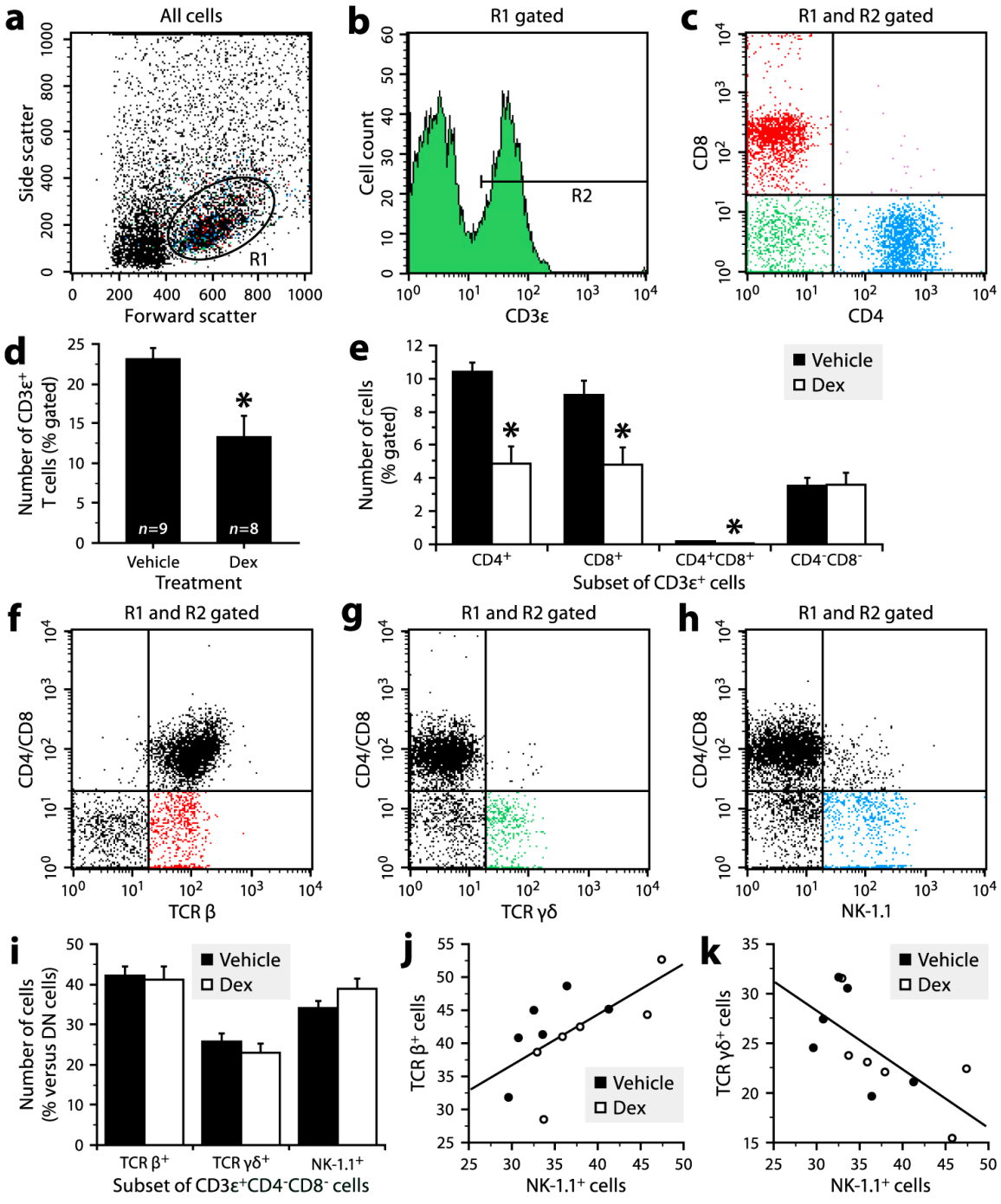
a
All cells
Side scatter
Forward scatter
R1
b
R1 gated
Cell count
CD3ε
R2
c
R1 and R2 gated
CD8
CD4
d
Number of CD3ε+ T cells (% gated)
n=9
n=8
Vehicle
Dex
Treatment
e
Number of cells (% gated)
Vehicle
Dex
CD4+
CD8+
CD4+CD8+
CD4-CD8-
Subset of CD3ε+ cells
f
R1 and R2 gated
CD4/CD8
TCR β
g
R1 and R2 gated
CD4/CD8
TCR γδ
h
R1 and R2 gated
CD4/CD8
NK-1.1
i
Number of cells (% versus DN cells)
Vehicle
Dex
TCR β+
TCR γδ+
NK-1.1+
Subset of CD3ε+CD4-CD8- cells
j
TCR β+ cells
Vehicle
Dex
NK-1.1+ cells
k
TCR γδ+ cells
Vehicle
Dex
NK-1.1+ cells

**Figure 15.** Dexamethasone selectively depletes tumor-infiltrating T cells with helper or cytotoxic function.

***a-c,*** Flow cytometric analysis of cells isolated from a 20-day glioma showing 3 predominant populations of $CD3\varepsilon^+$ T cells.

***d,*** Cell counts revealed a 43% decrease in the overall number of $CD3\varepsilon^+$ cells after treatment with dexamethasone (Dex; 1 mg/kg, twice daily). *Welch's *t* test, $P = 0.0067$. Data are mean ± SE.

***e,*** All populations of $CD3\varepsilon^+$ T cells were sensitive to dexamethasone, except $CD4^-CD8^-$ T cells. *Student's *t* test, $P \leq 0.02$. Data are mean ± SE.

***f-h,*** Phenotypic analysis showing $CD3\varepsilon^+CD4^-CD8^-$ T cells positively labeled for TCR β (red), TCR γδ (green) and NK-1.1 (blue).

***i,*** Cell counts showed no change in the number of double negative (DN) T cells expressing TCR β, TCR γδ or NK-1.1 after dexamethasone treatment. Student's *t* test, $P \geq 0.14$. Data are mean ± SE.

***j, k,*** The number of double negative T cells labeled for NK-1.1 correlated positively with that of TCR $\beta^+$ cells (Pearson correlation, $P = 0.022$, $R = 0.65$) and negatively with that of TCR $\gamma\delta^+$ cells (Pearson correlation, $P = 0.016$, $R = -0.68$).

### 3.5.3 GL261 cells are resistant to dexamethasone

Although it is unlikely that dexamethasone could be used in human at a dose high enough to inhibit brain tumor growth, we reasoned that understanding the mechanism by which dexamethasone exerts its antitumor effect might help to identify a more specific drug able to mimic its beneficial properties without its side effects. To begin exploring this mechanism, we cultured GL261 cells with or without dexamethasone for 3 or 5 days, after which the number of viable cells was counted by flow cytometry. As shown in Figure 16a, the growth of GL261 cells was not influenced by dexamethasone at a concentration as high as 1 μg/ml, suggesting that dexamethasone does not directly affect their proliferation and survival. To support this result and test whether dexamethasone alters the expression of genes important for tumor progression, we extracted RNA from GL261 cells cultured for 24 h with or without 1 μg/ml dexamethasone. The RNA samples were then analyzed using oligonucleotide microarrays interrogating over 39,000 different transcripts. Out of this number, only 16 genes (represented by 17 probe sets) were identified as being differentially expressed ($P < 0.05$) between the treated and control cells (Fig. 16b, Annexe III), and none of which has been previously associated with tumor progression, except Enpp2 (also named autotaxin). However, this secreted lysophospholipase, whose expression was upregulated by dexamethasone (Annexe III), has recently been shown to promote glioma cell migration in vitro [182], which is in contradiction with the possibility that it mediates the antitumor effect of dexamethasone. Overall, these results indicate that GL261 cells are largely insensitive to dexamethasone, suggesting that this drug reduces glioma growth by an indirect mechanism.

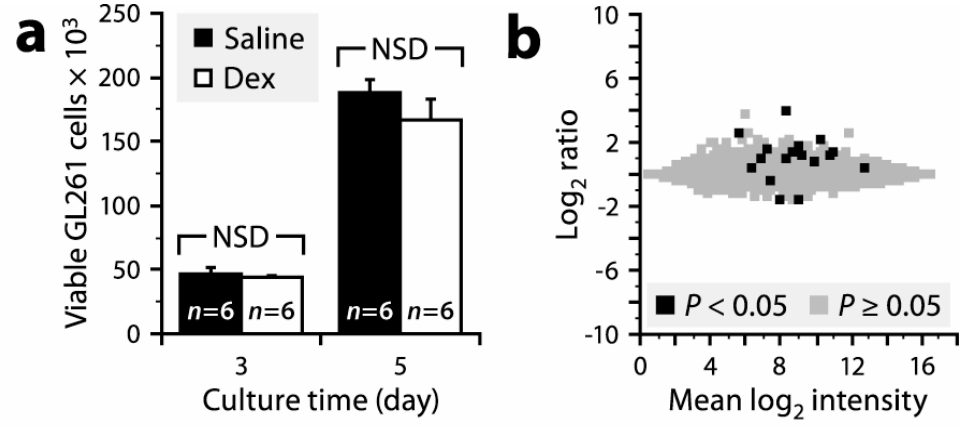


**Figure 16.** Cultured GL261 cells are virtually resistant to dexamethasone.

***a,*** As determined by flow cytometry, the number of viable cells (propidium iodide negative) did not differ between cultures supplemented or not with 1 µg/ml dexamethasone (Dex). Two-way ANOVA (treatment, $P = 0.23$; time, $P < 0.0001$; interaction, $P = 0.36$). Data are mean ± SE. NSD, not statistically different.

***b,*** Microarray analysis revealed minor changes in the transcriptional profile of GL261 cells after exposure to dexamethasone for 24 h. Each data point represents one of the 45,101 probe sets. Only 17 of these probe sets (black squares) had a *P*-value < 0.05 (see Annexe III for details). X-axis, mean of the hybridization intensities of all samples. Y-axis, ratio of the mean hybridization intensities for dexamethasone-treated cells versus control cells.

### 3.5.4 Dexamethasone decreases glioma vascularization

It has been shown that glioma cells grow by co-opting pre-existing blood vessels, which undergo morphological and functional changes and even regress to some extent [15, 17, 163, 183]. As shown in Figure 17a-c, the capillaries of GL261 gliomas are hypertrophied and irregularly shaped compared to those of the adjacent normal tissue. Because these changes are presumably important for glioma growth, we asked whether dexamethasone could normalize certain vascular parameters, such as capillary density and caliber. To address this question, glioma sections, from mice treated or not with dexamethasone and killed 20 days after tumor implantation, were immunostained for the endothelial marker CD31 and analyzed using unbiased stereological methods. We found a slightly decreased tumor vascular density in dexamethasone-treated mice (Fig. 17d), but no significant difference in tumor vessel diameter (Fig. 17e), although a tendency to decrease wasobserved. However, the volume of the tumors correlated better with vessel diameter (Fig.17f) than with vascular density (Fig. 17g). Therefore, these results suggest that although dexamethasone acts on the tumor endothelium, its antineoplastic effect is not a consequence of the reduction in vascularization.

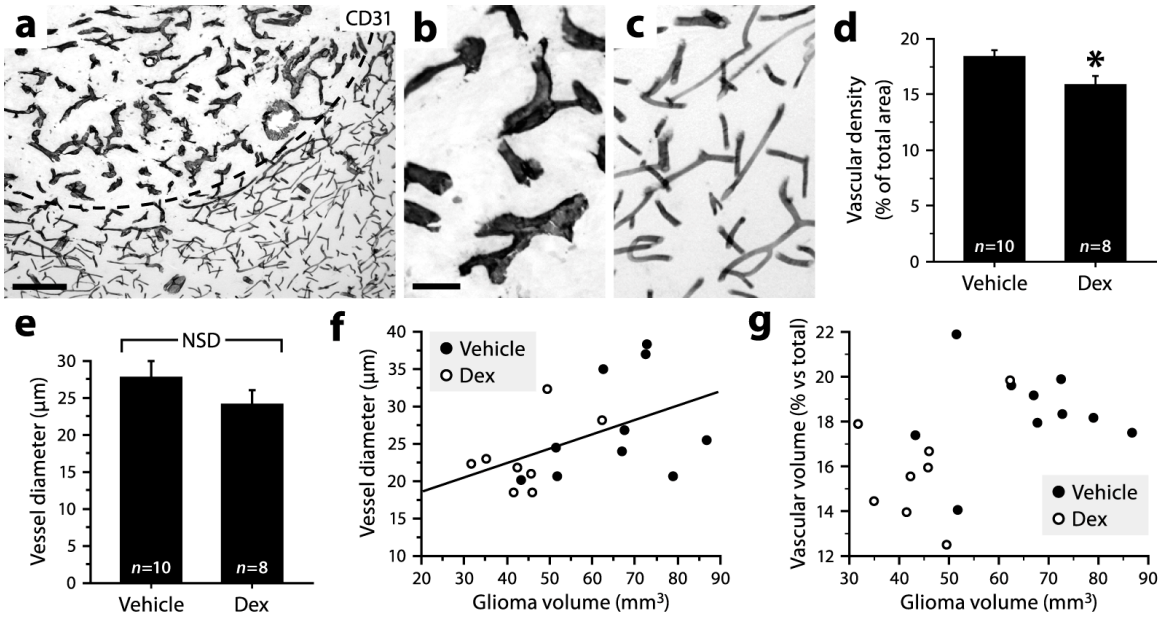


**Figure 17**. Dexamethasone slightly reduces tumor vascular density.

***a,*** Glioma section immunostained for CD31 showing morphological differences between the tumor and adjacent normal vasculature. The dashed line separates the tumor (top) from the non-neoplastic tissue (bottom). Scale bar: 200 µm.

***b, c,*** Higher magnification of capillaries in a glioma and the adjacent non-neoplastic tissue, respectively. Scale bar: 50 µm (b, c).

***d,*** Stereological analysis revealed a 14% decrease in tumor vascular density in mice treated twice daily with 1 mg/kg dexamethasone compared to mock-treated mice. *Student's *t* test, $P = 0.024$. Data are mean ± SE.

***e,*** No difference in tumor vessel caliber was recorded between mice treated or not with dexamethasone. Wilcoxon rank-sum test, $P = 0.2$. Data are mean ± SE.

***f, g,*** A positive correlation was found between glioma volume and vessel diameter (Pearson correlation, $P = 0.041$, $R = 0.49$), but no clear correlation was found between glioma volume and vascular volume (Pearson correlation, $P = 0.053$, $R = 0.46$). Each data point represents a mouse treated with dexamethasone or vehicle.

### 3.5.5 Dexamethasone reduces Angpt2 expression

An alternative hypothesis is that dexamethasone modulates the production of proneoplastic or antineoplastic factors by tumor endothelial cells. To investigate this possibility in a simplified model, we used oligonucleotide microarrays to compare the gene expression profiles of cerebral endothelial cells cultured for 24 h with or without dexamethasone (1 μg/ml). In contrast to what we observed with GL261 cells (Supplementary Table 1), 1253 dexamethasone-sensitive genes (represented by 1455 probe sets) with a P-value < 0.05 were found (Fig. 18a, Annexe IV). To narrow our search, we filtered out probe sets with a fold change between 0.5 and 2.0, and then retained only those classified as "extracellular" in the Gene Ontology database. Among the 83 remaining genes, we selected for further analysis 4 down-regulated ones, namely Angpt2, Tnc and TGFß2, which are known to be associated with certain cancers [184-186], and ESM1, a newly discovered proteoglycan that has been shown to induce tumor formation [187]. Quantitative RT-PCR analysis confirmed that all these genes were strongly repressed by dexamethasone at all doses tested in cultured cerebral endothelial cells (Fig. 18b-e).

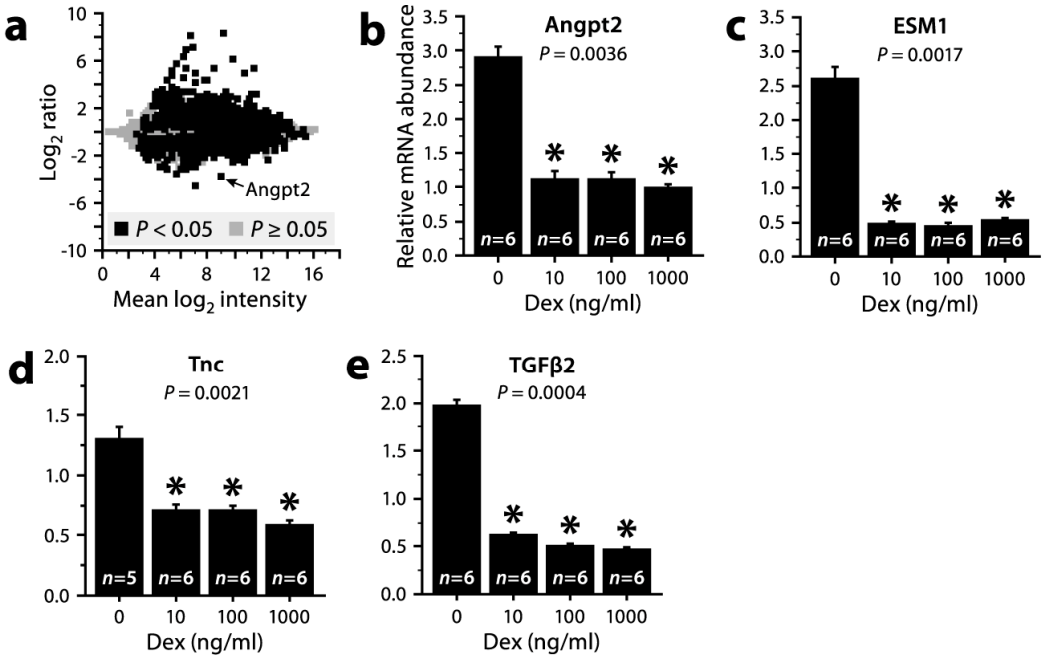


**Figure 18.** Genes modulated by dexamethasone in cultured cerebral endothelial cells.

***a,*** Microarray analysis revealed major changes in the transcriptional profile of bEnd.3 cells after exposure to dexamethasone for 24 h. Each data point represents one of the 45,101 probe sets. 1,455 of these probe sets (black squares) had a *P*-value < 0.05 (see Annexe IV for details). X-axis, mean of the hybridization intensities of all samples. Y-axis, ratio of the mean hybridization intensities for dexamethasone-treated cells versus control cells.
***b-e,*** Quantitative RT-PCR analysis showed reduced levels of Angpt2, ESM1, Tnc and TGFβ2 mRNAs in bEnd.3 cells cultured for 24 h in the presence of different concentrations of dexamethasone (Dex) compared to mock-treated cells. *Kruskal-Wallis test (*P* as indicated) followed by Dunn's test. Data (mean ± SE) are expressed as a ratio to 18S rRNA. Repeat analysis of Angpt2 with normalization to GADPH mRNA instead of 18S rRNA gave similar results (data not shown).

To validate these results in a more complex, in vivo system, glioma-bearing mice were injected twice daily with 1 mg/kg dexamethasone for 2 or 3 weeks, after which their brains were collected for in situ hybridization analysis. Two of the examined transcripts (TGFß2 and ESM1) were not reliably detected and were thus excluded from the study at this point (data not shown). Conversely, strong hybridization signals for Angpt2 and Tnc mRNAs were specifically detected along the tumor vasculature and not in the surrounding non-neoplastic tissue (Fig. 19a,b,e). Stereological analysis revealed an approximately 40% decrease in the number of Angpt2 mRNA+ cells within the tumors of dexamethasone-treated mice at both time points (Fig. 19c), but no change in the case of Tnc mRNA+ cells (Fig. 19f). To complement this result, we estimated the intensity of the hybridization signals for Angpt2 mRNA at the single-cell level by optical density readings, and found that the signals in dexamethasone-treated mice were 38 and 27% less intense than those in controls at 2 and 3 weeks, respectively (Fig. 19d). In other words, not only there were fewer Angpt2 mRNA+ cells in dexamethasone-treated mice, but also these positive cells expressed lower levels of Angpt2 mRNA. These results suggest that dexamethasone could influence glioma vascularization and growth, at least in part, by inhibiting the expression of Angpt2, which is known as a destabilizing factor for the endothelium [184].

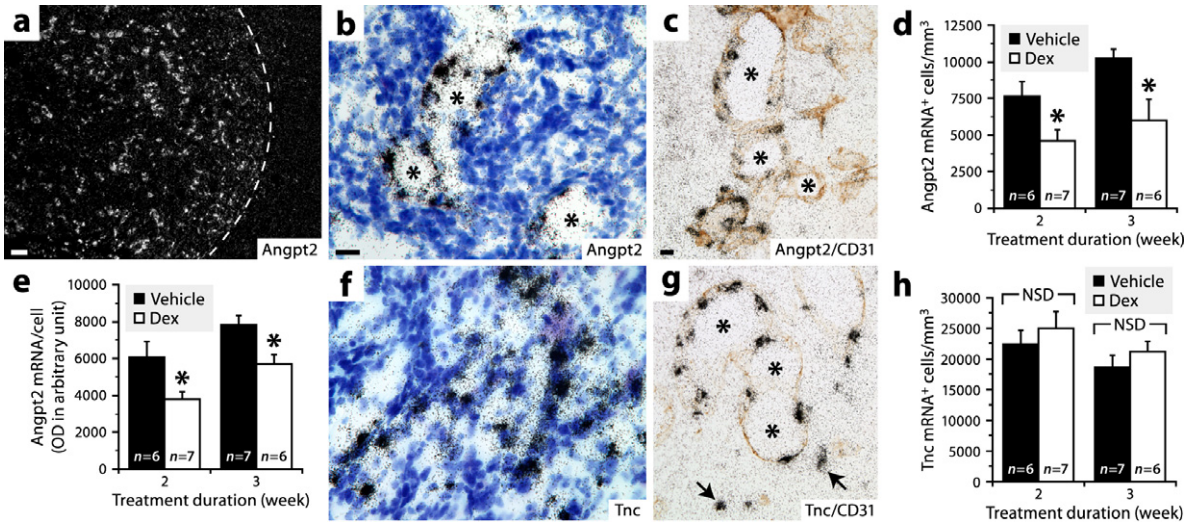


**Figure 19.** Dexamethasone inhibits the endothelial expression of Angpt2 in gliomas, but not that of Tnc.

***a,*** Dark-field photomicrograph showing *in situ* hybridization signals for Angpt2 mRNA in a 20-day glioma. The dashed line separates the tumor (left) from the normal tissue (right). Scale bar: 500 µm.

***b,*** Bright-field image at higher magnification of *in situ* hybridization signals for Angpt2 mRNA (black grains). Blue, thionin counterstaining. *Blood vessel. Scale bar: 20 µm (b, e).

***c,*** Double labeling for Angpt2 mRNA (*in situ* hybridization, black grains) and CD31 (immunohistochemistry, brown). *Blood vessel lumen. Scale bar: 20 µm (c, g).

***d,*** Stereological analysis revealed that the number of Angpt2 $mRNA^+$ cells was ~40% lower in mice treated for 2 or 3 weeks with 1 mg/kg dexamethasone compared to sham-treated mice. *Two-way ANOVA (treatment, $P = 0.0019$; time, $P = 0.065$; interaction, $P = 0.56$) followed by Student's *t* test. Data are mean ± SE.

***e,*** Optical density (OD) analysis of hybridization signals showed that the abundance of Angpt2 mRNA per positive cell was reduced after dexamethasone treatment by 38% at 2 weeks and 27% at 3 weeks. *Two-way ANOVA (treatment, $P = 0.0016$; time, $P = 0.0058$; interaction, $P = 0.87$) followed by Student's *t* test. Data are mean ± SE.

***f,*** Bright-field image of *in situ* hybridization signals for Tnc mRNA (black grains). Blue, thionin counterstaining. ***g,*** Double labeling for Tnc mRNA (*in situ* hybridization, black grains) and CD31 (immunohistochemistry, brown). Note that Tnc mRNA did not always colocalize with CD31 (arrows). *Blood vessel lumen.

***h,*** No intergroup difference in the number of Tnc $mRNA^+$ cells was detected. Two-way ANOVA (treatment, $P = 0.42$; time, $P = 0.12$; interaction, $P = 0.99$). Data are mean ± SE. NSD, not statistically different.

It has been reported that Angpt2 can induce glioma cell invasion by stimulating MMP2 expression [25, 28], which could thus be indirectly repressed by dexamethasone. Furthermore, it has been suggested that dexamethasone can reduce brain tumor-associated vascular permeability by inhibiting VEGFa expression [34, 35]. To determine whether these two genes are repressed in the model used here, we quantified MMP2 and VEGFa mRNAs in our RNA and tissue samples by qRT-PCR and in situ hybridization, respectively. We found that MMP2 was down-regulated by dexamethasone in cultured cerebral endothelial cells, but not in gliomas of mice treated for 2 or 3 weeks with the steroid, whereas VEGFa was not affected by dexamethasone, neither in vitro nor in vivo (Fig. 20).

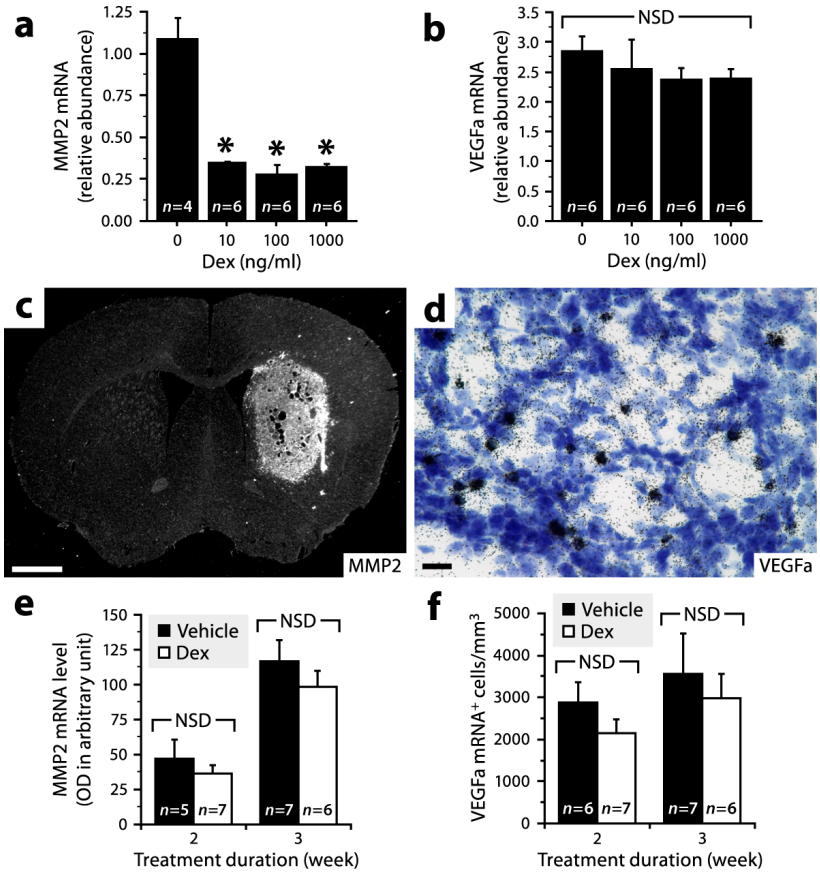


**Figure 20.** Dexamethasone does not affect MMP2 and VEGFa expression *in vivo*, but reduces MMP2 expression *in vitro*.

***a, b,*** Quantitative RT-PCR analysis showed reduced levels of MMP2 mRNA, but not of VEGFa mRNA, in bEnd.3 cells cultured for 24 h in the presence of different concentrations of dexamethasone (Dex) compared to mock-treated cells. *Kruskal-Wallis test ($P = 0.0173$) followed by Dunn's test. Data (mean ± SE) are expressed as a ratio to 18S rRNA.

***c,*** Dark-field photomicrograph of *in situ* hybridization signals for MMP2 mRNA in a 2-week glioma. Note that MMP2 expression is not restricted to the endothelium, but is widespread in the tumor. Scale bar: 1 mm.

***d,*** Bright-field photomicrograph of *in situ* hybridization signals for VEGFa mRNA (black grains) in a 3-week glioma. Blue, thionin counterstaining. Scale bar: 20 µm.

***e,*** Optical densitometric analysis revealed no difference in MMP2 mRNA levels in mice treated or not with 1 mg/kg dexamethasone. *Two-way ANOVA (treatment, $P = 0.24$; time, $P < 0.0001$; interaction, $P = 0.79$). Data are mean ± SE. f, Stereological analysis revealed no difference in the number of VEGFa $mRNA^+$ cells in mice treated or not with 1 mg/kg dexamethasone. *Two-way ANOVA (treatment, $P = 0.25$; time, $P = 0.06$; interaction, $P = 0.12$). Data are mean ± SE.

### 3.5.6 Selective inhibition of Angpt2 reduces glioma growth

Although Angpt2 is known to be expressed in human and experimental gliomas [188], its importance in the growth of these tumors is still unclear. To test the possibility that pharmacological neutralization of Angpt2 reproduces the effects of dexamethasone on glioma growth and vascularization, we treated glioma-bearing mice every other day with a synthetic anti-Angpt2 antibody called L1-10, which has recently been used with success to inhibit the development of epidermoid and colorectal tumor xenografts [189]. Remarkably, we found that L1-10 reduced glioma volume by 50% (Fig. 21a), as evaluated in mice killed 18 days after tumor implantation. Although L1-10 did not cure glioma-bearing mice, it produced a modest increase in their survival (Fig. 21b). No noticeable side effect, such as a chronic reduction in body weight, was associated with the use of L1-10 (Fig. 21c). The antitumor effect of L1-10 was indirect, because the growth of GL261 cells in vitro was not altered after the addition of 5 μM L1-10 to the culture media (Fig. 21d). To examine the effect of L1-10 on the tumor vasculature, we immunostained glioma sections for CD31, and found a small (9%) but significant decrease in tumor vascular density in L1-10-treated mice (Fig. 21e), as observed in the case of dexamethasone (Fig. 17d). In contrast to dexamethasone, L1-10 reduced by 29% tumor vessel diameter (Fig. 21f), which strongly correlated with glioma volume (Fig. 21g). Finally, because it has recently been shown that Angpt2 is involved in inflammatory processes, we asked whether L1-10 influenced the recruitment of immune cells into the tumors. Stereological analysis of sections immunostained for CD3e or Iba1 revealed no significant difference in T cells (Fig. 21h), but a small reduction (17%) in macrophages (Fig. 21i). Collectively, our results ascribed to Angpt2 an important role in glioma development and support the concept that dexamethasone slows glioma growth by a mechanism involving the suppression of Angpt2 expression.

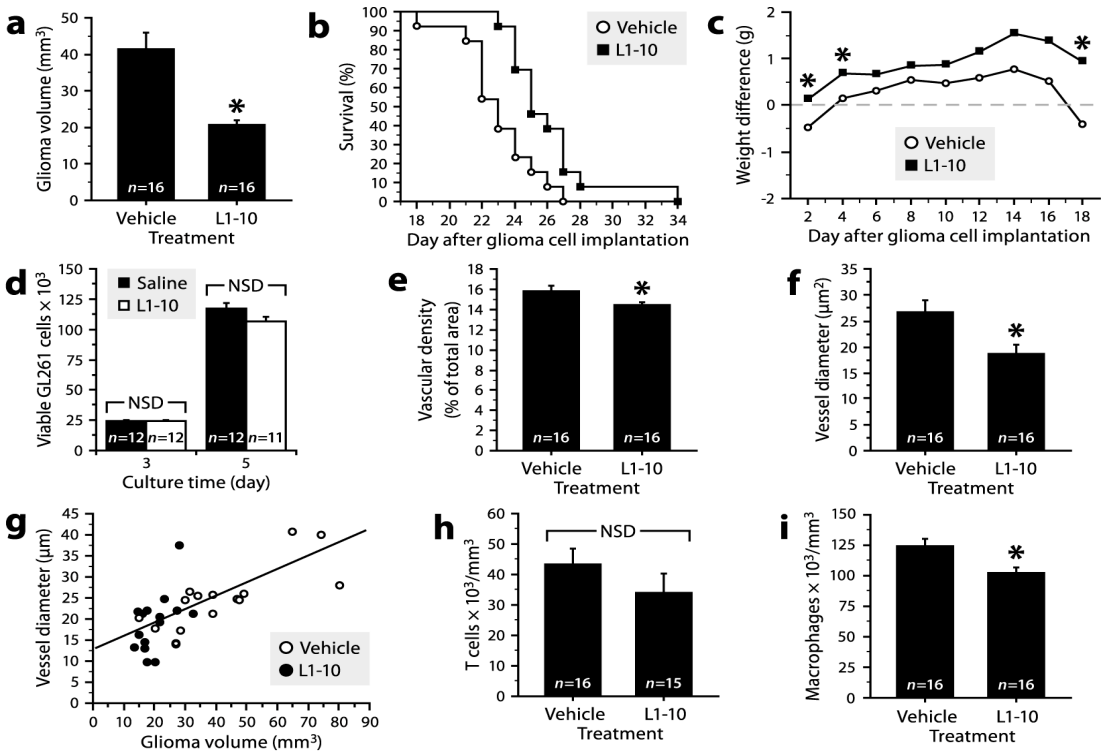


**Figure 21.** Specific neutralization of Angpt2 with L1-10 reduces glioma growth and vascular enlargement without affecting T cell infiltration.

***a,*** Volumetric analysis showed a 50% decrease in glioma volume in L1-10-treated mice. *Wilcoxon rank-sum test, $P = 0.0002$. Data are mean ± SE.

***b,*** Increases in body weight were recorded at the beginning and at the end of experimentation in mice injected with L1-10. *MANOVA with repeated measures ($P = 0.002$) followed by Student's $t$ test ($P < 0.05$). Data are mean change in body weight from the day of tumor implantation ($n = 16$ per group).

***c,*** Kaplan-Meier curves showing a modest increase in the probability of survival after treatment with dexamethasone. Log-rank test, $P = 0.005$ ($n = 13$ per group).

***d,*** As determined by flow cytometry, the growth of GL261 cells in culture was not affected in the presence of 5 μM L1-10. Two-way ANOVA (treatment, $P = 0.1$; time, $P < 0.0001$; interaction, $P = 0.07$). Data are mean ± SE. NSD, not statistically different.

***e,*** Stereological analysis revealed a 9% decrease in tumor vascular density in L1-10-treated mice. *Wilcoxon rank-sum test, $P = 0.03$. Data are mean ± SE.

***f, g,*** Tumor vessel diameter was reduced by 29% in L1-10-treated mice and correlated positively with glioma volume (Pearson correlation, $P = 0.0002$, $R = 0.61$). *Wilcoxon rank-sum test, $P = 0.0053$. Each data point represents a mouse treated with L1-10 or vehicle.

***h,*** No intergroup difference was detected in $CD3^+$ T cell density. Wilcoxon rank-sum test, $P = 0.07$. Data are mean ± SE. ***i,*** A 17% decrease in the number of tumor-associated $Iba1^+$ macrophages was observed after L1-10 treatment. Wilcoxon rank-sum test, $P = 0.004$. Data are mean ± SE.

## 3.4 Discussion

Dexamethasone is one of the most commonly prescribed drugs and is used since the 1960's for the management of edema associated with brain tumors, yet its effects on these tumors are not fully understood. The initial hypothesis tested in this work was that dexamethasone accelerates glioma growth by antagonizing antitumor immune responses. Although this hypothesis proved to be incorrect, four main findings emerge from our work: 1) dexamethasone can exert potential proneoplastic effects by neutralizing important components of the immune system (i.e., cytotoxic and helper T cells), but seems to leave intact other elements such as macrophages, gammadelta and NK T cells; 2) dexamethasone can also exert antineoplastic effects by reducing the expression of at least one angiogenic factor, Angpt2, leading to a partial normalization of the tumor vasculature; 3) the sum of the actions of dexamethasone results in a reduction of glioma growth, but only when it is used at a relatively high concentration associated with adverse effects; 4) selective blockade of Angpt2 with a synthetic antibody reduces glioma growth and vascular enlargement more efficiently than dexamethasone without depleting tumor-infiltrating T lymphocytes and causing notable side effects. This greater efficiency of Angpt2 is presumably due to a more complete neutralization of Angpt2, since dexamethasone only partially inhibits its expression.

Although the matrix-degrading enzyme MMP2 and the angiogenic regulator VEGFa were expressed in our glioma model and might play important growth-promoting roles, our results do not support their involvement in the mechanism by which dexamethasone reduced glioma growth. On the first hand, we expected that dexamethasone would have reduced MMP2 expression in vivo, at least indirectly, because it has been reported that Angpt2 stimulates glioma cells to produce MMP2 [25, 28], and because we found a reduction in MMP2 mRNA in cultured endothelial cells exposed to dexamethasone. However, no change in MMP2 expression was detectable in vivo after dexamethasone treatment. This lack of effect may be due to a difference between the glioma cells studied: GL261 cells strongly and constitutively expressed MMP2 after transplantation, whereas those used by Cheng and colleagues expressed MMP2 in an inducible-manner at the invasive border of the tumor [28]. Therefore, we cannot exclude the possibility that

dexamethasone can reduce the progression of other types of glioma cells by inhibiting MMP2 when this factor is not constitutively produced. On the other hand, we also expected a down-regulation of VEGFa expression by dexamethasone on the basis of two in vitro studies [34, 35]. Although the different nature of the cells used may again explain the difference in our results, it is important to note that one of the research team did not attempt to confirm their results in vivo [34], while the other group did not reproduce the same effect in a subcutaneous glioma model [35]. Similarly to the latter study, we found genes (MMP2 and Tnc) that were sensitive to dexamethasone in culture, but not in vivo, possibly due to differences in pharmacokinetic or the regulatory mechanisms involved. Together, these observations underscore the necessity of confirming in vitro results in more clinically relevant in vivo models.

It has been reported that anti-Angpt2 antibodies can inhibit the growth of subcutaneously implanted tumors and induce their regression [189]. In contrast, our results indicate that gliomas can only be slowed and not cured by anti-Angpt2 therapy. This difference may be explained by several possibilities. First, orthotopic gliomas are probably less dependent on angiogenesis than heterotopic tumors developing in the subcutaneous space. Indeed, it has been shown that glioma cells mainly grow by co-opting existing capillaries and that new blood vessels are only formed in a late phase in response to hypoxia or cell death [15, 17, 163, 183]. Second, the bioavailability of L1-10 might be lower in gliomas compared to peripheral tumors due to the presence of the blood-brain barrier. In future studies, it will be important to examine whether the effectiveness of L1-10 against cerebral tumors can be enhanced by using a higher dose or alternative delivery mean. Third, it is possible that GL261 cells are more resistant to hypoxia or inadequate supply of serum growth factors than other tumor cell lines. It remains to be determined whether all types of glioma cells are equally sensitive to Angpt2 inhibitors. Finally, we cannot exclude the possibility that another angiogenic factor partially compensates for the reduction in Angpt2 in gliomas, although no naturally occurring agonist of Angpt2 is currently known, except perhaps Angpt3 [190]. However, the latter was not detectable in GL261 gliomas by in situ hybridization (unpublished personal observation).

During glioma progression, the vasculature undergoes structural and functional changes, resulting in vascular cell apoptosis and blood vessel regression. It has been postulated that this regression is caused by the action of Angpt2 in the absence of VEGFa [15, 17, 163]. Our results do not support this concept, because VEGFa was expressed at all time examined and L1-10 treatment reduced vascular density, suggesting rather that Angpt2 somehow limits vascular regression in our model. However, this effect does not explain the proneoplastic activity of Angpt2, because we observed no clear correlation between vascular density and glioma volume. Another effect of Angpt2 that did correlate with glioma volume is the increase in vascular caliber. We propose that this effect is accompanied by changes in vascular physiology and that some of which are directly responsible for the proneoplastic activity of Angpt2. At least three mechanisms can be imagined: 1) Angpt2 could increase vascular permeability, thereby providing glioma cells with a better access to nutrients and growth factors; 2) it could induce structural alterations in the vascular wall that would facilitate the process of co-option and the migration of glioma cells along the vasculature, a phenomenon recently observed [183]; and 3) it could promote the recruitment of a subpopulation monocytic cells with proangiogenic activity, identified as Tie2-expressing monocytes [191], by stimulating the expression of adhesion molecules, such as ICAM1 and VCAM1 [192]. This latter effect would explain the reduction in tumor-associated macrophages observed after L1-10 treatment.

It is generally known that glucocorticoids can deplete lymphocytes by inducing apoptosis and inhibiting the expression of adhesion molecules and cytokines involved in their recruitment across the endothelium [168]. The reduced number of tumor-infiltrating helper and cytotoxic T cells observed after dexamethasone treatment in this study was thus predictable. Unexpected was the discovery of a new property of gammadelta and NK T cells, that of being resistant to dexamethasone. Gammadelta T cells distinguish from other T lymphocytes by their ability to recognize soluble protein and non-protein antigens in a MHC-independent manner [193]. NK T cells are also MHC-unrestricted, but recognize mainly glycolipids presented by the CD1d molecule [194]. Mounting evidence suggests that most gammadelta and NK T cells contribute to antitumor immunity by exerting cytotoxic effects or influencing the activity of other cell types by secreting a variety of cytokines [195-197]. On the contrary, however, a subset of NK T cells known as Type II

has been shown to repress antitumor immune responses [197, 198]. Interestingly, we found an inverse correlation between gammadelta and NK T cells, but further investigation is required to determine the significance of this observation; for example, whether one of these cells inhibits the other one. Nevertheless, it could be useful to develop immunotherapy using gammadelta and NK T cells, not only because patients with brain tumors are treated with dexamethasone, but also because MHC alleles are frequently down-regulated during cancer progression. Our ability to manipulate these cells for therapeutic purposes will depend on a better understanding of their roles and the mechanisms that govern their development and activities. In the mean time, the finding that NK T cells collected from patients with glioma can kill glioma cells in culture is encouraging [199].

In conclusion, this study not only helps to better understand the effects of dexamethasone on brain tumors, but also reveals a more specific agent, L1-10, that mimics beneficial properties of dexamethasone without the detrimental ones. In future work, it will be important to determine whether Angpt2 inhibitors could substitute dexamethasone or be used in combination with it, and whether they can enhance the efficacy of chemotherapeutic drugs, as recently proposed [200]. Finally, it could be useful to seek other proneoplastic genes repressed by dexamethasone in order to identify new potential targets for the treatment of malignant cerebral tumors.

# 4. Discussion générale et conclusion

Bien que le système immunitaire soit primordial pour la survie de l'être humain en le défendant contre plusieurs types d'agressions; une réponse inflammatoire persistante peut, à l'inverse, occasionner d'importants dommages à l'organisme. La réponse immune survenant durant le développement d'une tumeur illustre clairement cette réalité. Les macrophages, comptant parmi les effecteurs principaux de cette réponse, sont au centre de ce dilemme. La reconnaissance des cellules tumorales par les macrophages engendre, comme nous l'avons vu, la production d'une multitude de substances biologiquement actives, dont des cytokines, pouvant exercer des effets très variés. Ces composés ont souvent des actions chevauchantes et ne sont pas nécessairement produits uniquement par les macrophages. La situation est d'autant plus complexe que la tumeur démontre en plus une formidable capacité à s'y adapter.

L'intérêt principal du projet présenté dans ce mémoire est qu'il nous a permis de clarifier le rôle des macrophages dans le développement des tumeurs cérébrales malignes. Nos résultats démontrent que le recrutement des macrophages à l'intérieur de la tumeur corrèle avec une diminution de sa croissance. Cette conclusion apparaît en désaccord avec plusieurs études dont les résultats favorisent un rôle pro-tumoral des macrophages. Ces résultats sont, pour la plupart, issus d'expériences réalisées *in vitro*, et donc moins représentatives. Autrement, il est tout-à-fait possible que les macrophages sécrètent des agents pro-tumoraux. Seulement, l'effet de ces derniers doit être mineur relativement au pouvoir anti-tumoral des macrophages. Quant à notre modèle, il offre l'avantage de suivre l'évolution de la tumeur dans un contexte immunitaire et une localisation normale. Il s'agit sans doute, pour l'instant, d'un des paradigmes permettant de mimer le plus adéquatement une situation réelle. Bien sûr, ce résultat reste général et le mécanisme d'action précis demeure inconnu. Toutefois, certaines évidences permettent de croire que les macrophages peuvent exercer leur action de façon directe ou indirecte. C'est-à-dire, par exemple, en produisant des composés ayant une activité cytotoxique sur les cellules tumorales ou encore en aidant au recrutement d'autres populations cellulaires comme les lymphocytes T cytotoxiques.

Ces résultats permettront d'orienter les futures recherches, premièrement pour identifier plus précisément les mécanismes impliqués et ensuite pour développer de nouvelles thérapies. À ce titre, l'utilité de la réponse immune dans le contrôle de la croissance tumorale a engendré un questionnement sur l'efficacité d'une thérapie couramment utilisée : l'administration d'agents anti-inflammatoires. Nous avons donc vérifié l'effet d'un tel traitement sur les glioblastomes implantés chez la souris. Les résultats obtenus démontrent que l'action délétère de la dexaméthasone sur les lymphocytes T n'est pas observable sur toutes les sous-populations de lymphocytes T. En effet, les lymphocytes T γδ et NKT semblent insensibles à son influence. La dexaméthasone exerce en outre des effets indépendants de l'altération de la réponse inflammatoire permettant ainsi de réduire le développement tumoral. Pour l'instant, les recherches de notre équipe se sont principalement orientées vers l'élucidation de son action et ont permis de démontrer l'efficacité d'un anticorps synthétique (L1-10) contre l'Angpt-2 pour réduire la croissance tumorale de façon plus efficace que la dexamethasone. Cet agent présente donc un intérêt certain en chimiothérapie des gliomes malins.

Par ailleurs, les travaux présentés apportent un support considérable à la possibilité d'utiliser l'immunothérapie pour traiter les glioblastomes. Tout d'abord, puisque nos résultats démontrent l'utilité des macrophages pour limiter la croissance des tumeurs cérébrales, il serait intéressant d'exploiter ces cellules. Deux principaux moyens sont envisageables : favoriser leur activation *in vivo* par l'administration de cytokines telles que le TNF et l'INF-γ ou, alternativement, prélever des cellules chez le patient afin de les mettre en culture et de les activer *in vitro* avant de les leur réinjecter [84]. Cette dernière possibilité apparaît plus judicieuse en permettant la maturation des macrophages en l'absence des contraintes immunosuppressives de l'environnement tumoral. Pour l'instant, les études réalisées avec des procédés comme ceux-ci n'ont pas donné de résultats très encourageants. Toutefois, peu d'effets secondaires ont été observés chez les patients ayant participé à ces études, ce qui encourage à poursuivre et améliorer les tentatives de ce genre [84].

Dans un deuxième temps, nos résultats suggèrent qu'il serait aussi intéressant d'exploiter les lymphocytes T. Plusieurs stratégies d'activation et de transplantation de lymphocytes T cytotoxiques sont envisageables. Dans la mesure ou un antigène tumoral est connu, il est possible de prélever des lymphocytes chez les personnes atteintes afin de les activer *ex vivo* avant de les leur réinjecter. Ces cellules pourront par contre, une fois de plus, être la cible des mécanismes immunosuppresseurs de la tumeur. Il peut être envisageable de contrer, du moins en partie, ce problème en transfectant les cellules T avec des formes dominantes négatives de récepteurs pour des agents immunosuppresseurs produits par la tumeur comme le TGF-β [201]. Une autre stratégie, toute récente, permet aussi de contourner le problème de la diminution de la présentation antigénique par les cellules tumorales. Des cellules T sont prélevées et sont manipulées pour exprimer un récepteur de cellules T chimérique. Ce dernier se compose d'un domaine de reconnaissance à l'antigène cible jumelé avec les domaines signalétiques des molécules importantes à leur activation. Ce procédé permet aux lymphocytes T de reconnaître l'antigène sous forme native, sans qu'il ne soit présenté par une molécule de CMH [202]. De plus, l'activation survient même si la cellule tumorale ne fournit pas de signal de costimulation puisque la reconnaissance de l'antigène par le récepteur chimérique suffit à engendrer l'ensemble de la signalisation nécessaire à l'activation et la prolifération des lymphocytes T cytotoxiques [202].

Malheureusement, pour l'instant, peu d'antigènes tumoraux intéressants à exploiter en thérapie ont pu être identifiés. Cependant, quelques stratégies permettent de tirer profit des lymphocytes T sans connaître spécifiquement un antigène tumoral; ce qui est d'ailleurs une limitation particulièrement importante dans le cas des gliomes. L'une d'elles consiste à isoler plusieurs populations de lymphocytes T intra-tumorales (TIL) pour ensuite tester leur activité cytotoxique contre les cellules tumorales. Les lignées répondant positivement peuvent ensuite être multipliées *in vivo* avant d'être réinjectées au patient [203]. Une dernière possibilité consiste à vacciner le patient avec des CPA (préférablement des DC) qui ont été exposées, *ex vivo*, à un lysat de cellules tumorales. Les CPA pourront capter les antigènes tumoraux et les présenter efficacement aux lymphocytes T lorsqu'elles seront réintroduites chez le patient [204, 205].

Les lymphocytes T cytotoxiques ne constituent toutefois pas la seule population de lymphocytes retrouvée dans les glioblastomes. Comme nous avons pu le démontrer dans le deuxième volet de notre étude, des cellules T exprimant le récepteur constitué des sous-unités γ et δ et les cellules NKT y sont aussi présentes et ne semblent pas affectées par un traitement anti-inflammatoire. Ces deux types cellulaires pourraient donc se révéler particulièrement utiles en immunothérapie des tumeurs cérébrales. L'activité cytotoxique de cellules T γδ prélevées chez des patients atteints de gliomes a été démontrée *in vitro* [206]. Ces cellules peuvent être activées par plusieurs types d'antigènes non-conventionnels qui ne dépendent pas du CMH. *Ex vivo*, une des façon les plus efficaces de les activer est de les exposer à des phosphoantigènes synthétiques [196]. Ceux-ci permettent de les activer efficacement en plus de promouvoir leur activité cytotoxique dépendante de l'IFN-γ et du système perforine-granzyme. Il est probable que l'injection de phosphoantigènes pourrait être envisageable chez l'humain. D'autres molécules, dont les aminobiphosphonates, déjà utilisées dans le traitement de l'ostéoporose, ont un effet semblable sur les cellules γδ et sont donc d'un intérêt certain [207]. Les aminobiphosphonates présentent en plus l'avantage de pouvoir exercer une action directe sur les cellules tumorales en inhibant leurs propriétés adhésives et en induisant leur apoptose [208]. Toutefois, le développement de telles thérapies est freiné par le fait que les cellules γδ murines ne répondent pas aux phosphoantigènes, ce qui limite la conduite d'études pré-cliniques [196]. Pour l'instant, des résultats intéressants ont pu être obtenu en transplantant des cellules humaines chez des souris immunodéficientes [209].

De même, les cellules NKT sont indépendantes des molécules de CMH classiques et dépendent plutôt de la présentation d'antigènes lipidiques par la molécule CD1d. Il en existe différents types démontrant une activité cytotoxique contre les cellules tumorales via la production de perforine, de granzyme, de TNF ou l'expression de FasL. Elles peuvent être activées efficacement par l'utilisation de l'α-galactosylceramide (α-GalCer), un composé dérivé de l'éponge de mer [210]. Les études réalisées jusqu'à maintenant ont démontré que la réponse des cellules NKT était plus forte et prolongée lorsque les patients étaient vaccinés avec des cellules dendritiques préalablement exposées à l'α-GalCer plutôt que lorsque cette molécule était injectée directement [211]. Aussi, ce procédé a démontré son efficacité pour tuer des cellules gliomales en culture [199].

L'immunothérapie apparaît une avenue prometteuse dans l'élaboration de nouvelles thérapies contre les tumeurs cérébrales. Plusieurs stratégies sont imaginables et certaines font l'objet d'études cliniques. Les résultats sont souvent encourageants en permettant de prolonger la vie des patients. Cependant, il demeure extrêmement rare de pouvoir observer la régression de tumeurs. Puisque les approches testées jusqu'à maintenant sont apparues sécuritaires en ayant peu d'effets secondaires indésirables, il est primordial de poursuivre la recherche dans le but de perfectionner ces techniques. Pour ce faire, il est avant tout important d'investir des efforts dans la compréhension des mécanismes fondamentaux qui gouvernent la réponse immunitaire anti-tumorale. La poursuite d'études de qualité dans ce domaine nécessite aussi de développer des modèles animaux qui soient le plus représentatif possible de l'être humain. Les modèles actuels présentent certaines lacunes évidentes, l'une d'entre elles étant le manque d'hétérogénéité génétique et antigénique des tumeurs issues d'une même population cellulaire. Dans la réalité, plusieurs mutations différentes peuvent être à l'origine de la formation d'un gliome et ainsi influencer le comportement de ces tumeurs. Pour résoudre ce problème, il est nécessaire d'utiliser des animaux chez lesquels des tumeurs peuvent se former spontanément. Des modèles animaux plus représentatifs sont un outil essentiel pour faciliter la progression des études pré-cliniques vers la phase clinique.

Par ailleurs, le développement de l'immunothérapie ne signifie pas qu'il faille abandonner les méthodes conventionnelles de traitements. En effet, la chirurgie, la radiothérapie et la chimiothérapie resteront des traitements de première ligne nécessaires pour réduire le volume des tumeurs. Les fractions particulièrement envahissantes de la tumeur, impossibles à cibler efficacement avec ces approches, pourront être attaquées grâce à la grande spécificité de l'immunothérapie. De plus, pour éviter que la tumeur puisse contourner la réponse immunitaire, il sera nécessaire de combiner plusieurs approches. Idéalement, il faudrait pouvoir favoriser une augmentation de l'immunogénicité des cellules tumorales pour qu'elles soient facilement reconnaissables par les macrophages ou les lymphocytes T. Ces dernières cellules pourraient alors être manipulées afin d'accroître leurs fonctions effectrices permettant de tuer les cellules tumorales. Finalement, les mécanismes d'évasion de la tumeur devraient être supprimés.

Dans une perspective très pratique, un dernier obstacle à franchir demeure l'application de ces thérapies à grande échelle sur l'humain. Les approches imaginées nécessitent souvent des manipulations complexes qui doivent parfois être adaptées à chaque patient, en particulier dans le cas de thérapies cellulaires. L'élaboration de ces traitements requiert des installations et des produits dont la qualité est hautement contrôlée. Ces éléments peuvent se révéler particulièrement dispendieux et peu accessibles. Il sera donc important de chercher à développer des stratégies permettant d'augmenter la disponibilité de ces méthodes thérapeutiques.

En conclusion, cette étude a permis de révéler avec plus de précison le rôle joué par les macrophages dans le développement des tumeurs cérébrales malignes. Il apparaît maintenant qu'ils exercent une action positive en permettant de réduire la croissance de la tumeur. Beaucoup de travail reste encore à accomplir pour comprendre précisément les mécanismes impliqués, qu'ils soient directs ou indirects. Néanmoins, ces constatations soulevaient un questionnement quant à l'utilisation courante d'anti-inflammatoires, comme la dexaméthasone, dans la thérapie de ces tumeurs. En fait, nos travaux ont permis d'identifier de nouveaux mécanismes d'action de la dexaméthasone qui, étonnament, permettent de lutter contre l'invasion tumorale. De surcroît, l'un de ces mécanismes, l'inhibition de l'expression de l'Angpt2, a pu être recréé de façon plus spécifique grâce à un nouvel anticorps synthétique spécifique (L1-10). Ce traitement s'est révélé particulièrement efficace et constitue donc une nouvelle possibilité de traitement intéressante. Finalement, l'insensibilité de certaines cellules immunitaires à cet agent offre une voie avantageuse à explorer pour l'élaboration de traitements basés sur l'immunothérapie.

# 5. Bibliographie


1. Jemal, A., et al., *Cancer statistics, 2006.* CA Cancer J Clin, 2006. **56**(2): p. 106-30.
2. Dai, C. and E.C. Holland, *Astrocyte differentiation states and glioma formation.* Cancer J, 2003. **9**(2): p. 72-81.
3. Shih, A.H. and E.C. Holland, *Developmental neurobiology and the origin of brain tumors.* J Neurooncol, 2004. **70**(2): p. 125-36.
4. Agius, L.M., *Justification of glioma biology beyond a cellular basis of interpretation.* Med Hypotheses, 2003. **61**(4): p. 486-94.
5. Pilkington, G.J., *Cancer stem cells in the mammalian central nervous system.* Cell Prolif, 2005. **38**(6): p. 423-33.
6. Soltysova, A., V. Altanerova, and C. Altaner, *Cancer stem cells.* Neoplasma, 2005. **52**(6): p. 435-40.
7. Sanai, N., A. Alvarez-Buylla, and M.S. Berger, *Neural stem cells and the origin of gliomas.* N Engl J Med, 2005. **353**(8): p. 811-22.
8. Kleihues, *WorldHealth Organization classification of tumours: Vol. 1. Pathology and genetics of tumours of the nervous system.* 2000, Lyon: IARC Press.
9. DeAngelis, L.M., *Brain tumors.* N Engl J Med, 2001. **344**(2): p. 114-23.
10. Ichimura, K., et al., *Molecular pathogenesis of astrocytic tumours.* J Neurooncol, 2004. **70**(2): p. 137-60.
11. Ali-Osman, *Brain Tumors*. Comtemporary Cancer Research, ed. Nickoloff. 2005, Totowa: Humana Press.
12. Mitchell, P., D.W. Ellison, and A.D. Mendelow, *Surgery for malignant gliomas: mechanistic reasoning and slippery statistics.* Lancet Neurol, 2005. **4**(7): p. 413-22.
13. Berger, P., *Textbook of Neuro-Oncology*. 2005, Philadelphia: Elsevier Saunders.
14. McKinley, B.P., et al., *The impact of age and sex on the incidence of glial tumors in New York state from 1976 to 1995.* J Neurosurg, 2000. **93**(6): p. 932-9.
15. Zagzag, D., et al., *Vascular apoptosis and involution in gliomas precede neovascularization: a novel concept for glioma growth and angiogenesis.* Lab Invest, 2000. **80**(6): p. 837-49.
16. Hanahan, D. and J. Folkman, *Patterns and emerging mechanisms of the angiogenic switch during tumorigenesis.* Cell, 1996. **86**(3): p. 353-64.
17. Holash, J., et al., *Vessel cooption, regression, and growth in tumors mediated by angiopoietins and VEGF.* Science, 1999. **284**(5422): p. 1994-8.
18. Suri, C., et al., *Increased vascularization in mice overexpressing angiopoietin-1.* Science, 1998. **282**(5388): p. 468-71.
19. Maisonpierre, P.C., et al., *Angiopoietin-2, a natural antagonist for Tie2 that disrupts in vivo angiogenesis.* Science, 1997. **277**(5322): p. 55-60.
20. Wang, G.L. and G.L. Semenza, *General involvement of hypoxia-inducible factor 1 in transcriptional response to hypoxia.* Proc Natl Acad Sci U S A, 1993. **90**(9): p. 4304-8.
21. Semenza, G.L., *HIF-1 and tumor progression: pathophysiology and therapeutics.* Trends Mol Med, 2002. **8**(4 Suppl): p. S62-7.
22. Semenza, G.L., *Targeting HIF-1 for cancer therapy.* Nat Rev Cancer, 2003. **3**(10): p. 721-32.

23. Shweiki, D., et al., *Vascular endothelial growth factor induced by hypoxia may mediate hypoxia-initiated angiogenesis.* Nature, 1992. **359**(6398): p. 843-5.
24. Plate, K.H., et al., *Vascular endothelial growth factor is a potential tumour angiogenesis factor in human gliomas in vivo.* Nature, 1992. **359**(6398): p. 845-8.
25. Hu, B., et al., *Angiopoietin 2 induces glioma cell invasion by stimulating matrix metalloprotease 2 expression through the alphavbeta1 integrin and focal adhesion kinase signaling pathway.* Cancer Res, 2006. **66**(2): p. 775-83.
26. Lampert, K., et al., *Expression of matrix metalloproteinases and their tissue inhibitors in human brain tumors.* Am J Pathol, 1998. **153**(2): p. 429-37.
27. Chintala, S.K., J.C. Tonn, and J.S. Rao, *Matrix metalloproteinases and their biological function in human gliomas.* Int J Dev Neurosci, 1999. **17**(5-6): p. 495-502.
28. Hu, B., et al., *Angiopoietin-2 induces human glioma invasion through the activation of matrix metalloprotease-2.* Proc Natl Acad Sci U S A, 2003. **100**(15): p. 8904-9.
29. Kettenman, R., *Neuroglia*. 2005, New York: Oxford University Press.
30. Fadul, C., et al., *Morbidity and mortality of craniotomy for excision of supratentorial gliomas.* Neurology, 1988. **38**(9): p. 1374-9.
31. Sawaya, R., *Extent of resection in malignant gliomas: a critical summary.* J Neurooncol, 1999. **42**(3): p. 303-5.
32. Kaal, E.C. and C.J. Vecht, *The management of brain edema in brain tumors.* Curr Opin Oncol, 2004. **16**(6): p. 593-600.
33. Galicich, J.H., L.A. French, and J.C. Melby, *Use of dexamethasone in treatment of cerebral edema associated with brain tumors.* J Lancet, 1961. **81**: p. 46-53.
34. Heiss, J.D., et al., *Mechanism of dexamethasone suppression of brain tumor-associated vascular permeability in rats. Involvement of the glucocorticoid receptor and vascular permeability factor.* J Clin Invest, 1996. **98**(6): p. 1400-8.
35. Machein, M.R., et al., *Differential downregulation of vascular endothelial growth factor by dexamethasone in normoxic and hypoxic rat glioma cells.* Neuropathol Appl Neurobiol, 1999. **25**(2): p. 104-12.
36. Wen, P.Y.M.L.C.G.D., *Management of non-neoplastic problems in brain tumor patients in Cancer of the nervous system*. Black, P.M.; Loeffler J.S. ed. 2005, Philadelphia.
37. Walker, M.D., et al., *Evaluation of BCNU and/or radiotherapy in the treatment of anaplastic gliomas. A cooperative clinical trial.* J Neurosurg, 1978. **49**(3): p. 333-43.
38. Vaupel, P. and A. Mayer, *Hypoxia and anemia: effects on tumor biology and treatment resistance.* Transfus Clin Biol, 2005. **12**(1): p. 5-10.
39. DeAngelis, L.M., et al., *Malignant glioma: who benefits from adjuvant chemotherapy?* Ann Neurol, 1998. **44**(4): p. 691-5.
40. *Randomized trial of procarbazine, lomustine, and vincristine in the adjuvant treatment of high-grade astrocytoma: a Medical Research Council trial.* J Clin Oncol, 2001. **19**(2): p. 509-18.
41. Shapiro, W.R., et al., *Randomized trial of three chemotherapy regimens and two radiotherapy regimens and two radiotherapy regimens in postoperative treatment of malignant glioma. Brain Tumor Cooperative Group Trial 8001.* J Neurosurg, 1989. **71**(1): p. 1-9.

42. Regina, A., et al., *Multidrug resistance in brain tumors: roles of the blood-brain barrier.* Cancer Metastasis Rev, 2001. **20**(1-2): p. 13-25.
43. Mariani, L., et al., *Intratumoral arteriovenous shunting in malignant gliomas.* Neurosurgery, 2001. **48**(2): p. 353-7; discussion 357-8.
44. Brem, H. and P. Gabikian, *Biodegradable polymer implants to treat brain tumors.* J Control Release, 2001. **74**(1-3): p. 63-7.
45. Westphal, M., et al., *Gliadel((R)) wafer in initial surgery for malignant glioma: long-term follow-up of a multicenter controlled trial.* Acta Neurochir (Wien), 2006. **148**(3): p. 269-275.
46. Brem, H., et al., *Placebo-controlled trial of safety and efficacy of intraoperative controlled delivery by biodegradable polymers of chemotherapy for recurrent gliomas. The Polymer-brain Tumor Treatment Group.* Lancet, 1995. **345**(8956): p. 1008-12.
47. Liu, Y. and M. Hu, *P-glycoprotein and bioavailability-implication of polymorphism.* Clin Chem Lab Med, 2000. **38**(9): p. 877-81.
48. Rainov, N.G., *A phase III clinical evaluation of herpes simplex virus type 1 thymidine kinase and ganciclovir gene therapy as an adjuvant to surgical resection and radiation in adults with previously untreated glioblastoma multiforme.* Hum Gene Ther, 2000. **11**(17): p. 2389-401.
49. Prados, M.D., et al., *Treatment of progressive or recurrent glioblastoma multiforme in adults with herpes simplex virus thymidine kinase gene vector-producer cells followed by intravenous ganciclovir administration: a phase I/II multi-institutional trial.* J Neurooncol, 2003. **65**(3): p. 269-78.
50. Hoption Cann, S.A., J.P. van Netten, and C. van Netten, *Dr William Coley and tumour regression: a place in history or in the future.* Postgrad Med J, 2003. **79**(938): p. 672-80.
51. Malmberg, K.J., *Effective immunotherapy against cancer: a question of overcoming immune suppression and immune escape?* Cancer Immunol Immunother, 2004. **53**(10): p. 879-92.
52. Burnet, F.M., *The concept of immunological surveillance.* Prog Exp Tumor Res, 1970. **13**: p. 1-27.
53. Rygaard, J. and C.O. Povlsen, *The mouse mutant nude does not develop spontaneous tumours. An argument against immunological surveillance.* Acta Pathol Microbiol Scand [B] Microbiol Immunol, 1974. **82**(1): p. 99-106.
54. Van Pel, A. and T. Boon, *Protection against a nonimmunogenic mouse leukemia by an immunogenic variant obtained by mutagenesis.* Proc Natl Acad Sci U S A, 1982. **79**(15): p. 4718-22.
55. Dempsey, P.W., S.A. Vaidya, and G. Cheng, *The art of war: Innate and adaptive immune responses.* Cell Mol Life Sci, 2003. **60**(12): p. 2604-21.
56. Janeway, C., *Immunobiologie*. 2003, Paris: De Boeck Université.
57. Burke B, L.C., *The macrophage*. 2002, Oxford (NY): Oxford University Press.
58. Medzhitov, R. and C. Janeway, Jr., *The Toll receptor family and microbial recognition.* Trends Microbiol, 2000. **8**(10): p. 452-6.
59. Medzhitov, R. and C. Janeway, Jr., *Innate immune recognition: mechanisms and pathways.* Immunol Rev, 2000. **173**: p. 89-97.
60. Medzhitov, R. and C.A. Janeway, Jr., *How does the immune system distinguish self from nonself?* Semin Immunol, 2000. **12**(3): p. 185-8; discussion 257-344.

61. Takeda, K., T. Kaisho, and S. Akira, *Toll-like receptors.* Annu Rev Immunol, 2003. **21**: p. 335-76.
62. Rock, F.L., et al., *A family of human receptors structurally related to Drosophila Toll.* Proc Natl Acad Sci U S A, 1998. **95**(2): p. 588-93.
63. Srivastava, P., *Roles of heat-shock proteins in innate and adaptive immunity.* Nat Rev Immunol, 2002. **2**(3): p. 185-94.
64. Asea, A., et al., *Novel signal transduction pathway utilized by extracellular HSP70: role of toll-like receptor (TLR) 2 and TLR4.* J Biol Chem, 2002. **277**(17): p. 15028-34.
65. Ohashi, K., et al., *Cutting edge: heat shock protein 60 is a putative endogenous ligand of the toll-like receptor-4 complex.* J Immunol, 2000. **164**(2): p. 558-61.
66. Johnson, G.B., et al., *Receptor-mediated monitoring of tissue well-being via detection of soluble heparan sulfate by Toll-like receptor 4.* J Immunol, 2002. **168**(10): p. 5233-9.
67. Termeer, C., et al., *Oligosaccharides of Hyaluronan activate dendritic cells via toll-like receptor 4.* J Exp Med, 2002. **195**(1): p. 99-111.
68. Ichii, S., Y. Imai, and T. Irimura, *Initial steps in lymph node metastasis formation in an experimental system: possible involvement of recognition by macrophage C-type lectins.* Cancer Immunol Immunother, 2000. **49**(1): p. 1-9.
69. Utsugi, T., et al., *Elevated expression of phosphatidylserine in the outer membrane leaflet of human tumor cells and recognition by activated human blood monocytes.* Cancer Res, 1991. **51**(11): p. 3062-6.
70. Akira, S. and K. Takeda, *Toll-like receptor signalling.* Nat Rev Immunol, 2004. **4**(7): p. 499-511.
71. Kopp, E.B. and R. Medzhitov, *The Toll-receptor family and control of innate immunity.* Curr Opin Immunol, 1999. **11**(1): p. 13-8.
72. Mantovani, A., et al., *Chemokines in the recruitment and shaping of the leukocyte infiltrate of tumors.* Semin Cancer Biol, 2004. **14**(3): p. 155-60.
73. Nowicki, A., et al., *Impaired tumor growth in colony-stimulating factor 1 (CSF-1)-deficient, macrophage-deficient op/op mouse: evidence for a role of CSF-1-dependent macrophages in formation of tumor stroma.* Int J Cancer, 1996. **65**(1): p. 112-9.
74. Lin, E.Y., et al., *Colony-stimulating factor 1 promotes progression of mammary tumors to malignancy.* J Exp Med, 2001. **193**(6): p. 727-40.
75. Aharinejad, S., et al., *Colony-stimulating factor-1 blockade by antisense oligonucleotides and small interfering RNAs suppresses growth of human mammary tumor xenografts in mice.* Cancer Res, 2004. **64**(15): p. 5378-84.
76. Pollard, J.W., *Tumour-educated macrophages promote tumour progression and metastasis.* Nat Rev Cancer, 2004. **4**(1): p. 71-8.
77. Leung, S.Y., et al., *Monocyte chemoattractant protein-1 expression and macrophage infiltration in gliomas.* Acta Neuropathol (Berl), 1997. **93**(5): p. 518-27.
78. Sapolsky, R., et al., *Interleukin-1 stimulates the secretion of hypothalamic corticotropin-releasing factor.* Science, 1987. **238**(4826): p. 522-4.
79. Rivest, S., et al., *How the blood talks to the brain parenchyma and the paraventricular nucleus of the hypothalamus during systemic inflammatory and infectious stimuli.* Proc Soc Exp Biol Med, 2000. **223**(1): p. 22-38.

80. Wissink, S., et al., *A dual mechanism mediates repression of NF-kappaB activity by glucocorticoids.* Mol Endocrinol, 1998. **12**(3): p. 355-63.
81. De Bosscher, K., et al., *Glucocorticoid-mediated repression of nuclear factor-kappaB-dependent transcription involves direct interference with transactivation.* Proc Natl Acad Sci U S A, 1997. **94**(25): p. 13504-9.
82. Auphan, N., et al., *Immunosuppression by glucocorticoids: inhibition of NF-kappa B activity through induction of I kappa B synthesis.* Science, 1995. **270**(5234): p. 286-90.
83. Scheinman, R.I., et al., *Role of transcriptional activation of I kappa B alpha in mediation of immunosuppression by glucocorticoids.* Science, 1995. **270**(5234): p. 283-6.
84. Klimp, A.H., et al., *A potential role of macrophage activation in the treatment of cancer.* Crit Rev Oncol Hematol, 2002. **44**(2): p. 143-61.
85. Nathan, C., et al., *Activation of macrophages in vivo and in vitro. Correlation between hydrogen peroxide release and killing of Trypanosoma cruzi.* J Exp Med, 1979. **149**(5): p. 1056-68.
86. Mocellin, S., et al., *Tumor necrosis factor, cancer and anticancer therapy.* Cytokine Growth Factor Rev, 2005. **16**(1): p. 35-53.
87. Villeneuve, J., P. Tremblay, and L. Vallieres, *Tumor necrosis factor reduces brain tumor growth by enhancing macrophage recruitment and microcyst formation.* Cancer Res, 2005. **65**(9): p. 3928-36.
88. Soloski, M.J., *Recognition of tumor cells by the innate immune system.* Curr Opin Immunol, 2001. **13**(2): p. 154-62.
89. Mercer, J.C., M.J. Ragin, and A. August, *Natural killer T cells: rapid responders controlling immunity and disease.* Int J Biochem Cell Biol, 2005. **37**(7): p. 1337-43.
90. Smyth, M.J., et al., *NKT cells - conductors of tumor immunity?* Curr Opin Immunol, 2002. **14**(2): p. 165-71.
91. Boon, T., et al., *Tumor antigens recognized by T lymphocytes.* Annu Rev Immunol, 1994. **12**: p. 337-65.
92. Van Der Bruggen, P., et al., *Tumor-specific shared antigenic peptides recognized by human T cells.* Immunol Rev, 2002. **188**: p. 51-64.
93. Rosenberg, S.A., *A new era of cancer immunotherapy: converting theory to performance.* CA Cancer J Clin, 1999. **49**(2): p. 70-3, 65.
94. Pardoll, D., *Does the immune system see tumors as foreign or self?* Annu Rev Immunol, 2003. **21**: p. 807-39.
95. Zimmermann, V.S., F. Benigni, and A. Mondino, *Immune surveillance and anti-tumor immune responses: an anatomical perspective.* Immunol Lett, 2005. **98**(1): p. 1-8.
96. Wilson, N.S. and J.A. Villadangos, *Regulation of antigen presentation and cross-presentation in the dendritic cell network: facts, hypothesis, and immunological implications.* Adv Immunol, 2005. **86**: p. 241-305.
97. Yang, L., K.Y. Ng, and K.O. Lillehei, *Cell-mediated immunotherapy: a new approach to the treatment of malignant glioma.* Cancer Control, 2003. **10**(2): p. 138-47.
98. Dunn, G.P., L.J. Old, and R.D. Schreiber, *The three Es of cancer immunoediting.* Annu Rev Immunol, 2004. **22**: p. 329-60.

99. Khong, H.T. and N.P. Restifo, *Natural selection of tumor variants in the generation of "tumor escape" phenotypes.* Nat Immunol, 2002. **3**(11): p. 999-1005.
100. Svane, I.M., et al., *Chemically induced sarcomas from nude mice are more immunogenic than similar sarcomas from congenic normal mice.* Eur J Immunol, 1996. **26**(8): p. 1844-50.
101. Engel, A.M., et al., *MCA sarcomas induced in scid mice are more immunogenic than MCA sarcomas induced in congenic, immunocompetent mice.* Scand J Immunol, 1997. **45**(5): p. 463-70.
102. Koopman, L.A., et al., *Multiple genetic alterations cause frequent and heterogeneous human histocompatibility leukocyte antigen class I loss in cervical cancer.* J Exp Med, 2000. **191**(6): p. 961-76.
103. Groh, V., et al., *Tumour-derived soluble MIC ligands impair expression of NKG2D and T-cell activation.* Nature, 2002. **419**(6908): p. 734-8.
104. Catlett-Falcone, R., et al., *Constitutive activation of Stat3 signaling confers resistance to apoptosis in human U266 myeloma cells.* Immunity, 1999. **10**(1): p. 105-15.
105. Saas, P., et al., *Fas ligand expression by astrocytoma in vivo: maintaining immune privilege in the brain?* J Clin Invest, 1997. **99**(6): p. 1173-8.
106. Walker, P.R., P. Saas, and P.Y. Dietrich, *Role of Fas ligand (CD95L) in immune escape: the tumor cell strikes back.* J Immunol, 1997. **158**(10): p. 4521-4.
107. Walker, P.R., T. Calzascia, and P.Y. Dietrich, *All in the head: obstacles for immune rejection of brain tumours.* Immunology, 2002. **107**(1): p. 28-38.
108. Fontana, A., et al., *Glioblastoma cells release interleukin 1 and factors inhibiting interleukin 2-mediated effects.* J Immunol, 1984. **132**(4): p. 1837-44.
109. Walker, P.R. and P.Y. Dietrich, *Immune escape of gliomas.* Prog Brain Res, 2001. **132**: p. 685-98.
110. Ahuja, S.S., et al., *Effect of transforming growth factor-beta on early and late activation events in human T cells.* J Immunol, 1993. **150**(8 Pt 1): p. 3109-18.
111. Czarniecki, C.W., et al., *Transforming growth factor-beta 1 modulates the expression of class II histocompatibility antigens on human cells.* J Immunol, 1988. **140**(12): p. 4217-23.
112. Smyth, M.J., et al., *Regulation of lymphokine-activated killer activity and pore-forming protein gene expression in human peripheral blood CD8+ T lymphocytes. Inhibition by transforming growth factor-beta.* J Immunol, 1991. **146**(10): p. 3289-97.
113. Platten, M., W. Wick, and M. Weller, *Malignant glioma biology: role for TGF-beta in growth, motility, angiogenesis, and immune escape.* Microsc Res Tech, 2001. **52**(4): p. 401-10.
114. Huang, M., et al., *Non-small cell lung cancer cyclooxygenase-2-dependent regulation of cytokine balance in lymphocytes and macrophages: up-regulation of interleukin 10 and down-regulation of interleukin 12 production.* Cancer Res, 1998. **58**(6): p. 1208-16.
115. De Smedt, T., et al., *Effect of interleukin-10 on dendritic cell maturation and function.* Eur J Immunol, 1997. **27**(5): p. 1229-35.
116. Sharma, S., et al., *T cell-derived IL-10 promotes lung cancer growth by suppressing both T cell and APC function.* J Immunol, 1999. **163**(9): p. 5020-8.

117. Yue, F.Y., et al., *Interleukin-10 is a growth factor for human melanoma cells and down-regulates HLA class-I, HLA class-II and ICAM-1 molecules.* Int J Cancer, 1997. **71**(4): p. 630-7.
118. Lewis, C.E. and J.W. Pollard, *Distinct role of macrophages in different tumor microenvironments.* Cancer Res, 2006. **66**(2): p. 605-12.
119. Condeelis, J. and J.W. Pollard, *Macrophages: obligate partners for tumor cell migration, invasion, and metastasis.* Cell, 2006. **124**(2): p. 263-6.
120. Lafuente, J.V., et al., *Expression of vascular endothelial growth factor (VEGF) and platelet-derived growth factor receptor-beta (PDGFR-beta) in human gliomas.* J Mol Neurosci, 1999. **13**(1-2): p. 177-85.
121. Watters, J.J., J.M. Schartner, and B. Badie, *Microglia function in brain tumors.* J Neurosci Res, 2005. **81**(3): p. 447-55.
122. Jung, Y.J., et al., *IL-1beta-mediated up-regulation of HIF-1alpha via an NFkappaB/COX-2 pathway identifies HIF-1 as a critical link between inflammation and oncogenesis.* Faseb J, 2003. **17**(14): p. 2115-7.
123. Fries, G., A. Perneczky, and O. Kempski, *Glioblastoma-associated circulating monocytes and the release of epidermal growth factor.* J Neurosurg, 1996. **85**(4): p. 642-7.
124. Libermann, T.A., et al., *Amplification and overexpression of the EGF receptor gene in primary human glioblastomas.* J Cell Sci Suppl, 1985. **3**: p. 161-72.
125. Ryuto, M., et al., *Induction of vascular endothelial growth factor by tumor necrosis factor alpha in human glioma cells. Possible roles of SP-1.* J Biol Chem, 1996. **271**(45): p. 28220-8.
126. Adachi, K., et al., *Enhancement of epidermal growth factor receptor expression on glioma cells by recombinant tumor necrosis factor alpha.* Cancer Immunol Immunother, 1992. **34**(6): p. 370-6.
127. Esteve, P.O., et al., *Protein kinase C-zeta regulates transcription of the matrix metalloproteinase-9 gene induced by IL-1 and TNF-alpha in glioma cells via NF-kappa B.* J Biol Chem, 2002. **277**(38): p. 35150-5.
128. Maeda, H. and T. Akaike, *Nitric oxide and oxygen radicals in infection, inflammation, and cancer.* Biochemistry (Mosc), 1998. **63**(7): p. 854-65.
129. Chattopadhyay, S., N.G. Chakraborty, and B. Mukherji, *Regulatory T cells and tumor immunity.* Cancer Immunol Immunother, 2005. **54**(12): p. 1153-61.
130. Wang, R.F., *Immune suppression by tumor-specific CD4+ regulatory T-cells in cancer.* Semin Cancer Biol, 2006. **16**(1): p. 73-9.
131. Niederkorn, J.Y., *See no evil, hear no evil, do no evil: the lessons of immune privilege.* Nat Immunol, 2006. **7**(4): p. 354-9.
132. Johansson, B.B., *Immune and inflammatory responses in the nervous system*. molecular and cellular neurobiology, ed. N.L. Rothwell, S. 2002, New York: Oxford University press.
133. Blais, V. and S. Rivest, *[Role of the innate immune response in the brain].* Med Sci (Paris), 2003. **19**(10): p. 981-7.
134. Pachter, J.S., H.E. de Vries, and Z. Fabry, *The blood-brain barrier and its role in immune privilege in the central nervous system.* J Neuropathol Exp Neurol, 2003. **62**(6): p. 593-604.
135. Kim, S.U. and J. de Vellis, *Microglia in health and disease.* J Neurosci Res, 2005. **81**(3): p. 302-13.

136. Hanisch, U.K., *Microglia as a source and target of cytokines.* Glia, 2002. **40**(2): p. 140-55.
137. Aloisi, F., *Immune function of microglia.* Glia, 2001. **36**(2): p. 165-79.
138. Fabry, Z., C.S. Raine, and M.N. Hart, *Nervous tissue as an immune compartment: the dialect of the immune response in the CNS.* Immunol Today, 1994. **15**(5): p. 218-24.
139. Cserr, H.F. and P.M. Knopf, *Cervical lymphatics, the blood-brain barrier and the immunoreactivity of the brain: a new view.* Immunol Today, 1992. **13**(12): p. 507-12.
140. Pedemonte, E., et al., *Mechanisms of the adaptive immune response inside the central nervous system during inflammatory and autoimmune diseases.* Pharmacol Ther, 2006.
141. Ueno, T., et al., *Significance of macrophage chemoattractant protein-1 in macrophage recruitment, angiogenesis, and survival in human breast cancer.* Clin Cancer Res, 2000. **6**(8): p. 3282-9.
142. Leek, R.D. and A.L. Harris, *Tumor-associated macrophages in breast cancer.* J Mammary Gland Biol Neoplasia, 2002. **7**(2): p. 177-89.
143. Nishie, A., et al., *Macrophage infiltration and heme oxygenase-1 expression correlate with angiogenesis in human gliomas.* Clin Cancer Res, 1999. **5**(5): p. 1107-13.
144. Rossi, M.L., et al., *The mononuclear cell infiltrate compared with survival in high-grade astrocytomas.* Acta Neuropathol (Berl), 1989. **78**(2): p. 189-93.
145. Brooks, W.H., et al., *Relationship of lymphocyte invasion and survival of brain tumor patients.* Ann Neurol, 1978. **4**(3): p. 219-24.
146. Wheeler, C.J., et al., *Thymic CD8+ T cell production strongly influences tumor antigen recognition and age-dependent glioma mortality.* J Immunol, 2003. **171**(9): p. 4927-33.
147. Gowing, G., L. Vallieres, and J.P. Julien, *Mouse model for ablation of proliferating microglia in acute CNS injuries.* Glia, 2006. **53**(3): p. 331-7.
148. Heyman, R.A., et al., *Thymidine kinase obliteration: creation of transgenic mice with controlled immune deficiency.* Proc Natl Acad Sci U S A, 1989. **86**(8): p. 2698-702.
149. Cheng, Y.C., et al., *Unique spectrum of activity of 9-[(1,3-dihydroxy-2-propoxy)methyl]-guanine against herpesviruses in vitro and its mode of action against herpes simplex virus type 1.* Proc Natl Acad Sci U S A, 1983. **80**(9): p. 2767-70.
150. Black, M.E., et al., *Creation of drug-specific herpes simplex virus type 1 thymidine kinase mutants for gene therapy.* Proc Natl Acad Sci U S A, 1996. **93**(8): p. 3525-9.
151. Arnaout, M.A., *Structure and function of the leukocyte adhesion molecules CD11/CD18.* Blood, 1990. **75**(5): p. 1037-50.
152. Dziennis, S., et al., *The CD11b promoter directs high-level expression of reporter genes in macrophages in transgenic mice.* Blood, 1995. **85**(2): p. 319-29.
153. Graeber, M.B., B.W. Scheithauer, and G.W. Kreutzberg, *Microglia in brain tumors.* Glia, 2002. **40**(2): p. 252-9.
154. Diefenbach, A. and D.H. Raulet, *The innate immune response to tumors and its role in the induction of T-cell immunity.* Immunol Rev, 2002. **188**: p. 9-21.

155. Ackerman, A.L. and P. Cresswell, *Cellular mechanisms governing cross-presentation of exogenous antigens.* Nat Immunol, 2004. **5**(7): p. 678-84.
156. Drake, C.G., E. Jaffee, and D.M. Pardoll, *Mechanisms of immune evasion by tumors.* Adv Immunol, 2006. **90**: p. 51-81.
157. Balkwill, F. and A. Mantovani, *Inflammation and cancer: back to Virchow?* Lancet, 2001. **357**(9255): p. 539-45.
158. Seligman, A.S., MJ, *Studies in Carcinogenesis. VIII. Experimental production of brain tumors in mice with methylcholanthrene.* Am J Cancer, 1939. **37**: p. 364-395.
159. Watson, D.J., et al., *Targeted transduction patterns in the mouse brain by lentivirus vectors pseudotyped with VSV, Ebola, Mokola, LCMV, or MuLV envelope proteins.* Mol Ther, 2002. **5**(5 Pt 1): p. 528-37.
160. Vallières, L. and P.E. Sawchenko, *Bone marrow-derived cells that populate the adult mouse brain preserve their hematopoietic identity.* J Neurosci, 2003. **23**(12): p. 5197-207.
161. Simmons, D.A., JL; Swanson LW, *A complete protocol for in situ hybridization of messenger RNAs in brain and other tissues with radiolabeled single-stranded RNA probes.* J Histotechnol, 1989. **12**: p. 169-181.
162. Mazzone, A. and G. Ricevuti, *Leukocyte CD11/CD18 integrins: biological and clinical relevance.* Haematologica, 1995. **80**(2): p. 161-75.
163. Fischer, I., et al., *Angiogenesis in gliomas: biology and molecular pathophysiology.* Brain Pathol, 2005. **15**(4): p. 297-310.
164. McLendon, R.E., *Pathology of tumors of the central nervous system : a guide to histological diagnosis*. 1999, London: Arnold. 256.
165. Takano, T., et al., *Glutamate release promotes growth of malignant gliomas.* Nat Med, 2001. **7**(9): p. 1010-5.
166. Mrass, P., et al., *Random migration precedes stable target cell interactions of tumor-infiltrating T cells.* J Exp Med, 2006. **203**(12): p. 2749-61.
167. Bongartz, T., et al., *Anti-TNF antibody therapy in rheumatoid arthritis and the risk of serious infections and malignancies: systematic review and meta-analysis of rare harmful effects in randomized controlled trials.* Jama, 2006. **295**(19): p. 2275-85.
168. De Bosscher, K., W. Vanden Berghe, and G. Haegeman, *The interplay between the glucocorticoid receptor and nuclear factor-kappaB or activator protein-1: molecular mechanisms for gene repression.* Endocr Rev, 2003. **24**(4): p. 488-522.
169. Ashwell, J.D., F.W. Lu, and M.S. Vacchio, *Glucocorticoids in T cell development and function*.* Annu Rev Immunol, 2000. **18**: p. 309-45.
170. Reardon, D.A. and P.Y. Wen, *Therapeutic advances in the treatment of glioblastoma: rationale and potential role of targeted agents.* Oncologist, 2006. **11**(2): p. 152-64.
171. Stupp, R., et al., *Changing paradigms--an update on the multidisciplinary management of malignant glioma.* Oncologist, 2006. **11**(2): p. 165-80.
172. Ehtesham, M., K.L. Black, and J.S. Yu, *Recent progress in immunotherapy for malignant glioma: treatment strategies and results from clinical trials.* Cancer Control, 2004. **11**(3): p. 192-207.
173. Gagner, J.P., et al., *Angiogenesis in gliomas: imaging and experimental therapeutics.* Brain Pathol, 2005. **15**(4): p. 342-63.
174. Pulkkanen, K.J. and S. Yla-Herttuala, *Gene therapy for malignant glioma: current clinical status.* Mol Ther, 2005. **12**(4): p. 585-98.

175. Thapar, K.R., JJL, *Brain edema, increased intracranial pressure, vascular effects and other epiphenomena of human brain tumors. in Brain tumors: an encyclopedic approach*, ed. A.L. Kaye, ER. 1995, Edinburgh: Churchill Livingston.
176. Papadopoulos, M.C., et al., *Molecular mechanisms of brain tumor edema.* Neuroscience, 2004. **129**(4): p. 1011-20.
177. Das, A., et al., *Dexamethasone protected human glioblastoma U87MG cells from temozolomide induced apoptosis by maintaining Bax:Bcl-2 ratio and preventing proteolytic activities.* Mol Cancer, 2004. **3**(1): p. 36.
178. Sur, P., et al., *Dexamethasone decreases temozolomide-induced apoptosis in human gliobastoma T98G cells.* Glia, 2005. **50**(2): p. 160-7.
179. Robe, P.A., et al., *Dexamethasone inhibits the HSV-tk/ ganciclovir bystander effect in malignant glioma cells.* BMC Cancer, 2005. **5**(1): p. 32.
180. Benedetti, S., et al., *Dexamethasone inhibits the anti-tumor effect of interleukin 4 on rat experimental gliomas.* Gene Ther, 2003. **10**(2): p. 188-92.
181. Morley, J.E., D.R. Thomas, and M.M. Wilson, *Cachexia: pathophysiology and clinical relevance.* Am J Clin Nutr, 2006. **83**(4): p. 735-43.
182. Kishi, Y., et al., *Autotaxin is overexpressed in glioblastoma multiforme and contributes to cell motility of glioblastoma by converting lysophosphatidylcholine to lysophosphatidic acid.* J Biol Chem, 2006. **281**(25): p. 17492-500.
183. Farin, A., et al., *Transplanted glioma cells migrate and proliferate on host brain vasculature: a dynamic analysis.* Glia, 2006. **53**(8): p. 799-808.
184. Reiss, Y., M.R. Machein, and K.H. Plate, *The role of angiopoietins during angiogenesis in gliomas.* Brain Pathol, 2005. **15**(4): p. 311-7.
185. Chiquet-Ehrismann, R. and M. Chiquet, *Tenascins: regulation and putative functions during pathological stress.* J Pathol, 2003. **200**(4): p. 488-99.
186. Elliott, R.L. and G.C. Blobe, *Role of transforming growth factor Beta in human cancer.* J Clin Oncol, 2005. **23**(9): p. 2078-93.
187. Scherpereel, A., et al., *Overexpression of endocan induces tumor formation.* Cancer Res, 2003. **63**(18): p. 6084-9.
188. Tait, C.R. and P.F. Jones, *Angiopoietins in tumours: the angiogenic switch.* J Pathol, 2004. **204**(1): p. 1-10.
189. Oliner, J., et al., *Suppression of angiogenesis and tumor growth by selective inhibition of angiopoietin-2.* Cancer Cell, 2004. **6**(5): p. 507-16.
190. Valenzuela, D.M., et al., *Angiopoietins 3 and 4: diverging gene counterparts in mice and humans.* Proc Natl Acad Sci U S A, 1999. **96**(5): p. 1904-9.
191. De Palma, M., et al., *Tie2 identifies a hematopoietic lineage of proangiogenic monocytes required for tumor vessel formation and a mesenchymal population of pericyte progenitors.* Cancer Cell, 2005. **8**(3): p. 211-26.
192. Fiedler, U., et al., *Angiopoietin-2 sensitizes endothelial cells to TNF-alpha and has a crucial role in the induction of inflammation.* Nat Med, 2006. **12**(2): p. 235-9.
193. Carding, S.R. and P.J. Egan, *Gammadelta T cells: functional plasticity and heterogeneity.* Nat Rev Immunol, 2002. **2**(5): p. 336-45.
194. Kronenberg, M., *Toward an understanding of NKT cell biology: progress and paradoxes.* Annu Rev Immunol, 2005. **23**: p. 877-900.
195. Ferrarini, M., et al., *Human gammadelta T cells: a nonredundant system in the immune-surveillance against cancer.* Trends Immunol, 2002. **23**(1): p. 14-8.

196. Kabelitz, D., et al., *Potential of human gammadelta T lymphocytes for immunotherapy of cancer.* Int J Cancer, 2004. **112**(5): p. 727-32.
197. Seino, K., et al., *Natural killer T cell-mediated antitumor immune responses and their clinical applications.* Cancer Sci, 2006. **97**(9): p. 807-12.
198. Terabe, M. and J.A. Berzofsky, *Immunoregulatory T cells in tumor immunity.* Curr Opin Immunol, 2004. **16**(2): p. 157-62.
199. Dhodapkar, K.M., et al., *Invariant natural killer T cells are preserved in patients with glioma and exhibit antitumor lytic activity following dendritic cell-mediated expansion.* Int J Cancer, 2004. **109**(6): p. 893-9.
200. Kerbel, R.S., *Antiangiogenic therapy: a universal chemosensitization strategy for cancer?* Science, 2006. **312**(5777): p. 1171-5.
201. Bollard, C.M., et al., *Adapting a transforming growth factor beta-related tumor protection strategy to enhance antitumor immunity.* Blood, 2002. **99**(9): p. 3179-87.
202. Pule, M.A., et al., *A chimeric T cell antigen receptor that augments cytokine release and supports clonal expansion of primary human T cells.* Mol Ther, 2005. **12**(5): p. 933-41.
203. Quattrocchi, K.B., et al., *Pilot study of local autologous tumor infiltrating lymphocytes for the treatment of recurrent malignant gliomas.* J Neurooncol, 1999. **45**(2): p. 141-57.
204. Kew, Y. and V.A. Levin, *Advances in gene therapy and immunotherapy for brain tumors.* Curr Opin Neurol, 2003. **16**(6): p. 665-70.
205. Liau, L.M., et al., *Treatment of intracranial gliomas with bone marrow-derived dendritic cells pulsed with tumor antigens.* J Neurosurg, 1999. **90**(6): p. 1115-24.
206. Yamaguchi, T., et al., *Interleukin-15 effectively potentiates the in vitro tumor-specific activity and proliferation of peripheral blood gammadeltaT cells isolated from glioblastoma patients.* Cancer Immunol Immunother, 1998. **47**(2): p. 97-103.
207. Kunzmann, V., et al., *Stimulation of gammadelta T cells by aminobisphosphonates and induction of antiplasma cell activity in multiple myeloma.* Blood, 2000. **96**(2): p. 384-92.
208. Green, J.R., *Antitumor effects of bisphosphonates.* Cancer, 2003. **97**(3 Suppl): p. 840-7.
209. Zheng, B.J., et al., *Anti-tumor effects of human peripheral gammadelta T cells in a mouse tumor model.* Int J Cancer, 2001. **92**(3): p. 421-5.
210. Kawano, T., et al., *CD1d-restricted and TCR-mediated activation of valpha14 NKT cells by glycosylceramides.* Science, 1997. **278**(5343): p. 1626-9.
211. Fujii, S., et al., *Prolonged IFN-gamma-producing NKT response induced with alpha-galactosylceramide-loaded DCs.* Nat Immunol, 2002. **3**(9): p. 867-74.

# ANNEXE I

## Primers used for qRT-PCR.

| | **Primers[1] (5' to 3')** | |
|---|---|---|
| | **Forward** | **Reverse** |
| 18S rRNA | tgcatgtctaagtacgcacgg | aatgagccattcgcagtttca |
| Angpt2 | gtcacaatgacaaggccgtg | tccctggatactggctgcc |
| ESM1 | gcacccatatgtctccccat | aaacaagcaacattagggtaacttttc |
| GAPDH | ggctcatgaccacagtccatg | ccatccacagtcttctgggtg |
| MMP2 | ggtgtgccaaggtggaaatc | ggcagcagaaagggtgaaac |
| TGFß2 | cacgtgtctgccgaagctt | ttaacaggccttctgggcat |
| Tnc | cagtgaagctctccttgggc | tccgtgtggtctgcttgga |
| VEGFa | agcagaagtcccatgaagtgatc | agcttcgctggtagacatccat |

[1] The forward primers were flanked at their 5'-ends by the following sequence: actgaacctgaccgtaca.

# ANNEXE II

**cDNAS used for *in situ* hybridization.**

| | Primers[1] (5' to 3') | | Size[2] | Linearization[3] | | Transcription[4] | |
|---|---|---|---|---|---|---|---|
| **Gene symbol** | **Forward** | **Reverse** | **(bp)** | **Antisense** | **Sense** | **Antisense** | **Sense** |
| Angpt2 | ttctggacatggagggcaagcaca | ccgcattcaccaacatggcgctta | 1547 | EcoR V | Spe I | SP6 | T7 |
| ESM1 | tctcaggcatggacggggtcaagt | ctcccagcattggcaggacaacag | 1507 | EcoR V | Spe I | SP6 | T7 |
| MMP2 | ggacctgggactttggcacctact | gtcgttccctggacacccgaacag | 1129 | Not I | Spe I | SP6 | T7 |
| TGFß2 | tctcccacccagcgctacatcg | tccatgaagcttcggcagacacg | 1449 | EcoR V | Spe I | SP6 | T7 |
| Tnc | cccgggtgtagagtaccgcgtcag | gcccatcaaatgcccaagcccaaggagagc | 1411 | Xho I | Spe I | SP6 | T7 |
| VEGFa | cggacgggcctccgaaaccatg | cctgcagcctggctcaccgcc | 677 | EcoR V | Spe I | SP6 | T7 |

[1] Primer pairs used for PCR amplification.
[2] Size of the PCR product that was inserted into the pCR-Blunt II-TOPO vector.
[3] Restriction enzymes used to linearize the plasmid for antisense or sense riboprobe synthesis.
[4] Polymerase used for in vitro transcription.

# ANNEXE III

**Genes identified as being modulated in GL261 cells after 24-h incubation with 1 µg/ml dexamethasone (Dex). For concision only one probe set per gene is shown. A negative ratio indicates that the gene is down-regulated. Genes classified as "extracellular" in the Gene Ontology database are labeled with an x.**

| Probe set | Gene Symbol | Gene description | Average signal | | Expression change | | Extra-cellular |
|---|---|---|---|---|---|---|---|
| | | | Dex | Vehicle | ratio | P-value | |
| 1441972_at | 6230424C14Rik | RIKEN cDNA 6230424C14 gene | 292 | 842 | -2,9 | 0,0458 | |
| 1448952_at | A030009H04Rik | RIKEN cDNA A030009H04 gene | 138 | 189 | -1,4 | 0,0365 | |
| 1424059_at | Suv420h2 | suppressor of variegation 4-20 homolog 2 (Drosophila) | 87 | 68 | 1,3 | 0,0436 | |
| 1425780_a_at | 0610041E09Rik | RIKEN cDNA 0610041E09 gene | 8506 | 6440 | 1,3 | 0,0365 | |
| 1428288_at | 2310051E17Rik | RIKEN cDNA 2310051E17 gene | 1290 | 755 | 1,7 | 0,0458 | |
| 1452141_a_at | Sepp1 | selenoprotein P, plasma, 1 | 154 | 77 | 2,0 | 0,0365 | x |
| 1424775_at | Oas1g | 2'-5' oligoadenylate synthetase 1G | 452 | 221 | 2,0 | 0,0365 | |
| 1436202_at | Malat1 | metastasis associated lung adenocarcinoma transcript 1 (non-coding RNA) | 848 | 390 | 2,2 | 0,0392 | |
| 1427981_a_at | Csad | cysteine sulfinic acid decarboxylase | 2590 | 1116 | 2,3 | 0,0365 | |
| 1448136_at | Enpp2 | ectonucleotide pyrophosphatase/phosphodiesterase 2 | 3190 | 1185 | 2,7 | 0,0365 | x |
| 1455610_at | Dmn | desmuslin | 652 | 241 | 2,7 | 0,0436 | |
| 1454984_at | AW061234 | expressed sequence AW061234 | 264 | 92 | 2,9 | 0,0365 | |
| 1430697_at | Ammecr1 | Alport syndrome, mental retardation, midface hypoplasia and elliptocytosis chromosomal region gene 1 homolog (human) | 896 | 261 | 3,4 | 0,0365 | |
| 1416414_at | Emilin1 | elastin microfibril interfacer 1 | 2559 | 568 | 4,5 | 0,0365 | x |
| 1449851_at | Per1 | period homolog 1 (Drosophila) | 122 | 21 | 5,7 | 0,0365 | |
| 1419442_at | Matn2 | matrilin 2 | 1239 | 76 | 16,4 | 0,0365 | x |

# ANNEXE IV

**Genes identified as being modulated in BEnd3 cells after a 24-h incubation with 1 µG/ML dexamethasone (Dex). For concision, only one probe set per gene is shown. A negative ratio indicates that the gene is down-regulated. Genes classified as "extracellular" in the Gene Ontology database are labeled with an x.**

| Probe set | Gene symbol | Gene description | Average signal | | Expression change | | Extra-cellular |
|---|---|---|---|---|---|---|---|
| | | | Dex | Vehicle | Ratio | *P*-value | |
| 1417256_at | Mmp13 | matrix metallopeptidase 13 | 26 | 662 | -25,0 | 0,0084 | |
| 1448831_at | Angpt2 | angiopoietin 2 | 143 | 1784 | -12,5 | 0,0063 | x |
| 1452614_at | Gm566 | gene model 566, (NCBI) | 28 | 251 | -8,9 | 0,0035 | x |
| 1417155_at | Mycn | v-myc myelocytomatosis viral related oncogene, neuroblastoma derived (avian) | 26 | 212 | -8,2 | 0,0067 | |
| 1425681_a_at | Prnd | prion protein dublet | 9 | 70 | -8,1 | 0,0132 | |
| 1457032_at | Ak5 | adenylate kinase 5 | 39 | 303 | -7,9 | 0,0122 | |
| 1420992_at | Ankrd1 | ankyrin repeat domain 1 (cardiac muscle) | 49 | 360 | -7,4 | 0,0391 | |
| 1423597_at | Atp8a1 | ATPase, aminophospholipid transporter (APLT), class I, type 8A, member 1 | 10 | 68 | -6,6 | 0,0033 | |
| 1416342_at | Tnc | tenascin C | 672 | 4225 | -6,3 | 0,0011 | |
| 1429918_at | Arhgap20 | Rho GTPase activating protein 20 | 52 | 309 | -6,0 | 0,0170 | x |
| 1418945_at | Mmp3 | matrix metallopeptidase 3 | 423 | 2501 | -5,9 | 0,0094 | |
| 1427735_a_at | Acta1 | actin, alpha 1, skeletal muscle | 66 | 360 | -5,5 | 0,0342 | x |
| 1434411_at | --- | --- | 13 | 69 | -5,4 | 0,0018 | |
| 1454558_at | 5430416B10Rik | RIKEN cDNA 5430416B10 gene | 5 | 26 | -5,3 | 0,0135 | |
| 1424649_a_at | Tspan8 | tetraspanin 8 | 13 | 69 | -5,2 | 0,0073 | |
| 1449280_at | Esm1 | endothelial cell-specific molecule 1 | 2789 | 14181 | -5,1 | 0,0093 | |
| 1459978_x_at | Gm877 | gene model 877, (NCBI) | 4 | 22 | -5,0 | 0,0194 | x |
| 1422053_at | Inhba | inhibin beta-A | 581 | 2865 | -4,9 | 0,0015 | |
| 1420512_at | Dkk2 | dickkopf homolog 2 (Xenopus laevis) | 33 | 162 | -4,9 | 0,0340 | x |
| 1423104_at | Irs1 | insulin receptor substrate 1 | 8 | 41 | -4,9 | 0,0118 | x |
| 1422168_a_at | Bdnf | brain derived neurotrophic factor | 101 | 493 | -4,9 | 0,0008 | |
| 1454674_at | Fez1 | fasciculation and elongation protein zeta 1 (zygin I) | 155 | 735 | -4,8 | 0,0008 | x |
| 1427482_a_at | Car8 | carbonic anhydrase 8 | 64 | 300 | -4,7 | 0,0009 | |
| 1451236_at | Rerg | RAS-like, estrogen-regulated, growth-inhibitor | 11 | 47 | -4,3 | 0,0271 | |
| 1450241_a_at | Evi2a | ecotropic viral integration site 2a | 12 | 50 | -4,3 | 0,0358 | |
| 1428663_at | 5133401H06Rik | RIKEN cDNA 5133401H06 gene | 380 | 1533 | -4,0 | 0,0063 | |
| 1428114_at | Slc14a1 | solute carrier family 14 (urea transporter), member 1 | 416 | 1680 | -4,0 | 0,0109 | |
| 1451332_at | Zfp521 | zinc finger protein 521 | 812 | 3258 | -4,0 | 0,0047 | |
| 1416714_at | Irf8 | interferon regulatory factor 8 | 6 | 23 | -4,0 | 0,0019 | |
| 1429163_at | Dchs1 | dachsous 1 (Drosophila) | 7 | 26 | -3,8 | 0,0404 | |
| 1431176_at | 2310010I16Rik | RIKEN cDNA 2310010I16 gene | 85 | 320 | -3,8 | 0,0318 | |
| 1450923_at | Tgfb2 | transforming growth factor, beta 2 | 1062 | 3997 | -3,8 | 0,0089 | |
| 1418049_at | Ltbp3 | latent transforming growth factor beta binding protein 3 | 59 | 220 | -3,7 | 0,0153 | x |
| 1450971_at | Gadd45b | growth arrest and DNA-damage-inducible 45 beta | 549 | 2023 | -3,7 | 0,0034 | x |

| | | | | | | | |
|---|---|---|---|---|---|---|---|
| 1436910_at | Rasal2 | RAS protein activator like 2 | 105 | 386 | -3,7 | 0,0170 | |
| 1417235_at | Ehd3 | EH-domain containing 3 | 263 | 952 | -3,6 | 0,0056 | |
| 1437417_s_at | Gpc6 | glypican 6 | 261 | 923 | -3,5 | 0,0201 | |
| 1449531_at | Leprel2 | leprecan-like 2 | 33 | 115 | -3,5 | 0,0065 | x |
| 1455803_at | Slco4a1 | solute carrier organic anion transporter family, member 4a1 | 181 | 629 | -3,5 | 0,0156 | |
| 1437442_at | --- | Transcribed locus, strongly similar to XP_517139.1 PREDICTED: similar to protocadherin 7 isoform a precursor; brain-heart protocadherin; protocadherin 7 [Pan troglodytes] | 41 | 144 | -3,5 | 0,0082 | |
| 1456284_at | Gm905 | gene model 905, (NCBI) | 58 | 201 | -3,5 | 0,0065 | |
| 1448870_at | Ltbp1 | latent transforming growth factor beta binding protein 1 | 866 | 2982 | -3,4 | 0,0063 | |
| 1441461_at | --- | FERM domain containing 4A, mRNA (cDNA clone MGC:76363 IMAGE:6830456) | 5 | 16 | -3,4 | 0,0069 | x |
| 1435553_at | Pdzd2 | PDZ domain containing 2 | 141 | 475 | -3,4 | 0,0256 | |
| 1456524_at | Nrg1 | neuregulin 1 | 237 | 795 | -3,4 | 0,0138 | |
| 1448729_a_at | 36769 | septin 4 | 177 | 591 | -3,3 | 0,0089 | |
| 1418930_at | Cxcl10 | chemokine (C-X-C motif) ligand 10 | 166 | 550 | -3,3 | 0,0295 | |
| 1422256_at | Sstr2 | somatostatin receptor 2 | 158 | 520 | -3,3 | 0,0203 | x |
| 1426037_a_at | Rgs16 | regulator of G-protein signaling 16 | 572 | 1871 | -3,3 | 0,0061 | |
| 1449022_at | Nes | nestin | 646 | 2100 | -3,2 | 0,0035 | |
| 1416958_at | Nr1d2 | nuclear receptor subfamily 1, group D, member 2 | 758 | 2452 | -3,2 | 0,0045 | |
| 1448298_at | Tnk2 | tyrosine kinase, non-receptor, 2 | 82 | 262 | -3,2 | 0,0190 | |
| 1419324_at | Lhx9 | LIM homeobox protein 9 | 41 | 131 | -3,2 | 0,0389 | |
| 1449164_at | Cd68 | CD68 antigen | 332 | 1057 | -3,2 | 0,0054 | |
| 1448656_at | Cacnb3 | calcium channel, voltage-dependent, beta 3 subunit | 119 | 379 | -3,2 | 0,0118 | x |
| 1450651_at | Myo10 | myosin X | 38 | 120 | -3,2 | 0,0103 | |
| 1436719_at | Slc35f1 | solute carrier family 35, member F1 | 453 | 1435 | -3,2 | 0,0074 | |
| 1443230_at | --- | CDNA clone IMAGE:6514950 | 50 | 159 | -3,2 | 0,0144 | |
| 1421551_s_at | Ifi202b | interferon activated gene 202B | 1101 | 3454 | -3,1 | 0,0201 | |
| 1449254_at | Spp1 | secreted phosphoprotein 1 | 196 | 608 | -3,1 | 0,0361 | |
| 1422912_at | Bmp4 | bone morphogenetic protein 4 | 1315 | 4079 | -3,1 | 0,0023 | x |
| 1439925_at | --- | --- | 1166 | 3603 | -3,1 | 0,0042 | x |
| 1419728_at | Cxcl5 | chemokine (C-X-C motif) ligand 5 | 526 | 1605 | -3,1 | 0,0118 | |
| 1415983_at | Lcp1 | lymphocyte cytosolic protein 1 | 890 | 2665 | -3,0 | 0,0019 | x |
| 1429905_at | 3110009O07Rik | RIKEN cDNA 3110009O07 gene | 9 | 27 | -3,0 | 0,0158 | |
| 1417574_at | Cxcl12 | chemokine (C-X-C motif) ligand 12 | 3107 | 9155 | -2,9 | 0,0024 | |
| 1438674_a_at | Sfrs8 | splicing factor, arginine/serine-rich 8 | 57 | 168 | -2,9 | 0,0393 | x |
| 1452469_a_at | Smtn | smoothelin | 62 | 180 | -2,9 | 0,0348 | |
| 1449249_at | Pcdh7 | protocadherin 7 | 181 | 526 | -2,9 | 0,0099 | |
| 1420450_at | Mmp10 | matrix metallopeptidase 10 | 21 | 60 | -2,9 | 0,0136 | x |
| 1450414_at | Pdgfb | platelet derived growth factor, B polypeptide | 468 | 1354 | -2,9 | 0,0197 | x |
| 1418775_at | AI837181 | expressed sequence AI837181 | 285 | 818 | -2,9 | 0,0171 | x |
| 1441793_at | Rnf39 | ring finger protein 39 | 288 | 827 | -2,9 | 0,0038 | |

| | | | | | | | |
|---|---|---|---|---|---|---|---|
| 1451827_a_at | Nox4 | NADPH oxidase 4 | 1928 | 5482 | -2,8 | 0,0037 | |
| 1428867_at | 4933417E01Rik | RIKEN cDNA 4933417E01 gene | 192 | 544 | -2,8 | 0,0037 | |
| 1423303_at | Paxip1 | PAX interacting (with transcription-activation domain) protein 1 | 100 | 281 | -2,8 | 0,0364 | |
| 1417262_at | Ptgs2 | prostaglandin-endoperoxide synthase 2 | 5757 | 16173 | -2,8 | 0,0200 | |
| 1453076_at | 9130211I03Rik | RIKEN cDNA 9130211I03 gene | 139 | 382 | -2,8 | 0,0336 | x |
| 1434270_at | Nptxr | neuronal pentraxin receptor | 289 | 790 | -2,7 | 0,0422 | |
| 1431099_at | Hoxd8 | homeo box D8 | 1004 | 2741 | -2,7 | 0,0011 | x |
| 1433745_at | Trio | triple functional domain (PTPRF interacting) | 830 | 2267 | -2,7 | 0,0268 | |
| 1452210_at | Dna2l | DNA2 DNA replication helicase 2-like (yeast) | 189 | 516 | -2,7 | 0,0006 | |
| 1437869_at | 3222402P14Rik | RIKEN cDNA 3222402P14 gene | 75 | 204 | -2,7 | 0,0393 | |
| 1460223_a_at | Epb4.9 | erythrocyte protein band 4.9 | 41 | 112 | -2,7 | 0,0201 | |
| 1436311_at | Gemin5 | gem (nuclear organelle) associated protein 5 | 11 | 30 | -2,7 | 0,0473 | |
| 1434390_at | AI503316 | expressed sequence AI503316 | 34 | 91 | -2,7 | 0,0219 | |
| 1428808_at | Prickle2 | prickle-like 2 (Drosophila) | 184 | 493 | -2,7 | 0,0425 | |
| 1434116_at | Cbx2 | chromobox homolog 2 (Drosophila Pc class) | 28 | 76 | -2,7 | 0,0057 | |
| 1449363_at | Atf3 | activating transcription factor 3 | 293 | 784 | -2,7 | 0,0021 | |
| 1416612_at | Cyp1b1 | cytochrome P450, family 1, subfamily b, polypeptide 1 | 1979 | 5261 | -2,7 | 0,0141 | |
| 1444947_at | Lasp1 | LIM and SH3 protein 1 | 22 | 60 | -2,7 | 0,0477 | x |
| 1456498_at | Itga4 | integrin alpha 4 | 487 | 1286 | -2,6 | 0,0110 | |
| 1442082_at | C3ar1 | complement component 3a receptor 1 | 103 | 273 | -2,6 | 0,0095 | |
| 1442845_at | C130075A20Rik | RIKEN cDNA C130075A20 gene | 47 | 123 | -2,6 | 0,0113 | |
| 1447272_s_at | Atp10a | ATPase, class V, type 10A | 88 | 229 | -2,6 | 0,0348 | |
| 1459713_s_at | Tmem16a | transmembrane protein 16A | 848 | 2212 | -2,6 | 0,0058 | |
| 1427671_a_at | Fmn1 | formin 1 | 50 | 130 | -2,6 | 0,0276 | |
| 1426782_at | Gpr125 | G protein-coupled receptor 125 | 166 | 433 | -2,6 | 0,0218 | |
| 1452288_at | BB128963 | expressed sequence BB128963 | 2401 | 6226 | -2,6 | 0,0061 | |
| 1456429_at | Malt1 | mucosa associated lymphoid tissue lymphoma translocation gene 1 | 12 | 32 | -2,6 | 0,0218 | |
| 1428804_at | Mfap3l | microfibrillar-associated protein 3-like | 2663 | 6857 | -2,6 | 0,0144 | |
| 1422914_at | Sp5 | trans-acting transcription factor 5 | 5 | 12 | -2,6 | 0,0295 | |
| 1451382_at | Chac1 | ChaC, cation transport regulator-like 1 (E. coli) | 84 | 215 | -2,6 | 0,0189 | |
| 1442222_at | Ifnar1 | interferon (alpha and beta) receptor 1 | 16 | 42 | -2,6 | 0,0217 | |
| 1416564_at | Sox7 | SRY-box containing gene 7 | 713 | 1822 | -2,6 | 0,0339 | x |
| 1429158_at | Fbxo28 | F-box protein 28 | 158 | 402 | -2,6 | 0,0278 | |
| 1457522_at | 1110034C04Rik | RIKEN cDNA 1110034C04 gene | 28 | 72 | -2,5 | 0,0441 | |
| 1423417_at | Smarcc1 | SWI/SNF related, matrix associated, actin dependent regulator of chromatin, subfamily c, member 1 | 60 | 152 | -2,5 | 0,0313 | |
| 1438999_a_at | Nfat5 | nuclear factor of activated T-cells 5 | 380 | 948 | -2,5 | 0,0278 | |
| 1450209_at | Hoxd4 | homeo box D4 | 4 | 11 | -2,5 | 0,0224 | |
| 1448323_a_at | Bgn | biglycan | 75 | 186 | -2,5 | 0,0310 | |
| 1437065_at | 7330412A13Rik | RIKEN cDNA 7330412A13 gene | 153 | 381 | -2,5 | 0,0071 | x |
| 1437745_at | Chd7 | chromodomain helicase DNA binding protein 7 | 109 | 270 | -2,5 | 0,0253 | |
| 1434475_at | Ppig | peptidyl-prolyl isomerase G (cyclophilin G) | 31 | 76 | -2,5 | 0,0127 | |
| 1426642_at | Fn1 | fibronectin 1 | 9750 | 23923 | -2,5 | 0,0136 | |

| | | | | | | | |
|---|---|---|---|---|---|---|---|
| 1460056_at | 1700109F18Rik | RIKEN cDNA 1700109F18 gene | 387 | 949 | -2,4 | 0,0408 | x |
| 1424086_at | D9Ucla1 | DNA segment, Chr 9, University of California at Los Angeles 1 | 639 | 1565 | -2,4 | 0,0196 | |
| 1423721_at | Tpm1 | tropomyosin 1, alpha | 3646 | 8918 | -2,4 | 0,0400 | |
| 1418753_at | Gfpt2 | glutamine fructose-6-phosphate transaminase 2 | 1341 | 3278 | -2,4 | 0,0069 | |
| 1424099_at | 2310016C16Rik | RIKEN cDNA 2310016C16 gene | 1072 | 2617 | -2,4 | 0,0110 | |
| 1417008_at | Crat | carnitine acetyltransferase | 18 | 45 | -2,4 | 0,0271 | |
| 1429735_at | 1110003F05Rik | RIKEN cDNA 1110003F05 gene | 71 | 173 | -2,4 | 0,0175 | |
| 1421205_at | Atm | ataxia telangiectasia mutated homolog (human) | 34 | 82 | -2,4 | 0,0479 | |
| 1438271_at | Lpp | LIM domain containing preferred translocation partner in lipoma | 929 | 2233 | -2,4 | 0,0479 | |
| 1417175_at | Csnk1e | casein kinase 1, epsilon | 59 | 141 | -2,4 | 0,0354 | |
| 1415892_at | Sgpl1 | sphingosine phosphate lyase 1 | 47 | 113 | -2,4 | 0,0273 | |
| 1429183_at | Pkp2 | plakophilin 2 | 146 | 348 | -2,4 | 0,0070 | |
| 1439794_at | Ntn4 | netrin 4 | 157 | 375 | -2,4 | 0,0393 | |
| 1451924_a_at | Edn1 | endothelin 1 | 1881 | 4447 | -2,4 | 0,0418 | x |
| 1436003_at | Vcam1 | vascular cell adhesionmolecule1 | 657 | 1549 | -2,4 | 0,0470 | x |
| 1454877_at | Sertad4 | SERTA domain containing 4 | 338 | 795 | -2,4 | 0,0013 | x |
| 1428834_at | Dusp4 | dual specificity phosphatase 4 | 1458 | 3404 | -2,3 | 0,0195 | |
| 1443534_at | Mbnl1 | muscleblind-like 1 (Drosophila) | 242 | 566 | -2,3 | 0,0419 | |
| 1418350_at | Hbegf | heparin-binding EGF-like growth factor | 2012 | 4688 | -2,3 | 0,0189 | |
| 1455649_at | Ttc9 | tetratricopeptide repeat domain 9 | 1105 | 2571 | -2,3 | 0,0179 | x |
| 1439488_at | Dot1l | DOT1-like, histone H3 methyltransferase (S. cerevisiae) | 22 | 52 | -2,3 | 0,0195 | |
| 1424380_at | Vps37b | vacuolar protein sorting 37B (yeast) | 66 | 152 | -2,3 | 0,0446 | |
| 1449314_at | Zfpm2 | zinc finger protein, multitype 2 | 175 | 404 | -2,3 | 0,0400 | |
| 1455647_at | Ar | androgen receptor | 72 | 167 | -2,3 | 0,0418 | |
| 1454788_at | Arl4c | ADP-ribosylation factor-like 4C | 740 | 1704 | -2,3 | 0,0064 | |
| 1426848_at | Sec24b | SEC24 related gene family, member B (S. cerevisiae) | 145 | 333 | -2,3 | 0,0310 | |
| 1434967_at | Zswim6 | zinc finger, SWIM domain containing 6 | 274 | 627 | -2,3 | 0,0284 | |
| 1435078_at | 3526402J09Rik | RIKEN cDNA 3526402J09 gene | 22 | 50 | -2,3 | 0,0408 | |
| 1449158_at | Kcnk2 | potassium channel, subfamily K, member 2 | 75 | 171 | -2,3 | 0,0221 | |
| 1417476_at | Fbxw5 | F-box and WD-40 domain protein 5 | 114 | 259 | -2,3 | 0,0160 | |
| 1426297_at | Tcfe2a | transcription factor E2a | 98 | 223 | -2,3 | 0,0357 | |
| 1440195_at | Serbp1 | Serpine1 mRNA binding protein 1 | 36 | 81 | -2,3 | 0,0245 | |
| 1417962_s_at | Ghr | growth hormone receptor | 1585 | 3601 | -2,3 | 0,0066 | |
| 1419066_at | Ier5l | immediate early response 5-like | 215 | 489 | -2,3 | 0,0189 | |
| 1426951_at | Crim1 | cysteine rich transmembrane BMP regulator 1 (chordin like) | 2759 | 6264 | -2,3 | 0,0011 | |
| 1455002_at | Ptp4a1 | protein tyrosine phosphatase 4a1 | 3034 | 6877 | -2,3 | 0,0219 | x |
| 1434797_at | 6720469N11Rik | RIKEN cDNA 6720469N11 gene | 153 | 348 | -2,3 | 0,0291 | |
| 1438673_at | Slc4a7 | solute carrier family 4, sodium bicarbonate cotransporter, member 7 | 430 | 972 | -2,3 | 0,0098 | |
| 1433943_at | BC063749 | cDNA sequence BC063749 | 211 | 477 | -2,3 | 0,0195 | |
| 1429809_at | Tmtc2 | transmembrane and tetratricopeptide repeat containing 2 | 177 | 399 | -2,3 | 0,0157 | |
| 1438739_at | Cnbp1 | cellular nucleic acid binding protein 1 | 81 | 182 | -2,3 | 0,0067 | |
| 1419136_at | Akr1c18 | aldo-keto reductase family 1, member C18 | 268 | 602 | -2,2 | 0,0304 | |
| 1421344_a_at | Jub | ajuba | 1659 | 3715 | -2,2 | 0,0075 | |

| | | | | | | | |
|---|---|---|---|---|---|---|---|
| 1416981_at | Foxo1 | forkhead box O1 | 275 | 611 | -2,2 | 0,0272 | |
| 1433645_at | 2210409B22Rik | RIKEN cDNA 2210409B22 gene | 454 | 1009 | -2,2 | 0,0035 | |
| 1438133_a_at | Cyr61 | cysteine rich protein 61 | 3747 | 8326 | -2,2 | 0,0315 | |
| 1424005_at | B230219D22Rik | RIKEN cDNA B230219D22 gene | 788 | 1748 | -2,2 | 0,0305 | x |
| 1418606_at | Hoxd10 | homeo box D10 | 75 | 166 | -2,2 | 0,0451 | |
| 1423269_a_at | Nedd4l | neural precursor cell expressed, developmentally down-regulated gene 4-like | 465 | 1028 | -2,2 | 0,0151 | |
| 1418471_at | Pgf | placental growth factor | 687 | 1517 | -2,2 | 0,0439 | |
| 1438816_at | Ahctf1 | AT hook containing transcription factor 1 | 35 | 77 | -2,2 | 0,0297 | x |
| 1437862_at | 2600011C06Rik | RIKEN cDNA 2600011C06 gene | 265 | 583 | -2,2 | 0,0102 | |
| 1441358_at | Pcdhb16 | protocadherin beta 16 | 57 | 126 | -2,2 | 0,0364 | |
| 1426721_s_at | Tiparp | TCDD-inducible poly(ADP-ribose) polymerase | 951 | 2091 | -2,2 | 0,0006 | x |
| 1440355_at | Kctd12b | potassium channel tetramerisation domain containing 12b | 610 | 1340 | -2,2 | 0,0200 | |
| 1435455_at | C79267 | expressed sequence C79267 | 35 | 77 | -2,2 | 0,0084 | |
| 1434786_at | Ppp1r12b | protein phosphatase 1, regulatory (inhibitor) subunit 12B | 51 | 111 | -2,2 | 0,0252 | |
| 1424659_at | Slit2 | slit homolog 2 (Drosophila) | 886 | 1925 | -2,2 | 0,0147 | |
| 1436037_at | Cerkl | ceramide kinase-like | 662 | 1437 | -2,2 | 0,0122 | x |
| 1416892_s_at | 3110001A13Rik | RIKEN cDNA 3110001A13 gene | 2681 | 5821 | -2,2 | 0,0049 | |
| 1456201_at | 4632427E13Rik | RIKEN cDNA 4632427E13 gene | 99 | 215 | -2,2 | 0,0265 | |
| 1434959_at | Dhh | desert hedgehog | 224 | 484 | -2,2 | 0,0033 | |
| 1439364_a_at | Mmp2 | matrix metallopeptidase 2 | 112 | 241 | -2,2 | 0,0148 | x |
| 1423077_at | Snx9 | sorting nexin 9 | 741 | 1600 | -2,2 | 0,0200 | x |
| 1423967_at | Palm | paralemmin | 97 | 209 | -2,2 | 0,0103 | |
| 1429621_at | Cand2 | cullin-associated and neddylation-dissociated 2 (putative) | 5 | 12 | -2,2 | 0,0097 | |
| 1448155_at | Pdcd6ip | programmed cell death 6 interacting protein | 835 | 1797 | -2,2 | 0,0098 | |
| 1448128_at | Ppgb | protective protein for beta-galactosidase | 2593 | 5566 | -2,1 | 0,0031 | |
| 1420796_at | Ahrr | aryl-hydrocarbon receptor repressor | 127 | 274 | -2,1 | 0,0217 | |
| 1438038_at | 4930402H24Rik | RIKEN cDNA 4930402H24 gene | 405 | 865 | -2,1 | 0,0171 | |
| 1450397_at | Mtap1b | microtubule-associated protein 1 B | 145 | 308 | -2,1 | 0,0498 | |
| 1434186_at | Gpr23 | G protein-coupled receptor 23 | 303 | 643 | -2,1 | 0,0309 | |
| 1454894_at | Smurf2 | SMAD specific E3 ubiquitin protein ligase 2 | 4396 | 9327 | -2,1 | 0,0211 | |
| 1416658_at | Frzb | frizzled-related protein | 10 | 20 | -2,1 | 0,0357 | |
| 1433599_at | Baz1a | bromodomain adjacent to zinc finger domain 1A | 1454 | 3073 | -2,1 | 0,0298 | x |
| 1457166_at | AA536749 | expressed sequence AA536749 | 19 | 39 | -2,1 | 0,0340 | |
| 1433937_at | Trp53bp2 | transformation related protein 53 binding protein 2 | 52 | 109 | -2,1 | 0,0474 | |
| 1418058_at | Eltd1 | EGF, latrophilin seven transmembrane domain containing 1 | 705 | 1480 | -2,1 | 0,0298 | |
| 1425271_at | Psmc3ip | proteasome (prosome, macropain) 26S subunit, ATPase 3, interacting protein | 141 | 296 | -2,1 | 0,0219 | x |
| 1435867_at | A630082K20Rik | RIKEN cDNA A630082K20 gene | 144 | 302 | -2,1 | 0,0236 | |
| 1450669_at | Map3k11 | mitogen activated protein kinase kinase kinase 11 | 157 | 329 | -2,1 | 0,0222 | |
| 1434071_a_at | Pelo | pelota homolog (Drosophila) | 77 | 161 | -2,1 | 0,0379 | |
| 1428853_at | Ptch1 | patched homolog 1 | 1084 | 2242 | -2,1 | 0,0098 | |

| | | | | | | | |
|---|---|---|---|---|---|---|---|
| 1455750_at | BC053994 | cDNA sequence BC053994 | 181 | 374 | -2,1 | 0,0297 | |
| 1435284_at | Rtn4 | reticulon 4 | 1413 | 2915 | -2,1 | 0,0268 | |
| 1448650_a_at | Pole | polymerase (DNA directed), epsilon | 395 | 814 | -2,1 | 0,0259 | |
| 1422123_s_at | Ceacam1 | CEA-related cell adhesion molecule 1 | 344 | 708 | -2,1 | 0,0252 | |
| 1424156_at | Rbl1 | retinoblastoma-like 1 (p107) | 595 | 1223 | -2,1 | 0,0298 | |
| 1418539_a_at | Ptpre | protein tyrosine phosphatase, receptor type, E | 626 | 1284 | -2,1 | 0,0061 | |
| 1453069_at | Pik3cb | phosphatidylinositol 3-kinase, catalytic, beta polypeptide | 80 | 164 | -2,0 | 0,0241 | x |
| 1423165_a_at | Mta2 | metastasis-associated gene family, member 2 | 340 | 695 | -2,0 | 0,0356 | |
| 1436838_x_at | Cotl1 | coactosin-like 1 (Dictyostelium) | 17 | 35 | -2,0 | 0,0298 | |
| 1438081_at | Mcc | mutated in colorectal cancers | 350 | 714 | -2,0 | 0,0356 | |
| 1438211_s_at | Dbp | D site albumin promoter binding protein | 590 | 1201 | -2,0 | 0,0422 | |
| 1435013_at | BC053401 | cDNA sequence BC053401 | 94 | 192 | -2,0 | 0,0400 | |
| 1429290_at | Cbx6 | chromobox homolog 6 | 1418 | 2884 | -2,0 | 0,0033 | |
| 1454995_at | Ddah1 | dimethylarginine dimethylaminohydrolase 1 | 2315 | 4700 | -2,0 | 0,0037 | |
| 1428615_at | P2ry5 | purinergic receptor P2Y, G-protein coupled, 5 | 3366 | 6826 | -2,0 | 0,0015 | |
| 1448957_at | Rbpsuh | recombining binding protein suppressor of hairless (Drosophila) | 116 | 234 | -2,0 | 0,0311 | |
| 1433575_at | Sox4 | SRY-box containing gene 4 | 1442 | 2908 | -2,0 | 0,0190 | |
| 1428395_at | Smurf1 | SMAD specific E3 ubiquitin protein ligase 1 | 379 | 762 | -2,0 | 0,0256 | |
| 1427266_at | 2610016F04Rik | RIKEN cDNA 2610016F04 gene | 816 | 1640 | -2,0 | 0,0492 | |
| 1417487_at | Fosl1 | fos-like antigen 1 | 1176 | 2361 | -2,0 | 0,0035 | |
| 1422437_at | Col5a2 | procollagen, type V, alpha 2 | 4622 | 9269 | -2,0 | 0,0126 | |
| 1453107_s_at | Pebp1 | phosphatidylethanolamine binding protein 1 | 508 | 1015 | -2,0 | 0,0402 | x |
| 1436460_at | BC030440 | cDNA sequence BC030440 | 34 | 67 | -2,0 | 0,0364 | |
| 1455015_at | Tbc1d9 | TBC1 domain family, member 9 | 159 | 317 | -2,0 | 0,0452 | |
| 1449419_at | Dock8 | dedicator of cytokinesis 8 | 191 | 382 | -2,0 | 0,0146 | |
| 1438063_at | Mphosph9 | M-phase phosphoprotein 9 | 23 | 46 | -2,0 | 0,0495 | |
| 1422631_at | Ahr | aryl-hydrocarbon receptor | 846 | 1684 | -2,0 | 0,0297 | |
| 1436240_at | Sost | sclerostin | 108 | 216 | -2,0 | 0,0124 | |
| 1439673_at | Ppp1cb | protein phosphatase 1, catalytic subunit, beta isoform | 31 | 62 | -2,0 | 0,0245 | |
| 1416749_at | Htra1 | HtrA serine peptidase 1 | 403 | 800 | -2,0 | 0,0342 | |
| 1434177_at | Ece1 | endothelin converting enzyme 1 | 132 | 262 | -2,0 | 0,0472 | x |
| 1429560_at | Zfp422-rs1 | zinc finger protein 422, related sequence 1 | 507 | 1004 | -2,0 | 0,0183 | |
| 1426206_at | Robo4 | roundabout homolog 4 (Drosophila) | 798 | 1578 | -2,0 | 0,0272 | |
| 1453111_a_at | D11Ertd333e | DNA segment, Chr 11, ERATO Doi 333, expressed | 280 | 554 | -2,0 | 0,0418 | |
| 1452833_at | Rapgef2 | Rap guanine nucleotide exchange factor (GEF) 2 | 3637 | 7176 | -2,0 | 0,0093 | |
| 1427294_a_at | 1810073N04Rik | RIKEN cDNA 1810073N04 gene | 351 | 691 | -2,0 | 0,0065 | |
| 1451264_at | Frmd6 | FERM domain containing 6 | 471 | 925 | -2,0 | 0,0201 | |
| 1455352_at | AU023006 | expressed sequence AU023006 | 151 | 297 | -2,0 | 0,0305 | |
| 1423277_at | Ptprk | protein tyrosine phosphatase, receptor type, K | 948 | 1855 | -2,0 | 0,0069 | |
| 1417292_at | Ifi47 | interferon gamma inducible protein 47 | 696 | 1360 | -2,0 | 0,0005 | x |
| 1454967_at | A930001N09Rik | RIKEN cDNA A930001N09 gene | 140 | 273 | -1,9 | 0,0082 | |
| 1454034_a_at | Usp21 | ubiquitin specific peptidase 21 | 187 | 363 | -1,9 | 0,0149 | |
| 1424113_at | Lamb1-1 | laminin B1 subunit 1 | 507 | 985 | -1,9 | 0,0278 | |

| | | | | | | | |
|---|---|---|---|---|---|---|---|
| 1419168_at | Mapk6 | mitogen-activated protein kinase 6 | 203 | 393 | -1,9 | 0,0465 | x |
| 1439111_at | Tsc22d1 | TSC22 domain family, member 1 | 23 | 44 | -1,9 | 0,0418 | |
| 1429897_a_at | D16Ertd472e | DNA segment, Chr 16, ERATO Doi 472, expressed | 171 | 332 | -1,9 | 0,0099 | |
| 1448914_a_at | Csf1 | colony stimulating factor 1 (macrophage) | 231 | 447 | -1,9 | 0,0211 | |
| 1416308_at | Ugdh | UDP-glucose dehydrogenase | 4958 | 9579 | -1,9 | 0,0118 | x |
| 1448908_at | Ppap2b | phosphatidic acid phosphatase type 2B | 750 | 1449 | -1,9 | 0,0472 | |
| 1426981_at | Pcsk6 | proprotein convertase subtilisin/kexin type 6 | 97 | 187 | -1,9 | 0,0236 | |
| 1454656_at | Spata13 | spermatogenesis associated 13 | 349 | 672 | -1,9 | 0,0384 | |
| 1436985_at | Zfp644 | zinc finger protein 644 | 62 | 119 | -1,9 | 0,0108 | |
| 1417960_at | Cpeb1 | cytoplasmic polyadenylation element binding protein 1 | 280 | 539 | -1,9 | 0,0493 | |
| 1435349_at | Nrp2 | neuropilin 2 | 1694 | 3250 | -1,9 | 0,0207 | |
| 1438481_at | AW047464 | expressed sequence AW047464 | 24 | 46 | -1,9 | 0,0393 | x |
| 1434576_at | Tsga14 | testis specific gene A14 | 103 | 196 | -1,9 | 0,0451 | |
| 1425179_at | Shmt1 | serine hydroxymethyl transferase 1 (soluble) | 159 | 304 | -1,9 | 0,0444 | |
| 1416454_s_at | Acta2 | actin, alpha 2, smooth muscle, aorta | 546 | 1043 | -1,9 | 0,0283 | |
| 1455353_at | Tmcc1 | transmembrane and coiled coil domains 1 | 159 | 304 | -1,9 | 0,0093 | |
| 1449195_s_at | Cxcl16 | chemokine (C-X-C motif) ligand 16 | 58 | 112 | -1,9 | 0,0397 | |
| 1452521_a_at | Plaur | plasminogen activator, urokinase receptor | 799 | 1523 | -1,9 | 0,0386 | x |
| 1455197_at | Rnd1 | Rho family GTPase 1 | 1072 | 2039 | -1,9 | 0,0232 | x |
| 1417706_at | Naglu | alpha-N-acetylglucosaminidase (Sanfilippo disease IIIB) | 19 | 36 | -1,9 | 0,0427 | |
| 1428911_at | Ttll4 | tubulin tyrosine ligase-like family, member 4 | 463 | 879 | -1,9 | 0,0067 | x |
| 1429009_at | Snrp70 | U1 small nuclear ribonucleoprotein polypeptide A | 30 | 57 | -1,9 | 0,0350 | |
| 1427147_at | F730047E07Rik | RIKEN cDNA F730047E07 gene | 92 | 174 | -1,9 | 0,0481 | |
| 1430309_at | Nipbl | Nipped-B homolog (Drosophila) | 644 | 1220 | -1,9 | 0,0110 | |
| 1433909_at | Syt17 | synaptotagmin XVII | 352 | 666 | -1,9 | 0,0271 | |
| 1445037_at | 6430510B20Rik | RIKEN cDNA 6430510B20 gene | 42 | 80 | -1,9 | 0,0456 | |
| 1415703_at | Huwe1 | HECT, UBA and WWE domain containing 1 | 577 | 1088 | -1,9 | 0,0137 | |
| 1455160_at | 2610203C20Rik | RIKEN cDNA 2610203C20 gene | 1186 | 2234 | -1,9 | 0,0251 | |
| 1430388_a_at | Sulf2 | sulfatase 2 | 157 | 296 | -1,9 | 0,0144 | |
| 1456880_at | Hpvc2 | human papillomavirus 18 E5 central sequence motif gene 2 | 96 | 181 | -1,9 | 0,0386 | x |
| 1424843_a_at | Gas5 | growth arrest specific 5 | 47 | 88 | -1,9 | 0,0345 | |
| 1418090_at | Plvap | plasmalemma vesicle associated protein | 6788 | 12753 | -1,9 | 0,0043 | |
| 1451601_a_at | BC011467 | cDNA sequence BC011467 | 1691 | 3173 | -1,9 | 0,0466 | |
| 1428967_at | A330103N21Rik | RIKEN cDNA A330103N21 gene | 256 | 480 | -1,9 | 0,0413 | |
| 1422622_at | Nos3 | nitric oxide synthase 3, endothelial cell | 3517 | 6598 | -1,9 | 0,0118 | |
| 1429749_at | 9330180L21Rik | RIKEN cDNA 9330180L21 gene | 40 | 75 | -1,9 | 0,0058 | |
| 1430139_at | Hells | helicase, lymphoid specific | 368 | 688 | -1,9 | 0,0061 | |
| 1422546_at | Ilf3 | interleukin enhancer binding factor 3 | 45 | 85 | -1,9 | 0,0251 | |
| 1433460_at | Ttc7b | tetratricopeptide repeat domain 7B | 817 | 1523 | -1,9 | 0,0395 | |
| 1427891_at | Gimap6 | GTPase, IMAP family member 6 | 203 | 378 | -1,9 | 0,0019 | |
| 1452439_s_at | Sfrs2 | splicing factor, arginine/serine-rich 2 (SC-35) | 175 | 326 | -1,9 | 0,0241 | |
| 1456791_at | AA407452 | EST AA407452 | 174 | 323 | -1,9 | 0,0305 | |
| 1430075_at | Sf3b3 | splicing factor 3b, subunit 3 | 51 | 94 | -1,9 | 0,0304 | |

| | | | | | | | |
|---|---|---|---|---|---|---|---|
| 1418379_s_at | Gpr124 | G protein-coupled receptor 124 | 459 | 849 | -1,9 | 0,0276 | |
| 1420682_at | Chrnb1 | cholinergic receptor, nicotinic, beta polypeptide 1 (muscle) | 162 | 300 | -1,8 | 0,0454 | |
| 1428951_at | Nol8 | nucleolar protein 8 | 216 | 400 | -1,8 | 0,0405 | x |
| 1452072_at | Myct1 | myc target 1 | 877 | 1621 | -1,8 | 0,0089 | |
| 1424089_a_at | Tcf4 | transcription factor 4 | 4317 | 7975 | -1,8 | 0,0063 | |
| 1431293_a_at | Cldnd1 | claudin containing domain 1 | 842 | 1554 | -1,8 | 0,0163 | |
| 1434131_at | Rufy1 | RUN and FYVE domain containing 1 | 115 | 212 | -1,8 | 0,0297 | |
| 1434740_at | Scarf2 | scavenger receptor class F, member 2 | 13 | 24 | -1,8 | 0,0309 | |
| 1416818_at | Parva | parvin, alpha | 495 | 908 | -1,8 | 0,0246 | |
| 1416214_at | Mcm4 | minichromosome maintenance deficient 4 homolog (S. cerevisiae) | 2326 | 4264 | -1,8 | 0,0437 | |
| 1422272_at | Phxr4 | per-hexamer repeat gene 4 | 124 | 228 | -1,8 | 0,0165 | |
| 1426790_at | Ssrp1 | structure specific recognition protein 1 | 2565 | 4690 | -1,8 | 0,0478 | |
| 1437896_at | Zcrb1 | zinc finger CCHC-type and RNA binding motif 1 | 20 | 37 | -1,8 | 0,0194 | |
| 1417947_at | Pcna | proliferating cell nuclear antigen | 10255 | 18735 | -1,8 | 0,0236 | |
| 1452912_at | 2600005O03Rik | RIKEN cDNA 2600005O03 gene | 284 | 517 | -1,8 | 0,0189 | |
| 1418587_at | Traf3 | Tnf receptor-associated factor 3 | 583 | 1060 | -1,8 | 0,0170 | |
| 1438700_at | Fnbp4 | formin binding protein 4 | 5 | 10 | -1,8 | 0,0256 | |
| 1436520_at | AI450948 | expressed sequence AI450948 | 3341 | 6067 | -1,8 | 0,0095 | |
| 1452821_at | Tial1 | Tial1 cytotoxic granule-associated RNA binding protein-like 1 | 137 | 248 | -1,8 | 0,0398 | |
| 1423369_at | Fmr1 | fragile X mental retardation syndrome 1 homolog | 1076 | 1950 | -1,8 | 0,0340 | |
| 1448894_at | Akr1b8 | aldo-keto reductase family 1, member B8 | 3148 | 5704 | -1,8 | 0,0313 | |
| 1424230_at | Exoc6 | exocyst complex component 6 | 152 | 275 | -1,8 | 0,0412 | |
| 1417111_at | Man1a | mannosidase 1, alpha | 1359 | 2454 | -1,8 | 0,0223 | |
| 1448325_at | Myd116 | myeloid differentiation primary response gene 116 | 45 | 82 | -1,8 | 0,0170 | |
| 1438691_at | Zzef1 | zinc finger, ZZ-type with EF hand domain 1 | 559 | 1008 | -1,8 | 0,0412 | |
| 1454136_a_at | 4921524J17Rik | RIKEN cDNA 4921524J17 gene | 1714 | 3092 | -1,8 | 0,0309 | |
| 1436248_at | --- | Adult male spinal cord cDNA, RIKEN full-length enriched library, clone:A330033L11 product:unclassifiable, full insert sequence | 848 | 1529 | -1,8 | 0,0121 | |
| 1437645_at | Atf7 | activating transcription factor 7 | 182 | 327 | -1,8 | 0,0441 | |
| 1426238_at | Bmp1 | bone morphogenetic protein 1 | 62 | 112 | -1,8 | 0,0494 | |
| 1449109_at | Socs2 | suppressor of cytokine signaling 2 | 492 | 886 | -1,8 | 0,0470 | x |
| 1428497_at | Secisbp2 | SECIS binding protein 2 | 78 | 140 | -1,8 | 0,0351 | |
| 1449300_at | Cttnbp2nl | CTTNBP2 N-terminal like | 345 | 620 | -1,8 | 0,0197 | |
| 1416812_at | Tia1 | cytotoxic granule-associated RNA binding protein 1 | 336 | 604 | -1,8 | 0,0073 | |
| 1419853_a_at | Dnajb9 | DnaJ (Hsp40) homolog, subfamily B, member 9 | 95 | 170 | -1,8 | 0,0451 | |
| 1429559_at | Gnaq | guanine nucleotide binding protein, alpha q polypeptide | 2419 | 4342 | -1,8 | 0,0159 | |
| 1434211_at | Sh3bgrl2 | SH3 domain binding glutamic acid-rich protein like 2 | 88 | 157 | -1,8 | 0,0047 | |
| 1456681_at | AI848149 | expressed sequence AI848149 | 401 | 718 | -1,8 | 0,0271 | |
| 1455500_at | D11Ertd759e | DNA segment, Chr 11, ERATO Doi 759, expressed | 1283 | 2297 | -1,8 | 0,0471 | |
| 1433608_at | Scfd2 | sec1 family domain containing 2 | 22 | 40 | -1,8 | 0,0189 | |
| 1428725_at | Pias2 | protein inhibitor of activated STAT 2 | 183 | 326 | -1,8 | 0,0250 | |
| 1457357_at | Tlk2 | tousled-like kinase 2 (Arabidopsis) | 25 | 44 | -1,8 | 0,0470 | |

| | | | | | | | |
|---|---|---|---|---|---|---|---|
| 1422771_at | Smad6 | MAD homolog 6 (Drosophila) | 306 | 546 | -1,8 | 0,0381 | |
| 1417371_at | Peli1 | pellino 1 | 238 | 425 | -1,8 | 0,0201 | |
| 1428231_at | Cpsf6 | cleavage and polyadenylation specific factor 6 | 740 | 1317 | -1,8 | 0,0132 | |
| 1422549_at | Arl2 | ADP-ribosylation factor-like 2 | 181 | 321 | -1,8 | 0,0457 | |
| 1416122_at | Ccnd2 | cyclin D2 | 842 | 1498 | -1,8 | 0,0138 | |
| 1423584_at | Igfbp7 | insulin-like growth factor binding protein 7 | 1663 | 2957 | -1,8 | 0,0149 | |
| 1435597_at | C130052G03Rik | RIKEN cDNA C130052G03 gene | 266 | 473 | -1,8 | 0,0295 | x |
| 1416377_at | Pdcd7 | programmed cell death protein 7 | 182 | 323 | -1,8 | 0,0347 | |
| 1416805_at | 1110032E23Rik | RIKEN cDNA 1110032E23 gene | 2230 | 3954 | -1,8 | 0,0412 | |
| 1460303_at | Nr3c1 | nuclear receptor subfamily 3, group C, member 1 | 1069 | 1894 | -1,8 | 0,0158 | |
| 1415973_at | Marcks | myristoylated alanine rich protein kinase C substrate | 2040 | 3615 | -1,8 | 0,0076 | |
| 1460633_at | Prpf19 | PRP19/PSO4 pre-mRNA processing factor 19 homolog (S. cerevisiae) | 206 | 364 | -1,8 | 0,0305 | |
| 1416845_at | Tmem132a | transmembrane protein 132A | 45 | 79 | -1,8 | 0,0336 | |
| 1438345_at | --- | Transcribed locus | 10 | 17 | -1,8 | 0,0027 | |
| 1424008_a_at | Rbpms2 | RNA binding protein with multiple splicing 2 | 354 | 625 | -1,8 | 0,0295 | |
| 1453257_at | Agpat5 | 1-acylglycerol-3-phosphate O-acyltransferase 5 (lysophosphatidic acid acyltransferase, epsilon) | 753 | 1331 | -1,8 | 0,0110 | |
| 1435880_at | Ankrd50 | ankrin repeat domain 50 | 2331 | 4111 | -1,8 | 0,0422 | |
| 1448402_at | Tln1 | talin 1 | 2144 | 3780 | -1,8 | 0,0392 | |
| 1419652_s_at | 2610200G18Rik | RIKEN cDNA 2610200G18 gene | 18 | 31 | -1,8 | 0,0472 | |
| 1452954_at | Ube2c | ubiquitin-conjugating enzyme E2C | 2214 | 3898 | -1,8 | 0,0298 | x |
| 1452306_at | Zfyve26 | zinc finger, FYVE domain containing 26 | 229 | 401 | -1,8 | 0,0320 | |
| 1451253_at | Pxk | PX domain containing serine/threonine kinase | 266 | 466 | -1,8 | 0,0402 | |
| 1428509_at | Myo1e | myosin IE | 504 | 882 | -1,8 | 0,0434 | |
| 1419255_at | Spnb2 | spectrin beta 2 | 242 | 423 | -1,7 | 0,0251 | |
| 1431892_a_at | Plcd3 | phospholipase C, delta 3 | 153 | 267 | -1,7 | 0,0141 | |
| 1455238_at | Mum1l1 | melanoma associated antigen (mutated) 1-like 1 | 953 | 1664 | -1,7 | 0,0149 | |
| 1434334_at | Prkd2 | protein kinase D2 | 273 | 477 | -1,7 | 0,0335 | |
| 1416216_at | Reps1 | RalBP1 associated Eps domain containing protein | 224 | 390 | -1,7 | 0,0159 | |
| 1421164_a_at | Arhgef1 | Rho guanine nucleotide exchange factor (GEF) 1 | 262 | 457 | -1,7 | 0,0179 | |
| 1435260_at | Sdccag8 | serologically defined colon cancer antigen 8 | 115 | 201 | -1,7 | 0,0252 | |
| 1450622_at | Bcar1 | breast cancer anti-estrogen resistance 1 | 190 | 330 | -1,7 | 0,0427 | |
| 1455356_at | Camsap1 | calmodulin regulated spectrin-associated protein 1 | 392 | 681 | -1,7 | 0,0413 | |
| 1420028_s_at | Mcm3 | minichromosome maintenance deficient 3 (S. cerevisiae) | 3378 | 5859 | -1,7 | 0,0360 | |
| 1417209_at | Sertad2 | SERTA domain containing 2 | 340 | 590 | -1,7 | 0,0491 | |
| 1423350_at | Socs5 | suppressor of cytokine signaling 5 | 2724 | 4715 | -1,7 | 0,0170 | |
| 1448851_a_at | Dnajc5 | DnaJ (Hsp40) homolog, subfamily C, member 5 | 137 | 238 | -1,7 | 0,0095 | |
| 1424748_at | Galnt11 | UDP-N-acetyl-alpha-D-galactosamine:polypeptide N-acetylgalactosaminyltransferase 11 | 346 | 599 | -1,7 | 0,0279 | |
| 1424594_at | Lgals7 | lectin, galactose binding, soluble 7 | 983 | 1698 | -1,7 | 0,0340 | |
| 1417065_at | Egr1 | early growth response 1 | 132 | 227 | -1,7 | 0,0134 | |
| 1433640_at | Fubp1 | far upstream element (FUSE) binding protein 1 | 612 | 1057 | -1,7 | 0,0298 | |
| 1460121_at | 9630010G10Rik | RIKEN cDNA 9630010G10 gene | 310 | 534 | -1,7 | 0,0187 | |

| | | | | | | | |
|---|---|---|---|---|---|---|---|
| 1434924_at | Phf2 | PHD finger protein 2 | 205 | 354 | -1,7 | 0,0031 | |
| 1418098_at | Adcy4 | adenylate cyclase 4 | 1311 | 2259 | -1,7 | 0,0084 | |
| 1418571_at | Tnfrsf12a | tumor necrosis factor receptor superfamily, member 12a | 2261 | 3892 | -1,7 | 0,0134 | |
| 1438008_at | Gga3 | golgi associated, gamma adaptin ear containing, ARF binding protein 3 | 116 | 200 | -1,7 | 0,0340 | |
| 1434737_at | Obfc1 | oligonucleotide/oligosaccharide-binding fold containing 1 | 116 | 199 | -1,7 | 0,0089 | |
| 1419203_at | Gtlf3a | gene trap locus F3a | 91 | 157 | -1,7 | 0,0065 | |
| 1454086_a_at | Lmo2 | LIM domain only 2 | 715 | 1225 | -1,7 | 0,0298 | |
| 1435484_at | BF642829 | expressed sequence BF642829 | 2750 | 4712 | -1,7 | 0,0041 | |
| 1452178_at | Plec1 | plectin 1 | 126 | 216 | -1,7 | 0,0335 | |
| 1455333_at | Tns3 | tensin 3 | 3420 | 5851 | -1,7 | 0,0065 | |
| 1435434_at | Braf | Braf transforming gene | 128 | 219 | -1,7 | 0,0323 | |
| 1455733_at | A430105I05Rik | RIKEN cDNA A430105I05 gene | 211 | 361 | -1,7 | 0,0225 | |
| 1420979_at | Pak1 | p21 (CDKN1A)-activated kinase 1 | 100 | 171 | -1,7 | 0,0303 | |
| 1437632_at | 1810030O07Rik | RIKEN cDNA 1810030O07 gene | 920 | 1571 | -1,7 | 0,0138 | |
| 1452058_a_at | Rnf11 | ring finger protein 11 | 1162 | 1984 | -1,7 | 0,0095 | |
| 1451803_a_at | Vegfb | vascular endothelial growth factor B | 272 | 463 | -1,7 | 0,0366 | |
| 1426825_at | Fmnl3 | formin-like 3 | 242 | 413 | -1,7 | 0,0387 | x |
| 1435461_at | Magi3 | membrane associated guanylate kinase, WW and PDZ domain containing 3 | 598 | 1019 | -1,7 | 0,0284 | |
| 1433595_at | Slc35d1 | solute carrier family 35 (UDP-glucuronic acid/UDP-N-acetylgalactosamine dual transporter), member D1 | 317 | 539 | -1,7 | 0,0145 | |
| 1439972_at | Etnk1 | ethanolamine kinase 1 | 28 | 48 | -1,7 | 0,0306 | |
| 1417540_at | Elf1 | E74-like factor 1 | 595 | 1012 | -1,7 | 0,0142 | |
| 1415869_a_at | Trim28 | tripartite motif protein 28 | 1872 | 3181 | -1,7 | 0,0297 | |
| 1451069_at | Pim3 | proviral integration site 3 | 36 | 60 | -1,7 | 0,0115 | |
| 1454664_a_at | Eif5 | eukaryotic translation initiation factor 5 | 2828 | 4801 | -1,7 | 0,0438 | |
| 1434805_at | Mllt1 | myeloid/lymphoid or mixed lineage-leukemia translocation to 1 homolog (Drosophila) | 188 | 319 | -1,7 | 0,0199 | |
| 1428694_at | 5033413D16Rik | RIKEN cDNA 5033413D16 gene | 66 | 111 | -1,7 | 0,0427 | |
| 1458440_at | Specc1 | spectrin domain with coiled-coils 1 | 431 | 728 | -1,7 | 0,0365 | |
| 1416953_at | Ctgf | connective tissue growth factor | 11259 | 19014 | -1,7 | 0,0173 | |
| 1448430_a_at | Naca | nascent polypeptide-associated complex alpha polypeptide | 10798 | 18226 | -1,7 | 0,0384 | x |
| 1448558_a_at | Pla2g4a | phospholipase A2, group IVA (cytosolic, calcium-dependent) | 3542 | 5978 | -1,7 | 0,0136 | |
| 1417419_at | Ccnd1 | cyclin D1 | 9064 | 15272 | -1,7 | 0,0282 | |
| 1438400_at | 4632411B12Rik | RIKEN cDNA 4632411B12 gene | 415 | 698 | -1,7 | 0,0305 | |
| 1423577_at | Ankrd32 | ankyrin repeat domain 32 | 62 | 105 | -1,7 | 0,0159 | |
| 1436897_at | Mfhas1 | malignant fibrous histiocytoma amplified sequence 1 | 76 | 128 | -1,7 | 0,0063 | |
| 1437041_at | 5730406M06Rik | RIKEN cDNA 5730406M06 gene | 195 | 327 | -1,7 | 0,0341 | |
| 1434337_at | Cmtm3 | CKLF-like MARVEL transmembrane domain containing 3 | 125 | 210 | -1,7 | 0,0320 | |
| 1417189_at | Psme2 | proteasome (prosome, macropain) 28 subunit, beta | 662 | 1107 | -1,7 | 0,0422 | x |
| 1423809_at | Tcf19 | transcription factor 19 | 1278 | 2136 | -1,7 | 0,0219 | |
| 1425972_a_at | Zfx | zinc finger protein X-linked | 673 | 1124 | -1,7 | 0,0276 | |
| 1433623_at | Zfp367 | zinc finger protein 367 | 1401 | 2337 | -1,7 | 0,0089 | |

| | | | | | | | |
|---|---|---|---|---|---|---|---|
| 1452828_at | Fbxo21 | F-box only protein 21 | 565 | 940 | -1,7 | 0,0208 | |
| 1446835_at | --- | --- | 445 | 742 | -1,7 | 0,0221 | |
| 1428452_at | 2810025M15Rik | RIKEN cDNA 2810025M15 gene | 880 | 1465 | -1,7 | 0,0152 | |
| 1427310_at | Falz | fetal Alzheimer antigen | 1037 | 1726 | -1,7 | 0,0285 | |
| 1434393_at | Usp34 | ubiquitin specific peptidase 34 | 393 | 653 | -1,7 | 0,0400 | |
| 1424175_at | Tef | thyrotroph embryonic factor | 152 | 252 | -1,7 | 0,0460 | |
| 1451293_at | Rnu3ip2 | RNA, U3 small nucleolar interacting protein 2 | 262 | 435 | -1,7 | 0,0212 | |
| 1426389_at | Camk1d | calcium/calmodulin-dependent protein kinase ID | 58 | 96 | -1,7 | 0,0236 | |
| 1427228_at | Palld | palladin, cytoskeletal associated protein | 2252 | 3737 | -1,7 | 0,0302 | |
| 1452612_at | Zfp294 | zinc finger protein 294 | 504 | 836 | -1,7 | 0,0244 | |
| 1418936_at | Maff | v-maf musculoaponeurotic fibrosarcoma oncogene family, protein F (avian) | 581 | 962 | -1,7 | 0,0487 | |
| 1417324_at | Mast2 | microtubule associated serine/threonine kinase 2 | 321 | 531 | -1,7 | 0,0099 | |
| 1454776_at | Ehmt1 | euchromatic histone methyltransferase 1 | 349 | 577 | -1,7 | 0,0447 | |
| 1434037_s_at | Pcaf | p300/CBP-associated factor | 953 | 1574 | -1,7 | 0,0121 | |
| 1418516_at | Mtf2 | metal response element binding transcription factor 2 | 1195 | 1972 | -1,7 | 0,0448 | |
| 1422866_at | Col13a1 | procollagen, type XIII, alpha 1 | 3132 | 5158 | -1,6 | 0,0448 | |
| 1438049_at | A430108E01Rik | RIKEN cDNA A430108E01 gene | 625 | 1028 | -1,6 | 0,0186 | |
| 1426524_at | Gnpda2 | glucosamine-6-phosphate deaminase 2 | 1098 | 1805 | -1,6 | 0,0078 | |
| 1426900_at | Jmjd1c | jumonji domain containing 1C | 967 | 1589 | -1,6 | 0,0298 | |
| 1418293_at | Ifit2 | interferon-induced protein with tetratricopeptide repeats 2 | 1035 | 1696 | -1,6 | 0,0271 | |
| 1430435_at | Aff3 | AF4/FMR2 family, member 3 | 133 | 217 | -1,6 | 0,0285 | |
| 1429499_at | Fbxo5 | F-box only protein 5 | 2220 | 3633 | -1,6 | 0,0328 | |
| 1455084_x_at | Shmt2 | serine hydroxymethyl transferase 2 (mitochondrial) | 2063 | 3375 | -1,6 | 0,0129 | |
| 1447910_x_at | BC052688 | cDNA sequence BC052688 | 40 | 66 | -1,6 | 0,0273 | |
| 1417547_at | Sart3 | squamous cell carcinoma antigen recognized by T-cells 3 | 270 | 440 | -1,6 | 0,0197 | |
| 1437878_s_at | Ccdc39 | coiled-coil domain containing 39 | 235 | 384 | -1,6 | 0,0310 | |
| 1438844_x_at | Spata5 | spermatogenesis associated 5 | 160 | 260 | -1,6 | 0,0118 | |
| 1428230_at | Prkcn | protein kinase C, nu | 1239 | 2018 | -1,6 | 0,0251 | |
| 1418440_at | Col8a1 | procollagen, type VIII, alpha 1 | 2538 | 4132 | -1,6 | 0,0387 | |
| 1419536_a_at | Rela | v-rel reticuloendotheliosis viral oncogene homolog A (avian) | 1076 | 1751 | -1,6 | 0,0494 | x |
| 1429017_at | Smcr8 | Smith-Magenis syndrome chromosome region, candidate 8 homolog (human) | 271 | 440 | -1,6 | 0,0090 | |
| 1433862_at | Espl1 | extra spindle poles-like 1 (S. cerevisiae) | 424 | 689 | -1,6 | 0,0254 | |
| 1433736_at | Hcfc1 | host cell factor C1 | 539 | 874 | -1,6 | 0,0278 | |
| 1428213_at | 2410003A14Rik | RIKEN cDNA 2410003A14 gene | 890 | 1441 | -1,6 | 0,0195 | |
| 1419126_at | Hoxd9 | homeo box D9 | 476 | 771 | -1,6 | 0,0376 | |
| 1416591_at | Rab34 | RAB34, member of RAS oncogene family | 505 | 818 | -1,6 | 0,0297 | |
| 1428500_at | 2210419D22Rik | RIKEN cDNA 2210419D22 gene | 348 | 562 | -1,6 | 0,0061 | |
| 1438246_at | Ppib | peptidylprolyl isomerase B | 114 | 184 | -1,6 | 0,0256 | |
| 1421844_at | Il1rap | interleukin 1 receptor accessory protein | 624 | 1006 | -1,6 | 0,0475 | |
| 1450044_at | Fzd7 | frizzled homolog 7 (Drosophila) | 318 | 511 | -1,6 | 0,0242 | |
| 1435847_at | Cdc42bpa | Cdc42 binding protein kinase alpha | 206 | 329 | -1,6 | 0,0310 | x |

| | | | | | | | |
|---|---|---|---|---|---|---|---|
| 1433485_x_at | Gpr56 | G protein-coupled receptor 56 | 585 | 937 | -1,6 | 0,0419 | |
| 1457908_at | Zfp407 | zinc finger protein 407 | 41 | 65 | -1,6 | 0,0297 | x |
| 1433755_at | Mier1 | mesoderm induction early response 1 homolog (Xenopus laevis | 397 | 633 | -1,6 | 0,0285 | |
| 1450051_at | Atrx | alpha thalassemia/mental retardation syndrome X-linked homolog (human) | 458 | 727 | -1,6 | 0,0475 | |
| 1427959_at | Abhd10 | abhydrolase domain containing 10 | 327 | 519 | -1,6 | 0,0171 | |
| 1452858_at | Elavl1 | ELAV (embryonic lethal, abnormal vision, Drosophila)-like 1 (Hu antigen R) | 27 | 43 | -1,6 | 0,0276 | |
| 1452220_at | Dock1 | dedicator of cyto-kinesis 1 | 936 | 1479 | -1,6 | 0,0311 | |
| 1429660_s_at | Smc2l1 | SMC2 structural maintenance of chromosomes 2-like 1 (yeast) | 1153 | 1821 | -1,6 | 0,0309 | |
| 1419428_a_at | Gaa | glucosidase, alpha, acid | 131 | 207 | -1,6 | 0,0420 | |
| 1439840_at | Polb | polymerase (DNA directed), beta | 8 | 13 | -1,6 | 0,0135 | |
| 1428411_at | 1700020I14Rik | RIKEN cDNA 1700020I14 gene | 1059 | 1670 | -1,6 | 0,0099 | |
| 1448529_at | Thbd | thrombomodulin | 7877 | 12422 | -1,6 | 0,0069 | |
| 1452310_at | Tada2l | transcriptional adaptor 2 (ADA2 homolog, yeast)-like | 253 | 399 | -1,6 | 0,0224 | x |
| 1449227_at | Ch25h | cholesterol 25-hydroxylase | 3066 | 4830 | -1,6 | 0,0280 | |
| 1424991_s_at | Tyms | thymidylate synthase | 1532 | 2409 | -1,6 | 0,0420 | |
| 1434620_s_at | Pkd2l2 | polycystic kidney disease 2-like 2 | 2520 | 3947 | -1,6 | 0,0160 | |
| 1429491_s_at | Rif1 | Rap1 interacting factor 1 homolog (yeast) | 965 | 1509 | -1,6 | 0,0460 | |
| 1451567_a_at | Ifi203 | interferon activated gene 203 | 1424 | 2228 | -1,6 | 0,0309 | |
| 1433702_at | D19Wsu12e | DNA segment, Chr 19, Wayne State University 12, expressed | 861 | 1347 | -1,6 | 0,0470 | |
| 1433641_at | Smad5 | MAD homolog 5 (Drosophila) | 333 | 520 | -1,6 | 0,0091 | |
| 1439496_at | 4921524J06Rik | RIKEN cDNA 4921524J06 gene | 946 | 1479 | -1,6 | 0,0476 | |
| 1429503_at | 2900024C23Rik | RIKEN cDNA 2900024C23 gene | 797 | 1246 | -1,6 | 0,0069 | |
| 1434210_s_at | Lrig1 | leucine-rich repeats and immunoglobulin-like domains 1 | 824 | 1288 | -1,6 | 0,0102 | |
| 1436367_at | --- | Adult male urinary bladder cDNA, RIKEN full-length enriched library, clone:9530071L19 product:unclassifiable, full insert sequence | 1843 | 2879 | -1,6 | 0,0206 | x |
| 1441005_at | 2610304G08Rik | RIKEN cDNA 2610304G08 gene | 8 | 12 | -1,6 | 0,0158 | |
| 1460227_at | Timp1 | tissue inhibitor of metalloproteinase 1 | 1878 | 2930 | -1,6 | 0,0283 | |
| 1436174_at | Atad2 | ATPase family, AAA domain containing 2 | 1791 | 2788 | -1,6 | 0,0064 | x |
| 1415986_at | Clcn4-2 | chloride channel 4-2 | 431 | 672 | -1,6 | 0,0314 | |
| 1460444_at | Arrb1 | arrestin, beta 1 | 667 | 1038 | -1,6 | 0,0170 | |
| 1453270_a_at | Phf14 | PHD finger protein 14 | 180 | 280 | -1,6 | 0,0298 | |
| 1435225_s_at | Brpf3 | bromodomain and PHD finger containing, 3 | 13 | 20 | -1,6 | 0,0069 | |
| 1452885_at | Sfrs2ip | splicing factor, arginine/serine-rich 2, interacting protein | 500 | 778 | -1,6 | 0,0446 | |
| 1434385_at | Tom1l2 | target of myb1-like 2 (chicken) | 418 | 648 | -1,6 | 0,0481 | |
| 1418347_at | Ccdc22 | coiled-coil domain containing 22 | 534 | 828 | -1,6 | 0,0303 | |
| 1416532_at | Trrap | transformation/transcription domain-associated protein | 255 | 396 | -1,6 | 0,0375 | |
| 1438320_s_at | Mcm7 | minichromosome maintenance deficient 7 (S. cerevisiae) | 6219 | 9638 | -1,5 | 0,0075 | |
| 1426949_s_at | Tpr | translocated promoter region | 2843 | 4405 | -1,5 | 0,0095 | |
| 1424686_at | 2700008B19Rik | RIKEN cDNA 2700008B19 gene | 220 | 341 | -1,5 | 0,0429 | |
| 1417904_at | Dclre1a | DNA cross-link repair 1A, PSO2 homolog (S. cerevisiae) | 141 | 217 | -1,5 | 0,0434 | |
| 1424033_at | Sfrs7 | splicing factor, arginine/serine-rich 7 | 1691 | 2598 | -1,5 | 0,0303 | |

| | | | | | | | |
|---|---|---|---|---|---|---|---|
| 1427978_at | 4732418C07Rik | RIKEN cDNA 4732418C07 gene | 248 | 380 | -1,5 | 0,0063 | |
| 1434802_s_at | Ntf3 | neurotrophin 3 | 324 | 496 | -1,5 | 0,0177 | |
| 1417519_at | Plagl2 | pleiomorphic adenoma gene-like 2 | 45 | 69 | -1,5 | 0,0193 | x |
| 1450642_at | 3110001I20Rik | RIKEN cDNA 3110001I20 gene | 4246 | 6504 | -1,5 | 0,0421 | |
| 1426983_at | Fnbp1 | formin binding protein 1 | 332 | 508 | -1,5 | 0,0342 | |
| 1422731_at | Limd1 | LIM domains containing 1 | 478 | 730 | -1,5 | 0,0324 | |
| 1425265_a_at | Prnpip1 | prion protein interacting protein 1 | 103 | 157 | -1,5 | 0,0404 | |
| 1451977_at | Dyrk1a | dual-specificity tyrosine-(Y)-phosphorylation regulated kinase 1a | 159 | 242 | -1,5 | 0,0248 | |
| 1451462_a_at | Ifnar2 | interferon (alpha and beta) receptor 2 | 1063 | 1621 | -1,5 | 0,0223 | |
| 1435338_at | Cdk6 | cyclin-dependent kinase 6 | 3812 | 5810 | -1,5 | 0,0149 | x |
| 1448721_at | D1Ertd622e | DNA segment, Chr 1, ERATO Doi 622, expressed | 1422 | 2167 | -1,5 | 0,0411 | |
| 1417295_at | Mta1 | metastasis associated 1 | 312 | 475 | -1,5 | 0,0394 | |
| 1417056_at | Psme1 | proteasome (prosome, macropain) 28 subunit, alpha | 793 | 1208 | -1,5 | 0,0409 | |
| 1429478_at | 6720463M24Rik | RIKEN cDNA 6720463M24 gene | 130 | 198 | -1,5 | 0,0227 | |
| 1440282_at | Tulp4 | tubby like protein 4 | 1558 | 2370 | -1,5 | 0,0304 | |
| 1429564_at | Pcgf5 | polycomb group ring finger 5 | 843 | 1282 | -1,5 | 0,0240 | |
| 1454952_s_at | B130055D15Rik | RIKEN cDNA B130055D15 gene | 1309 | 1989 | -1,5 | 0,0298 | |
| 1448907_at | Thop1 | thimet oligopeptidase 1 | 257 | 390 | -1,5 | 0,0113 | |
| 1425072_at | Skp2 | S-phase kinase-associated protein 2 (p45) | 30 | 46 | -1,5 | 0,0414 | |
| 1436303_at | Mllt4 | myeloid/lymphoid or mixed lineage-leukemia translocation to 4 homolog (Drosophila) | 1827 | 2769 | -1,5 | 0,0115 | |
| 1417409_at | Jun | Jun oncogene | 1966 | 2980 | -1,5 | 0,0144 | |
| 1460326_at | Pik3ca | phosphatidylinositol 3-kinase, catalytic, alpha polypeptide | 107 | 163 | -1,5 | 0,0115 | |
| 1436585_at | BB182297 | expressed sequence BB182297 | 141 | 214 | -1,5 | 0,0193 | |
| 1426060_at | Cul4a | cullin 4A | 78 | 118 | -1,5 | 0,0063 | |
| 1416036_at | Fkbp1a | FK506 binding protein 1a | 5338 | 8070 | -1,5 | 0,0448 | |
| 1456505_at | Ndufb2 | NADH dehydrogenase (ubiquinone) 1 beta subcomplex, 2 | 55 | 84 | -1,5 | 0,0082 | |
| 1456523_at | C77713 | expressed sequence C77713 | 313 | 472 | -1,5 | 0,0010 | |
| 1438761_a_at | Odc1 | ornithine decarboxylase, structural 1 | 9081 | 13702 | -1,5 | 0,0298 | |
| 1454705_at | D15Ertd621e | DNA segment, Chr 15, ERATO Doi 621, expressed | 1635 | 2466 | -1,5 | 0,0393 | |
| 1416830_at | 0610031J06Rik | RIKEN cDNA 0610031J06 gene | 1084 | 1636 | -1,5 | 0,0499 | |
| 1418024_at | Narg1 | NMDA receptor-regulated gene 1 | 867 | 1308 | -1,5 | 0,0280 | x |
| 1430535_at | Tsc22d2 | TSC22 domain family 2 | 2124 | 3201 | -1,5 | 0,0035 | |
| 1432827_x_at | Ubc | ubiquitin C | 6762 | 10186 | -1,5 | 0,0116 | |
| 1436308_at | Zfp292 | zinc finger protein 292 | 170 | 256 | -1,5 | 0,0438 | |
| 1428869_at | Nolc1 | nucleolar and coiled-body phosphoprotein 1 | 2659 | 4002 | -1,5 | 0,0051 | |
| 1416492_at | Ccne1 | cyclin E1 | 226 | 340 | -1,5 | 0,0206 | |
| 1429028_at | Dock11 | dedicator of cytokinesis 11 | 1346 | 2025 | -1,5 | 0,0434 | |
| 1435769_at | Akap9 | A kinase (PRKA) anchor protein (yotiao) 9 | 325 | 488 | -1,5 | 0,0171 | |
| 1428260_at | Spg3a | spastic paraplegia 3A homolog (human) | 143 | 215 | -1,5 | 0,0415 | |
| 1454006_a_at | Ubxd6 | UBX domain containing 6 | 83 | 124 | -1,5 | 0,0110 | |
| 1433614_at | Snx27 | sorting nexin family member 27 | 194 | 291 | -1,5 | 0,0476 | |
| 1435006_s_at | Abcb7 | ATP-binding cassette, sub-family B (MDR/TAP), member 7 | 665 | 997 | -1,5 | 0,0285 | |

| | | | | | | | |
|---|---|---|---|---|---|---|---|
| 1426269_at | Sybl1 | synaptobrevin like 1 | 1082 | 1620 | -1,5 | 0,0140 | |
| 1460682_s_at | Ceacam2 | CEA-related cell adhesion molecule 2 | 639 | 956 | -1,5 | 0,0178 | |
| 1426852_x_at | Nov | nephroblastoma overexpressed gene | 520 | 775 | -1,5 | 0,0211 | |
| 1452919_a_at | 1700012G19Rik | RIKEN cDNA 1700012G19 gene | 1259 | 1873 | -1,5 | 0,0439 | x |
| 1429004_at | Phip | pleckstrin homology domain interacting protein | 740 | 1102 | -1,5 | 0,0043 | |
| 1433455_at | Lnk | linker of T-cell receptor pathways | 1111 | 1652 | -1,5 | 0,0098 | |
| 1435777_at | E030018N11Rik | RIKEN cDNA E030018N11 gene | 5624 | 8346 | -1,5 | 0,0200 | |
| 1460180_at | Hexb | hexosaminidase B | 648 | 961 | -1,5 | 0,0409 | |
| 1460210_at | Pkd1 | polycystic kidney disease 1 homolog | 217 | 322 | -1,5 | 0,0224 | |
| 1422547_at | Ranbp1 | RAN binding protein 1 | 6177 | 9136 | -1,5 | 0,0207 | |
| 1417622_at | Slc12a2 | solute carrier family 12, member 2 | 8113 | 12000 | -1,5 | 0,0278 | |
| 1434570_at | AK122525 | cDNA sequence AK122525 | 352 | 521 | -1,5 | 0,0203 | |
| 1424141_at | Hectd1 | HECT domain containing 1 | 2042 | 3015 | -1,5 | 0,0121 | |
| 1436036_at | Whsc1 | Wolf-Hirschhorn syndrome candidate 1 (human) | 265 | 391 | -1,5 | 0,0182 | |
| 1444111_at | 2200002K05Rik | RIKEN cDNA 2200002K05 gene | 8 | 11 | -1,5 | 0,0254 | |
| 1444065_at | BC051585 | PREDICTED: Mus musculus similar to novel ZZ type zinc finger domain containing protein (LOC544797), mRNA | 19 | 27 | -1,5 | 0,0118 | |
| 1418843_at | Slc30a4 | solute carrier family 30 (zinc transporter), member 4 | 4176 | 6136 | -1,5 | 0,0200 | |
| 1452681_at | Dtymk | deoxythymidylate kinase | 461 | 678 | -1,5 | 0,0266 | |
| 1433893_s_at | Spag5 | sperm associated antigen 5 | 239 | 350 | -1,5 | 0,0468 | |
| 1441272_at | Matr3 | matrin 3 | 94 | 137 | -1,5 | 0,0414 | |
| 1456477_at | Ccnt1 | cyclin T1 | 180 | 263 | -1,5 | 0,0176 | |
| 1436181_at | Itgb1bp1 | integrin beta 1 binding protein 1 | 379 | 554 | -1,5 | 0,0186 | |
| 1449934_at | Pura | purine rich element binding protein A | 687 | 1002 | -1,5 | 0,0089 | |
| 1454919_at | Nmt2 | N-myristoyltransferase 2 | 1856 | 2706 | -1,5 | 0,0467 | |
| 1416816_at | Nek7 | NIMA (never in mitosis gene a)-related expressed kinase 7 | 8312 | 12101 | -1,5 | 0,0246 | |
| 1452659_at | Dek | DEK oncogene (DNA binding) | 8412 | 12229 | -1,5 | 0,0095 | |
| 1423656_x_at | 1500010J02Rik | RIKEN cDNA 1500010J02 gene | 238 | 345 | -1,5 | 0,0260 | |
| 1421923_at | Capn7 | calpain 7 | 6603 | 9585 | -1,5 | 0,0309 | |
| 1451221_at | BC018507 | cDNA sequence BC018507 | 459 | 665 | -1,4 | 0,0478 | |
| 1460436_at | Ndst1 | N-deacetylase/N-sulfotransferase (heparan glucosaminyl) 1 | 2109 | 3054 | -1,4 | 0,0291 | |
| 1434506_at | Arid2 | AT rich interactive domain 2 (Arid-rfx like) | 25 | 37 | -1,4 | 0,0276 | |
| 1455686_at | 5730507H05Rik | RIKEN cDNA 5730507H05 gene | 231 | 334 | -1,4 | 0,0345 | |
| 1417446_at | Slc12a4 | solute carrier family 12, member 4 | 492 | 710 | -1,4 | 0,0318 | |
| 1449702_at | Zfand2a | zinc finger, AN1-type domain 2A | 1392 | 2006 | -1,4 | 0,0171 | |
| 1429057_at | Narg1l | NMDA receptor regulated 1-like | 515 | 741 | -1,4 | 0,0251 | |
| 1434791_at | Atp6v0a2 | ATPase, H+ transporting, lysosomal V0 subunit A2 | 508 | 731 | -1,4 | 0,0034 | |
| 1417179_at | Tspan5 | tetraspanin 5 | 929 | 1336 | -1,4 | 0,0103 | x |
| 1429085_at | Vezf1 | vascular endothelial zinc finger 1 | 1435 | 2064 | -1,4 | 0,0493 | |
| 1454698_at | Ptplad1 | protein tyrosine phosphatase-like A domain containing 1 | 442 | 636 | -1,4 | 0,0404 | |
| 1454652_at | Zfp265 | zinc finger protein 265 | 1993 | 2863 | -1,4 | 0,0306 | |
| 1423249_at | Nktr | natural killer tumor recognition sequence | 167 | 239 | -1,4 | 0,0311 | |
| 1424778_at | D10Ucla1 | DNA segment, Chr 10, University of California at Los Angeles 1 | 308 | 440 | -1,4 | 0,0493 | |

| | | | | | | | |
|---|---|---|---|---|---|---|---|
| 1427953_at | BC025462 | cDNA sequence BC025462 | 86 | 122 | -1,4 | 0,0213 | |
| 1439787_at | P2rx7 | purinergic receptor P2X, ligand-gated ion channel, 7 | 9 | 13 | -1,4 | 0,0345 | |
| 1416768_at | 1110003E01Rik | RIKEN cDNA 1110003E01 gene | 1804 | 2569 | -1,4 | 0,0155 | |
| 1428243_at | 1700021K19Rik | RIKEN cDNA 1700021K19 gene | 119 | 169 | -1,4 | 0,0284 | |
| 1426754_x_at | Ckap4 | cytoskeleton-associated protein 4 | 582 | 825 | -1,4 | 0,0409 | |
| 1423622_a_at | Ccnl1 | cyclin L1 | 612 | 867 | -1,4 | 0,0154 | |
| 1429618_at | Cyld | cylindromatosis (turban tumor syndrome) | 2340 | 3303 | -1,4 | 0,0110 | |
| 1418562_at | Sf3b1 | splicing factor 3b, subunit 1 | 1495 | 2106 | -1,4 | 0,0192 | |
| 1417800_at | Parp2 | poly (ADP-ribose) polymerase family, member 2 | 384 | 540 | -1,4 | 0,0395 | |
| 1429883_at | Actl6a | actin-like 6A | 192 | 271 | -1,4 | 0,0413 | |
| 1426364_at | Mrrf | mitochondrial ribosome recycling factor | 561 | 788 | -1,4 | 0,0232 | |
| 1426454_at | Arhgdib | Rho, GDP dissociation inhibitor (GDI) beta | 1963 | 2759 | -1,4 | 0,0298 | |
| 1454648_s_at | D10Wsu102e | DNA segment, Chr 10, Wayne State University 102, expressed | 449 | 629 | -1,4 | 0,0463 | |
| 1455768_at | Npc2 | Niemann Pick type C2 | 300 | 421 | -1,4 | 0,0280 | |
| 1418012_at | Sh3glb1 | SH3-domain GRB2-like B1 (endophilin) | 661 | 927 | -1,4 | 0,0278 | x |
| 1427878_at | 0610010O12Rik | RIKEN cDNA 0610010O12 gene | 68 | 95 | -1,4 | 0,0421 | |
| 1418501_a_at | Oxr1 | oxidation resistance 1 | 3491 | 4889 | -1,4 | 0,0168 | |
| 1423389_at | Smad7 | MAD homolog 7 (Drosophila) | 531 | 743 | -1,4 | 0,0460 | |
| 1434646_s_at | Sap18 | Sin3-associated polypeptide 18 | 8797 | 12312 | -1,4 | 0,0277 | |
| 1426739_at | Donson | downstream neighbor of SON | 113 | 157 | -1,4 | 0,0274 | |
| 1416254_a_at | Vps16 | vacuolar protein sorting 16 (yeast) | 274 | 383 | -1,4 | 0,0473 | |
| 1454927_at | Zfp41 | zinc finger protein 41 | 71 | 99 | -1,4 | 0,0376 | |
| 1452032_at | Prkar1a | protein kinase, cAMP dependent regulatory, type I, alpha | 7297 | 10179 | -1,4 | 0,0137 | |
| 1449933_a_at | 5730449L18Rik | RIKEN cDNA 5730449L18 gene | 213 | 297 | -1,4 | 0,0192 | |
| 1428169_at | Atg16l1 | autophagy-related 16-like 1 (yeast) | 235 | 327 | -1,4 | 0,0309 | |
| 1449839_at | Casp3 | caspase 3 | 1603 | 2233 | -1,4 | 0,0198 | |
| 1416903_at | Nucb1 | nucleobindin 1 | 974 | 1357 | -1,4 | 0,0318 | |
| 1455437_at | 9030204A07Rik | RIKEN cDNA 9030204A07 gene | 977 | 1360 | -1,4 | 0,0434 | |
| 1457111_at | AA415038 | expressed sequence AA415038 | 61 | 84 | -1,4 | 0,0450 | |
| 1416171_at | 2310037I24Rik | RIKEN cDNA 2310037I24 gene | 2354 | 3267 | -1,4 | 0,0099 | |
| 1434507_at | Npepl1 | aminopeptidase-like 1 | 562 | 778 | -1,4 | 0,0065 | |
| 1425560_a_at | S100a16 | S100 calcium binding protein A16 | 3803 | 5252 | -1,4 | 0,0399 | |
| 1453183_at | 1110034A24Rik | RIKEN cDNA 1110034A24 gene | 152 | 210 | -1,4 | 0,0220 | |
| 1417941_at | Nanp | N-acetylneuraminic acid phosphatase | 542 | 748 | -1,4 | 0,0328 | |
| 1448703_at | Lsm8 | LSM8 homolog, U6 small nuclear RNA associated (S. cerevisiae) | 4003 | 5516 | -1,4 | 0,0414 | |
| 1448684_at | Ppp1r2 | protein phosphatase 1, regulatory (inhibitor) subunit 2 | 5552 | 7650 | -1,4 | 0,0348 | |
| 1452868_at | Usp24 | ubiquitin specific peptidase 24 | 315 | 434 | -1,4 | 0,0453 | |
| 1419647_a_at | Ier3 | immediate early response 3 | 3770 | 5189 | -1,4 | 0,0298 | |
| 1435000_at | Gspt1 | G1 to S phase transition 1 | 298 | 409 | -1,4 | 0,0396 | |
| 1422854_at | Shc1 | src homology 2 domain-containing transforming protein C1 | 834 | 1147 | -1,4 | 0,0231 | |
| 1417138_s_at | Polr2e | polymerase (RNA) II (DNA directed) polypeptide E | 717 | 986 | -1,4 | 0,0151 | |
| 1438688_at | Srrm2 | serine/arginine repetitive matrix 2 | 5595 | 7690 | -1,4 | 0,0194 | |
| 1450958_at | Tm4sf1 | transmembrane 4 superfamily member 1 | 21467 | 29481 | -1,4 | 0,0447 | |

| | | | | | | | |
|---|---|---|---|---|---|---|---|
| 1448797_at | Elk3 | ELK3, member of ETS oncogene family | 5088 | 6985 | -1,4 | 0,0297 | |
| 1455227_at | Aadacl1 | arylacetamide deacetylase-like 1 | 335 | 460 | -1,4 | 0,0334 | |
| 1416641_at | Lig1 | ligase I, DNA, ATP-dependent | 1230 | 1684 | -1,4 | 0,0255 | |
| 1451083_s_at | Aars | alanyl-tRNA synthetase | 2272 | 3110 | -1,4 | 0,0043 | |
| 1421963_a_at | Cdc25b | cell division cycle 25 homolog B (S. cerevisiae) | 454 | 620 | -1,4 | 0,0330 | |
| 1427987_at | Safb2 | scaffold attachment factor B2 | 296 | 405 | -1,4 | 0,0313 | |
| 1426397_at | Tgfbr2 | transforming growth factor, beta receptor II | 2125 | 2901 | -1,4 | 0,0065 | |
| 1417674_s_at | Golga4 | golgi autoantigen, golgin subfamily a, 4 | 1218 | 1656 | -1,4 | 0,0135 | |
| 1425745_a_at | Tacc2 | transforming, acidic coiled-coil containing protein 2 | 881 | 1198 | -1,4 | 0,0305 | |
| 1427425_at | 9130208E07Rik | RIKEN cDNA 9130208E07 gene | 8 | 10 | -1,4 | 0,0263 | |
| 1417490_at | Ctsb | cathepsin B | 6495 | 8827 | -1,4 | 0,0242 | |
| 1455586_at | Rnf168 | ring fnger protein 168 | 217 | 295 | -1,4 | 0,0269 | |
| 1433995_s_at | D16Bwg1543e | DNA segment, Chr 16, Brigham & Women's Genetics 1543 expressed | 1284 | 1745 | -1,4 | 0,0404 | |
| 1456495_s_at | Osbpl6 | oxysterol binding protein-like 6 | 229 | 311 | -1,4 | 0,0250 | |
| 1439128_at | --- | Acyl-Coenzyme A binding domain containing 6, mRNA (cDNA clone IMAGE:3465595) | 1474 | 1999 | -1,4 | 0,0136 | |
| 1426631_at | Pus7 | pseudouridylate synthase 7 homolog (S. cerevisiae) | 945 | 1281 | -1,4 | 0,0103 | |
| 1418236_s_at | Atg5 | autophagy-related 5 (yeast) | 109 | 147 | -1,4 | 0,0125 | |
| 1425615_a_at | Pck2 | phosphoenolpyruvate carboxykinase 2 (mitochondrial) | 497 | 674 | -1,4 | 0,0364 | |
| 1448579_at | Glg1 | golgi apparatus protein 1 | 1381 | 1867 | -1,4 | 0,0308 | |
| 1422669_at | Ebag9 | estrogen receptor-binding fragment-associated gene 9 | 446 | 601 | -1,3 | 0,0468 | |
| 1450852_s_at | F2r | coagulation factor II (thrombin) receptor | 5103 | 6867 | -1,3 | 0,0283 | x |
| 1423507_a_at | Sirt2 | sirtuin 2 (silent mating type information regulation 2, homolog) 2 (S. cerevisiae) | 1370 | 1841 | -1,3 | 0,0413 | x |
| 1434643_at | Tbl1x | transducin (beta)-like 1 X-linked | 334 | 447 | -1,3 | 0,0429 | |
| 1448320_at | Stim1 | stromal interaction molecule 1 | 160 | 213 | -1,3 | 0,0446 | |
| 1448597_at | Cstf1 | cleavage stimulation factor, 3' pre-RNA, subunit 1 | 375 | 500 | -1,3 | 0,0436 | x |
| 1416441_at | Pgcp | plasma glutamate carboxypeptidase | 2238 | 2983 | -1,3 | 0,0220 | |
| 1452797_at | 2310010B21Rik | RIKEN cDNA 2310010B21 gene | 162 | 215 | -1,3 | 0,0026 | |
| 1434300_at | 2610101N10Rik | RIKEN cDNA 2610101N10 gene | 516 | 687 | -1,3 | 0,0303 | |
| 1448899_s_at | Rad51ap1 | RAD51 associated protein 1 | 530 | 705 | -1,3 | 0,0304 | |
| 1435379_at | AK122209 | cDNA sequence AK122209 | 347 | 461 | -1,3 | 0,0480 | |
| 1433699_at | Tnfaip3 | tumor necrosis factor, alpha-induced protein 3 | 850 | 1128 | -1,3 | 0,0439 | |
| 1435739_at | AW208599 | expressed sequence AW208599 | 234 | 309 | -1,3 | 0,0158 | |
| 1431131_s_at | A630007B06Rik | RIKEN cDNA A630007B06 gene | 83 | 109 | -1,3 | 0,0251 | |
| 1452737_at | 2810008M24Rik | RIKEN cDNA 2810008M24 gene | 3721 | 4921 | -1,3 | 0,0089 | |
| 1448195_at | Taf5l | TAF5-like RNA polymerase II, p300/CBP-associated factor (PCAF)-associated factor | 335 | 443 | -1,3 | 0,0239 | |
| 1438030_at | Rasgrp3 | RAS, guanyl releasing protein 3 | 5726 | 7547 | -1,3 | 0,0344 | |
| 1435141_at | Sft2d2 | SFT2 domain containing 2 | 1228 | 1616 | -1,3 | 0,0323 | |
| 1450981_at | Cnn2 | calponin 2 | 5850 | 7696 | -1,3 | 0,0376 | |
| 1455311_at | Dgcr8 | DiGeorge syndrome critical region gene 8 | 276 | 363 | -1,3 | 0,0182 | |
| 1423755_at | Zcchc8 | zinc finger, CCHC domain containing 8 | 2080 | 2735 | -1,3 | 0,0062 | |

| | | | | | | | |
|---|---|---|---|---|---|---|---|
| 1434344_at | Gpkow | G patch domain and KOW motifs | 803 | 1057 | -1,3 | 0,0496 | |
| 1415792_at | AL033326 | expressed sequence AL033326 | 348 | 458 | -1,3 | 0,0395 | |
| 1416029_at | Klf10 | Kruppel-like factor 10 | 857 | 1127 | -1,3 | 0,0160 | |
| 1420664_s_at | Procr | protein C receptor, endothelial | 41788 | 54874 | -1,3 | 0,0281 | |
| 1419248_at | Rgs2 | regulator of G-protein signaling 2 | 6330 | 8311 | -1,3 | 0,0099 | |
| 1453174_at | 2310076G13Rik | RIKEN cDNA 2310076G13 gene | 924 | 1212 | -1,3 | 0,0301 | |
| 1419455_at | Il10rb | interleukin 10 receptor, beta | 1301 | 1704 | -1,3 | 0,0162 | |
| 1434958_at | Sacs | sacsin | 3290 | 4307 | -1,3 | 0,0076 | |
| 1416501_at | Pdpk1 | 3-phosphoinositide dependent protein kinase-1 | 957 | 1252 | -1,3 | 0,0248 | |
| 1426485_at | Ubxd2 | UBX domain containing 2 | 4173 | 5416 | -1,3 | 0,0076 | |
| 1423128_at | Aip | aryl-hydrocarbon receptor-interacting protein | 953 | 1236 | -1,3 | 0,0384 | x |
| 1426861_at | 9130023F12Rik | RIKEN cDNA 9130023F12 gene | 560 | 724 | -1,3 | 0,0282 | |
| 1427689_a_at | Tnip1 | TNFAIP3 interacting protein 1 | 774 | 995 | -1,3 | 0,0164 | |
| 1437198_at | Rffl | ring finger and FYVE like domain containing protein | 283 | 363 | -1,3 | 0,0189 | |
| 1438233_at | 6030443O07Rik | RIKEN cDNA 6030443O07 gene | 1228 | 1577 | -1,3 | 0,0292 | |
| 1456059_at | Psmd11 | proteasome (prosome, macropain) 26S subunit, non-ATPase, 11 | 408 | 523 | -1,3 | 0,0201 | |
| 1420636_a_at | Dusp12 | dual specificity phosphatase 12 | 363 | 466 | -1,3 | 0,0414 | |
| 1439278_at | Zbtb20 | zinc finger and BTB domain containing 20 | 742 | 950 | -1,3 | 0,0118 | |
| 1438735_at | Hbxap | hepatitis B virus x associated protein | 312 | 399 | -1,3 | 0,0208 | |
| 1434117_at | Tceb3 | transcription elongation factor B (SIII), polypeptide 3 | 101 | 128 | 1,3 | 0,0310 | |
| 1423375_at | 1700023B02Rik | RIKEN cDNA 1700023B02 gene | 28 | 36 | -1,3 | 0,0105 | |
| 1452321_at | Brwd1 | bromodomain and WD repeat domain containing 1 | 48 | 61 | -1,3 | 0,0348 | |
| 1442287_at | --- | Transcribed locus | 89 | 114 | -1,3 | 0,0299 | |
| 1450887_at | Rqcd1 | rcd1 (required for cell differentiation) homolog 1 (S. pombe) | 521 | 663 | -1,3 | 0,0389 | |
| 1416531_at | Gsto1 | glutathione S-transferase omega 1 | 9569 | 12172 | -1,3 | 0,0204 | |
| 1423731_at | Aldh16a1 | aldehyde dehydrogenase 16 family, member A1 | 92 | 117 | -1,3 | 0,0311 | |
| 1451431_a_at | D2Bwg0891e | DNA segment, Chr 2, Brigham & Women's Genetics 0891 expressed | 428 | 543 | -1,3 | 0,0297 | |
| 1452806_at | 1500016O10Rik | RIKEN cDNA 1500016O10 gene | 7 | 10 | -1,3 | 0,0298 | |
| 1418616_at | Mafk | v-maf musculoaponeurotic fibrosarcoma oncogene family, protein K (avian) | 362 | 459 | -1,3 | 0,0330 | |
| 1416060_at | Tbc1d15 | TBC1 domain family, member 15 | 2867 | 3633 | -1,3 | 0,0465 | |
| 1434671_at | B230337E12Rik | RIKEN cDNA B230337E12 gene | 588 | 744 | -1,3 | 0,0174 | |
| 1422517_a_at | Znrd1 | zinc ribbon domain containing, 1 | 1742 | 2198 | -1,3 | 0,0298 | |
| 1420046_s_at | Maf1 | MAF1 homolog (S. cerevisiae) | 921 | 1157 | -1,3 | 0,0463 | |
| 1416270_at | Polr2g | polymerase (RNA) II (DNA directed) polypeptide G | 4844 | 6082 | -1,3 | 0,0171 | |
| 1454834_at | Nfib | nuclear factor I/B | 4843 | 6068 | -1,3 | 0,0467 | |
| 1434161_at | 5830457H20Rik | RIKEN cDNA 5830457H20 gene | 441 | 551 | -1,3 | 0,0361 | |
| 1423461_a_at | Ubl3 | ubiquitin-like 3 | 1408 | 1760 | -1,2 | 0,0436 | |
| 1422801_at | RP23-336J1.4 | Ras-GTPase-activating protein SH3-domain binding protein | 3521 | 4390 | -1,2 | 0,0210 | |
| 1436069_at | Ing5 | inhibitor of growth family, member 5 | 345 | 429 | -1,2 | 0,0323 | |
| 1428000_at | Tmem60 | transmembrane protein 60 | 1517 | 1885 | -1,2 | 0,0451 | |
| 1434219_at | Stim2 | stromal interaction molecule 2 | 2178 | 2702 | -1,2 | 0,0330 | |
| 1421821_at | Ldlr | low density lipoprotein receptor | 937 | 1162 | -1,2 | 0,0415 | |

| | | | | | | | |
|---|---|---|---|---|---|---|---|
| 1436795_at | 9630058J23Rik | RIKEN cDNA 9630058J23 gene | 148 | 183 | -1,2 | 0,0385 | x |
| 1424640_at | Arl8a | ADP-ribosylation factor-like 8A | 519 | 640 | -1,2 | 0,0409 | |
| 1425837_a_at | Ccrn4l | CCR4 carbon catabolite repression 4-like (S. cerevisiae) | 2788 | 3435 | -1,2 | 0,0315 | |
| 1448619_at | Dhcr7 | 7-dehydrocholesterol reductase | 132 | 162 | -1,2 | 0,0287 | |
| 1450705_at | Rdbp | RD RNA-binding protein | 1168 | 1433 | -1,2 | 0,0277 | |
| 1433666_s_at | Vps41 | vacuolar protein sorting 41 (yeast) | 615 | 754 | -1,2 | 0,0236 | |
| 1423539_at | Pms2 | postmeiotic segregation increased 2 (S. cerevisiae) | 257 | 315 | -1,2 | 0,0438 | |
| 1434665_at | Aga | aspartylglucosaminidase | 721 | 881 | -1,2 | 0,0252 | |
| 1426968_a_at | Rdh10 | retinol dehydrogenase 10 (all-trans) | 163 | 198 | -1,2 | 0,0143 | x |
| 1451291_at | Obfc2b | oligonucleotide/oligosaccharide-binding fold containing 2B | 430 | 521 | -1,2 | 0,0351 | |
| 1416544_at | Ezh2 | enhancer of zeste homolog 2 (Drosophila) | 1811 | 2195 | -1,2 | 0,0138 | |
| 1456026_at | 8030451K01Rik | RIKEN cDNA 8030451K01 gene | 527 | 638 | -1,2 | 0,0377 | |
| 1422613_a_at | Rpl7a | ribosomal protein L7a | 19659 | 23764 | -1,2 | 0,0480 | x |
| 1452702_at | Clcn7 | chloride channel 7 | 517 | 624 | -1,2 | 0,0414 | |
| 1423047_at | Tollip | toll interacting protein | 1628 | 1950 | -1,2 | 0,0478 | |
| 1424149_at | 1110014D18Rik | RIKEN cDNA 1110014D18 gene | 708 | 847 | -1,2 | 0,0481 | |
| 1417086_at | Pafah1b1 | platelet-activating factor acetylhydrolase, isoform 1b, beta1 subunit | 267 | 320 | -1,2 | 0,0474 | |
| 1438578_a_at | Btbd10 | BTB (POZ) domain containing 10 | 2609 | 3120 | -1,2 | 0,0195 | |
| 1428842_a_at | Ngfrap1 | nerve growth factor receptor (TNFRSF16) associated protein 1 | 3255 | 3889 | -1,2 | 0,0471 | |
| 1426817_at | Mki67 | antigen identified by monoclonal antibody Ki 67 | 8730 | 10421 | -1,2 | 0,0441 | |
| 1452151_at | BC021523 | cDNA sequence BC021523 | 501 | 597 | -1,2 | 0,0127 | |
| 1423975_s_at | Numa1 | nuclear mitotic apparatus protein 1 | 816 | 968 | -1,2 | 0,0441 | |
| 1435679_at | Optn | optineurin | 347 | 410 | -1,2 | 0,0330 | |
| 1419867_a_at | Ankhd1 | ankyrin repeat and KH domain containing 1 | 522 | 614 | -1,2 | 0,0387 | |
| 1423275_at | Ddx26 | DEAD/H (Asp-Glu-Ala-Asp/His) box polypeptide 26 | 600 | 697 | -1,2 | 0,0446 | |
| 1416963_at | Ubadc1 | ubiquitin associated domain containing 1 | 705 | 812 | -1,2 | 0,0413 | x |
| 1417451_a_at | Ppia | peptidylprolyl isomerase A | 24814 | 28344 | -1,1 | 0,0445 | |
| 1442198_at | --- | --- | 5 | 6 | -1,1 | 0,0303 | |
| 1416642_a_at | Tpt1 | tumor protein, translationally-controlled 1 | 31232 | 35179 | -1,1 | 0,0393 | |
| 1423772_x_at | Slc25a5 | solute carrier family 25 (mitochondrial carrier, adenine nucleotide translocator), member 5 | 17483 | 19690 | -1,1 | 0,0439 | |
| 1422994_at | Pip5k3 | phosphatidylinositol-3-phosphate/phosphatidylinositol 5-kinase, type III | 10 | 9 | 1,1 | 0,0493 | |
| 1435811_a_at | Unc50 | unc-50 homolog (C. elegans) | 2761 | 2471 | 1,1 | 0,0274 | |
| 1425298_a_at | Birc1a | baculoviral IAP repeat-containing 1a | 10 | 9 | 1,1 | 0,0366 | |
| 1418203_at | Pmaip1 | phorbol-12-myristate-13-acetate-induced protein 1 | 12 | 10 | 1,2 | 0,0418 | |
| 1426386_at | Rpl7l1 | ribosomal protein L7-like 1 | 963 | 837 | 1,2 | 0,0492 | |
| 1424670_s_at | Zfyve21 | zinc finger, FYVE domain containing 21 | 897 | 778 | 1,2 | 0,0307 | |
| 1416524_at | Spop | speckle-type POZ protein | 3813 | 3296 | 1,2 | 0,0257 | |
| 1436921_at | Atp7a | ATPase, Cu++ transporting, alpha polypeptide | 3480 | 2977 | 1,2 | 0,0227 | |
| 1428345_at | 4430402I18Rik | RIKEN cDNA 4430402I18 gene | 74 | 63 | 1,2 | 0,0375 | |
| 1460621_x_at | Ywhaq | tyrosine 3-monooxygenase/tryptophan 5-monooxygenase activation protein, theta polypeptide | 22991 | 19587 | 1,2 | 0,0220 | |
| 1428624_at | 2810482I07Rik | RIKEN cDNA 2810482I07 gene | 5132 | 4369 | 1,2 | 0,0283 | |

| | | | | | | | |
|---|---|---|---|---|---|---|---|
| 1460359_at | Armcx3 | armadillo repeat containing, X-linked 3 | 1133 | 958 | 1,2 | 0,0493 | |
| 1456205_x_at | Tbca | tubulin cofactor a | 14281 | 12036 | 1,2 | 0,0420 | |
| 1449351_s_at | Pdgfc | platelet-derived growth factor, C polypeptide | 29 | 25 | 1,2 | 0,0145 | |
| 1455174_at | Rps19bp1 | ribosomal protein S19 binding protein 1 | 625 | 525 | 1,2 | 0,0382 | x |
| 1444602_at | --- | Transcribed locus | 13 | 11 | 1,2 | 0,0324 | |
| 1426378_at | Eif4b | eukaryotic translation initiation factor 4B | 2113 | 1757 | 1,2 | 0,0404 | |
| 1455816_a_at | Kctd3 | potassium channel tetramerisation domain containing 3 | 7392 | 6134 | 1,2 | 0,0422 | |
| 1434056_a_at | Ndufb6 | NADH dehydrogenase (ubiquinone) 1 beta subcomplex, 6 | 22759 | 18872 | 1,2 | 0,0171 | |
| 1448771_a_at | Fth1 | ferritin heavy chain 1 | 42224 | 34871 | 1,2 | 0,0201 | |
| 1454829_at | Rundc1 | RUN domain containing 1 | 155 | 126 | 1,2 | 0,0225 | |
| 1423333_at | 1200007D18Rik | RIKEN cDNA 1200007D18 gene | 741 | 605 | 1,2 | 0,0241 | |
| 1424639_a_at | Hmgcl | 3-hydroxy-3-methylglutaryl-Coenzyme A lyase | 470 | 383 | 1,2 | 0,0468 | |
| 1448867_at | Tmem9b | TMEM9 domain family, member B | 1866 | 1518 | 1,2 | 0,0251 | x |
| 1438760_x_at | Adam15 | a disintegrin and metallopeptidase domain 15 (metargidin) | 750 | 610 | 1,2 | 0,0142 | |
| 1451044_at | Sip1 | survivor of motor neuron protein interacting protein 1 | 708 | 574 | 1,2 | 0,0288 | x |
| 1424366_at | Tmem15 | transmembrane protein 15 | 1334 | 1081 | 1,2 | 0,0280 | |
| 1428369_s_at | Arhgap21 | Rho GTPase activating protein 21 | 3776 | 3059 | 1,2 | 0,0408 | |
| 1449142_a_at | Yipf5 | Yip1 domain family, member 5 | 866 | 700 | 1,2 | 0,0221 | |
| 1447977_x_at | --- | --- | 1055 | 852 | 1,2 | 0,0393 | |
| 1455795_at | Sart2 | squamous cell carcinoma antigen recognized by T cells 2 | 25 | 20 | 1,2 | 0,0245 | |
| 1439401_x_at | Ppp2r5e | protein phosphatase 2, regulatory subunit B (B56), epsilon isoform | 733 | 587 | 1,2 | 0,0149 | |
| 1450407_a_at | Anp32a | acidic (leucine-rich) nuclear phosphoprotein 32 family, member A | 910 | 724 | 1,3 | 0,0246 | |
| 1439622_at | Rassf4 | Ras association (RalGDS/AF-6) domain family 4 | 9 | 7 | 1,3 | 0,0162 | |
| 1436848_x_at | Impa1 | inositol (myo)-1(or 4)-monophosphatase 1 | 6535 | 5185 | 1,3 | 0,0241 | |
| 1416465_a_at | Vapa | vesicle-associated membrane protein, associated protein A | 11456 | 9080 | 1,3 | 0,0203 | |
| 1420809_a_at | 1500003O03Rik | RIKEN cDNA 1500003O03 gene | 10421 | 8248 | 1,3 | 0,0061 | |
| 1442097_at | --- | --- | 13 | 10 | 1,3 | 0,0243 | |
| 1439561_at | 2010012O05Rik | RIKEN cDNA 2010012O05 gene | 26 | 20 | 1,3 | 0,0218 | |
| 1422996_at | Acot2 | acyl-CoA thioesterase 2 | 21 | 16 | 1,3 | 0,0413 | |
| 1420641_a_at | Sqrdl | sulfide quinone reductase-like (yeast) | 1433 | 1122 | 1,3 | 0,0267 | |
| 1454678_s_at | A130022J15Rik | RIKEN cDNA A130022J15 gene | 2765 | 2164 | 1,3 | 0,0404 | |
| 1427760_s_at | Plf | proliferin | 9 | 7 | 1,3 | 0,0075 | x |
| 1453021_at | Stxbp5 | syntaxin binding protein 5 (tomosyn) | 179 | 140 | 1,3 | 0,0397 | x |
| 1439268_x_at | Eif3s6 | eukaryotic translation initiation factor 3, subunit 6 | 20085 | 15699 | 1,3 | 0,0179 | |
| 1451318_a_at | Lyn | Yamaguchi sarcoma viral (v-yes-1) oncogene homolog | 1237 | 965 | 1,3 | 0,0306 | |
| 1449338_at | D10Ertd641e | DNA segment, Chr 10, ERATO Doi 641, expressed | 2891 | 2238 | 1,3 | 0,0238 | |
| 1421275_s_at | Socs4 | suppressor of cytokine signaling 4 | 70 | 54 | 1,3 | 0,0283 | |
| 1418164_at | Epim | epimorphin | 430 | 332 | 1,3 | 0,0040 | |
| 1456013_x_at | Slc35a4 | solute carrier family 35, member A4 | 1444 | 1114 | 1,3 | 0,0174 | |
| 1439368_a_at | Slc9a3r2 | solute carrier family 9 (sodium/hydrogen exchanger), isoform 3 regulator 2 | 9050 | 6977 | 1,3 | 0,0400 | |
| 1448334_a_at | Ccni | cyclin I | 7542 | 5813 | 1,3 | 0,0328 | |

| | | | | | | | |
|---|---|---|---|---|---|---|---|
| 1428074_at | 2310037P21Rik | RIKEN cDNA 2310037P21 gene | 9263 | 7136 | 1,3 | 0,0240 | |
| 1448517_at | Timm22 | translocase of inner mitochondrial membrane 22 homolog (yeast) | 815 | 627 | 1,3 | 0,0124 | |
| 1438646_x_at | 2510039O18Rik | RIKEN cDNA 2510039O18 gene | 615 | 474 | 1,3 | 0,0266 | |
| 1441811_x_at | 0610011I04Rik | RIKEN cDNA 0610011I04 gene | 1649 | 1267 | 1,3 | 0,0206 | |
| 1425486_s_at | Mtmr6 | myotubularin related protein 6 | 4975 | 3797 | 1,3 | 0,0412 | |
| 1416808_at | Nid1 | nidogen 1 | 13524 | 10296 | 1,3 | 0,0423 | |
| 1438928_x_at | Ninj1 | ninjurin 1 | 920 | 698 | 1,3 | 0,0404 | x |
| 1437014_x_at | LOC545161 | NA | 11223 | 8516 | 1,3 | 0,0231 | |
| 1416179_a_at | Rdx | radixin | 14090 | 10690 | 1,3 | 0,0482 | |
| 1456604_a_at | Pcmt1 | protein-L-isoaspartate (D-aspartate) O-methyltransferase 1 | 4138 | 3138 | 1,3 | 0,0095 | |
| 1424574_at | Tmed5 | transmembrane emp24 protein transport domain containing 5 | 7315 | 5541 | 1,3 | 0,0024 | |
| 1417162_at | Tmbim1 | transmembrane BAX inhibitor motif containing 1 | 3931 | 2976 | 1,3 | 0,0060 | |
| 1416911_a_at | 6330407G11Rik | RIKEN cDNA 6330407G11 gene | 4252 | 3214 | 1,3 | 0,0241 | |
| 1454748_at | Naprt1 | nicotinate phosphoribosyltransferase domain containing 1 | 92 | 70 | 1,3 | 0,0065 | |
| 1418029_at | Faim | Fas apoptotic inhibitory molecule | 3062 | 2308 | 1,3 | 0,0357 | |
| 1426436_at | 8430420C20Rik | RIKEN cDNA 8430420C20 gene | 234 | 176 | 1,3 | 0,0460 | |
| 1437385_at | Ccbe1 | collagen and calcium binding EGF domains 1 | 1081 | 810 | 1,3 | 0,0167 | |
| 1434267_at | Nek1 | NIMA (never in mitosis gene a)-related expressed kinase 1 | 141 | 105 | 1,3 | 0,0305 | |
| 1434692_at | 1110034B05Rik | RIKEN cDNA 1110034B05 gene | 611 | 455 | 1,3 | 0,0340 | |
| 1456872_a_at | D230010M03Rik | RIKEN cDNA D230010M03 gene | 59 | 44 | 1,3 | 0,0195 | |
| 1452342_at | Apbb2 | amyloid beta (A4) precursor protein-binding, family B, member 2 | 2278 | 1689 | 1,3 | 0,0451 | |
| 1434853_x_at | Mkrn1 | makorin, ring finger protein, 1 | 2165 | 1604 | 1,3 | 0,0364 | |
| 1423402_at | Creb1 | cAMP responsive element binding protein 1 | 363 | 268 | 1,4 | 0,0453 | |
| 1422539_at | Extl2 | exotoses (multiple)-like 2 | 569 | 419 | 1,4 | 0,0318 | |
| 1452929_at | Rsn | restin (Reed-Steinberg cell-expressed intermediate filament-associated protein) | 1310 | 963 | 1,4 | 0,0395 | x |
| 1434084_at | 5730601F06Rik | RIKEN cDNA 5730601F06 gene | 2351 | 1726 | 1,4 | 0,0214 | |
| 1436834_x_at | Mdh1 | malate dehydrogenase 1, NAD (soluble) | 11835 | 8689 | 1,4 | 0,0049 | |
| 1424309_a_at | Mocs2 | molybdenum cofactor synthesis 2 | 2653 | 1945 | 1,4 | 0,0138 | |
| 1456739_x_at | Armcx2 | armadillo repeat containing, X-linked 2 | 10713 | 7844 | 1,4 | 0,0078 | |
| 1447277_s_at | Pcyox1 | prenylcysteine oxidase 1 | 5792 | 4217 | 1,4 | 0,0271 | |
| 1448707_at | Taf13 | TAF13 RNA polymerase II, TATA box binding protein (TBP)-associated factor | 1948 | 1416 | 1,4 | 0,0336 | x |
| 1420827_a_at | Ccng1 | cyclin G1 | 19660 | 14288 | 1,4 | 0,0457 | |
| 1441931_x_at | BB125219 | expressed sequence BB125219 | 204 | 148 | 1,4 | 0,0456 | |
| 1460346_at | Arsa | arylsulfatase A | 1732 | 1256 | 1,4 | 0,0089 | |
| 1441866_s_at | Ptdss1 | phosphatidylserine synthase 1 | 2775 | 2011 | 1,4 | 0,0474 | x |
| 1434839_s_at | Tbl1xr1 | transducin (beta)-like 1X-linked receptor 1 | 701 | 507 | 1,4 | 0,0386 | |
| 1420967_at | Slc25a15 | solute carrier family 25 (mitochondrial carrier ornithine transporter), member 15 | 2151 | 1553 | 1,4 | 0,0145 | |
| 1427925_at | Stx17 | syntaxin 17 | 709 | 512 | 1,4 | 0,0381 | |
| 1435740_at | Rai17 | retinoic acid induced 17 | 1252 | 902 | 1,4 | 0,0196 | |
| 1437358_at | Wdfy1 | WD repeat and FYVE domain containing 1 | 1220 | 878 | 1,4 | 0,0204 | |

| | | | | | | | |
|---|---|---|---|---|---|---|---|
| 1449023_a_at | Ezh1 | enhancer of zeste homolog 1 (Drosophila) | 489 | 352 | 1,4 | 0,0309 | |
| 1448724_at | Cish | cytokine inducible SH2-containing protein | 72 | 52 | 1,4 | 0,0451 | |
| 1451751_at | Ddit4l | DNA-damage-inducible transcript 4-like | 244 | 174 | 1,4 | 0,0304 | |
| 1456728_x_at | Aco1 | aconitase 1 | 4639 | 3304 | 1,4 | 0,0148 | |
| 1418854_at | Birc2 | baculoviral IAP repeat-containing 2 | 640 | 456 | 1,4 | 0,0293 | |
| 1428394_at | Phyhd1 | phytanoyl-CoA dioxygenase domain containing 1 | 21 | 15 | 1,4 | 0,0413 | |
| 1416458_at | Arf2 | ADP-ribosylation factor 2 | 451 | 321 | 1,4 | 0,0277 | |
| 1459782_x_at | Abcc5 | ATP-binding cassette, sub-family C (CFTR/MRP), member 5 | 57 | 41 | 1,4 | 0,0297 | |
| 1455152_at | AI462493 | expressed sequence AI462493 | 789 | 560 | 1,4 | 0,0475 | |
| 1416881_at | Mcl1 | myeloid cell leukemia sequence 1 | 3680 | 2609 | 1,4 | 0,0170 | |
| 1426345_at | Prepl | prolyl endopeptidase-like | 325 | 230 | 1,4 | 0,0278 | |
| 1447522_s_at | Tnks2 | tankyrase, TRF1-interacting ankyrin-related ADP-ribose polymerase 2 | 2652 | 1876 | 1,4 | 0,0061 | |
| 1424782_at | Tmem77 | transmembrane protein 77 | 670 | 474 | 1,4 | 0,0115 | |
| 1434986_a_at | Sec61a1 | Sec61 alpha 1 subunit (S. cerevisiae) | 3140 | 2218 | 1,4 | 0,0035 | |
| 1441906_x_at | Syap1 | synapse associated protein 1 | 409 | 288 | 1,4 | 0,0361 | |
| 1424058_at | 1190002C06Rik | RIKEN cDNA 1190002C06 gene | 447 | 314 | 1,4 | 0,0259 | |
| 1448673_at | Pvrl3 | poliovirus receptor-related 3 | 1489 | 1048 | 1,4 | 0,0156 | |
| 1427912_at | Cbr3 | carbonyl reductase 3 | 1642 | 1153 | 1,4 | 0,0095 | x |
| 1437763_at | Dcun1d3 | DCN1, defective in cullin neddylation 1, domain containing 3 (S. cerevisiae) | 224 | 157 | 1,4 | 0,0441 | |
| 1435616_at | Cyp20a1 | cytochrome P450, family 20, subfamily A, polypeptide 1 | 6942 | 4873 | 1,4 | 0,0382 | |
| 1434534_at | Dsc3 | desmocollin 3 | 15 | 10 | 1,4 | 0,0245 | |
| 1453745_at | 2700038G22Rik | RIKEN cDNA 2700038G22 gene | 719 | 504 | 1,4 | 0,0145 | |
| 1450744_at | Ell2 | elongation factor RNA polymerase II 2 | 3878 | 2717 | 1,4 | 0,0037 | |
| 1439047_s_at | BC027061 | cDNA sequence BC027061 | 1188 | 832 | 1,4 | 0,0278 | |
| 1449014_at | Lactb | lactamase, beta | 462 | 323 | 1,4 | 0,0381 | |
| 1455787_x_at | Minpp1 | multiple inositol polyphosphate histidine phosphatase 1 | 2137 | 1492 | 1,4 | 0,0395 | x |
| 1418406_at | Pde8a | phosphodiesterase 8A | 200 | 139 | 1,4 | 0,0458 | |
| 1454727_at | AI173486 | expressed sequence AI173486 | 1437 | 1002 | 1,4 | 0,0277 | |
| 1439189_at | D630023B12Rik | RIKEN cDNA D630023B12 gene | 571 | 397 | 1,4 | 0,0211 | |
| 1450333_a_at | Gata2 | GATA binding protein 2 | 699 | 486 | 1,4 | 0,0207 | |
| 1426375_s_at | Oxnad1 | oxidoreductase NAD-binding domain containing 1 | 143 | 99 | 1,4 | 0,0217 | |
| 1418506_a_at | Prdx2 | peroxiredoxin 2 | 12270 | 8529 | 1,4 | 0,0418 | |
| 1421209_s_at | Ikbkg | inhibitor of kappaB kinase gamma | 500 | 347 | 1,4 | 0,0068 | |
| 1420381_a_at | Rpl31 | ribosomal protein L31 | 1504 | 1045 | 1,4 | 0,0451 | |
| 1448720_at | Lrrc40 | leucine rich repeat containing 40 | 2444 | 1692 | 1,4 | 0,0406 | |
| 1426922_s_at | Hrb | HIV-1 Rev binding protein | 1462 | 1012 | 1,4 | 0,0494 | |
| 1435753_a_at | Nucks1 | nuclear casein kinase and cyclin-dependent kinase substrate 1 | 2920 | 2019 | 1,4 | 0,0048 | |
| 1438024_at | 6230416A05Rik | RIKEN cDNA 6230416A05 gene | 1025 | 705 | 1,5 | 0,0439 | |
| 1450724_at | Drctnnb1a | down-regulated by Ctnnb1, a | 6684 | 4581 | 1,5 | 0,0171 | |
| 1437009_a_at | Zfp364 | zinc finger protein 364 | 4185 | 2845 | 1,5 | 0,0245 | |
| 1421644_at | Slfn3 | schlafen 3 | 168 | 114 | 1,5 | 0,0269 | |
| 1452011_a_at | Uxs1 | UDP-glucuronate decarboxylase 1 | 5857 | 3972 | 1,5 | 0,0230 | |

| | | | | | | | |
|---|---|---|---|---|---|---|---|
| 1443870_at | Abcc4 | ATP-binding cassette, sub-family C (CFTR/MRP), member 4 | 2659 | 1800 | 1,5 | 0,0344 | |
| 1455032_at | 9630037P07Rik | RIKEN cDNA 9630037P07 gene | 6272 | 4227 | 1,5 | 0,0108 | |
| 1452193_a_at | Wasl | Wiskott-Aldrich syndrome-like (human) | 3064 | 2065 | 1,5 | 0,0310 | |
| 1429019_s_at | Pon2 | paraoxonase 2 | 1658 | 1117 | 1,5 | 0,0048 | |
| 1437991_x_at | Rusc1 | RUN and SH3 domain containing 1 | 337 | 227 | 1,5 | 0,0454 | x |
| 1434302_at | Raph1 | Ras association (RalGDS/AF-6) and pleckstrin homology domains 1 | 6333 | 4262 | 1,5 | 0,0099 | |
| 1416989_at | Vps53 | vacuolar protein sorting 53 (yeast) | 2127 | 1428 | 1,5 | 0,0100 | |
| 1431582_at | Itgb4bp | integrin beta 4 binding protein | 249 | 167 | 1,5 | 0,0090 | |
| 1428132_at | Cdc42se1 | CDC42 small effector 1 | 655 | 438 | 1,5 | 0,0297 | |
| 1455053_a_at | Dcun1d1 | DCUN1D1 DCN1, defective in cullin neddylation 1, domain containing 1 (S. cerevisiae) | 402 | 269 | 1,5 | 0,0201 | |
| 1433781_a_at | Cldn12 | claudin 12 | 2191 | 1464 | 1,5 | 0,0295 | |
| 1453228_at | Stx11 | syntaxin 11 | 447 | 298 | 1,5 | 0,0147 | |
| 1429307_s_at | Lzic | leucine zipper and CTNNBIP1 domain containing | 351 | 234 | 1,5 | 0,0172 | |
| 1417764_at | Ssr1 | signal sequence receptor, alpha | 956 | 636 | 1,5 | 0,0236 | |
| 1435727_s_at | D15Ertd366e | DNA segment, Chr 15, ERATO Doi 366, expressed | 1110 | 738 | 1,5 | 0,0297 | |
| 1441942_x_at | Rnut1 | RNA, U transporter 1 | 284 | 189 | 1,5 | 0,0425 | |
| 1428202_at | 1810037C20Rik | RIKEN cDNA 1810037C20 gene | 358 | 237 | 1,5 | 0,0257 | |
| 1424084_at | Rod1 | ROD1 regulator of differentiation 1 (S. pombe) | 94 | 62 | 1,5 | 0,0238 | |
| 1428586_at | Tmem41b | transmembrane protein 41B | 1668 | 1104 | 1,5 | 0,0101 | |
| 1422895_at | Vamp4 | vesicle-associated membrane protein 4 | 1379 | 910 | 1,5 | 0,0189 | |
| 1424852_at | Mef2c | myocyte enhancer factor 2C | 849 | 559 | 1,5 | 0,0040 | |
| 1419641_at | Purb | purine rich element binding protein B | 1294 | 852 | 1,5 | 0,0043 | |
| 1420116_s_at | Golph3 | golgi phosphoprotein 3 | 1327 | 872 | 1,5 | 0,0231 | |
| 1446737_a_at | Hook3 | hook homolog 3 (Drosophila) | 570 | 374 | 1,5 | 0,0158 | |
| 1428644_at | Mgat5 | mannoside acetylglucosaminyltransferase 5 | 1019 | 664 | 1,5 | 0,0115 | |
| 1454685_at | Gpr146 | G protein-coupled receptor 146 | 676 | 440 | 1,5 | 0,0297 | |
| 1429581_at | Acad9 | acyl-Coenzyme A dehydrogenase family, member 9 | 408 | 265 | 1,5 | 0,0288 | |
| 1452054_at | Ube2w | ubiquitin-conjugating enzyme E2W (putative) | 1660 | 1075 | 1,5 | 0,0218 | |
| 1455646_at | 2010004M13Rik | RIKEN cDNA 2010004M13 gene | 57 | 37 | 1,5 | 0,0102 | |
| 1435524_at | --- | CDNA clone IMAGE:4036503, with apparent retained intron | 6776 | 4376 | 1,5 | 0,0325 | |
| 1425476_at | Col4a5 | procollagen, type IV, alpha 5 | 230 | 148 | 1,6 | 0,0224 | |
| 1435488_at | 1110019K23Rik | RIKEN cDNA 1110019K23 gene | 643 | 414 | 1,6 | 0,0256 | |
| 1455959_s_at | Gclc | glutamate-cysteine ligase, catalytic subunit | 1526 | 982 | 1,6 | 0,0305 | |
| 1440173_x_at | Selp | selectin, platelet | 9248 | 5935 | 1,6 | 0,0065 | |
| 1449263_at | Ufm1 | ubiquitin-fold modifier 1 | 851 | 545 | 1,6 | 0,0342 | |
| 1435653_at | Abhd2 | abhydrolase domain containing 2 | 525 | 336 | 1,6 | 0,0387 | |
| 1443672_at | Lars2 | leucyl-tRNA synthetase, mitochondrial | 405 | 258 | 1,6 | 0,0201 | |
| 1424604_s_at | Sumf1 | sulfatase modifying factor 1 | 3319 | 2114 | 1,6 | 0,0470 | |
| 1436549_a_at | Hnrpa1 | heterogeneous nuclear ribonucleoprotein A1 | 1741 | 1108 | 1,6 | 0,0263 | |
| 1452451_at | Bean | brain expressed, associated with Nedd4 | 31 | 20 | 1,6 | 0,0427 | |
| 1417839_at | Cldn5 | claudin 5 | 2430 | 1537 | 1,6 | 0,0071 | |
| 1435641_at | 9530018I07Rik | RIKEN cDNA 9530018I07 gene | 765 | 484 | 1,6 | 0,0399 | x |

| | | | | | | | |
|---|---|---|---|---|---|---|---|
| 1436724_a_at | Lgtn | ligatin | 2850 | 1800 | 1,6 | 0,0049 | |
| 1427934_at | 2610208E05Rik | RIKEN cDNA 2610208E05 gene | 264 | 166 | 1,6 | 0,0466 | |
| 1433639_at | 5730593F17Rik | RIKEN cDNA 5730593F17 gene | 262 | 165 | 1,6 | 0,0468 | |
| 1442060_at | Slc3a1 | solute carrier family 3, member 1 | 30 | 19 | 1,6 | 0,0371 | |
| 1416824_at | B230118H07Rik | RIKEN cDNA B230118H07 gene | 716 | 449 | 1,6 | 0,0174 | |
| 1450942_at | Ccdc16 | coiled-coil domain containing 16 | 381 | 238 | 1,6 | 0,0171 | |
| 1428963_at | Rwdd2 | RWD domain containing 2 | 68 | 42 | 1,6 | 0,0279 | |
| 1426646_at | 9130011J15Rik | RIKEN cDNA 9130011J15 gene | 563 | 351 | 1,6 | 0,0369 | |
| 1455137_at | Rapgef5 | Rap guanine nucleotide exchange factor (GEF) 5 | 2356 | 1469 | 1,6 | 0,0280 | |
| 1436736_x_at | D0H4S114 | DNA segment, human D4S114 | 7918 | 4920 | 1,6 | 0,0310 | |
| 1460371_at | Hspa12b | heat shock protein 12B | 1330 | 826 | 1,6 | 0,0171 | |
| 1417369_at | Hsd17b4 | hydroxysteroid (17-beta) dehydrogenase 4 | 2346 | 1447 | 1,6 | 0,0297 | |
| 1417822_at | D17H6S56E-5 | DNA segment, Chr 17, human D6S56E 5 | 8227 | 5072 | 1,6 | 0,0497 | |
| 1454397_at | 4632418H02Rik | RIKEN cDNA 4632418H02 gene | 60 | 37 | 1,6 | 0,0300 | |
| 1451240_a_at | Glo1 | glyoxalase 1 | 17533 | 10790 | 1,6 | 0,0034 | |
| 1447308_at | Lass5 | longevity assurance homolog 5 (S. cerevisiae) | 401 | 246 | 1,6 | 0,0095 | |
| 1451277_at | Zadh2 | zinc binding alcohol dehydrogenase, domain containing 2 | 1229 | 755 | 1,6 | 0,0288 | |
| 1423176_at | Tob1 | transducer of ErbB-2.1 | 1569 | 962 | 1,6 | 0,0162 | |
| 1433985_at | Abi2 | abl-interactor 2 | 1310 | 803 | 1,6 | 0,0285 | |
| 1417045_at | Bid | BH3 interacting domain death agonist | 390 | 239 | 1,6 | 0,0134 | |
| 1457265_at | B230333C21Rik | RIKEN cDNA B230333C21 gene | 183 | 112 | 1,6 | 0,0170 | |
| 1425193_at | 2010106G01Rik | RIKEN cDNA 2010106G01 gene | 693 | 424 | 1,6 | 0,0134 | |
| 1420731_a_at | Csrp2 | cysteine and glycine-rich protein 2 | 1799 | 1096 | 1,6 | 0,0330 | |
| 1418762_at | Daf1 | decay accelerating factor 1 | 1159 | 704 | 1,6 | 0,0165 | |
| 1456516_x_at | Uap1 | UDP-N-acetylglucosamine pyrophosphorylase 1 | 220 | 134 | 1,6 | 0,0048 | x |
| 1455775_at | --- | --- | 365 | 221 | 1,6 | 0,0496 | |
| 1448793_a_at | Sdc4 | syndecan 4 | 1570 | 952 | 1,6 | 0,0446 | |
| 1449107_at | Nudt4 | nudix (nucleoside diphosphate linked moiety X)-type motif 4 | 1603 | 969 | 1,7 | 0,0212 | |
| 1453221_at | Gopc | golgi associated PDZ and coiled-coil motif containing | 611 | 369 | 1,7 | 0,0342 | |
| 1419132_at | Tlr2 | toll-like receptor 2 | 494 | 298 | 1,7 | 0,0192 | |
| 1436915_x_at | Laptm4b | lysosomal-associated protein transmembrane 4B | 9056 | 5459 | 1,7 | 0,0030 | |
| 1428548_at | Pak4 | p21 (CDKN1A)-activated kinase 4 | 430 | 259 | 1,7 | 0,0392 | |
| 1434408_at | Mjd | Machado-Joseph disease (spinocerebellar ataxia 3, olivopontocerebellar ataxia 3, autosomal dominant, ataxin 3) homolog (human) | 635 | 382 | 1,7 | 0,0254 | |
| 1457658_x_at | Anxa4 | annexin A4 | 429 | 258 | 1,7 | 0,0345 | |
| 1442608_at | Layn | layilin | 503 | 300 | 1,7 | 0,0208 | |
| 1426875_s_at | Srxn1 | sulfiredoxin 1 homolog (S. cerevisiae) | 1501 | 890 | 1,7 | 0,0089 | |
| 1416262_at | Tmem19 | transmembrane protein 19 | 170 | 101 | 1,7 | 0,0125 | |
| 1437447_s_at | Ercc1 | excision repair cross-complementing rodent repair deficiency, complementation group 1 | 4489 | 2657 | 1,7 | 0,0011 | |
| 1415795_at | Spin | spindlin | 55 | 33 | 1,7 | 0,0375 | |
| 1437635_at | St3gal6 | ST3 beta-galactoside alpha-2,3-sialyltransferase 6 | 1267 | 748 | 1,7 | 0,0020 | |
| 1433544_at | Als2cr2 | amyotrophic lateral sclerosis 2 (juvenile) chromosome region, candidate | 302 | 178 | 1,7 | 0,0200 | |

| | | | | | | | |
|---|---|---|---|---|---|---|---|
| | | 2 (human) | | | | | |
| 1449137_at | Pdha1 | pyruvate dehydrogenase E1 alpha 1 | 511 | 301 | 1,7 | 0,0318 | |
| 1421172_at | Adam12 | a disintegrin and metallopeptidase domain 12 (meltrin alpha) | 859 | 505 | 1,7 | 0,0149 | x |
| 1424358_at | Ube2e2 | ubiquitin-conjugating enzyme E2E 2 (UBC4/5 homolog, yeast) | 1888 | 1109 | 1,7 | 0,0310 | x |
| 1433795_at | Tgfbr3 | transforming growth factor, beta receptor III | 141 | 82 | 1,7 | 0,0134 | |
| 1426640_s_at | Trib2 | tribbles homolog 2 (Drosophila) | 2450 | 1427 | 1,7 | 0,0493 | x |
| 1459867_x_at | Unc45a | unc-45 homolog A (C. elegans) | 39 | 23 | 1,7 | 0,0104 | |
| 1437831_at | --- | --- | 34 | 20 | 1,7 | 0,0184 | |
| 1424820_a_at | Ndfip1 | Nedd4 family interacting protein 1 | 6502 | 3771 | 1,7 | 0,0095 | |
| 1434590_at | B230209C24Rik | RIKEN cDNA B230209C24 gene | 560 | 323 | 1,7 | 0,0251 | |
| 1419706_a_at | Akap12 | A kinase (PRKA) anchor protein (gravin) 12 | 25962 | 14946 | 1,7 | 0,0162 | |
| 1455345_at | Phf15 | PHD finger protein 15 | 1562 | 899 | 1,7 | 0,0196 | |
| 1430986_at | Farslb | phenylalanine-tRNA synthetase-like, beta subunit | 229 | 132 | 1,7 | 0,0404 | |
| 1448600_s_at | Vav3 | vav 3 oncogene | 862 | 495 | 1,7 | 0,0097 | |
| 1428570_at | Ccnc | cyclin C | 605 | 347 | 1,7 | 0,0471 | |
| 1451527_at | Pcolce2 | procollagen C-endopeptidase enhancer 2 | 1972 | 1129 | 1,7 | 0,0024 | |
| 1443486_at | --- | Component of oligomeric golgi complex 7 (Cog7), mRNA | 1474 | 844 | 1,7 | 0,0413 | x |
| 1436771_x_at | Pgd | phosphogluconate dehydrogenase | 17451 | 9981 | 1,7 | 0,0466 | |
| 1435167_at | Ranbp6 | RAN binding protein 6 | 379 | 215 | 1,8 | 0,0110 | |
| 1448864_at | Snrk | SNF related kinase | 5185 | 2945 | 1,8 | 0,0272 | |
| 1421571_a_at | Ly6c | lymphocyte antigen 6 complex, locus C | 13879 | 7869 | 1,8 | 0,0145 | |
| 1450784_at | Reck | reversion-inducing-cysteine-rich protein with kazal motifs | 465 | 263 | 1,8 | 0,0011 | x |
| 1437694_at | --- | Transcribed locus, weakly similar to NP_795929.1 hypothetical protein LOC319587 [Mus musculus] | 744 | 419 | 1,8 | 0,0339 | x |
| 1436544_at | Atp10d | ATPase, Class V, type 10D | 564 | 316 | 1,8 | 0,0047 | |
| 1434751_at | Ids | iduronate 2-sulfatase | 630 | 353 | 1,8 | 0,0047 | |
| 1427491_at | Nsun6 | NOL1/NOP2/Sun domain family 6 | 66 | 37 | 1,8 | 0,0117 | x |
| 1416077_at | Adm | adrenomedullin | 817 | 457 | 1,8 | 0,0475 | |
| 1426569_a_at | Frk | fyn-related kinase | 94 | 52 | 1,8 | 0,0215 | x |
| 1418394_a_at | Cd97 | CD97 antigen | 32 | 18 | 1,8 | 0,0069 | x |
| 1434687_at | C730026J16 | hypothetical protein C730026J16 | 4692 | 2602 | 1,8 | 0,0056 | x |
| 1418209_a_at | Pfn2 | profilin 2 | 1900 | 1052 | 1,8 | 0,0288 | |
| 1436737_a_at | Sorbs1 | sorbin and SH3 domain containing 1 | 8762 | 4846 | 1,8 | 0,0381 | |
| 1422184_a_at | Ak1 | adenylate kinase 1 | 403 | 223 | 1,8 | 0,0080 | |
| 1422619_at | Ppap2a | phosphatidic acid phosphatase 2a | 3136 | 1725 | 1,8 | 0,0381 | |
| 1422433_s_at | Idh1 | isocitrate dehydrogenase 1 (NADP+), soluble | 2094 | 1149 | 1,8 | 0,0197 | |
| 1416429_a_at | Cat | catalase | 5168 | 2821 | 1,8 | 0,0395 | |
| 1434828_at | B430201A12Rik | RIKEN cDNA B430201A12 gene | 1145 | 624 | 1,8 | 0,0095 | |
| 1447757_x_at | Inpp5f | inositol polyphosphate-5-phosphatase F | 239 | 130 | 1,8 | 0,0241 | |
| 1451828_a_at | Acsl4 | acyl-CoA synthetase long-chain family member 4 | 429 | 233 | 1,8 | 0,0419 | |
| 1451415_at | 1810011O10Rik | RIKEN cDNA 1810011O10 gene | 750 | 407 | 1,8 | 0,0136 | |
| 1419272_at | Myd88 | myeloid differentiation primary response gene 88 | 260 | 141 | 1,8 | 0,0205 | |
| 1423871_at | Tmem63a | transmembrane protein 63a | 492 | 266 | 1,8 | 0,0206 | |

| | | | | | | | |
|---|---|---|---|---|---|---|---|
| 1429590_at | Tacc1 | transforming, acidic coiled-coil containing protein 1 | 625 | 338 | 1,8 | 0,0156 | |
| 1453622_s_at | Mllt3 | myeloid/lymphoid or mixed lineage-leukemia translocation to 3 homolog (Drosophila) | 174 | 94 | 1,9 | 0,0291 | |
| 1452016_at | Alox5ap | arachidonate 5-lipoxygenase activating protein | 647 | 348 | 1,9 | 0,0063 | |
| 1449334_at | Timp3 | tissue inhibitor of metalloproteinase 3 | 1844 | 990 | 1,9 | 0,0313 | x |
| 1426356_at | 6330578E17Rik | RIKEN cDNA 6330578E17 gene | 363 | 194 | 1,9 | 0,0095 | x |
| 1454617_at | Arrdc3 | arrestin domain containing 3 | 250 | 134 | 1,9 | 0,0134 | |
| 1422518_at | Cask | calcium/calmodulin-dependent serine protein kinase (MAGUK family) | 170 | 91 | 1,9 | 0,0457 | |
| 1429310_at | Flrt3 | fibronectin leucine rich transmembrane protein 3 | 148 | 79 | 1,9 | 0,0421 | |
| 1421840_at | Abca1 | ATP-binding cassette, sub-family A (ABC1), member 1 | 1298 | 691 | 1,9 | 0,0374 | |
| 1430030_at | 5330426P16Rik | RIKEN cDNA 5330426P16 gene | 269 | 143 | 1,9 | 0,0379 | |
| 1419301_at | Fzd4 | frizzled homolog 4 (Drosophila) | 6265 | 3332 | 1,9 | 0,0040 | |
| 1415824_at | Scd1 | stearoyl-Coenzyme A desaturase 1 | 136 | 72 | 1,9 | 0,0481 | x |
| 1449125_at | Tnfaip8l1 | tumor necrosis factor, alpha-induced protein 8-like 1 | 1333 | 704 | 1,9 | 0,0063 | |
| 1426573_at | Me2 | malic enzyme 2, NAD(+)-dependent, mitochondrial | 290 | 153 | 1,9 | 0,0060 | |
| 1437342_x_at | Pttg1ip | pituitary tumor-transforming 1 interacting protein | 11619 | 6128 | 1,9 | 0,0063 | |
| 1425029_a_at | Oact2 | O-acyltransferase (membrane bound) domain containing 2 | 522 | 275 | 1,9 | 0,0325 | |
| 1449118_at | Dbt | dihydrolipoamide branched chain transacylase E2 | 1441 | 755 | 1,9 | 0,0203 | |
| 1458996_at | Itga5 | integrin alpha 5 (fibronectin receptor alpha) | 210 | 110 | 1,9 | 0,0076 | |
| 1452209_at | Pkp4 | plakophilin 4 | 2351 | 1230 | 1,9 | 0,0276 | x |
| 1420888_at | Bcl2l1 | Bcl2-like 1 | 5449 | 2834 | 1,9 | 0,0182 | |
| 1443673_x_at | --- | --- | 387 | 200 | 1,9 | 0,0456 | |
| 1435517_x_at | Ralb | v-ral simian leukemia viral oncogene homolog B (ras related) | 1273 | 657 | 1,9 | 0,0111 | |
| 1442350_at | --- | 0 day neonate skin cDNA, RIKEN full-length enriched library, clone:4632424N07 product:unclassifiable, full insert sequence | 600 | 310 | 1,9 | 0,0290 | |
| 1426236_a_at | Glul | glutamate-ammonia ligase (glutamine synthetase) | 1742 | 897 | 1,9 | 0,0124 | |
| 1436678_at | Sgcb | sarcoglycan, beta (dystrophin-associated glycoprotein) | 321 | 165 | 1,9 | 0,0305 | |
| 1449984_at | Cxcl2 | chemokine (C-X-C motif) ligand 2 | 2619 | 1344 | 1,9 | 0,0310 | |
| 1448812_at | Hpcal1 | hippocalcin-like 1 | 2958 | 1517 | 1,9 | 0,0191 | x |
| 1448610_a_at | Sod2 | superoxide dismutase 2, mitochondrial | 11757 | 6005 | 2,0 | 0,0121 | |
| 1431302_a_at | Nudt7 | nudix (nucleoside diphosphate linked moiety X)-type motif 7 | 648 | 330 | 2,0 | 0,0102 | |
| 1454604_s_at | Tspan12 | tetraspanin 12 | 227 | 116 | 2,0 | 0,0297 | |
| 1416592_at | Glrx | glutaredoxin | 4000 | 2033 | 2,0 | 0,0340 | |
| 1416825_at | Snta1 | syntrophin, acidic 1 | 72 | 36 | 2,0 | 0,0098 | |
| 1435396_at | Stxbp6 | syntaxin binding protein 6 (amisyn) | 26 | 13 | 2,0 | 0,0127 | |
| 1435058_x_at | Stxbp3a | syntaxin binding protein 3A | 1454 | 731 | 2,0 | 0,0075 | |
| 1456482_at | Pik3r3 | phosphatidylinositol 3 kinase, regulatory subunit, polypeptide 3 (p55) | 1076 | 538 | 2,0 | 0,0169 | |
| 1436116_x_at | 2900057D21Rik | RIKEN cDNA 2900057D21 gene | 593 | 296 | 2,0 | 0,0039 | |
| 1456288_at | Slfn5 | schlafen 5 | 342 | 171 | 2,0 | 0,0170 | |
| 1427097_at | Wwp1 | WW domain containing E3 ubiquitin protein ligase 1 | 1421 | 709 | 2,0 | 0,0084 | |
| 1421594_a_at | Sytl2 | synaptotagmin-like 2 | 462 | 231 | 2,0 | 0,0196 | |
| 1436756_x_at | Hadhsc | L-3-hydroxyacyl-Coenzyme A dehydrogenase, short chain | 591 | 293 | 2,0 | 0,0451 | |
| 1417777_at | Ltb4dh | leukotriene B4 12-hydroxydehydrogenase | 952 | 472 | 2,0 | 0,0067 | |

| | | | | | | | |
|---|---|---|---|---|---|---|---|
| 1424711_at | Tmem2 | transmembrane protein 2 | 356 | 176 | 2,0 | 0,0013 | |
| 1435735_x_at | H47 | histocompatibility 47 | 5452 | 2696 | 2,0 | 0,0438 | |
| 1427347_s_at | Tubb2a | tubulin, beta 2a | 11058 | 5456 | 2,0 | 0,0302 | |
| 1438610_a_at | Cryz | crystallin, zeta | 3203 | 1578 | 2,0 | 0,0276 | |
| 1455735_at | Ap1s3 | adaptor-related protein complex AP-1, sigma 3 | 364 | 179 | 2,0 | 0,0061 | |
| 1426260_a_at | Ugt1a6a | UDP glucuronosyltransferase 1 family, polypeptide A6A | 6628 | 3260 | 2,0 | 0,0110 | |
| 1428196_a_at | 1200015F23Rik | RIKEN cDNA 1200015F23 gene | 2541 | 1245 | 2,0 | 0,0253 | |
| 1431802_a_at | D5Wsu178e | DNA segment, Chr 5, Wayne State University 178, expressed | 1323 | 647 | 2,0 | 0,0490 | |
| 1436194_at | C330008K14Rik | RIKEN cDNA C330008K14 gene | 210 | 102 | 2,0 | 0,0160 | |
| 1422601_at | Serpinb9 | serine (or cysteine) peptidase inhibitor, clade B, member 9 | 859 | 419 | 2,0 | 0,0021 | |
| 1448489_at | Pafah2 | platelet-activating factor acetylhydrolase 2 | 1105 | 539 | 2,1 | 0,0475 | |
| 1424800_at | Enah | enabled homolog (Drosophila) | 116 | 56 | 2,1 | 0,0384 | |
| 1433453_a_at | Abtb2 | ankyrin repeat and BTB (POZ) domain containing 2 | 835 | 406 | 2,1 | 0,0413 | |
| 1438667_at | 5730410E15Rik | RIKEN cDNA 5730410E15 gene | 12 | 6 | 2,1 | 0,0206 | |
| 1417533_a_at | Itgb5 | integrin beta 5 | 186 | 90 | 2,1 | 0,0149 | |
| 1429690_at | 1300003B13Rik | RIKEN cDNA 1300003B13 gene | 1385 | 672 | 2,1 | 0,0069 | x |
| 1440230_at | Lrrc54 | leucine rich repeat containing 54 | 75 | 36 | 2,1 | 0,0274 | |
| 1430526_a_at | Smarca2 | SWI/SNF related, matrix associated, actin dependent regulator of chromatin, subfamily a, member 2 | 266 | 128 | 2,1 | 0,0472 | x |
| 1434350_at | Axud1 | AXIN1 up-regulated 1 | 542 | 262 | 2,1 | 0,0348 | |
| 1421992_a_at | Igfbp4 | insulin-like growth factor binding protein 4 | 2080 | 1003 | 2,1 | 0,0196 | |
| 1429527_a_at | Plscr1 | phospholipid scramblase 1 | 2465 | 1188 | 2,1 | 0,0341 | x |
| 1435771_at | Plcb4 | phospholipase C, beta 4 | 1427 | 686 | 2,1 | 0,0076 | |
| 1455096_at | Flrt2 | fibronectin leucine rich transmembrane protein 2 | 2423 | 1165 | 2,1 | 0,0142 | |
| 1439558_at | Zfp75 | zinc finger protein 75 | 506 | 243 | 2,1 | 0,0236 | |
| 1428636_at | Steap2 | six transmembrane epithelial antigen of prostate 2 | 5127 | 2457 | 2,1 | 0,0215 | |
| 1438156_x_at | Cpt1a | carnitine palmitoyltransferase 1a, liver | 2443 | 1171 | 2,1 | 0,0239 | |
| 1451112_s_at | Dap | death-associated protein | 3088 | 1478 | 2,1 | 0,0108 | |
| 1418280_at | Klf6 | Kruppel-like factor 6 | 721 | 345 | 2,1 | 0,0170 | |
| 1416165_at | Rab31 | RAB31, member RAS oncogene family | 1435 | 684 | 2,1 | 0,0415 | |
| 1449983_a_at | Nqo2 | NAD(P)H dehydrogenase, quinone 2 | 716 | 340 | 2,1 | 0,0038 | |
| 1447903_x_at | Ap1s2 | adaptor-related protein complex 1, sigma 2 subunit | 8243 | 3911 | 2,1 | 0,0132 | |
| 1460694_s_at | Svil | supervillin | 4025 | 1902 | 2,1 | 0,0073 | |
| 1428914_at | 2310014D11Rik | RIKEN cDNA 2310014D11 gene | 1224 | 575 | 2,1 | 0,0119 | |
| 1426593_a_at | Fbxo22 | F-box only protein 22 | 7603 | 3569 | 2,1 | 0,0115 | |
| 1434010_at | Als2cr13 | amyotrophic lateral sclerosis 2 (juvenile) chromosome region, candidate 13 (human) | 1410 | 659 | 2,1 | 0,0337 | |
| 1455150_at | --- | 13 days embryo forelimb cDNA, RIKEN full-length enriched library, clone:5930438H13 product:unclassifiable, full insert sequence | 137 | 64 | 2,1 | 0,0423 | |
| 1434089_at | Synpo | synaptopodin | 2840 | 1318 | 2,2 | 0,0069 | |
| 1451989_a_at | Mapre2 | microtubule-associated protein, RP/EB family, member 2 | 5666 | 2628 | 2,2 | 0,0218 | |
| 1424029_at | Tspyl4 | TSPY-like 4 | 182 | 84 | 2,2 | 0,0445 | |
| 1433992_at | Apxl | apical protein, Xenopus laevis-like | 914 | 422 | 2,2 | 0,0156 | |

| | | | | | | | |
|---|---|---|---|---|---|---|---|
| 1419435_at | Aox1 | aldehyde oxidase 1 | 331 | 152 | 2,2 | 0,0480 | |
| 1451508_at | 1700108L22Rik | RIKEN cDNA 1700108L22 gene | 142 | 65 | 2,2 | 0,0387 | |
| 1423747_a_at | Pdk1 | pyruvate dehydrogenase kinase, isoenzyme 1 | 2055 | 935 | 2,2 | 0,0292 | |
| 1416021_a_at | Fabp5 | fatty acid binding protein 5, epidermal | 6846 | 3104 | 2,2 | 0,0381 | x |
| 1429177_x_at | Sox17 | SRY-box containing gene 17 | 2462 | 1113 | 2,2 | 0,0345 | |
| 1436155_at | Nmnat2 | nicotinamide nucleotide adenylyltransferase 2 | 134 | 61 | 2,2 | 0,0195 | |
| 1422524_at | Abcb6 | ATP-binding cassette, sub-family B (MDR/TAP), member 6 | 233 | 105 | 2,2 | 0,0171 | |
| 1434329_s_at | Adipor2 | adiponectin receptor 2 | 1404 | 627 | 2,2 | 0,0189 | |
| 1424783_a_at | Ugt1a9 | UDP glucuronosyltransferase 1 family, polypeptide A9 | 5224 | 2312 | 2,3 | 0,0019 | |
| 1454858_x_at | Mettl7a | methyltransferase like 7A | 214 | 95 | 2,3 | 0,0142 | |
| 1434379_at | Mxd4 | Max dimerization protein 4 | 14 | 6 | 2,3 | 0,0470 | |
| 1452847_at | 2410008K03Rik | RIKEN cDNA 2410008K03 gene | 352 | 156 | 2,3 | 0,0037 | |
| 1425814_a_at | Calcrl | calcitonin receptor-like | 12194 | 5357 | 2,3 | 0,0030 | |
| 1418302_at | Ppt2 | palmitoyl-protein thioesterase 2 | 973 | 427 | 2,3 | 0,0453 | x |
| 1416619_at | 4632428N05Rik | RIKEN cDNA 4632428N05 gene | 118 | 52 | 2,3 | 0,0482 | x |
| 1436538_at | Lrp2bp | Lrp2 binding protein | 78 | 34 | 2,3 | 0,0308 | x |
| 1424383_at | Tmem51 | transmembrane protein 51 | 1739 | 758 | 2,3 | 0,0048 | |
| 1439433_a_at | Slc35a2 | solute carrier family 35 (UDP-galactose transporter), member 2 | 6450 | 2807 | 2,3 | 0,0381 | |
| 1460360_at | Asrgl1 | asparaginase like 1 | 162 | 70 | 2,3 | 0,0254 | |
| 1457270_at | B230343A10Rik | RIKEN cDNA B230343A10 gene | 349 | 151 | 2,3 | 0,0092 | |
| 1456341_a_at | Klf9 | Kruppel-like factor 9 | 8265 | 3575 | 2,3 | 0,0153 | |
| 1438931_s_at | Sesn1 | sestrin 1 | 410 | 177 | 2,3 | 0,0276 | |
| 1433820_a_at | 1110012D08Rik | RIKEN cDNA 1110012D08 gene | 570 | 246 | 2,3 | 0,0281 | |
| 1418649_at | Egln3 | EGL nine homolog 3 (C. elegans) | 3006 | 1281 | 2,3 | 0,0063 | |
| 1419599_s_at | Ms4a6d | membrane-spanning 4-domains, subfamily A, member 6D | 8160 | 3469 | 2,4 | 0,0110 | |
| 1440999_at | Zfp697 | zinc finger protein 697 | 1251 | 531 | 2,4 | 0,0015 | |
| 1451364_at | Polr3gl | polymerase (RNA) III (DNA directed) polypeptide G like | 743 | 315 | 2,4 | 0,0236 | |
| 1424613_at | Gprc5b | G protein-coupled receptor, family C, group 5, member B | 386 | 163 | 2,4 | 0,0295 | |
| 1453238_s_at | E430024C06Rik | RIKEN cDNA E430024C06 gene | 482 | 202 | 2,4 | 0,0498 | x |
| 1443829_x_at | Coasy | Coenzyme A synthase | 789 | 331 | 2,4 | 0,0201 | |
| 1459860_x_at | Trim2 | tripartite motif protein 2 | 3738 | 1569 | 2,4 | 0,0312 | |
| 1433710_at | Lsm16 | LSM16 homolog (EDC3, S. cerevisiae) | 1328 | 553 | 2,4 | 0,0124 | |
| 1425214_at | P2ry6 | pyrimidinergic receptor P2Y, G-protein coupled, 6 | 169 | 70 | 2,4 | 0,0259 | |
| 1417288_at | Plekha2 | pleckstrin homology domain-containing, family A (phosphoinositide binding specific) member 2 | 1423 | 592 | 2,4 | 0,0051 | |
| 1437277_x_at | Tgm2 | transglutaminase 2, C polypeptide | 11758 | 4858 | 2,4 | 0,0144 | |
| 1435065_x_at | Vav2 | Vav2 oncogene | 25 | 10 | 2,4 | 0,0258 | x |
| 1449888_at | Epas1 | endothelial PAS domain protein 1 | 474 | 192 | 2,5 | 0,0262 | |
| 1417220_at | Fah | fumarylacetoacetate hydrolase | 39 | 16 | 2,5 | 0,0248 | |
| 1420715_a_at | Pparg | peroxisome proliferator activated receptor gamma | 387 | 154 | 2,5 | 0,0084 | |
| 1435694_at | Arhgap26 | Rho GTPase activating protein 26 | 80 | 32 | 2,5 | 0,0058 | |
| 1425503_at | Gcnt2 | glucosaminyl (N-acetyl) transferase 2, I-branching enzyme | 837 | 332 | 2,5 | 0,0184 | |
| 1438756_at | Ankrd29 | ankyrin repeat domain 29 | 61 | 24 | 2,5 | 0,0297 | |

| | | | | | | | |
|---|---|---|---|---|---|---|---|
| 1437463_x_at | Tgfbi | transforming growth factor, beta induced | 43 | 17 | 2,5 | 0,0201 | |
| 1455446_x_at | Acadsb | acyl-Coenzyme A dehydrogenase, short/branched chain | 1317 | 522 | 2,5 | 0,0048 | x |
| 1428289_at | 2310051E17Rik | RIKEN cDNA 2310051E17 gene | 3298 | 1300 | 2,5 | 0,0387 | |
| 1456500_at | Aph1b | anterior pharynx defective 1b homolog (C. elegans) | 193 | 75 | 2,6 | 0,0098 | |
| 1447448_s_at | --- | --- | 1943 | 751 | 2,6 | 0,0194 | |
| 1419440_at | Trim54 | tripartite motif-containing 54 | 281 | 108 | 2,6 | 0,0108 | |
| 1442019_at | --- | 16 days neonate cerebellum cDNA, RIKEN full-length enriched library, clone:9630033M11 product:unclassifiable, full insert sequence | 2229 | 850 | 2,6 | 0,0135 | |
| 1418739_at | Sgk2 | serum/glucocorticoid regulated kinase 2 | 103 | 39 | 2,6 | 0,0477 | |
| 1448613_at | Ecm1 | extracellular matrix protein 1 | 2456 | 926 | 2,7 | 0,0030 | |
| 1417862_at | A830059I20Rik | RIKEN cDNA A830059I20 gene | 1178 | 436 | 2,7 | 0,0061 | x |
| 1416778_at | Sdpr | serum deprivation response | 18149 | 6680 | 2,7 | 0,0095 | |
| 1418673_at | Snai2 | snail homolog 2 (Drosophila) | 341 | 125 | 2,7 | 0,0063 | |
| 1426306_a_at | Maged2 | melanoma antigen, family D, 2 | 1812 | 663 | 2,7 | 0,0162 | |
| 1460230_at | Syn2 | synapsin II | 37 | 13 | 2,8 | 0,0325 | |
| 1428535_at | 9430020K01Rik | RIKEN cDNA 9430020K01 gene | 4564 | 1650 | 2,8 | 0,0201 | |
| 1428650_at | Tns1 | tensin 1 | 1518 | 546 | 2,8 | 0,0070 | |
| 1456603_at | 1500005K14Rik | RIKEN cDNA 1500005K14 gene | 4099 | 1473 | 2,8 | 0,0065 | |
| 1422478_a_at | Acss2 | acyl-CoA synthetase short-chain family member 2 | 34 | 12 | 2,8 | 0,0061 | |
| 1418545_at | Wasf1 | WASP family 1 | 92 | 33 | 2,8 | 0,0197 | |
| 1417591_at | Ptges2 | prostaglandin E synthase 2 | 289 | 101 | 2,9 | 0,0121 | |
| 1438385_s_at | Gpt2 | glutamic pyruvate transaminase (alanine aminotransferase) 2 | 101 | 35 | 2,9 | 0,0170 | x |
| 1428579_at | Fmnl2 | formin-like 2 | 947 | 323 | 2,9 | 0,0273 | |
| 1456979_at | Plcg1 | Phospholipase C, gamma 1 (Plcg1), mRNA | 115 | 39 | 3,0 | 0,0329 | |
| 1448182_a_at | Cd24a | CD24a antigen | 11210 | 3799 | 3,0 | 0,0130 | |
| 1417426_at | Prg1 | proteoglycan 1, secretory granule | 4478 | 1508 | 3,0 | 0,0104 | |
| 1456003_a_at | Slc1a4 | solute carrier family 1 (glutamate/neutral amino acid transporter), member 4 | 477 | 161 | 3,0 | 0,0236 | x |
| 1451532_s_at | Steap1 | six transmembrane epithelial antigen of the prostate 1 | 3810 | 1268 | 3,0 | 0,0039 | |
| 1437928_at | Pcdh12 | protocadherin 12 | 943 | 314 | 3,0 | 0,0099 | |
| 1421818_at | Bcl6 | B-cell leukemia/lymphoma 6 | 300 | 100 | 3,0 | 0,0124 | x |
| 1435060_at | Tmod2 | tropomodulin 2 | 43 | 14 | 3,0 | 0,0099 | |
| 1435486_at | Pak3 | p21 (CDKN1A)-activated kinase 3 | 106 | 35 | 3,0 | 0,0136 | |
| 1436791_at | Wnt5a | wingless-related MMTV integration site 5A | 301 | 100 | 3,0 | 0,0280 | |
| 1459718_x_at | --- | --- | 903 | 298 | 3,0 | 0,0071 | x |
| 1441228_at | Apold1 | apolipoprotein L domain containing 1 | 1491 | 491 | 3,0 | 0,0015 | |
| 1450716_at | Adamts1 | a disintegrin-like and metallopeptidse (reprolysin type) with thrombospondin type 1 motif, 1 | 7645 | 2497 | 3,1 | 0,0076 | |
| 1429399_at | Rnf125 | ring finger protein 125 | 575 | 187 | 3,1 | 0,0096 | x |
| 1450448_at | Stc1 | stanniocalcin 1 | 331 | 107 | 3,1 | 0,0217 | |
| 1436991_x_at | Gsn | gelsolin | 3652 | 1180 | 3,1 | 0,0066 | x |
| 1455257_at | Itgb3 | integrin beta 3 | 4199 | 1334 | 3,1 | 0,0037 | x |
| 1443777_at | --- | --- | 197 | 62 | 3,2 | 0,0277 | |

| | | | | | | | |
|---|---|---|---|---|---|---|---|
| 1450769_s_at | Stard5 | StAR-related lipid transfer (START) domain containing 5 | 196 | 61 | 3,2 | 0,0278 | |
| 1433836_a_at | 8430408G22Rik | RIKEN cDNA 8430408G22 gene | 2170 | 674 | 3,2 | 0,0147 | |
| 1424713_at | Calml4 | calmodulin-like 4 | 415 | 126 | 3,3 | 0,0358 | |
| 1428413_at | 5730405I09Rik | RIKEN cDNA 5730405I09 gene | 1946 | 591 | 3,3 | 0,0091 | |
| 1421041_s_at | Gsta2 | glutathione S-transferase, alpha 2 (Yc2) | 226 | 67 | 3,3 | 0,0218 | |
| 1433481_at | Fkbp14 | FK506 binding protein 14 | 1048 | 313 | 3,4 | 0,0065 | |
| 1455251_at | Itga1 | integrin alpha 1 | 41 | 12 | 3,4 | 0,0218 | |
| 1422787_at | Fkbpl | FK506 binding protein-like | 247 | 72 | 3,4 | 0,0110 | |
| 1437604_x_at | Napg | N-ethylmaleimide sensitive fusion protein attachment protein gamma | 69 | 20 | 3,4 | 0,0160 | |
| 1419468_at | Clec14a | C-type lectin domain family 14, member a | 3867 | 1097 | 3,5 | 0,0042 | |
| 1447928_at | Car5b | carbonic anhydrase 5b, mitochondrial | 91 | 25 | 3,6 | 0,0162 | |
| 1455377_at | 4921517B04Rik | RIKEN cDNA 4921517B04 gene | 846 | 233 | 3,6 | 0,0025 | |
| 1435137_s_at | 1200016E24Rik | RIKEN cDNA 1200016E24 gene | 1082 | 295 | 3,7 | 0,0241 | |
| 1456404_at | Adamts5 | a disintegrin-like and metallopeptidase (reprolysin type) with thrombospondin type 1 motif, 5 (aggrecanase-2) | 428 | 114 | 3,7 | 0,0048 | |
| 1417133_at | Pmp22 | peripheral myelin protein | 4487 | 1166 | 3,8 | 0,0156 | x |
| 1451313_a_at | 1110067D22Rik | RIKEN cDNA 1110067D22 gene | 2335 | 595 | 3,9 | 0,0098 | x |
| 1436870_s_at | AU041783 | expressed sequence AU041783 | 69 | 17 | 4,0 | 0,0451 | |
| 1439322_at | --- | 15 days embryo head cDNA, RIKEN full-length enriched library, clone:D930042L20 product:hypothetical protein, full insert sequence | 314 | 76 | 4,1 | 0,0156 | |
| 1418674_at | Osmr | oncostatin M receptor | 966 | 235 | 4,1 | 0,0040 | |
| 1437360_at | Pcdh19 | protocadherin 19 | 177 | 43 | 4,1 | 0,0065 | x |
| 1456862_at | Six4 | sine oculis-related homeobox 4 homolog (Drosophila) | 664 | 159 | 4,2 | 0,0143 | |
| 1437722_x_at | Pcbp3 | poly(rC) binding protein 3 | 2641 | 629 | 4,2 | 0,0204 | |
| 1426431_at | Jag2 | jagged 2 | 212 | 50 | 4,2 | 0,0298 | |
| 1449440_at | Lpin3 | lipin 3 | 60 | 14 | 4,3 | 0,0312 | x |
| 1434369_a_at | Cryab | crystallin, alpha B | 2137 | 493 | 4,3 | 0,0201 | |
| 1420150_at | Spsb1 | splA/ryanodine receptor domain and SOCS box containing 1 | 569 | 130 | 4,4 | 0,0040 | |
| 1427919_at | Srpx2 | sushi-repeat-containing protein, X-linked 2 | 203 | 46 | 4,4 | 0,0298 | |
| 1417507_at | Cyb561 | cytochrome b-561 | 1167 | 255 | 4,6 | 0,0064 | |
| 1428306_at | Ddit4 | DNA-damage-inducible transcript 4 | 1313 | 286 | 4,6 | 0,0064 | |
| 1451355_at | Asah3l | N-acylsphingosine amidohydrolase 3-like | 482 | 104 | 4,6 | 0,0099 | |
| 1435749_at | Gda | guanine deaminase | 748 | 160 | 4,7 | 0,0160 | |
| 1422943_a_at | Hspb1 | heat shock protein 1 | 285 | 60 | 4,7 | 0,0066 | x |
| 1456226_x_at | Ddr1 | discoidin domain receptor family, member 1 | 482 | 102 | 4,7 | 0,0379 | |
| 1453586_at | Entpd1 | ectonucleoside triphosphate diphosphohydrolase 1 | 275 | 58 | 4,8 | 0,0058 | x |
| 1426127_x_at | Klra18 | killer cell lectin-like receptor, subfamily A, member 18 | 6551 | 1363 | 4,8 | 0,0056 | |
| 1449851_at | Per1 | period homolog 1 (Drosophila) | 100 | 21 | 4,8 | 0,0047 | |
| 1423467_at | Ms4a4b | membrane-spanning 4-domains, subfamily A, member 4B | 36 | 7 | 4,9 | 0,0221 | |
| 1424271_at | Dcamkl1 | double cortin and calcium/calmodulin-dependent protein kinase-like 1 | 72 | 15 | 4,9 | 0,0222 | |
| 1433919_at | Asb4 | ankyrin repeat and SOCS box-containing protein 4 | 99 | 20 | 4,9 | 0,0135 | |
| 1459890_s_at | 1110008P14Rik | RIKEN cDNA 1110008P14 gene | 786 | 158 | 5,0 | 0,0260 | |
| 1435084_at | C730049O14Rik | RIKEN cDNA C730049O14 gene | 1545 | 309 | 5,0 | 0,0071 | |

| | | | | | | | |
|---|---|---|---|---|---|---|---|
| 1455978_a_at | Matn2 | matrilin 2 | 4798 | 934 | 5,1 | 0,0048 | |
| 1442659_at | Pcdh9 | protocadherin 9 | 675 | 130 | 5,2 | 0,0008 | x |
| 1455145_at | --- | 14, 17 days embryo head cDNA, RIKEN full-length enriched library, clone:3222402J19 product:unclassifiable, full insert sequence | 298 | 57 | 5,2 | 0,0127 | |
| 1456873_at | Clic5 | chloride intracellular channel 5 | 877 | 166 | 5,3 | 0,0236 | |
| 1420804_s_at | Clec4d | C-type lectin domain family 4, member d | 37 | 7 | 5,3 | 0,0064 | |
| 1449027_at | Rhou | ras homolog gene family, member U | 1067 | 201 | 5,3 | 0,0021 | |
| 1437785_at | Adamts9 | a disintegrin-like and metallopeptidase (reprolysin type) with thrombospondin type 1 motif, 9 | 358 | 67 | 5,3 | 0,0098 | |
| 1441799_at | 6030422H21Rik | RIKEN cDNA 6030422H21 gene | 67 | 12 | 5,3 | 0,0037 | x |
| 1424701_at | Pcdh20 | protocadherin 20 | 242 | 45 | 5,3 | 0,0023 | |
| 1422177_at | Il13ra2 | interleukin 13 receptor, alpha 2 | 66 | 12 | 5,4 | 0,0001 | |
| 1430062_at | 1600002O04Rik | RIKEN cDNA 1600002O04 gene | 140 | 26 | 5,4 | 0,0231 | x |
| 1435040_at | Irak3 | interleukin-1 receptor-associated kinase 3 | 44 | 8 | 5,4 | 0,0014 | |
| 1416318_at | Serpinb1a | serine (or cysteine) peptidase inhibitor, clade B, member 1a | 57 | 10 | 5,5 | 0,0086 | x |
| 1451804_a_at | Lrrc16 | leucine rich repeat containing 16 | 136 | 25 | 5,5 | 0,0064 | |
| 1452977_at | Zhx3 | zinc fingers and homeoboxes 3 | 336 | 59 | 5,7 | 0,0007 | |
| 1420772_a_at | Tsc22d3 | TSC22 domain family 3 | 573 | 101 | 5,7 | 0,0118 | |
| 1419703_at | Col5a3 | procollagen, type V, alpha 3 | 75 | 13 | 5,7 | 0,0080 | |
| 1443536_at | Slc7a11 | solute carrier family 7 (cationic amino acid transporter, y+ system), member 11 | 1246 | 216 | 5,8 | 0,0028 | x |
| 1436598_at | Icos | inducible T-cell co-stimulator | 58 | 10 | 5,9 | 0,0020 | |
| 1435701_at | --- | 13 days embryo lung cDNA, RIKEN full-length enriched library, clone:D430017B04 product:unclassifiable, full insert sequence | 143 | 23 | 6,1 | 0,0023 | x |
| 1423100_at | Fos | FBJ osteosarcoma oncogene | 395 | 62 | 6,4 | 0,0195 | |
| 1436448_a_at | Ptgs1 | prostaglandin-endoperoxide synthase 1 | 251 | 39 | 6,4 | 0,0014 | |
| 1416935_at | Trpv2 | transient receptor potential cation channel, subfamily V, member 2 | 69 | 11 | 6,4 | 0,0054 | x |
| 1427256_at | Cspg2 | chondroitin sulfate proteoglycan 2 | 41 | 6 | 6,5 | 0,0019 | |
| 1418901_at | Cebpb | CCAAT/enhancer binding protein (C/EBP), beta | 1952 | 298 | 6,5 | 0,0015 | x |
| 1424408_at | Lims2 | LIM and senescent cell antigen like domains 2 | 1057 | 154 | 6,9 | 0,0071 | |
| 1418601_at | Aldh1a7 | aldehyde dehydrogenase family 1, subfamily A7 | 70 | 10 | 6,9 | 0,0002 | |
| 1428433_at | Hipk2 | homeodomain interacting protein kinase 2 | 845 | 123 | 6,9 | 0,0063 | |
| 1437347_at | Ednrb | endothelin receptor type B | 1116 | 162 | 6,9 | 0,0348 | |
| 1416125_at | Fkbp5 | FK506 binding protein 5 | 3245 | 464 | 7,0 | 0,0035 | x |
| 1420753_at | Tll1 | tolloid-like | 697 | 99 | 7,0 | 0,0283 | |
| 1449408_at | Jam2 | junction adhesion molecule 2 | 700 | 99 | 7,0 | 0,0040 | |
| 1429379_at | Xlkd1 | extra cellular link domain-containing 1 | 6307 | 883 | 7,1 | 0,0084 | x |
| 1447773_x_at | 6330409D20Rik | RIKEN cDNA 6330409D20 gene | 133 | 18 | 7,2 | 0,0093 | |
| 1448550_at | Lbp | lipopolysaccharide binding protein | 501 | 68 | 7,3 | 0,0065 | |
| 1448470_at | Fbp1 | fructose bisphosphatase 1 | 447 | 60 | 7,5 | 0,0063 | x |
| 1437595_at | E030010A14Rik | RIKEN cDNA E030010A14 gene | 1591 | 209 | 7,6 | 0,0037 | |
| 1418382_at | Apcdd1 | adenomatosis polyposis coli down-regulated 1 | 958 | 117 | 8,2 | 0,0011 | |
| 1460601_at | Myrip | myosin VIIA and Rab interacting protein | 69 | 8 | 8,2 | 0,0200 | |

| | | | | | | | |
|---|---|---|---|---|---|---|---|
| 1423062_at | Igfbp3 | insulin-like growth factor binding protein 3 | 7341 | 844 | 8,7 | 0,0006 | |
| 1434013_at | Ablim3 | actin binding LIM protein family, member 3 | 129 | 15 | 8,8 | 0,0130 | x |
| 1435790_at | Olfm2 | olfactomedin 2 | 109 | 12 | 9,0 | 0,0064 | |
| 1460039_at | Clec1a | C-type lectin domain family 1, member a | 369 | 40 | 9,2 | 0,0259 | |
| 1429018_at | 3830408D24Rik | RIKEN cDNA 3830408D24 gene | 150 | 16 | 9,6 | 0,0215 | |
| 1435092_at | Arl4a | ADP-ribosylation factor-like 4A | 175 | 17 | 10,3 | 0,0072 | |
| 1439163_at | Zbtb16 | zinc finger and BTB domain containing 16 | 64 | 6 | 10,4 | 0,0236 | |
| 1430352_at | 8430417A20Rik | RIKEN cDNA 8430417A20 gene | 155 | 14 | 11,3 | 0,0067 | |
| 1439878_at | Ivl | involucrin | 134 | 10 | 13,1 | 0,0002 | |
| 1442025_a_at | AI467657 | expressed sequence AI467657 | 90 | 6 | 14,6 | 0,0441 | |
| 1416164_at | Fbln5 | fibulin 5 | 608 | 31 | 19,8 | 0,0049 | |
| 1453678_at | Mbd1 | methyl-CpG binding domain protein 1 | 1058 | 49 | 21,6 | 0,0040 | x |
| 1457707_at | Gm489 | gene model 489, (NCBI) | 141 | 6 | 22,3 | 0,0130 | |
| 1455859_at | A330021E22Rik | RIKEN cDNA A330021E22 gene | 358 | 14 | 25,8 | 0,0018 | |
| 1450291_s_at | Ms4a4c | membrane-spanning 4-domains, subfamily A, member 4C | 201 | 7 | 27,5 | 0,0006 | |
| 1427034_at | Ace | angiotensin I converting enzyme (peptidyl-dipeptidase A) 1 | 727 | 23 | 31,9 | 0,0018 | |
| 1434202_a_at | BC055107 | cDNA sequence BC055107 | 10170 | 312 | 32,6 | 0,0006 | x |
| 1427345_a_at | Sult1a1 | sulfotransferase family 1A, phenol-preferring, member 1 | 250 | 7 | 37,7 | 0,0068 | |
| 1427747_a_at | Lcn2 | lipocalin 2 | 18710 | 464 | 40,4 | 0,0037 | |
| 1450826_a_at | Saa3 | serum amyloid A 3 | 512 | 12 | 42,2 | 0,0026 | |
| 1419491_at | Defb1 | defensin beta 1 | 343 | 6 | 53,9 | 0,0026 | x |
| 1451263_a_at | Fabp4 | fatty acid binding protein 4, adipocyte | 8478 | 121 | 69,9 | 0,0007 | x |
| 1451596_a_at | Sphk1 | sphingosine kinase 1 | 926 | 7 | 136,2 | 0,0006 | |
| 1422639_at | Calcb | calcitonin-related polypeptide, beta | 1331 | 10 | 138,5 | 0,0006 | |
| 1422557_s_at | Mt1 | metallothionein 1 | 1719 | 5 | 316,9 | 0,0002 | x |
| 1428942_at | Mt2 | metallothionein 2 | 11202 | 31 | 359,0 | 0,0000 | |